BIOGEOCHEMICAL WEATHERING PROCESSES IN THE GLACIERISED RHÔNE AND OBERAAR CATCHMENTS, SWITZERLAND, AND THE APURE CATCHMENT, VENEZUELA

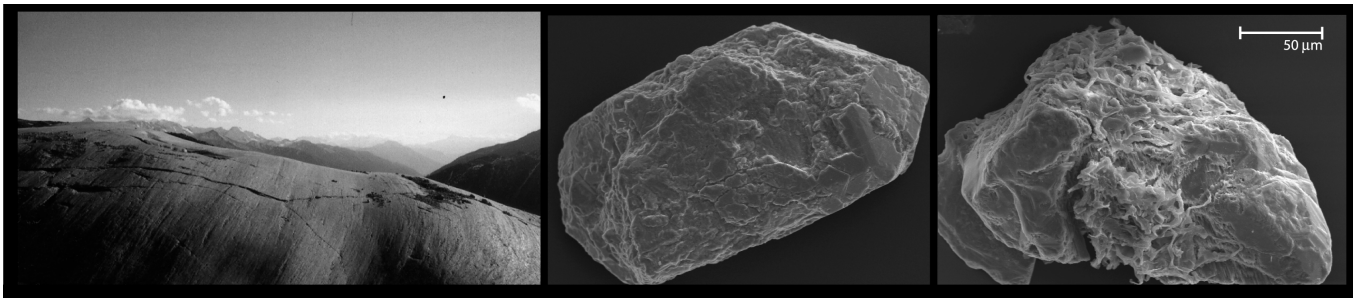
RACHEL HOSEIN: Ph.D. THESIS (2002)

Geochemical and Environmental Analysis Research Group

Institut de Géologie
Université de Neuchâtel

Thesis Jury:

Prof. Karl B. Föllmi (Neuchâtel; Supervisor)
Dr. Sylvain Huon (Pierre & Marie Curie, Paris)
Dr. Martin R. Lee (Glasgow)
Prof. James I. Drever (Wyoming)
Prof. Angelika Kalt (Neuchâtel)
Dr. Philipp Steinmann (Neuchâtel)



Th. 1662

IMPRIMATUR POUR LA THESE

Biogeochemical weathering processes in the glacierised Rhône and Oberaar catchments, Switzerland, and the Apure catchment, Venezuela

de Mme Rachel Hosein

UNIVERSITE DE NEUCHATEL

FACULTE DES SCIENCES

La Faculté des sciences de l'Université de Neuchâtel sur le rapport des membres du jury,

Mme A. Kalt, MM. K. Föllmi (directeur de thèse),
P. Steinmann, S. Huon (Paris),
M. Lee (Glasgow UK) et J. Drever (Wyoming USA)

autorise l'impression de la présente thèse.

Neuchâtel, le 10 janvier 2003

Le doyen:

F. Zwahlen

SERVICE DES BIBLIOTHEQUES DE L'UNIVERSITE NEUCHATEL

CONTENTS

PREFACE *I*

ABSTRACT : ENGLISH/ GERMAN/ FRENCH *V*

CHAPTER 1: INTRODUCTION *1-1*

CHAPTER 2: METHODS *2-1*

CHAPTER 3: CARBONATE AND SILICATE WEATHERING IN TWO PRESENTLY GLACIATED, CRYSTALLINE CATCHMENTS *3-1*

CHAPTER 4: ELEVATED APATITE WEATHERING RATES *4-1*

CHAPTER 5: PHOSPHORUS WEATHERING: FOUR CASE STUDIES *5-1*

CHAPTER 6: CHEMICAL WEATHERING: RATE AND MECHANISM OF BIOTITE WEATHERING *6-1*

CHAPTER 7: SR ISOTOPE SYSTEMATICS IN GLACIATED CRYSTALLINE CATCHMENTS *7-1*

CHAPTER 8: DISCUSSION *8-1*

Chapter 2 Appendicies

Appendix 2-1: Rhône discharge 99-2001 **2-15**
Appendix 2-2: Field Methods 2-17
Appendix 2-3: Soluble Reactive Phosphorus (SRP) 2-18
Appendix 2-4: Total and Total Dissolved Phosphorus (TP; TDP) 2-19
Appendix 2-5: SEDEX, Sequential Extraction Of Phosphorus Phases 2-21
Appendix 2-6: Picture Plate A *2-25*

Chapter 3 Appendicies

Appendix 3-1: Cations

Appendix 3-1-1a: Rhône meltwater Ca^{2+} composition **3-25**
Appendix 3-1-1b: Oberaar meltwater Ca^{2+} composition 3-27
Appendix 3-1-2a: Rhône meltwater Mg^{2+} composition 3-29
Appendix 3-1-2b: Oberaar meltwater Mg^{2+} composition 3-31
Appendix 3-1-3a: Rhône meltwater Na^{+} composition 3-33
Appendix 3-1-3b: Oberaar meltwater Na^{+} composition 3-35
Appendix 3-1-4a: Rhône meltwater K^{+} composition 3-37
Appendix 3-1-4b: Oberaar meltwater K^{+} composition 3-39
Appendix 3-1-5a: Rhône meltwater Adsorbed Cations 3-41
Appendix 3-1-5b: Oberaar meltwater Adsorbed Cations 3-42

CONTENTS

Appendix 3-2: Anions

Appendix 3-2-1a: Rhône meltwater Cl^- composition **3-43**
Appendix 3-2-1b: Oberaar meltwater Cl^- composition 3-45
Appendix 3-2-2a: Rhône meltwater NO_3^- composition 3-47
Appendix 3-2-2b: Oberaar meltwater NO_3^- composition 3-49
Appendix 3-2-3a: Rhône meltwater SO_4^- composition 3-51
Appendix 3-2-3b: Oberaar meltwater SO_4^- composition 3-53
Appendix 3-2-4a: Rhône meltwater measured HCO_3^- 3-55
Appendix 3-2-4b: Rhône meltwater calculated HCO_3^- 3-57
Appendix 3-2-4c: Oberaar meltwater calculated HCO_3^- 3-59

Appendix 3-3: Miscellaneous

Appendix 3-3-1a: Rhône meltwater Si content **3-61**
Appendix 3-3-1b: Oberaar meltwater Si content 3-63
Appendix 3-3-2a: Rhône meltwater suspended sediment 3-65
Appendix 3-3-2b: Oberaar meltwater suspended sediment 3-67
Appendix 3-3-3a: Rhône meltwater pH 3-69
Appendix 3-3-3b: Oberaar meltwater pH 3-71
Appendix 3-3-4a: Rhône meltwater conductivity 3-73
Appendix 3-3-4b: Oberaar meltwater conductivity 3-75
Appendix 3-3-5:: Oberaar meltwater discharge 3-77
Appendix 3-3-6: Suspended sediment XRF values 3-79
Appendix 3-3-7: Suspended sediment mineralogy 3-81
Appendix 3-3-8a: Rhône Suspended sediment granulometry 3-83
Appendix 3-3-8b: Oberaar Suspended sediment granulometry 3-84

Chapter 4 Appendicies

Appendix 4-1: Apatite grain images **4-15**
Appendix 4-2: Apatite grain descriptions 4-37
Appendix 4-3: Apatite grain grading 4-41
Appendix 4-4: suspended sediment SEDEX values 4-45
Appendix 4-5a: Rhône profiles sedex, TOC and pH values 4-47
Appendix 4-5b: Oberaar profiles sedex, TOC and pH values 4-48
Appendix 4-6a: Rhône profiles granulometry 4-49
Appendix 4-6b: Oberaar profiles granulometry 4-50
Appendix 4-7: Picture Plate B 4-51

Chapter 5 Appendicies

Appendix 5-1a: Rhône meltwater SRP concentrations **5-23**
Appendix 5-1b: Oberaar meltwater SRP concentrations 5-25
Appendix 5-2a: Total P concentrations in the Rhône meltwaters 5-27
Appendix 5-2b: Total P concentrations in the Oberaar meltwaters 5-28

Chapter 6 Appendicies

Appendix 6-1: Rhône and Oberaar XRD values **6-25**

General Appendicies

APPENDIX I: GRAIN SIZE AND THE SEDEX METHOD *AI-1*
APPENDIX II: CONFERENCE ABSTRACTS *AII-1*
APPENDIX III: A SHORT CV *AIII-1*

PREFACE

My thesis is part of the research project "***continent-ocean interactions and their long-term records***" presently being undertaken by the ***Geological Environmental Analysis*** (GEA) group of the ***Institut de Géologie, Université de Neuchâtel***. It was the inspiration of my thesis supervisor, ***Karl Föllmi***, resulting from his work comparing total and organic phosphorus concentrations in marine sediments sampled by the ODP-DP projects, encompassing sediments deposited in the world's oceans from the Mesozoic to the end of the Pleistocene. Karl observed an inverse correlation between sea-level and the phosphorus flux to the oceans from the Oligocene onwards and wanted to explore how glaciers and glacial processes might affect both chemical weathering fluxes in general and specifically how they modify the release of the biolimiting nutrient phosphorus (P) to the biosphere, because the main source of P on geological timescales is the weathering of continental rocks.

With these questions in mind, and with the support of the GEA researchers ***Philipp Steinmann***, ***Thierry Adatte*** and others, he initiated three Ph. D. theses: My thesis compliments the thesis of ***Federica Tamburini***, who studied marine phosphorus deposition during the last 150,000 years using sediment cores from a range of oceanic sites. It is also a "joint project" whose purpose is to compare present-day and longer term glacial weathering processes in the geographically, glaciologically and geologically comparable, crystalline catchments of the Rhône and Oberaar glaciers, Central Switzerland. To this end I have shared the last four years, an office, a field apartment and many hours of challenging discussion with my fellow Ph. D. colleague, ***Kaspar Arn***. A large part of our thesis time was passed in the field, collecting a comprehensive 2-year data set of rain, snow, meltwater, suspended sediment, dust and moraine samples. Six months of fieldwork were required to obtain this data set, including two winter campaigns when samples were taken on a monthly basis. Kaspar Arn is responsible for the ***Oberaar glacier*** data set and the ***Rhône glacier*** data set was collected by myself.

During my thesis I had the opportunity to further my research experience through two further collaborations: I was invited to participate in a project studying the hydrochemistry of the Apure watershed, Venezuela, organised by ***Sylvain Huon***, of the ***Biogéochimie Isotopique*** group of the ***Université Pierre & Marie Curie, Paris***. Additionally I initiated my own collaboration with ***Martin Lee*** of the ***Division of Earth Sciences*** at the ***University of Glasgow*** examining the surface morphologies of apatite grains from glacial sediments of different ages.

These fulfilling and enlightening opportunities were enabled thanks to the people and groups named above and two grants from the ***Swiss National Science Foundation*** 21-53997.98 and 20-61485.00, which are most gratefully acknowledged.

There are also many other people who have sculpted and enriched both my personal and academic experiences over the years, and whom I would most sincerely like to thank:

Colin Reynolds and Mr Hately, formerly of *the Institute for Freshwater Biology* and the *Queen Katherine School, Kendal* respectively, for introducing me to Redfield ratios and the colorimetric measurement of chlorophyll during my A-level biology project on "The Relative Eutrophicity of the Lakes in the English Lake District" (1991).

Dave Evans, *Department of Geography, University of Glasgow,* for fostering my interest in glacial environments through his leadership of our Glasgow University Exploration Society student expedition to Spitsbergen (1996).

Mike Russell, Chris Burton and Bill Higginson then of the *Department of Geology, University of Glasgow,* for their openness in the supervision of my B.Sc. final year project (1998) studying the total phosphorus and iron "chemostratigraphy" in sediments from Dobb's Linn, Scotland (the global stratatype for the Ordovician-Silurian boundary) and their colleagues in the department for their enthusiasm in teaching Geology.

Fellow members of the British Branch of the International Glaciological Society whose ideas, experiences and research helped me orientate my thesis and made me feel part of a research community, particularly Darrel Swift (Melv), Pete Nienow and Martyn Tranter**.**

Other Staff, fellow Ph. D.'s, post docs and undergraduate students associated with Neuchâtel's Institut de Géologie, the Science Faculty, the canton of Neuchâtel and BENEFRI: Khaoula Hamila, José, Sebastian Ryser, Roberto Costa, François Bourret, André Villar, Tong, Charles-Henri and Ivann; Sabine Erb, Elisabeth Kuster, Pierre Tissot, Manuel da Silva and Gianfranca Cerrito; Jean-Paul Schaer, Martin Burkhard, Angelika Kalt, Eric Verrecchia; Othmar Müntener, Virginie Matera and Urs Eichenberger; Massoud Dadras and Mireille Leboeuf (Institut de Microtechnologie, Neuchâtel), J. Ondrus and S. Pierrehumbert (SCPE-laboratory, Neuchâtel), Giulio Galetti (University of Fribourg), Barbera Seth (formerly of Bern University). Julia, Natalie, Pierre, Laurent, Bas, Fedy, Baba, Urs, Sévérine, Bernd, Mahmoud, Ronny, Bastien, J.D., Olivier, Guillaume, Alexey Claire, Charles and Ray.

Herr Carlen-Philipp for allowing me access to the Rhône glacier via the Rhône Glacier Boutique and by helicopter!

The scientists and technicians I had the chance to meet in Venezuela Vincent Vallés, Toto, Manuel, Manuel and Herado...

Brigitte Hool, my singing teacher for her patience and wisdom in helping my find my voice and for giving me the chance to sing in the Neuchâtel University Choir.

My friends: Manna, Astri, Morag, Miranda, Helen, Siân and Angus, Sam, Kat and Ruedi, Neil, Dan, Andy, Silvia and Kristian, Ken, Jim, Alison and Matt, Roddy, Dru, Karen and Matt, Sandra and Gilbert, the Berneys, Paul, Mark, Sarah, Gary and Catlin, Morgan and Lucy, Dave and Gail, Heather and Gareth, Matt and Mari, John, Enrique, Ellie and Dave for sharing in our swiss adventures.

Jean Reynolds and her family together with ***Pauline and David Alker,*** whose continuing love, support and prayers have helped our family keep its strength over the last year.

My in-laws Mike and Penny, Katharine and Stephen and the whole of the extended Nisbet family for keenly sharing in the adventures of Dave and myself.

My grandparents, Elsie and Lloyd Greenwood.

My sister, Loren

My Mum

and Dad, who told me on my 24th birthday " ... you too my daughter first, will soon be another year in front of yesteryear which has gone past and strangely it is Time that lasts".

My husband, Dave.

ABSTRACT

In my Ph. D. thesis I assess the biogeochemical and physical weathering rates in the sub- and proglacial environments of the Rhône and Oberaar glaciers, Switzerland in collaboration with Kaspar Arn, whose Ph. D. thesis compliments my own and whose results are also presented within my thesis (*chapters 6 and 7*) they give pertinent background data on our joint field areas. I also compare the weathering of phosphorus (P) in these glaciated catchments with P forms in the tropical Apure catchment, Venezuela. The relative contribution to each chapter from Kaspar and I is as follows:

Chapter one: Rachel Hosein 100%
Chapter two: Rachel Hosein 100%
Chapter three: Rachel Hosein 60%, Kaspar Arn 40%
Chapter four: Rachel Hosein 90%, Kaspar Arn 10%
Chapter five: Rachel Hosein 80%, Kaspar Arn 20%
Chapter six: Rachel Hosein 10%, Kaspar Arn 90%
Chapter seven: Rachel Hosein 10%, Kaspar Arn 90%
Chapter eight: Rachel Hosein 100%

Our quantification of the composition of inputs to and outputs from the Rhône and Oberaar watersheds has allowed us to calculate present-day chemical and physical denudation fluxes from these catchments. The Rhône and Oberaar basins were chosen for this study because the mineralogy of their crystalline bedrock geology is well documented (*chapter 2*). Since crystalline rocks also cropped out underneath large areas of the ice sheets at the last glacial maximum I attempt to draw some wider inferences about biogeochemical weathering in glacial environments (*chapter 8*).

Calcium dominates the cation denudation flux from presently glaciated Oberaar catchment and is the second most important dissolved cation in the Rhône meltwaters after silica. In *chapter 3* we calculate that calcium represents 81 % and 55 % of the total cation flux from the Oberaar and Rhône catchments respectively. Chemical and physical weathering rates are elevated in the Oberaar catchment compared to the Rhône: The Oberaar meltwaters contain an order of magnitude more Ca^{2+} than the Rhône meltwaters (i.e. 555 and 82-96 keq km^{-2} yr^{-1}) and its SO_4^{2-}, HCO_3^-, K^+, and Mg^{2+} and suspended sediment fluxes are also elevated (e.g. Oberaar suspension = 773 t km^{-2} yr^{-1}; Rhône suspension = 388-491 t km^{-2} yr^{-1}). We attribute this to the presence of a strongly foliated gneissic zone in the centre of the Oberaar catchment, which is eroded more easily than the surrounding granites and granodiorites that crop-out in the Rhône catchment. The gneissic zone is also enriched in calcite (up to 9 %; *chapter 7*) compared to other local lithologies where calcite concentrations are < 1 % and we infer the presence of more metal sulphides in the

Abstract

Oberaar catchment from the greater weight percent of FeO in the Oberaar suspension (0.32 %; Rhône = 1.8 %) and the elevated rain corrected sulphide flux issuing from the Oberaar glacier relative to the Rhône glacier (204 and 33- 39 keq km^{-2} yr^{-1} respectively). Calcite and suphides are highly reactive minerals in the subglacial environment, due to their rapid oxidation (sulphides) and rapid rates of dissolution at neutral pH compared to silicate minerals (calcite). Sulphide oxidation provides a source of protons for the acid hydrolysis of freshly abraded finely comminuted mineral grains that are generated at the glacier sole. Therefore differences in the erodability of bedrock, together with small contrasts in the calcite and sulphide content of the bedrock appear to have a major impact on denudation rates, even in crystalline catchments. This observation is also supported by the Sr isotope data collected on the waters, suspended sediments and bedrock in our respective field areas (*chapter 7*). In contrast the Na^+ and Si fluxes from the two catchments are similar, indicating that silicate-weathering rates are comparable between the two catchments. A comparison with the available published denudation data for other presently glaciated catchments with crystalline bedrock implies that neither the congruent nor the incongruent weathering of silicate minerals is elevated in presently glaciated catchments, suggesting that increased glacial cover does not increase silicate weathering rates or the rate of sequestration of atmospheric CO_2 associated with these weathering processes.

The second part of my thesis was to analyse the physical and biogeochemical weathering of phosphorus (P) in glacial environments: In *chapter 4* I assess the fate of detrital P in the proglacial zone, by comparing chronosequences from the Rhône and Oberaar catchments that are comprised of samples of recent meltout sediment and sediments from profiles dug into Little Ice Age moraines and Younger Dryas aged tills. ESEM pictures were taken of apatite grain surface morphologies and a sequential phosphorus extraction method (SEDEX) was used to measure the concentrations of ironbound, detrital and organic P in the sediment samples. We use these data to assess the evolution of phosphorus forms in the pedosphere on a 11.6 kyr time frame and to calculate integrated dissolution rates for detrital P over 140 yr, 270 yr and 11.6 kyr time steps. Our rates suggest that P dissolution rates in proglacial systems may be ≈ 70 faster than the average continental weathering rate (based on the P concentrations in unpolluted rivers) in the first 300 years post deglaciation, due to bio-corrosion and the oxidisation of sulphide minerals in the evolving acidic pedosphere, with mechanical indentations on grains acting as sites for preferential dissolution. *Chapter 4* draws on data generated by Kasper Arn: sediment granulometry, chemistry and mineralogy, as part of his assessment of the long-term weathering of detrital minerals (particularly biotite) in the proglacial environments of the Rhône and Oberaar

glaciers (*chapter 6*; here Kaspar observes that biotite concentrations are reduced by 25 – 50 % in proglacial sediments 140 – 270 yr after deglaciation and that they are replaced by vermiculite).

In *chapter 5* I examine the forms of P in the runoff from presently glaciated Rhône, and Oberaar catchments and the recently glaciated Rhône Tributary catchment and compare them to those in the runoff from the tropical Apure watershed. To this end we measured the concentrations of dissolved and particulate forms of P in river waters, rain and snow: soluble reactive P (SRP), dissolved organic P (DOP) and total P (TP). The ironbound, detrital and organic P content of the particulate material was also measured using the SEDEX sequential extraction method. We found that the runoff from the Apure watershed contains more conditionally bioavailable P (dissolved inorganic, and organic P and particulate ironbound and organic P; 1.97 kmol km^{-2} yr^{-1}) than glacial meltwaters from the Rhône and Oberaar glaciers (0.29 - 0-39 kmol km^{-2} yr^{-1}). But the eolian input of bioavailable P to the Apure watershed by Saharan dust is greater than the output flux of conditionally bioavailable P, which implies that soils in our largely transport limited tropical catchment act as a reservoir for P. In contrast, while runoff from the presently glaciated catchments is dominated by scarcely bioavailable detrital P (97 %), the role subglacial weathering processes play in bringing large volumes of freshly comminuted, detrital P to the biosphere (7 & 11 kmol km^{-2} yr^{-1} in our presently glaciated catchments) may be important in controlling inputs of bioavailable P to the oceans on glacial-interglacial timescales: The weathering-derived SRP flux from the recently deglaciated Rhône Tributary catchment (0.17 kmol km^{-2} yr^{-1}) is elevated compared to the weathering-derived SRP flux from the Rhône and Oberaar subglacial environments (0.04 - 0.05 kmol km^{-2} yr^{-1}) and global mean riverine SRP flux (0.13 kmol km^{-2} yr^{-1}). This indicates that the dissolution of detrital P is accelerated in proglacial sediments and that the low P binding capacity of immature, weathering limited, glacial soils allows the transfer of bioavailable P into aquatic ecosystems. These data strengthen the argument for changes in the biolimiting P flux from the continents on glacial-interglacial timescales.

Zusammenfassung

In meiner Dissertation studierte ich biogeochemische und physikalische Verwitterungsraten im sub- und proglazialen Bereich vom Rhône- und Oberaargletscher (Schweizer Alpen). Die Arbeit entstand in Zusammenarbeit mit Kaspar Arn, dessen Dissertation die vorliegende Arbeit ergänzt und dessen Resultate im Nachfolgenden auch gezeigt werden (*Kapitel 6 und 7*; diese enthalten weitere erhobene Daten aus unseren gemeinsamen Feldgebieten). Im weiteren verglich ich die Verwitterung von Phosphor (P) in den vergletscherten Gebieten mit den P-Formen im tropischen Apure-Einzugsgebiet, Venezuela. Die relativen Beiträge von mir und Kaspar Arn an den einzelnen Kapiteln belaufen sich wie folgt:

Kapitel 1: Rachel Hosein 100%
Kapitel 2: Rachel Hosein 100%
Kapitel 3: Rachel Hosein 60%, Kaspar Arn 40%
Kapitel 4: Rachel Hosein 90%, Kaspar Arn 10%
Kapitel 5: Rachel Hosein 80%, Kaspar Arn 20%
Kapitel 6: Rachel Hosein 10%, Kaspar Arn 90%
Kapitel 7: Rachel Hosein 10%, Kaspar Arn 90%
Kapitel 8: Rachel Hosein 100%

Die Quantifizierung der Zusammensetzung von input und output vom Rhône- und vom Oberaar-Einzugsgebiet erlaubte uns, die aktuellen (rezenten) chemischen und physikalischen Denudationsfluxe der Gebiete zu errechnen. Die zwei Einzugsgebiete dieser Studie wurden aufgrund der guten Kenntnisse über die Mineralogie ihrer kristallinen Grundgesteine ausgewählt. Auch während dem letzten glazialen Maximum lagen grosse Gebiete der kontinentalen Eisschilder auf kristallinen Gesteinen, woraus ich einige generelle Folgerungen über die biogeochemische Verwitterung in glazialen Gebieten ziehe (*Kapitel 8*).

Calcium dominiert den Kationenflux vom Oberaar-Einzugsgebiet, in den Rhoneschmelzwässern ist Calcium das zweitwichtigste Element nach Silizium. In *Kapitel 3* errechnen wir, dass Calcium im Oberaar- und im Rhône-Einzugsgebiet 81 und 55 % vom totalen Kationenflux ausmachen. Die chemischen und physikalischen Verwitterungsraten vom Oberaar-Einzugsgebiet werden mit dem Rhône-Einzugsgebiet verglichen: Die Oberaar-Schmelzwässer enthalten mehr als fünf mal mehr Ca^{2+} als die Rhône-Schmelzwässer (555 und 82-96 keq km^{-2} yr^{-1}), auch die Fluxe von SO_4^{2-}, HCO_3^-, K^+, und Mg^{2+} und suspendiertem Sediment vom Oberaar sind erhöht (Oberaar Suspension = 773 t km^{-2} yr^{-1}; Rhône Suspension = 388-491 t km^{-2} yr^{-1}). Wir schreiben dies der leichteren Erodierbarkeit einer stark verfalteten Zone von Gneisen im mittleren Teil dieses Gebietes zu, verglichen mit den umliegenden Graniten und Granodioriten, welche auch im Rhôneeinzugsgebiet anstehen. Diese Gneise enthalten bis zu 9 % Calcit (*Kapitel 7*)

sowie einen höheren Sulphidanteil (mehr Gewichts% FeO in der Oberaar Suspension; 0.32 %, Rhône = 1.8 %), was zu einem erhöhten, regenkorrigierten SO_4^{2-}Flux vom Oberaargletscher führt (204 im Vergleich zu 33 – 39 keq km^{-2} yr^{-1} am Rhônegletscher). Calcit und Sulphide sind sehr reaktive Minerale im Subglazialen Bereich aufgrund von dessen hohen Lösungsraten bei neutralem pH verglichen mit Silikatmineralen (Calcit) resp. der schnellen Oxidation (Sulphide). Die Oxidation von Sulphiden ist eine wichtige Quelle von Protonen für die saure Hydrolyse von frisch erodierten, fein gemahlenen Mineralkörnern, welche an der Gletscherbasis produziert werden. Deswegen haben Unterschiede in der Erodierbarkeit des Grundgesteins zusammen mit geringen Unterschieden im Calcit- und Sulphidgehalt desselben einen starken Einfluss auf die Denudationsraten, dies sogar in Einzugsgebieten kristalliner Geologie. Diese Beobachtung wurde in unseren Feldgebieten mit Sr-Isotopen-Daten von Schmelzwasser, Suspension und Grundgestein bestätigt (*Kapitel 7*). Si- und Na^+-Flux sowie daraus folgernd Silikatverwitterungsraten sind dagegen in beiden Einzugsgebieten vergleichbar. Ein Vergleich mit publizierten Daten aus nichtvergletscherten Einzugsgebieten mit kristallinem Grundgestein und analogen, temperierten Bedingungen zeigt, dass weder die kongruente noch die inkongruente Verwitterung von Silikatmineralen in unseren vergletscherten Gebieten erhöht sind, was wiederum darauf hinweist, dass eine stärkere Vergletscherung die Silikatverwitterungsraten sowie den mit dem Verwitterungsprozess verbundene Entzug von CO_2 aus der Atmosphäre kaum erhöht.

Der zweite Teil dieser Dissertation beinhaltet die Analyse der physikalischen und biogeochemischen Verwitterung von Phosphorus (P) in vergletscherten Gebieten. In *Kapitel 4* wird, anhand eines Vergleiches von Chronosequenzen von den Vorfeldern des Rhône- und Oberaargletschers, das Schicksal von detritischem P in der proglazialen Zone untersucht. Die Chronosequenzen bestehen aus Proben von rezentem Ausschmelzsediment sowie aus Proben von Bodenprofilen in den Moränenablagerungen der Kleinen Eiszeit und der Jüngeren Dryas. Von Apatitkörnern wurde mit dem Rasterelektronenmikroskop (REM) die Oberflächenmorphologie untersucht und fotographiert. Ferner wurde eine Methode der sequentiellen Extraktion von Phosphor (SEDEX) angewendet, um die Konzentrationen von eisengebundenem, detritischem und organischem P in den Sedimentproben zu messen. Mit diesen Daten wird die Entwicklung verschiedener Formen von P in der Pedosphäre über einen zeitlichen Rahmen von 11.6 ka aufgezeigt sowie durchschnittliche Lösungsraten für detritisches P über Zeiträume von 140 a, 270 a und 11.6 ka errechnet. Diese Daten weisen daraufhin, dass die P-Lösungsraten in proglazialen Systemen, im Vergleich zu der durchschnittlichen kontinentalen P-Verwitterungsrate (welche auf den P-Konzentrationen in unverschmutzten Flüssen beruht), über die ersten 300 Jahre nach einem

Gletscherrückzug bis zu 70 mal schneller sein können. Dies aufgrund von Bio-Korrosion und der Oxidation von Sulphidmineralen in der sich entwickelnden sauren Pedosphäre sowie aufgrund von mechanischen Defekten auf den Apatitoberflächen, welche als Orte der bevorzugten Lösung gelten.

Kapitel 4 baut auf Daten von Kaspar Arn auf: Sedimentgranulometrie, chemische und mineralogische Zusammensetzung, welche einen Teil seiner Untersuchung der langfristigen Verwitterung von primären Mineralien (im Speziellen Biotit) in der proglazialen Zone der beiden Gletscher darstellt. In *Kapitel 6* wird der Zerfall von Biotit zu Gunsten des sekundären Minerals Vermikulit beschrieben (Der Biotitgehalt nimmt in den proglazialen Sedimenten über 140 – 270 Jahre nach dem Gletscherrückzug um 25 – 50 % ab).

In *Kapitel 5* vergleiche ich die Formen von P im Schmelzwasser der beiden Gletscher mit denjenigen im Abfluss eines bis vor kurzem vergletscherten Seiteneinzugsgebiet vom Rhônegletscher sowie mit dem Abfluss vom tropischen Apure-Einzugsgebiet. Hierzu haben wir die Konzentrationen von gelösten und partikulären Formen von P im Abflusswasser, im Regen und im Schnee gemessen: Gelöster reaktiver P (SRP), gelöster organischer P (DOP) und totaler P (TP). Der Gehalt an eisengebundenem, detritischem und organischem P wurde ebenfalls gemessen, anhand der sequentiellen Extraktionsmethode (SEDEX). Wir konnten aufzeigen, dass die Wässer des Apure-Einzugsgebietes mehr teilweise biologisch nutzbaren P (gelöster inorganischer und organischer P, partikulärer eisengebundener P sowie organischer P; 1.97 kmol km^{-2} yr^{-1}) enthalten als die Schmelzwässer der beiden Gletscher (0.29 - 0-39 kmol km^{-2} yr^{-1}). Der äolische input von biologisch nutzbarem P durch Saharastaub in das Apure-Einzugsgebiet jedoch ist grösser als der output von teilweise biologisch nutzbarem P, was auf den Reservoireffekt der Böden in diesem hauptsächlich transportlimitierten, tropischen Einzugsgebiet hinweist. Im Gegensatz dazu, obwohl der Abfluss von vergletscherten Gebieten durch kaum biologisch nutzbaren P (97 %) dominiert ist, spielen die subglazialen Verwitterungsprozesse eine wichtige Rolle, indem sie grosse Mengen von frisch gemahlenem, detritischem P in die Biosphäre bringen (7 & 11 kmol km^{-2} yr^{-1} in den beiden Gletschergebieten). Damit könnte der input von biologisch nutzbarem P in die Ozeane in glazial-interglazialen Zeiträumen beeinflusst werden: Der von der Verwitterung herrührende SRP-Flux vom kürzlich entgletscherten Seitenfluss der Rhône (0.17 kmol km^{-2} yr^{-1}) ist höher verglichen mit denjenigen der beiden Gletscher (0.04 - 0.05 kmol km^{-2} yr^{-1}) sowie mit dem globalen Abflussmittel (0.13 kmol km^{-2} yr^{-1}). Dies weisst auf die beschleunigte Lösung von detritischem P in proglazialen Sedimenten hin sowie darauf, dass die geringe Bindungskapazität der kaum entwickelten, verwitterungslimitierten Böden in Gletschervorfeldern den Transfer von biologisch nutzbarem P in aquatische Ökosysteme

vereinfacht. Diese Daten stärken das Argument für einen sich ändernden biolimitierenden P-Flux von Kontinenten über glazial-interglaziale Zeiträume.

RESUME

Dans cette thèse de doctorat, j'évalue les taux d'altération biogéochimique et physique dans les environnements sous- et proglaciaire des glaciers du Rhône et de l'Oberaar en Suisse. Ce travail a à mettre en relation avec celui de Kaspar Arn, dont certains résultats sont présentés avec les miens (*les chapitres 6 et 7*). Ils offrent des éléments d'information pertinents (en arrière plan) sur nos bassins versants étudiés simultanément. En outre, je mets en comparaison l'altération du phosphore (P) dans ces bassins versants glaciaires avec l'altération du P dans le bassin tropical d'Apure, au Venezuela. La participation relative dans chaque chapitre est la suivante :

Chapitre un : Rachel Hosein 100 %
Chapitre deux : Rachel Hosein 100 %
Chapitre trois : Rachel Hosein 60 %, Kaspar Arn 40 %
Chapitre quatre : Rachel Hosein 90 %, Kaspar Arn 10 %
Chapitre cinq : Rachel Hosein 80 %, Kaspar Arn 20 %
Chapitre six : Rachel Hosein 10 %, Kaspar Arn 90 %
Chapitre sept : Rachel Hosein 10 %, Kaspar Arn 90 %
Chapitre huit : Rachel Hosein 100 %

Notre quantification de la composition des précipitations et des eaux de fonte des bassins hydrographiques du Rhône et de l'Oberaar nous ont permis de calculer les taux d'altération chimiques et physiques actuels de ces captages. Nous avons pris la décision d'étudier les bassins du Rhône et de l'Oberaar du fait de l'importante documentation à disposition sur leur minéralogie (pour les roches cristallines ; *chapitre 2*). Puisque les roches cristallines ont affleuré sous les grandes surfaces des champs de glace au dernier maximum glaciaire, j'essaie de tirer des conclusions étendues au sujet de la désagrégation biogéochimique dans les environnements glaciaires (*chapitre 8*).

Le calcium domine le flux de dénudation du bassin de l'Oberaar et c'est le deuxième ion le plus présent dans les eaux de fonte du Rhône après la silice. Dans le *chapitre 3*, nous calculons que le calcium représente 81 % et 55 % du flux de cation total des bassins versants respectifs de l'Oberaar et du Rhône. Les dénudations physiques et chimiques sont plus élevées dans le bassin de l'Oberaar en comparaison de celui du Rhône. Les eaux de fontes de l'Oberaar contiennent un ordre de magnitude de plus pour le Ca^{2+} que les eaux de fontes du Rhône (c'est-à-dire 555 et 88 –96 keq km^{-2} yr^{-1}) et ses flux de le SO_4^{2-}, K^+, Mg^{2+} et de matières en suspension sont également élevés (Oberaar : matières en suspension = 773 t km^{-2} yr^{-1}; Rhône : matières en suspension = 388-491 t km^{-2} yr^{-1}). Nous attribuons ces résultats à la présence d'une zone gneissique avec une foliation très prononcée au centre du bassin de l'Oberaar qui est érodée plus facilement que les environs granitiques et granodioritiques qui affleurent dans le bassin versant du Rhône. En outre, la zone gneissique est enrichie en calcite (jusqu'à 9 %. *Chapitre 7*) en comparaison avec des

autres lithologies locales où les concentrations en calcites sont < 1 %. Nous déduisons également la présence des sulfures métalliques supplémentaires dans le bassin versant de l'Oberaar car la concentration de FeO dans la suspension de l'Oberaar est plus élevée que dans celui du Rhône (0.32 % ; Rhône = 1.8 %) ainsi qu'un flux élevé de SO_4^{2-} qui provient du glacier de l'Oberaar. Le calcite et les sulfures sont des minéraux extrêmement réactifs dans l'environnement sous-glaciaire, à cause de leur oxydation rapide (sulfures) et de leur rapide taux de la dissolution à pH neutre en comparaison avec les silicates (les calcites). L'oxydation des sulfures fournit une source de protons pour l'hydrolyse acide des grains minéraux récemment érodés et finement broyées qui sont engendrés au fond du glacier.

Ainsi, des différences d'érodabilité entre lithologies en même temps que des petits contrastes dans le contenu en calcite et en sulfure de la roche semblent avoir un impact majeur sur taux de dénudation, même dans les bassins cristallins. (En outre, l'étude du rapport isotopique du Sr des eaux, des matières en suspension et de la roche mère dans nos terrains respectifs *chapitre 7*). Par contre, les flux de Na^+ et de Si des deux bassins se ressemblent, indiquant une similitude entre les deux bassins versants du point de vue de l'altération des silicates. Une comparaison avec les informations publiées pour d'autres bassins versant actuellement glaciaires, suggèrent que l'augmentation de la couverture glaciaire n'augmente ni l'altération des silicates ni les taux de séquestration de CO_2 atmosphérique, phénomènes associés à ces processus de d'altération.

La deuxième partie de ma thèse a pour but d'analyser l'altération physique et biogéochimique du phosphore (P) dans les environnements glaciaires. Dans le *chapitre 4*, j'évalue le devenir du P détritique dans la zone proglaciaire, en comparant les chronoséquences des bassins du Rhône et de l'Oberaar qui maintient des spécimens de sédiments provenant de la fonte de la glace et des profiles creusés dans les moraines Petit Age glaciaire et du Drayas Récent. Des photos de la morphologie des surfaces des apatites ont été réalisées à l'aide d'un microscope de balayage électronique et l'on a utilisé la méthode d'extraction séquentielle de phosphore (SEDEX) pour mesurer les concentrations de P lié au fer, détritique et organique dans les échantillons de sédiment. Nous employons ces données pour évaluer l'évolution des formes de phosphores dans la pédosphère durant une période de 11.6 ka et pour calculer les taux d'altération intégrés pour le P détritique pendant des périodes de 140 ans, 270 ans et 11.6 ka. Nos données suggèrent que la dissolution de P détritique dans les systèmes proglaciaire pourrait être~ 70 plus rapide que le flux moyen d'altération continentale dans les 300 premières années après la déglaciation. Cette déduction et basée sur les concentrations de P mesurées dans les fleuves non- pollués, et serait due à la bio-corrosion et à l'oxydation des minéraux sulfurés dans la pédosphère qui deviennent

de plus en plus acides, avec des déformations mécaniques sur les grains qui sont les sites pour la dissolution préférentielle. Le *chapitre 4* utilise les éléments d'information issu de la thèse de Kaspar Arn, la granulométrie, la chimie et la minéralogie de sédiment, pour évaluer l'altération des minéraux détritiques (surtout la biotite) dans les environnements proglaciaires du Rhône et de l'Oberaar. (Dans le *Chapitre 6,* Kaspar Arn remarque que les concentrations en biotite sont réduites de 25- 50 % dans les sédiments proglaciaires 140 à 270 ans après la déglaciation et qu'elles sont remplacées par la vermiculite).

Dans le *chapitre 5*, j'examine les formes de P dans l'écoulement des bassins versants actuellement glaciaires du Rhône et de l'Oberaar et du bassin du tributaire du Rhône récemment glaciaire et j'entreprends également la comparaison entre ces derniers et ceux d'écoulement du bassin versant tropical de l'Apure. Dans ce but, nous avons mesuré les concentrations de P dissout et en suspension dans l'eau des rivières, de la pluie et de la neige : P soluble et réactif (SRP), P dissout et organique (POP) et P total. Nous avons aussi mesuré le contenu en P lié avec le fer, le P détritique et organique de la matière en suspension par la méthode d'extraction séquentielle SEDEX. Nous avons observé que l'écoulement de l'Apure contient du P plus essentiellement bio-disponible (sous forme de P organique et inorganique dissout, et du P en suspension lié avec le fer et la matière organique) que les eaux glaciaires du Rhône et de l'Oberaar (0.29 – 0.39 kmol km^{-2} yr^{-1}). Mais le flux de P entrant dans le bassin d'Apure, essentiellement bio-disponible, issu des poussières du Sahara qui entre le bassin d'Apure est plus important que le flux de P essentiellement bio-disponible qui sort dans les rivières, ce qui implique que les sols de bassin tropical à "transport limité" servent de réservoir pour le P. Par ailleurs, tandis que les ruissellements glaciaires actuels sont dominés par du P détritique faiblement bio-disponible (97 %), le rôle que jouent les processus de d'altération sous glaciaires, en apportant de grands flots de P détritique à la biosphère (7 et 11 kmol km^{-2} yr^{-1} dans nos bassins actuellement glaciaux) peuvent êtres importants dans le commande des transfers de P bio-disponible aux océans dans les temps glaciaires-interglaciaires. Le flux de SRP issu de la d'altération du bassin versant du tributaire du Rhône récemment englacé est plus élevé que le flux qui émane des environnements sous- glaciaires du Rhône et de l'Oberaar et le flux moyen global de SRP des rivières. En fait la dissolution de P détritique est accélérée dans les sédiments proglaciaires et la faible capacité du P à se lier dans les sols glaciaires, immatures et à altération limitée, permet le transfert du P bio-disponible dans les écosystèmes aquatiques. Ces données renforcent l'argumentation en faveur des changements du flux de P bio-limitant depuis les continents pour des échelles de temps de l'ordre glaciaire-interglaciaire.

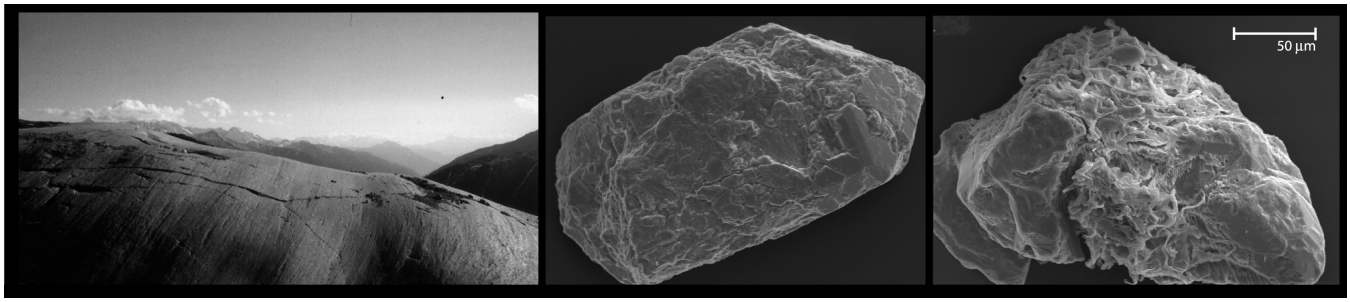
CHAPTER 1

A Spanish Mountain Poem

Does the mountain feel
As it unravels and crumbles
And is eaten into soils
Hard yielding
To softer ground.

The soil fleshing itself
Into poppies, lizards, olives
And us- our tounges rooted
In more tones and textures
Than they can ever name.

But can we lick away our edges
With such astounding grace.



INTRODUCTION

What Drives Changes in CO_2 on Glacial-Interglacial Timescales?

The earth has experienced periods of glaciation throughout its geological record, evinced for example by the occurrence of glaciomarine sediments in the late Proterozoic, late Ordovician, Permo-Carboniferous and Pleistocene. The timing of climate oscillations is controlled by many factors. The main pacer of the earth's climate is its position relative to the sun: The periodicity of Earth's eccentricity, obliquity (tilt) and precession are all echoed by changes in the Late Cenozoic climate on 100,000, 41,000 and 23,000-19,000 timescales respectively (Imbrie and Imbrie, 1979; Menzies, 1995 and references therein). The positioning of the continental plates and biological evolution may also influence climate (Berner, 1992) and detailed ice core records show evidence of reduced atmospheric CO_2 during "ice-house periods". A 50 % reduction in the atmospheric content of this "greenhouse gas" would cool the surface of the planet by 3° C (± 1.5° C; Broecker and Peng, 1982).

The relationship between CO_2 and the $\partial^{18}O$ (temperature proxy) curves over the last 400 kyr is striking (Fig. 1): with a gradual, saw-toothed decrease in CO_2 and $\partial^{18}O$ as the worlds' climate cools down and a rapid rebound to preglacial values upon warming. This points towards a complex, internal regulation of the climate system that is non-linear, with negative

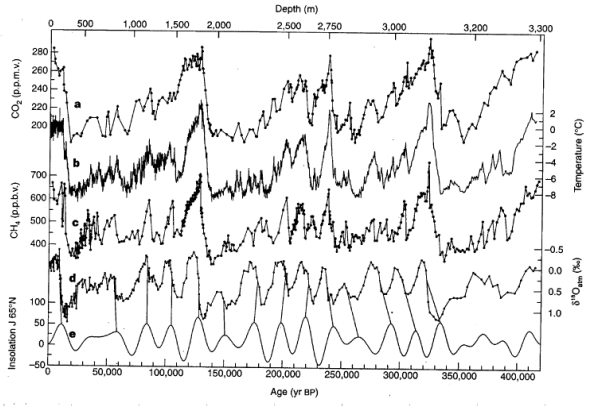


Fig. 1: *The synchronous changes in atmospheric CO_2 and $\partial^{18}O$ over the last 400 kyr (Petit et al., 1999)*

feedbacks operating (Fig. 2; e.g. Broecker, 2000). The processes controlling these changes in CO_2 are not fully understood. Decreased oceanic temperature, increased oceanic salinity and albedo can only account for 30 % of the CO_2 reduction at the last glacial maximum (Neftel et al., 1988).

To date a number of alternative mechanisms have been suggested for reducing atmospheric CO_2 during the Tertiary, particularly during the Pleistocene: Elevated rates of physical erosion owing to the uplift and erosion of the Himalayan and Alpine orogens (e.g. Raymo, 1991) and increased glacial cover (Sharp, 1995) may have lead to increased chemical erosion on the continents (Berner et al., 1983; Berner, 1994; reactions 1 & 2)

$$2CO_2 + 3\,H_2O + CaAl_2Si_2O_8 \rightarrow Al_2Si_2O_5(OH)_4 + Ca^{2+} + 2HCO_3^- \quad (1)$$

$$CaCO_3 + CO_2 + H_2O \rightarrow Ca^{2+} + 2HCO_3^- \quad (2)$$

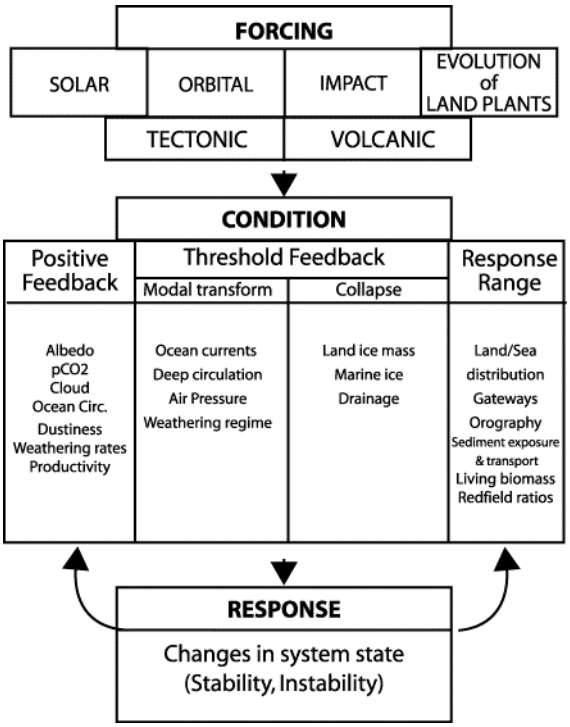


Fig. 2: *The path to "stability" and "instability" in the climate system from astronomic (and evolutionary) forcing,paced by internal adaptions in the condition of the system. Adapted from Berger (1990)*

Silicate weathering is a long-term sink of atmospheric CO_2, but the weathering of carbonates may also reduce atmospheric CO_2 punctually within glacial-interglacial cycles, as dissolved inorganic carbon is retained within the oceans on timescales of a 1000 years (Fig. 3).

An increased biological carbon pump might also serve to lower atmospheric CO_2 during glacial times (Broecker, 1982). The rate at which biolimiting nutrients are supplied to the biosphere controls productivity and on geological timescales the main biolimiting nutrient is likely to be phosphorus (P; Broecker and Peng, 1982; Tyrell, 1999). The P concentration of oceanic surface waters may be raised during glacial stadials by the enhanced upwelling of deep ocean waters that are enriched in P (Broecker and Peng, 1982; Sigman and Boyle, 2000; Fig. 4, after Compton et al., 2000). But, since the residence time of P in the oceans is between 38,000 and 10,000 yr (Ruttenberg, 1993; Colman and Holland, 2000) the deep oceanic resevoir of P would not be able to sustain enhanced levels of productivity over a full glacial cycle without a concomitant increase in phosphorus input to the oceans. (Föllmi, 1995, 1996). The primary source of P to the biosphere is the weathering of detrital minerals, as phosphorus does not have a gaseous phase. Therefore increasing the chemical weathering rate of detrital P minerals on the continents is the main way by which P inputs to the oceans can be augmented on glacial-interglacial timescales. But, both rates of oceanic overturn and continental mechanisms should be considered as potential pacemakers of glacial-interglacial changes in atmospheric CO_2.

Increased inputs of other micro nutrients to the oceans during the last glacial cycle may also have increased primary productivity. The increased oceanic iron flux due to increased aridity and

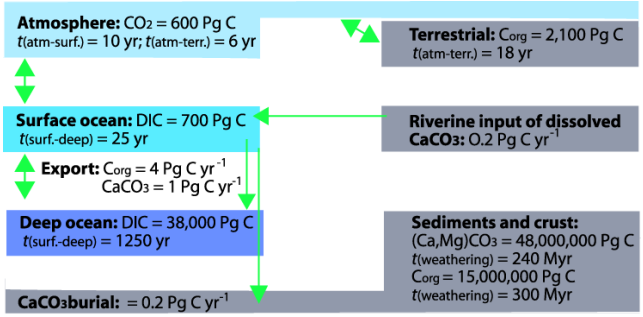


Fig. 3: *A simplified view of the Holocene carbon cycle, (Sigman and Boyle 2000 and references therein).*

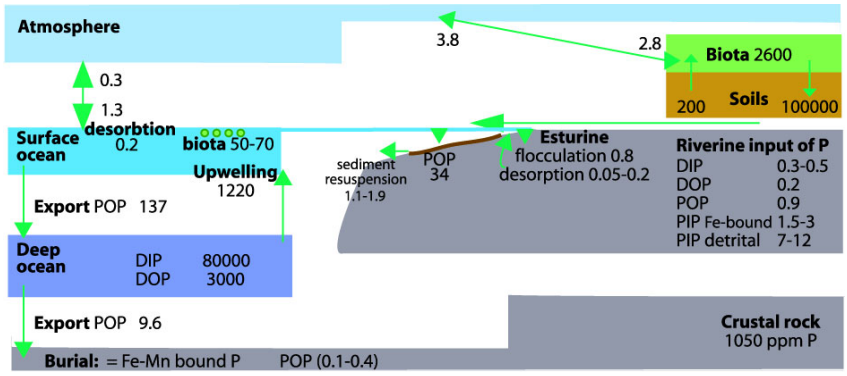


Fig. 4: *"Natural" P cycles in terrestrial and aquatic environments in units of grams * 10^{12} (After Compton et al., 2000 and references therein)*

dustiness during glacial stadials may have been particularly important (Martin, 1990; Falkowski, 1997).

In order to significantly reduce atmospheric CO_2 the carbon sequestered by biological organisms must not be reoxidised. But, the residence time of carbon in organic resevoirs is very short; i.e., 18 yr in terrestrial systems (Fig. 3). For this reason several authors have argued for a fundamental shift in traditional Redfield ratios during glacial periods to accentuate the biological sequestration of CO_2 from the atmosphere (e.g. Broecker, 1982).

A combined biogeochemical weathering equation, where C: P molar ratios are fixed by terrestrial organic matter (C: P 250:1) shows how biological and abiological CO_2 draw down mechanisms are related (3). Alowances must also be made for the reoxidation of this carbon. The diagram of Sigman and Boyle (2000; Fig. 3) shows that this reservoir of C is recycled on a 18 yr time frame.

$$2CaSiO_3P_{0.002} + 3CO_2 + 1H_2O = 2CaCO_3 + 2SiO_2 + CH_2OP_{0.004} + O_2 \quad (3)$$

Chemical weathering reactions may be concomitantly biologically controlled and controlling (Föllmi et al., 2003): Land plants, their associated microbes and fungi have the capacity to increase terrestrial weathering rates by the gradual acidification of the immature pedosphere, for example by the secretion of organic acids:

$$2NaAlSi_3O_8 + H_2C_2O_4 + 9H_2O = 2Na^+ + C_2O_4^{2-} + 4H_4SiO_4 + Al_2Si_2O_5(OH)_4 \quad (4)$$

In turn their "reward" is the mobilisation of growth limiting nutrients (e.g. PO_4^{3-}, Fe^{2+}, Mg^{2+} and K^+; Berner, 1992; Drever, 1994; Föllmi et al., 2002). The high fluxes of sulphate from proglacial areas (Anderson et al., 2000; Wadham et al., 2001) that are generated by the oxidation of finely comminuted sulphide minerals may also provide a strong acid proton-source for the accelerated dissolution of mechanically preconditioned minerals in the proglacial environment.

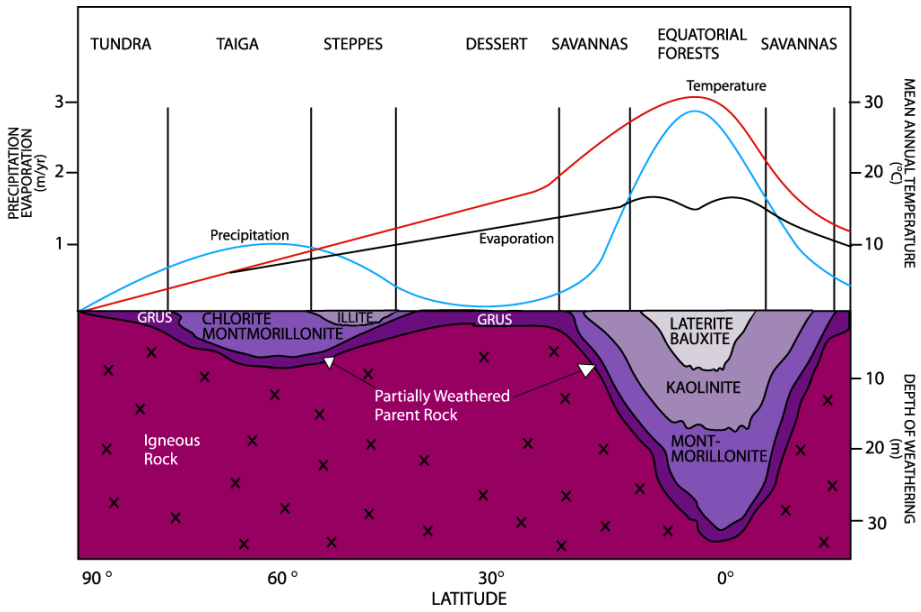


Fig. 5: *Schematic view of silicate weathering system, showing the relationship between precipitation, evaporation, temperature, depth of weathering and nature of residuum (after Strakhov, 1967; Hay, 1998)*

Quantifying Weathering Rates

The study of weathering has been an important facet of geological research for over a century. The concept of a series of mineral weatherability was introduced by Goldich (1938). The least resistant minerals are the ones which are most chemically reactive: halite, and calcite have low solubility constants and pyrite is rapidly oxidised at the earth's surface. The most stable minerals are quartz, kaolinite and gibbsite (Berner and Berner, 1996). Kaolinite and gibbsite are examples of secondary products formed by the weathering of detrital minerals. The type of secondary minerals formed by weathering reactions depends on the primary minerals present and the temperature and aridity of the environment (Fig. 5; after Strakhov, 1967 and Hay, 1998).

Chemical weathering can be studied using two main approaches: either "in vitro" or in the field. Laboratory studies measure weathering rates using very specific mineral surface areas, mineral substrates, solute compositions, temperatures and pH's. One major advantage of such work is that each condition can be varied independently and monitored continuously over a period of months or years in order to characterise trends in weathering rates over ranges of conditions and scales that can not be found in the natural environment (e.g. Blum and Stillings, 1995). Laboratory weathering rates are expressed in mol m^{-2} s^{-1}, where the reactive surface area of the substrate in contact with the weathering solution is quantified either geometrically or by the Brunauer Emmett Teller (BET) method, which uses the physyadsorbtion of a gas on mineral surface areas. The reactive surface area parameter therefore exerts a

fundamental control on laboratory weathering rate calculations.

The trends observed in such laboratory studies can be used to identify patterns that may also exist in the natural environment, for example the positive relationship between silicate weathering and temperature (Vebel, 1993; White et al., 1999a).

Field weathering rates, which are generally normalised by catchment area (e.g. mol km^{-2} yr^{-1}), permit the geochemist to obtain an integrated view of weathering processes and rates in natural environments. Multiple variables may interact to accelerate or inhibit the weathering of bedrock in the field; vegetation, temperature, relief, elevation, runoff, aridity, mineral coatings, geology, acid aerosols and physical erosion rates are all important factors. Geochemists treat the world as natural laboratory, seeking to quantify the impact of these different parameters on weathering rates. One approach is to observe the solute composition of catchment runoff. The Amazon River in South America has the highest annual discharge in the world (6300 km^3 yr^{-1}, or 17 % of the total global runoff; Berner and Berner, 1996). The combined annual discharge of the top 13 rivers represents 38 % of the total water discharged into the oceans, or a 10 cm thick layer of water were it spread over the entire ocean surface (Berner and Berner, 1996; Stumm and Morgan, 1996). Catchment studies of the world's major rivers show the global transfer of elements from the continents to the oceans (Table 1).

Table 1 The long-term input-output balance for major seawater ions and alkalinity

Ion	Ocean Inventory (10^{18} mol)	River Input	Atmospheric-Evaporite Cycling	Ion Exchange	Hydrothermal Activity	Pyrite burial or other	Carbonate Deposition
Cl^-	710	6.1	(-6.1)				
Na^+	608	8.5	-5.7	-1.9	(-0.9)		
Mg^{2+}	69	5.2	-0.3	-1.2	(-3.1)		-0.6
SO_4^{2-}	37	3.2	-0.3		(-1.7)	-1.2	
K^+	13	1.2	-0.06	-0.4	(-0.6)	-0.1	
Ca^{2+}	13	12.5	-0.06	2.6	(+2.0)		-17
Alk	3.1	31.9		0.5	-0.4	2.4	-35

(data compiled by Stumm and Morgan, 1996)

Meybeck (1979) and Milliman and Meade (1983) have measured the chemical compositions and suspended sediment concentrations running down these major arteries in order to calculate global physical and chemical continental weathering fluxes and the relative importance of different lithologies. Meybeck (1987) showed that although crystalline rocks crop out over 33.9 % of the continental area they only contribute 11.6 % of the solutes to the oceans, whereas the 1.25 % of evaporites outcropping generates 17.2 % of the weathering derived dissolved mineral load and the input from carbonates weathering represents 50 % of the total denudation-derived load. Similar data sets have also been used to demonstrate the linear relationship between runoff and dissolved fluxes of ions and the control geology exerts on dissolved compositions (sandstone < granite < basalt < shale < carbonates; Bluth and Kump, 1994). Catchment studies can also be made on a smaller scale to decipher the role of interrelated variables under conditions where solute budgets are more tightly constrained. Having compared 68 (< 58 km^2) catchments that are underlain by granitoid rock White and Blum (1995) proposed that precipitation and temperature are co-variable with respect to silicate weathering; i.e. warm wet localities have elevated fluxes of SiO_4 compared to dry cold areas. They did not find a connection between K^+, Ca^{2+},

Table 2: Erosion regimes: Features and processes associated with transport-limited and weathering limited erosion. Adapted from Stallard (1992).

Transport-limited	Weathering-limited
Thick soils	Thin or no soils
Slight-slopes that are convexo-concave	(Steep slopes that are straight and at a threshold angle
Erosion rates indepentent of lithology	Erosion rates depend on bedrock susceptibility
Processes:	Processes:
soil creep	rock slides
removal of dissolved phases	strong sheet wash
	soil and snow avalanches
	glacial plucking and abrasion
	removal of dissolved phases

Notes: Weathering-limited - potential transport processes greater than weathering supply. Transport-limited - supply by weathering greater than the capacity of transport processes to remove material (until weathering is slowed by feedback).

Mg^{2+} and climate in their study, nor a correlation between chemical fluxes and topographic relief or extent of recent glaciation, unlike other authors (Drever and Zobrist, 1992; Anderson et al., 1997; see below). They interpret this as evidence that physical erosion has a weaker influence on chemical weathering than temperature and precipitation. The linkages between relief, physical erosion and chemical weathering probably cannot be expressed in a linear fashion (Drever and Clow, 1995). Changes in relief may modify the erosion regimes operating on the land surface; uplift and glaciations rejuvenate physical erosion, allowing continental denudation processes to switch from being predominantly transport-limited to weathering-limited regimes (Table 2, after Stallard, 1992)

Catchment studies give us a "here and now" picture of natural weathering rates, but natural environments also provide an opportunity to assess weathering rates integrated over longer time steps i.e. on centennial, millennial and millenary timescales. The prerequisites for such studies are a set of precisely datable surfaces or sediment deposits, the original composition of which can be determined and which have not been subsequently reworked. The hot-spot related sequence of basaltic eruptions leading to the formation of the Hawaiian Islands is one such example and the mineral composition of the regolith on islands of different ages is used to assess progressive weathering (e.g. Chadwick et al., 1999). Freshly ground glacial deposits of different ages can also provide the basis for a chronosequence (e.g. Taylor and Blum, 1995). Chronosequences can be used to assess the rate of primary mineral dissolution (this study, *chapters 4 and 6*) and the rate of secondary mineralogy formation (Darmody et al.1987; Egli et al., 2001; this study *chapter 6*).

Finally the data from chronosequence and catchment studies can be modeled using parameterisations of rates derived in the laboratory, data on flushing times and chemical compositions of fluids entering and exiting catchments in order to

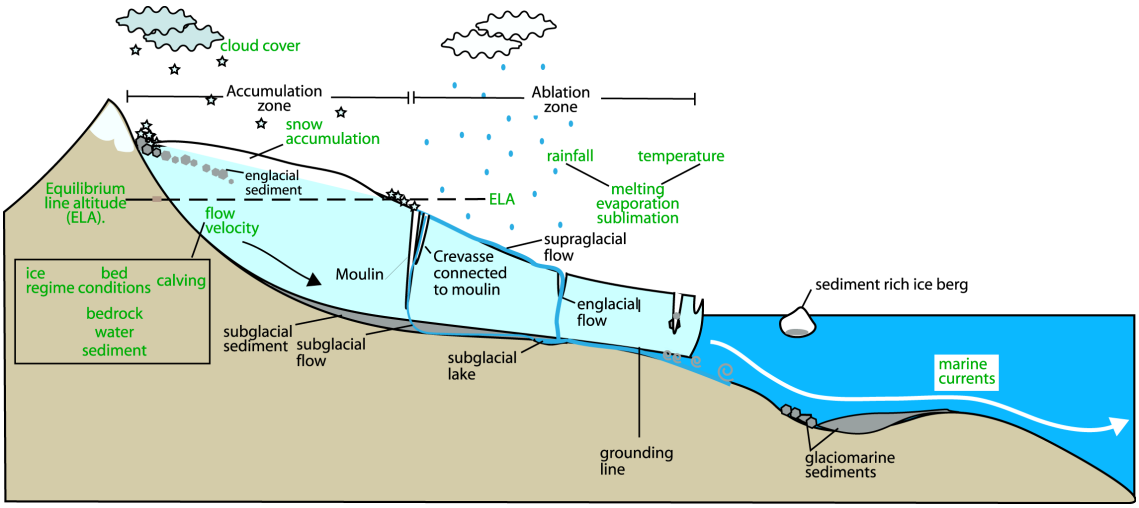


Fig. 6: *Generalised features of glacial systems: factors controlling ice mass balance are written in green, (after Röthlisberger and Lang, 1987 and Powell, 1991)*

calculate the contribution of different minerals to solute denudation.

Glaciers and Glacial Weathering

"The development of these huge ice sheets must have led to the destruction of all organic life at the Earth's surface. The ground of Europe, previously covered with tropical vegetation and inhabited by herds of great elephants, enormous hippopotami, and gigantic carnivora became suddenly buried under a vast expanse of ice covered plains, lakes, seas, and plateaus alike. The silence of death followed... springs dried up, streams ceased to flow and sunrays rising over that frozen shore...were met only by the whistling of northern winds and the rumbling of the crevasses as they opened across the surface of that huge ocean of ice."

Louis Agassiz.

Introduction: 2.97 % (or 43.4 * 10^6 km^3) of the earth's water is presently stored in the cryosphere (Berner and Berner, 1996). Mass balance, a concept universally applicable to glacial systems, explains the dynamic interactions of this ice with the rest of the water cycle. An equilibrium line divides terrestrial ice masses into two parts: an upper accumulation zone and a lower ablation zone and changes in the form and the volume of the ice mass are the result of the waxing and waning of these two components of the glacial system. Relative volume gain, through increased snowfall, results in the altitude of the equilibrium line descending, whereas relative volume loss, by melting and sublimation leads to a rise in the altitude of the equilibrium line. There are many interdependent factors controlling this mass balance, which should be considered when thinking about connections between glacial weathering and climate (Fig. 6 after Powell, 1991).

Subglacial weathering: Glaciers can potentially increase weathering rates by generating large amounts of fine rock flour through abrading and plucking away the bedrock at their bases (Boulton, 1979). Dilute glacial meltwaters drain through crevasses, course through the subglacial system and emerge at glacier portals as milks charged with

freshly comminuted fines and ions (SO_4^{2-} , Ca^{2+} and K^+) dissolved from the most reactive mineral phases: (pyrite, calcite and mica, respectively) and depressed with respect to silicic acid (Drever and Hurcomb, 1986; Sharp et al., 1995; Nienow, 1996 and Anderson et al., 1997, West et al., 2002; Figs. 6 & 7). The chemical reactions that result from the mixing of milled rock flour and dilute, close to neutral meltwaters lead to solute fluxes from glacial catchments that are three times Summerfield's (1991) estimated global average denudation rate of 14.8 t km^{-2} yr^{-1} (Sharp et al., 1995). Calcium is the dominant cation in all glacial meltwaters and its presence is mainly due to the dissolution of carbonates. Calcite is not confined to catchments with carbonate or metasedimentary geology, but is also present as an accessory phase in crystalline rocks and provided up to 98% of the calcium flux from freshly ground granitoid rocks in laboratory leaching experiments (White et al., 1999b). The dissolution of calcite, mica and other less reactive silicate minerals in meltwaters acts as a sink for CO_2 (see equations 1 & 2). Effective chemical weathering in the subglacial environment depends on the production, mixing and export of sediments and meltwaters and a degree of contact between the subglacial and supraglacial environments for the draw down of CO_2. Therefore maximal chemical weathering occurs under wet-based glaciers (Table 3; Figs. 6 & 7; Raiswell, 1984). Indeed it is as a result of catchments studies in just such basins that the idea was first conceived (Sharp et al., 1995). Wet based glaciers are not universal; polythermal and frozen glacier beds are more commonly found in polar and sub-polar settings where the majority of the present-day cryosphere is located. Areas of the glacier bed are frozen to bedrock or basal sediments in such cold-based systems and the temperatures at the ice-rock interface range from –13 to -18°C (Menzies, 1995 and references therein). In the last 5 years a growing number of studies of weathering have been undertaken in polar regions to investigate weathering rates under cold-based and polythermal glaciers (Table 3).

Although there is evidence of cold-based glaciers eroding sediment (e.g. Atkins et al., 2002), erosion is generally conceded to be greatly reduced, both under frozen glaciers and under warm-based glaciers with soft basal sediments (e.g. Boulton, 1979). Moreover meltwaters are "minimal" in frozen systems. In polythermal regimes weathering rates are heavily influenced by the routing of glacial melts: At sub-zero temperatures englacial ice plugs crevasses, causing melt to drain down sediment-poor marginal channels and weathering is minimal (Hodson and Ferguson, 1999). In contrast, when melt does drain

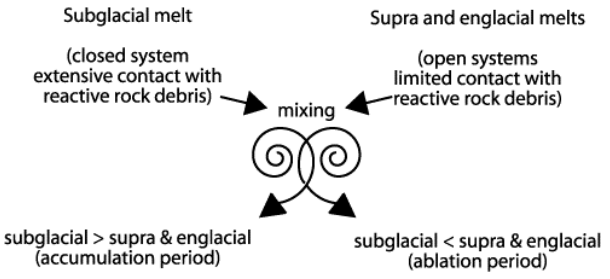


Fig. 7: *Glacial hydrology, modified after Raiswell (1984) *Groundwater is not included in the diagram as this is minimal in the Rhône and Oberaar catchments since they have crystalline bedrock.*

into the subglacial environment it may remain in contact with fine sediments for longer periods of time compared to waters in warm based glacial systems. Thus it becomes highly concentrated in dissolved species. Charged waters may be released when portals are created in the previously frozen glacier margin (Skidmore and Sharp, 1999). A comparison of cation fluxes from wet-based, polythermal and cold-based glaciers indicates that chemical weathering occurs in all three subglacial environments, although it is notably lower under cold-based glaciers (Table 3). Perhaps the key point to remember is that the cryosphere is a dynamic system and that over periods of 100-1000's of years basal conditions can vary, even in polar latitudes (Menzies, 1995 and references therein). Moreover at the last glacial maximum (LGM) the Laurentide ice sheet was composed of cold-based, warm-melting and warm-freezing areas according to Sugden (1978). Therefore a range of subglacial erosion processes coexisted, related to both the thermal regime and the geology underlying different areas of the ice sheet (Fig. 8, after Sugden, 1978). Geology and bedrock permeability can also effect the routing of basal meltwaters and in turn basal pressures, ice sliding rates and subglacial erosion. Water leaks through porous carbonate lithologies and the ice sticks, whereas water pressure builds up under less permeable crystalline lithologies enabling the ice to slide (Sugden, 1978).

Mechanical weathering: The global importance of glacial chemical weathering is intimately linked to the question- do glaciers and ice sheets mechanically erode more sediment than rivers? This is a subject of intense debate. The conclusion appears to depend on the way physical weathering is measured; the storage of sediment within basins should be accounted for if such comparisons are to be effective (Harbour and Warburton, 1993). The damming of many rivers, and prior deposition of glacial sediments in what are presently riverine catchments has complicated such an appraisal (Harbour and Warburton, 1993; Hay, 1998). Hallet et al. (1996) demonstrate that sediment yields are higher from presently glaciated valleys compared to un-glaciated valleys incised in the same bedrock. They present glacial erosion rates ranging from 0.01-100 mm yr^{-1}; the lowest rate is for polar glaciers on crystalline rock, the highest are for large surging glaciers in tectonically active Alaskan mountain ranges. In addition they compare glaciated basins to small mountain basins, identified by Milliman and Syvitski (1992) as having statistically elevated yield, and find that glacier dominated basins produce more sediment than mountainous catchments in general. Ice sheets also appear to be superior agents of physical erosion: Bell and Laine (1985) estimate that the Canadian shield was lowered by 120 m during the Pleistocene, whereas contemporary erosion rates measured on the shield could only have lower it by 40 m if they continued for the same period of time 3 My; Stallard, 1992). But Hay, (1998) recalculated Bell and Laine's estimate as 16 m and suggested that the inclusion data from the Alaskan glaciers which erode tectonically active mountain ranges, in the global comparisons made by Hallet et al., (1996) biased

Catchment	Specific runoff (m yr^{-1})	Bedrock	Catchment area (Km^2)	Ice cover (%)	Thermal regime	Cationic denudation rate (∑meq+ m-2 yr-1)	Transient CO_2 drawdown (kg C km^{-2} yr^{-1})
Ice Sheet							
Lewis River draining Barnes Ice Cap	0.71	migmatic granite-gneiss	205	89	Polythermal ?	94	
Maritime glaciers (Svalbard)							
Scott Turnerbreen	0.52	Sedimentary/mixed	13	32	Cold-based	160	110
Austre Broggernbreen	1.3	Sandstone, shale, phyllite, schists, quartzite & carbonate	9.9	71	Cold-based	240	1100
Broggernbreen (lower site)	0.99	Sandstone, shale, phyllite, schists, quartzite & extensive carbonate	32	53	Polythermal	500	2600
Finsterwalderbreen	0.60	Phyllites, quartzites, sandstones, shales, limestones & siltstones	69	65	Polythermal	325	915
Hannabreen	0.8	Carbonate, schist & sandstone	13.3	69	Polythermal	320	2300
Erdmanbreen	0.81	Sandstone, dolerite, phyllite, schist, quartzite	16	70	Polythermal	190	490
Midre Lovénbreen	1.4	Schist, quartzite, phyllite, minor carbonate & sandstone	6.2	80	Polythermal	560	765
Maritime glaciers (Iceland)							
Tungufljot	2.1	Basalt	720	25		720	9800
Hvita-south, Gullfoss	2.1	Basalt	2000	19		1100	13000
Hvita-west kljafoss	1.8	Basalt	1700	21		650	8300
Temperate valley glaciers							
Europe							
Rhône[†]	3.1	granite	26.6	73	Warm-based	147-178	774
Oberaar[†]	2.4	granite & strongly foliated gneiss	11.03	57	Warm-based	681	2317
Haut Glacier d'Arolla	2	schists and gneisses	12	54	Warm-based	640	2000
Gornergletscher	1.4	gneisse, micaschist, gabbro,serpentine, 5% - calcareous micaschist and dolomite	82	83	Warm-based	450	
Tsidjiore Nouve		Metamorphosed Limestones	4.8	97	Warm-based	510	
N. America							
South Cascade Glacier	3.9	phlogopite-actinolite schists, greenstones, quartz diorite, basaltic and lamprophyric dykes	6.1	34	Warm-based	676	3300
Worthington Glacier	7.7	metagraywake, metapelite	13	83	Warm-based	1600	
Berendon Glacier	3.7	siltstones, conglomerates and volcanoclastic	53	62	Warm-based	947	
Asia							
Batura Glacier	2	Carbonate-rich	608	60	Warm-based	1500	
Chhota-Shigri Glacier	3.5	Plutonic/metamorphic	40	25	Warm-based	750	
Dokriani Glacier	1.1	Plutonic/metamorphic	23	45	Warm-based	462	
Continental/global averages			390[*]				3000[§]

[†] This study:

[*] Livingstone (1963)

[§] Gaillardet et al. (1999)

Other data are from a compilation by Hodson et al. (2000)

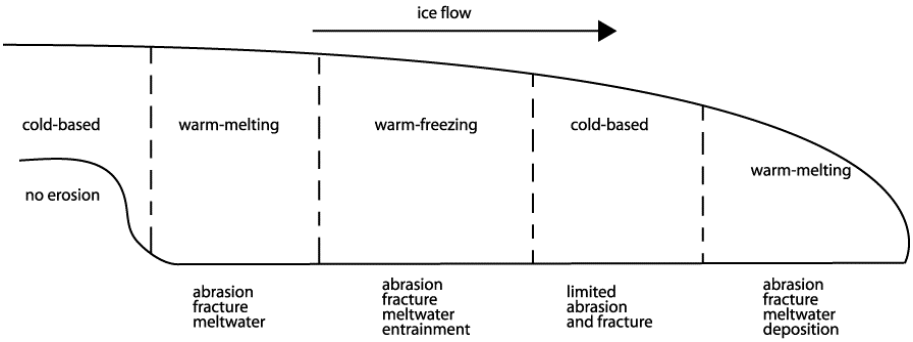


Fig. 8: *Idealised model of the relationship between processes of glacial erosion and the basal thermal regime of an ice sheet (after Sugden, 1978).*

their conclusion incorrectly in favour of glacial weathering. Furthermore he suggested that the volume of sediment transferred to the Northern Atlantic by a Heinrich event ($1.3 * 10^{12}$ m^2; Alley and MacAyeal, 1994) is in keeping with typical erosion values for temperate glacier basins. His conclusion is that fluvial and glacial sediment yield may have been equal before the advent of man. Of course yield is not the only determinant of chemical weathering rate, and the finely comminuted nature of glacial sediments may well predispose them to chemical weathering in sub- and proglacial environments (Kump and Alley, 1996).

Weathering beyond glacier margins: Sediments which are eroded subglacially can be transferred to the proglacial environment by glaciofluvial transport, or by retreat of the ice margin. 28 % of land area in the northern hemisphere lay in the proglacial zone after breakdown of the LGM ice sheets (Gibbs and Kump, 1994). Thus glaciers provided a mechanism of rejuvenating chemical weathering in previously weathering limited areas, by cleaning out thick soils depleted in minerals during glacial advance and leaving behind freshly comminuted minerals upon their retreat (Stallard, 1992; Sigman and Boyle 2000). Therefore weathering rates may increase on centennial to millennial timescales following glacial retreat. Elevated rates of sulphide and carbonate weathering (with respect to those observed in the subglacial environment) have been identified in approximately 200 year old proglacial areas (Anderson et al., 2000, Wadham et al., 2001). Furthermore silicate-weathering rates are also elevated once sediments become vegetated (Anderson et al., 2000; Fig. 9, after Smith et al., 2001). Proglacial sediments can also be distributed by eolian means: loess deposition was widespread during the LGM and glacially derived dust has been recognised as an important source of "fertiliser" for marine and terrestrial ecosystems (e.g. Martin; 1990; Chadwick, 1999; Kump and Alley, 1996 and references therein).

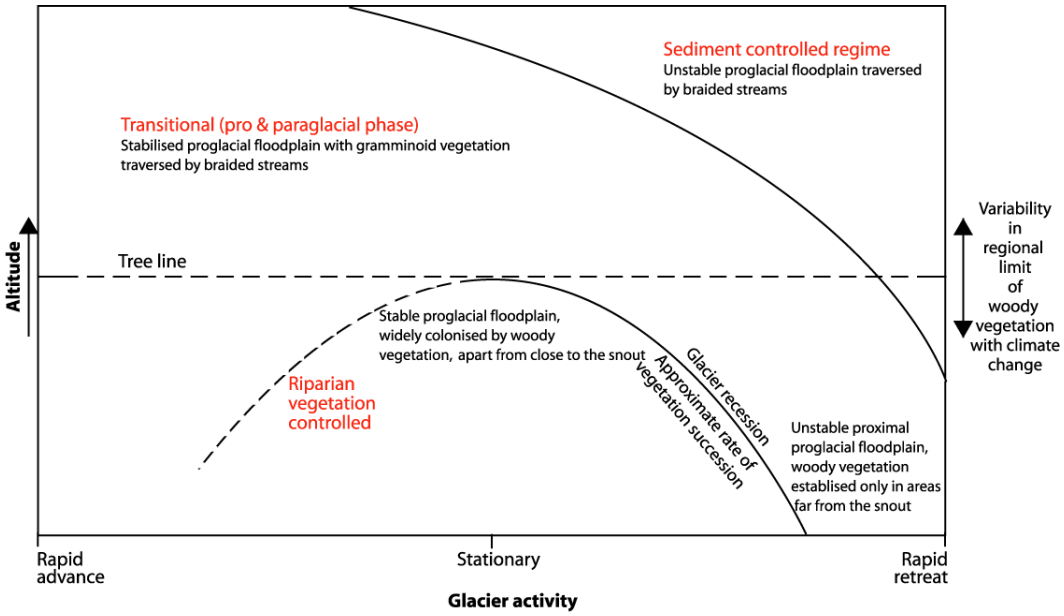


Fig. 9 *The dynamics of the proglacial area over time, after Smith et al., 2001.*

My thesis studies the weathering rates of silicate, carbonate and phosphate-bearing minerals in two glaciated catchments in the crystalline Aar Massif of the Swiss Alps as part of a program to test the plausibility of linkages between continental weathering, productivity and climate (Continent-Ocean Interactions and their Geological Records). It is part of a joint project with Kaspar Arn.

The weathering fluxes of total phosphorus we have calculated from the Rhône and Oberaar catchments rank among the highest in the world (*Chapter 5, table 6*), but 97 % of this phosphorus is in the particulate form of detrital phosphorus, which in our catchments will be principally apatite (*see chapters 4 & 5*). This phosphorus is scarcely bio-available, but the sediments derived from crystalline rocks by the mechanical erosion associated with the Rhône glacier, which are subsequently exposed by glacial retreat and colonised by plants, release soluble P into aquatic ecosystems at rates that are at least as high as the global average riverine dissolved P flux (Rhône Tributary = 0.17 kmol km^{-2} yr^{-1}; global average = 0.13 kmol km^{-2} yr^{-1} Meybeck, 1993). We also detected the accelerated dissolution of detrital P in the Rhône and Oberaar proglacial areas using a chronosequence approach (*Chapters 4 & 5*). The detrital P chemical weathering rates integrated over 145 yr; 270 yr and 11.6 kyr are calculated as 10, 9 and 0.32 kmol km^{-2} yr^{-1}, respectively. We measured an increase in ironbound and organic P forms in the older chronosequences showing that detrital P is being transformed into forms which are also retained within the pedosphere. If these observations hold for proglacial areas in general, upon glacial retreat and exposure of large areas of freshly comminuted detrital P the transfer of P from detrital to soluble reactive, ironbound and organic forms could be significant (see also Filippelli and Souch, 1999).

A second finding of this thesis, which is supported by an accompanying study of Sr fluxes and Sr ratios (*chapter 7*), is that variations in the calcite and sulphide content of the crystalline bedrock and associated hydrothermal veining in the Rhône and Oberaar catchments lead to the dissolution of 5 times as much calcium and a 4-fold increase in the HCO_3^- flux (*chapter 3)* in the Oberaar catchment. This underlines the effectiveness with which traces of carbonates in granitoid rocks are weathered in the subglacial environment. Mean annual CO_2 draw down (as C) for the 1999-2001 study period is calculated as 2317 Kg km^{-2} yr^{-1} in the Oberaar catchment and 774 Kg km^{-2} yr^{-1} in the Rhône catchment. The Oberaar value is comparable with CO_2 drawdown calculated for the Haut Glacier d'Arolla catchment, which has a schistose bedrock geology (2000 Kg km^{-2} yr^{-1}; Sharp et al., 1995), but CO_2 draw down rates in presently glaciated areas are generally lower than the continental average (3000 Kg km^{-2} yr^{-1}; Gaillardet et al., 1999; table 3).

The third topic of the thesis (which is largely the work of Kaspar Arn) is the weathering of biotite in the glacier forefields (*chapter 6*). Present-day suspended sediments are derived from freshly eroded bedrock as secondary weathering products are not observed. But, chemical weathering becomes increasingly important once glacial sediment is deposited in the proglacial area. With increasing age a vegetation cover develops on the morainic deposits and the initial umbrepts undergo podzolisation. XRD data in this chronosequence shows an increase in pedogenically formed vermiculite and a continuous decrease in biotite with increasing sediment age. Biotite contents in the top 30 cm of the soils decrease by 25 – 50 % within 140 – 270 years.

References

Alley H.B. and MacAyeal D.R. (1994) Ice rafted debris associated with binge/purge oscillations of the Laurentide Ice Sheet. *Paleoceanography* **9**: 503-511.

Anderson S.P., Drever J.I. and Humphery N.F. (1997) Chemical weathering in glacial environments. *Geology*, **25**: 399-402.

Anderson S.P., Drever J.I., Frost C.D. and Holden P. (2000) Chemical weathering in the foreland of a retreating glacier. *Geochimica et Cosmochimica Acta* **64**: 1173-1189.

Archer D. and Maier-Reimer E. (1994) Effect of deep-sea sedimentary calcite preservation on atmospheric CO2 concentration. *Nature* **367**: 260-263.

Atkins C.B., Barret P.J., and Hicock S.R. (2002) Cold glaciers erode and deposit: Evidence from Allan Hills, Antarctica. *Geology* **30**: 659-662.

Barnola J.M., Raynaud D., Korotkevich Y.S. and Lorius C. (1987) Vostock ice core provides 160,000 year record of atmospheric CO_2. *Nature* **329**: 408-414.

Bell M. and Laine E.P. (1985) Erosion of the Laurentide region of North America by glacial and glaciofluvial processes. *Quaternary Research* **23**: 154-174.

Berger W.H. (1990) The Younger Dryas cold spell-a quest for causes. *Palaeogeography, Palaeoclimatology, Palaeoecology* **89**: 219-237.

Berner R.A. (1992) Weathering, plants, and the long-term carbon cycle. *Geochimica et Cosmochimica Acta* **56**: 3225-3231.

Berner R.A., Lasaga A.C. and Garrels R.M. (1983) The carbonate-silicate geochemical cycle and its effect on atmospheric carbon dioxide and climate. *American Journal of Science* **283**: 641-683.

Berner R.A. (1994) Geocarb II: A revised model of Atmospheric CO_2 over Phanerozoic time. *American Journal of Science* **294**: 56-91.

Berner E.K. and Berner R.A. (1996) Global Environment: Water, Air and Geochemical Cycles. Prentice-Hall, Inc. New Jersey **pp.** 376.

Blum A.E. and Stillings L.L. (1995) Feldspar Dissolution Kinetics. *In* White A.F. and Brantley S.L. eds., Chemical Weathering Rates of Silicate Minerals: Reviews in Mineralogy **31**: 291-351.

Bluth G.S. and Kump L.R. (1994) Lithological and climatological controls of river chemistry. *Geochimica et Cosmochimica Acta* **58**: 2341-2359.

Boulton G.S. (1979) Processes of glacier erosion on different substrata. *Journal of glaciology* **23**: 15-38.

Broecker W.S. (1982) Ocean geochemistry during glacial time. *Geochimica et Cosmochimica Acta* **46**: 1689-1705.

Broecker W.S. and Peng T.-H. (1982) Tracers in the sea: Lamont-Doherty Geological Observatory, Palisades, N.Y, pp 690.

Broecker W.S. and Peng T.-H. (1989) The cause of the glacial to interglacial atmospheric CO_2 change: A polar alkalinity hypothesis. *Global Biogeochemical Cycles* **3**: 215-239.

Broecker W.S. (2000) Abrupt climate change:causal constraints provided by the paleoclimate record. Earth-Science Reviews **51**: 137-154.

Chadwick O.A., Derry L.A., Vitousek P.M., Huebert B.J., and Hedin L.O., (1999) Changing sources of nutrients during four million years of ecosystem development. *Nature* **397**: 491-497.

Colman A.S. and Holland H.D (2000) The global diagenetic flux of phosphorus from marine sediments to the oceans: Redox sensitivity and the control of atmospheric oxygen levels. *In*: Marine Authigenesis. From Global to Microbial, *SEPM Special Publication* **66**: 21-33.

Compton J., Mallinson D., Glenn C.R., Filippelli G., Föllmi K., Shields G. and Zanin Y. (2000) Variations in the Global Phosphorus Cycle: *In:* Marine Authigenesis. From Global to Microbial, *SEPM Special Publication* **66**: 21-33.

Darmody R.G, Thorn C.E. and Rissing J.M. (1987) Chemical Weathering of Fine Debris from a series of Holocenee Moraines: Storbreen, Jotunheimen, Southern Norway. *Geografiska Annaler* **69**: 405-413.

Drever J.I. and Hurcomb D.R. (1986) Neutralization of atmospheric acidity by chemical weathering in an alpine drainage basin in the North Cascade Mountains. *Geology* **14**: 221-224.

Drever J.I. and Zobrist J. (1992) Chemical weathering of silicate rocks as a function of elevation in the southern Swiss Alps. Geochimica et Cosmochimica Acta **56**: 3290-3216.

Drever J.I. (1994) The effect of land plants on weathering rates of silicate minerals. *Geochimica et Cosmochimica Acta* **58**: 2325-2332.

Drever J.I. and Clow D.W. (1995) Weathering rates in Catchments. *In* White A.F. and Brantley S.L. eds., Chemical Weathering Rates of Silicate Minerals: Reviews in Mineralogy **31**: 463-483.

Egli M., Fitze P., and Mirabella A. (2001) Weathering and evolution of soils formed on granitic, glacial deposits: results from chronosequences of Swiss alpine environments. *Catena* **45**: 19-47.

Falkovski P.G. (1997) Evolution of the nitrogen cycle and its influence on the biological sequestration of CO_2 in the ocean. *Nature* **387**: 272-275.

Filippelli G.M., and Souch C. (1999) Effects of climate and landscape development on the terrestrial phosphorus cycle. *Geology* **27**:171-174.

Föllmi F.B. (1995) 160 m.y. Record of marine sedimentary phosphorus burial: Coupling of climate and continental weathering under greenhouse and icehouse conditions. *Geology* 23: 859-862.

Föllmi K.B. (1996) The phosphorus cycle, phosphogenesis and marine phosphate-rich deposits. *Earth-Science Reviews* **40**:55-124.

Föllmi K.B., Tamburini F., Hosein R., van de Schootbrugge B., Arn K. and Rambeau C. (2003) Phosphorus, a servant faithful to Gaia? Biosphere remediation rather than regulation. *In* Miller, J., Boston, P., and Schneider, S., (Eds.) *Scientists on Gaia*: MIT Press.

Gaillardet J., Dupré B., Louvat P. and Allégre C.J. (1999) Global silicate weatheirng and CO_2 consumption rates deduced from the chemistry of large rivers. *Chemical Geology* **159**: 3-30.

Gibbs M.T. and Kump L.R. (1994) Global chemical erosion during the last glacial maximum and the present: Sensitivity to changes in lithology and hydrology. *Paleoceanography* **9**: 529-543.

Goldich S.S. (1938) A study in rock weathering. *Journal of Geology* **46**: 17-58.

Hallet B., Hunter L. and Bogen J. (1996) Rates of erosion and sediment evacuation by glaciers: A review of field data and their implications. *Global and Planetary Change* **12**: 213-235.

Harbour J. and Warburton J (1993) Relative rates of glacial and nonglacial erosion in Alpine Environments. *Arctic and Alpine Research* **25**: 1-7.

Hay W.W. (1998) Detrital sediment fluxes from continents to oceans. *Chemical Geology* **145**: 287-323.

Hodson A.J. and Ferguson R.I. (1999) Fluvial suspended sediment transport from cold- and warm-based glaciers in Svalbard. *Earth Surface Processes and Landforms* **24**: 957-974.

Hodson A., Tranter M., and Vatne G. (2000) Contemporary rates of chemical denudation and atmospheric CO_2 sequestration in glacier basins: an Arctic perspective. *Earth Surface Processes and Landforms* **25**: 1447-1471.

Imbrie J. and Imbrie K.P. (1979) *Ice Ages: Solving the mystery*. The Macmillan press LTD, London and Basingstoke. **pp** 224

Kump L.R. and Alley R.B. (1994) Global chemical weathering on glacial time scales. *In*: Usselman TM and Hay WW (Eds). *Material Fluxes on the Surface of the Earth*: 46-60. Geophysics Study Committee, National Research Council, National Academy Press, Washington D.C.

Livingstone D.A. (1963) Chemical compositions of rivers and lakes. *U.S. Geological Survey Proffesional Paper* **440-G**: 64 pp.

Martin J.H. (1990) Glacial-interglacial CO_2 change: The iron hypothesis. *Paleoceanography* **5**: 1-13.

Menzies J. (1995) Glaciers and Ice Sheets: 139-196. *In:* Menzies J. (Ed) *Modern Glacial Environments: Processes, Dynamics and Sediments*. Glacial Environments: **1**. Butterworth-Heinemann, Oxford: **pp** 621.

Meybeck (1979) Concentration de eaux fluviales en éléments majeurs et apports en solution aux oceans. *Revue de Géologie Dynamique et Géographie Physique* **21**: 215-246.

Meybeck M. (1987) Global chemical weathering of surficial rocks estimated from river dissolved loads. *American Journal of Sci*ence **287**: 401-428.

Meybeck M. (1993) Natural sources of C, N, P and S: 163-193. *In*: Wollast R., Mackenzie F.T., and Chou L., (Eds.) *Interactions of C, N, P and S Biogeochemical Cycles and Global Change*: NATO ASI Series **I 4**, Springer-Verlarg: Berlin Heidelberg.

Milliman J.D. and Meade R.H. (1983) World-wide delivery of river sediment to the oceans. *The Journal of Geology* **91**: 1-21.

Milliman J.D. and Syvitski J.P.M. (1992) Geomorphic/Techtonic Control of Sediment Discharge to the Ocean: The Importance of Small Mountainous Rivers. *The Jounal of Geology* **100**: 525-544.

Neftel A., Oeschger H., Staffelbach T. and Stauffer B. (1988) CO_2 records in the Byrd ice core 50,000-5,000 years BP. *Nature* **331**: 609-611.

Nienow P., Sharp M. and Willis I. (1996) Temporal switching between englacial and subglacial drainage pathways: Dye tracer evidence from the Haut glacier d'Arrola, Switzerland. *Geografiska Annaler* **78**: 51-59.

Petit J.-R. et al., (1999) Climate and atmospheric history of the past 420,000 years from the Vostok ice core, Antarctica. *Nature* **399**: 429-436.

Powell R.D. (1991) Grounding-line systems as second order controls on the fluctuations of tide water termini of temperate glaciers: 75-93. *In:* Anderson J.B. and Ashley G.M. (Eds) Glacial Marine Sedimentation; Palaeoclimatic Significance. *Geological Society of America Special Paper* **261**:

Raiswell R. (1984) Chemical models of solute aquisition in glacial meltwaters. *Journal of Glaciology* **30**: 49-57.

Raymo M.E., (1991) Geochemical evidence supporting T.C. Chamberlin's theory of glaciation. *Geology* **19**: 344-347.

Röthlisberger H and Lang H, (1987) Glacial hydrology: 207-284. *In.* Gurnell A.M. and Clark M.J. (Eds) *Glaciofluvial Sediment Transfer-an Alpine Perspective*. John Wiley, Chichester.

Sharp M., Tranter M., Brown G.H. and Skidmore M. (1995) Rates of chemical denudation and CO_2 draw down in a glacier-covered alpine catchment. *Geology* **23:** 61-64.

Sigman D.M. and Boyle E.A. (2000) Glacial/interglacial variations in atmospheric carbon dioxide. *Nature* **407**: 859-869.

Skidmore M.L. and Sharp M.J (1999) Drainage system behaviour of a High Arctic polythermal glacier. *Annals of Glaciology* **28**: 209-215.

Smith B.P.G., Hannah D.M., Gurnell A.M. and Petts G.E. (2001) A hydrogeomorphological context for ecological research on alpine glacial rivers *Freshwater Biology* **46**: 1579-1596.

Southam J.R. and Hay W.W. (1981) Global sedimentary mass balance and sea level changes. *The Sea* **7**: 1617-1684.

Stallard R.F. (1992) Tectonic Processes, Continental Freeboard, and the Rate-controlling Step for Continental Denudation. *In*: Butcher S.S. et al., (Eds) Global Biogeochemical Cycles. Academic Press, New York. **pp.** 93-121.

Strakhov N.M. (1967) *Principles of Lithogenesis* Vol. 1, London, Oliver & Boyd, **pp** 245.

Stumm W. and Morgan J.J. (1996) *Aquatic Chemistry*. (Eds Schnoor J.L. & Zehnder A.) John Wiley & Sons **pp** 1022.

Sugden D.E. (1978) Glacial erosion by the Laurentide ice sheet. *Journal of Glaciology* **20**: 367-394.

Summerfield M. (1991) *Global geomorphology:* Harlow, United Kingdom, Longman **pp** 537.

Taylor A. and Blum J.D. (1995) Relation between soil age and silicate weathering rates from the chemical evolution of a glacial chronosequence. *Geology* **23**: 979-982.

Tranter M., Sharp M.J., Lamb H.R., Brown G.H., Hubbard B.P. and Willis I.C. (2002) Geochemical weathering at the bed of Haut Glacier d'Arolla, Switzerland – a new model. *Hydrological Processes* **16**: 959-993.

Tyrell T. (1999) The relative influences of nitrogen and phosphorus on oceanic primary production. *Nature* **400**: 525-531.

Vebel M.A. (1993) Temperature dependence of silicate weathering in nature: How strong a negative feedback on longterm accumulation of atmospheric CO_2 and global greenhouse warming? *Geology* **21**: 1059-1062.

Wadham J.L., Cooper R.J., Tranter M., and Hodgkins R (2001) Enhancement of solute fluxes in the proglacial zone of a polythermal glacier, *Journal of Glaciology* **47**: 378-386.

West J.A., Bickle M.J., Collins R. and Brasington J. (2002) Small-catchment perspective on Himalayan weathering fluxes. *Geology* **30**: 355-358.

White A.F. and Blum A.E. (1995) Effects of climate on chemical weathering in watersheds. *Geochimica Cosmochimica Acta* **59**: 1729-1747.

White A.F., Blum A.E., Bullen T.D., Vivit D.V., Schulz M.S. and Fitzpatrick J. (1999a) The effect of temperature on experimental and natural chemical weathering rates of granitoid rocks. *Geochimica Cosmochimica Acta* **63**: 3277-3291.

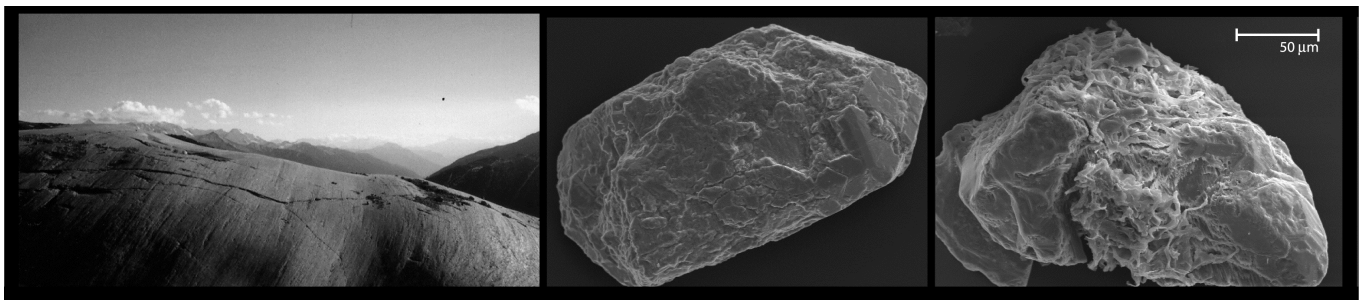
White A.F., Bullen T.D., Vivit, D.V., Schulz M.S. and Clow D.W. (1999b) The role of disseminated calcite in the chemical weathering of granitoid rocks. *Geochimica Cosmochimica Acta* **63**: 1939-1953.

CHAPTER 2

Der Fippeli

Der Fippeli u d Mungge
hocke ir Bschuettiglungge
si chosle u si chaedere
u baden ihri Faedere

Roland Zoss



RATIONALE AND METHODS FOR STUDYING WEATHERING IN THE RHÔNE AND OBERAAR CATCHMENTS, LOCATED IN THE SWISS ALPS

The Rhône and Oberaar Catchments

The Rhône and Oberaar catchments have figured in Swiss glaciology since the late 18th century, when the position of the Rhône glacier snout was mapped in 1777 by Besson (Carlen, 1997). Agassiz's research group reportedly visited the Oberaar glacier in 1840, the year they constructed a field center, the Hôtel Neuchâteloise, at the neighboring Unteraar glacier. Agassiz subsequently acted as a catalyst and publicist for the subject (Schaer, 2000) and in 1874 the Rhône glacier was chosen by the Swiss Glacier Commission and the Swiss Scientific Society as the field locality for their beautiful measurements of glacier mass balance (1874-1915; Mercanton, 1916). In his foreword to the publication Albert Heim, ETH Professor of Geology, wrote:

> "*The glacier is a giant image of the climate which depicts the sum effect of many influences acting together over decades, which in its internal interplay between renewal and melting, brings about a balance between the years and the decades*".

Aptly setting the context for this thesis. Not only do glaciers allow us to measure an integrated response to decadal climate change, but catchment studies of glacierised basins also allow us to quantify chemical and physical weathering rates in glaciated environments. By combining the knowledge gained from the study of different types of glacierised catchments the potential for glacial erosion and weathering to influence climate, by drawing down CO_2, can be assessed. A small catchment should have an easily discernable watershed boundary, denoted by a topographical divide within which all the components effecting the weathering balance occur: atmosphere, bedrock, sediments, vegetation, soils, groundwater and perennial streams (Moldan and Cern, 1994). The way

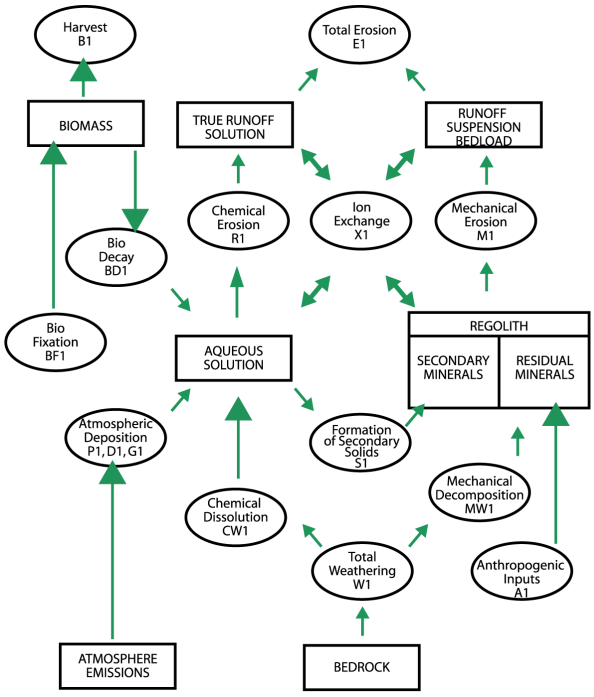


Fig. 1: *A model of weathering and erosion in catchments After Paces, 1986.*

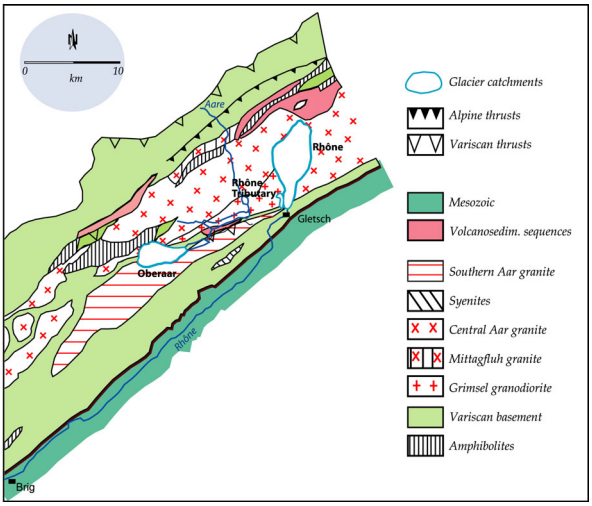


Fig. 2: *Tectonic map of the Aar Massif (modified after Oberhänsli and Schenker, 1988).*

these components interact to generate a solute flux depends on the nature of the catchment (Fig. 1 after Paces, 1986). The Rhône and Oberaar glacier catchments both fit the definition of Moldan and Cern (1994), although vegetation, soils and groundwater are negligible in these watersheds (Amman, 1977; Degueldre, 1994; *chapter 6*). The two catchments have similar bedrock geology, as they are cut into the crystalline Aar massif in central Switzerland (Fig. 2 & *chapter 3*, Table 1). But the presence of a strongly foliated gneissic band in the central third of the Oberaar catchment (Oberhänsli and Schenker, 1988) has a dominant effect on WI (Fig. 1). The increased erodablity and higher calcite content of the zone leads to elevated RI and MI values from this catchment relative to the Rhône (Fig. 1 & *chapter 3*). The difference in the size of the watersheds and their percentage ice cover may also effect the calculation of R1 and M1 (*chapter 3*; Table 1). The thickness of the Rhône glacier was mapped by Wächter (1981), his data indicates the presence of a croissant shaped trough running from north east of the Tieralplistock to the seracs west of the Galenstock (Fig 3). The ice attains its maximum thickness (> 350 m) in this depression. There is also a second narrower bowl located 2.5 km up glacier from the snout which is > 250 m in depth. Equivalent ice thickness data are not available for the Oberaar glacier, but since the Oberaar catchment is approximately half the size of the Rhône catchment, its capacity for sediment storage is likely to be reduced. Otherwise the catchments are located at similar altitudes, have similar mean annual temperatures and receive similar volumes of precipitation (*chapter 3*, Table 1). Direct measurement of the ice mass balance of the two glaciers and their rates of advance was beyond the scope of this thesis, but data for the hydrological years of 1997/1998 and 1999/2000 have been published by the Glaciological commision of the Swiss Academy of Sciences. This corresponds to the year before this study and our first ablation period field season. Unfortunately the Oberaar data pertain to the year 1997/1998, when the glacier receded 32.9 m, whereas the Rhône data are for 1998/1999, it receded 11.2 m in this year. The year 1998/1999 was the 5th warmest year on record since 1860, and in the first half of the year much of Switzerland received the highest levels of precipitation for a century (World Met Organisation, quoted in The Swiss Glaciers 1997/1997 & 1998/1999 report).

In order to quantify WI, the total weathering of bedrock, chemical and mechanical erosion rates must be determined (RI & MI, respectively). Therefore runoff volumes, meltwater compositions and suspended sediment concentrations must be measured

in order to calculate denudation fluxes. Runoff is normally measured by a gauging station, whose positioning defines a catchment's size. The nearest hydrographic gauging station in the Rhône watershed is located at Gletsch (no 2268; Fig 3). It records runoff from the presently glaciated Rhône basin at this point, as well as from the Mutt valley and other minor tributaries that contribute 14 -18 % of the total runoff, according to a 5 year field study by Bernath (1991). This portion of runoff is subtracted from the daily discharges recorded by the gauging station in order to estimate the daily minimum and maximum volumes of meltwater discharged from the presently glaciated Rhône catchment. It was felt that this was a more accurate approach than making our own gauging station up river. The Oberaar catchment does not have a permanent gauging station and average ablation period meltwater discharges were therefore measured using a salt dilution method and daily discharge was estimated by eye, as a function of water speed, channel depth and width, at the meltwater sampling point (Fig. 4). Accumulation period discharges were estimated by eye in both catchments. In 1999 meltwater sampling commenced on the 6/7/99, due to the late clearance of snow from the mountain passes. But discharge started to rise at Gletsch on the 1/5/99 and we interpret this as the start of the ablation period (*chapter 3*, Fig. 2). We estimate that the ablation period ended on the 1/11/99. The discharge dropped below 1 m^3 s^{-1} at Gletsch on this date and continued to fall, with the first snowfall lying on the 7/11/99. In 2000 discharge began to rise on the 20/4/00. Discharge dropped below 1 m^3 s^{-1} on the 8/11/00 and the regression continued from this date until the last of the winter's snow fell on the 25/4/00 and flow picked up (see appendix 1). We

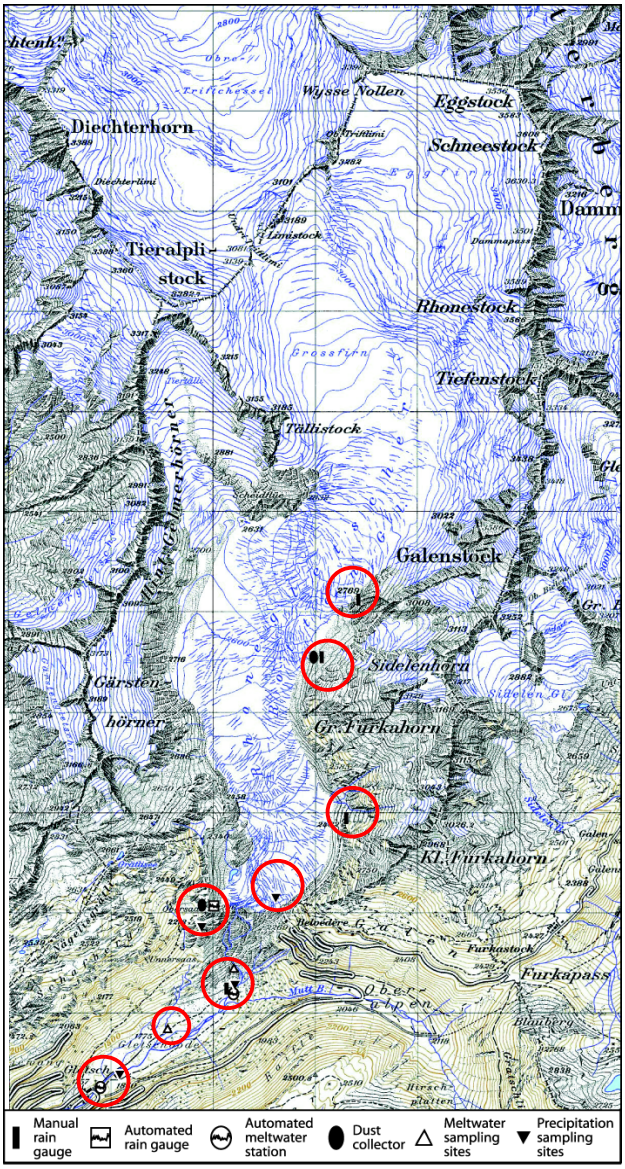


***Fig 3**: Sampling grid to measure the volumes and chemistries of precipitation inputs to and meltwater outputs from the Rhône and Rhône Tributary catchments.*
Reproduced with the permission of the Swiss National Office of Cartography (BA024559).

therefore consider the months May to October inclusively as the ablation period. Rhône meltwaters were sampled above the Mutt stream and the streamlets south of the Belvedere and north of the Mutt (Fig. 3). These streams drain metasediments, therefore their solute concentrations are higher than the Rhône's during the accumulation period when the discharge of the two streams is similar (Mutt, 110 μs cm^{-1}; Rhône, $\approx$ 20 μs cm^{-1}). Oberaar meltwaters were sampled between the glacier snout and the Oberaarsee (Fig. 4). Meltwater samples were collected on a daily basis during the 1999 and 2000 ablation periods.

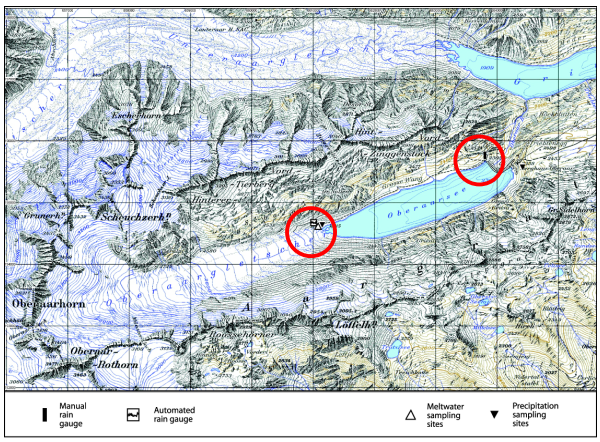


Fig 4: *Sampling grid to measure the volumes and chemistries of precipitation inputs to and meltwater outputs from the Oberaar catchment. Further stations, maintained by Meteosuisse are sited (Table 2).*
Reproduced with the permission of the Swiss National Office of Cartography (BA024559).

Samples were taken at 10:00 and 17:00 hours, when the daily minimum and maximum discharges occur (Gurnell et al., 1994). Several 24-hour sampling campaigns were used to check this (Fig. 5). Throughout the winters of 1999-2000 and 2000-2001 samples were taken on a monthly basis. MI, mechanical erosion was quantified by filtering the meltwaters through 0.45 μm cellulose acetate filters and weighing the sediment retained (see *chapter 3*). We do not consider the bed load component.

Solid and liquid atmospheric depositions (D1, and P1 respectively) were also measured in the catchments. Rain and snow samples were collected in order to determine the chemistry of wet atmospheric deposition, using collecting bottles and pits respectively (see *chapter 3*). The volume of wet deposition was measured in the field areas using a net of cumulative rain gauges that contained paraffin in order to limit evaporation (Otz, 1998; Fig. 3 & 4; Pict. -plates-1). An automatic rain gauge, coupled to a data logger that registered precipitation as pulses per minute over half hour periods, was also installed in each field area during the ablation periods 1999, 2000 and 2001 (Pluviometer 3029, Précis Mechanique; Mitec Satelite-U, data logger; Fig. 3 & 4; Pict. -plates-2). Our data were compared to values from local weather stations and maps where mean annual precipitation data is contoured (Schwab, 2001): There is a good agreement between the Rhône and Hospiz data, and the Oberaar and Hospiz data (Table 1; Fig 6). Annual precipitation volumes were estimated based on a range of sources in order to determine P1 (see *chapter 3*). D1 volumes were measured in the Rhône catchment using two dust collectors based on a system designed by Martin Reis (Personal communication; Fig. 7; Pict. -plates-3).

The Rhône Tributary Catchment

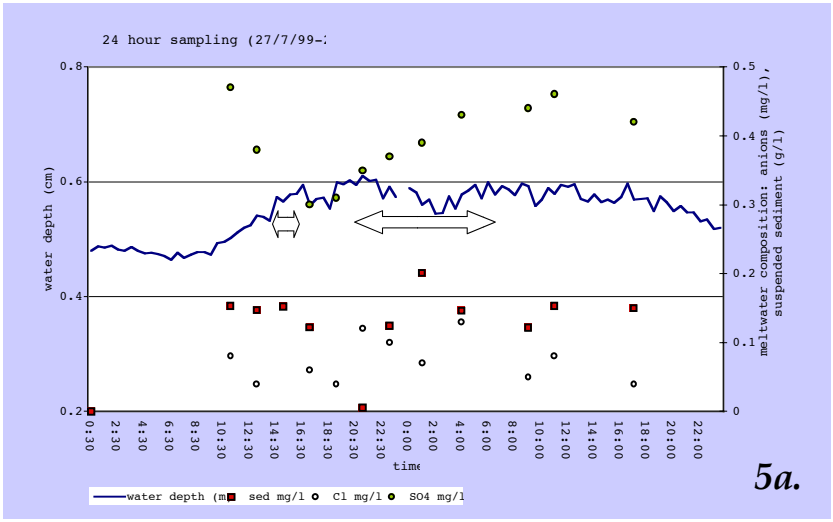
This catchment drains a steep 1.5 km^{-2} parcel immediately to the southwest of the Rhône glacier

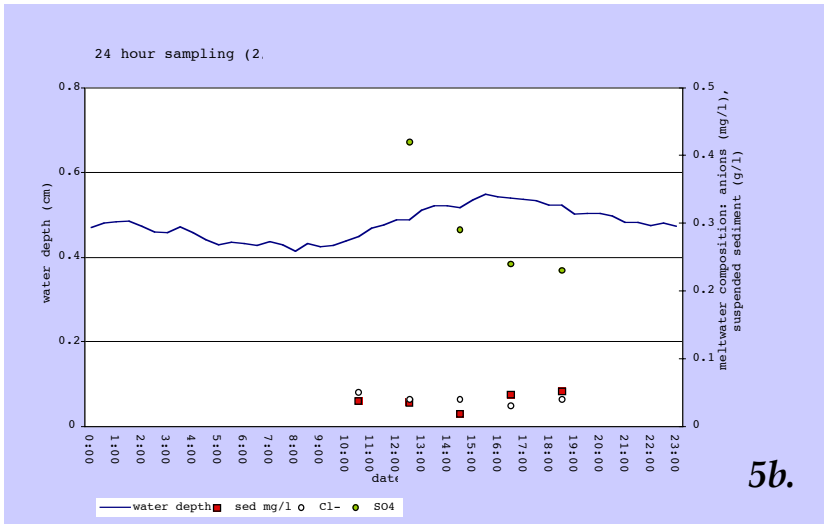
Table 1: Precipitation data from in and around the field areas

Station	Gauge Type	Time		Precipitation	Precipitation Grimsel Hospiz (1980 m)
		Start	Finish	(mm)	mm
Oberaar snout (2320 m)	Automatic gauge	12-Aug-99	30-Sep-99	244	156
		27-Jul-00	21-Sep-00	453	456
		3-Aug-01	1-Oct-01	269	366
	Manual gauge	3-Aug-99	4-Oct-99	264	242
		1-Jan	31-Dec	1800-2000[§]	2089/ 1800-2000[§]
Oberaar above dam (2360)	Manual gauge	3-Aug-99	1-Oct-99	267	186
		1-Oct-99	17-May-00	817	1552
		17-May-00	20-Jun-00	69	105
		21-Jun-00	16-Oct-00	641	647
		16-Oct-00	4-Jul-01	655	1174
		4-Jul-01	1-Oct-01	340	474
		1-Oct-99	*1-Oct-01*	*2522*	*3952*
		1-Jan	31-Dec	1600[§]	–
Oberaar Joch gauge no 5008[†] (3333 m)	Manual gauge	1/1/99	12/1/01	1143	2089
	Manual gauge	1/1/91	12/1/01	2364	2047
		1-Jan	31-Dec	2500-3000[§]	2089/ 1800-2000[§]
Rhone (1790 m)	Manual gauge	4-Aug-99	17-Oct-99	310	243
Rhone (2296 m)	Automatic gauge	12-Aug-99	2-Oct-99	203	162
		18-Jun-00	22-Sep-00	547	483
		10-Jul-01	26-Sep-01	171	470
Rhone (2462 m)	Manual gauge	4-Aug-99	17-Oct-99	210	243
Rhone (2600 m)	Manual gauge	31-Jul-99	17-Oct-99	250	246
Rhone (2796 m)	Manual gauge	31-Jul-99	17-Oct-99	170	246
mean August - November 1999				*266*	*299*
Rhone (1790 m)	Manual gauge	16-May-99	24-Sep-99	440	470
Rhone (2462 m)	Manual gauge	11-Jun-99	fell down		
Rhone (2600 m)	Manual gauge	25-Jun-99	24-Sep-99	350	388
Rhone (2796 m)	Manual gauge	-	-		
mean May-October 2000				*395*	*429*
Rhône average		1-Jan	31-Dec	2000[§]	
Kl. Sidelhorn[†] (no 7015; 2428 m)	Manual gauge	1/1/99	12/1/01	2033/ 1800-2000[§]	
	Manual gauge	1/1/91	12/1/01	1789/ 1800-2000[§]	
Albert Heim Hütte[†] (no 4004; 2530 m)	Manual gauge	1/1/99	12/1/01	2043/ 1600-1800[§]	
	Manual gauge	1/1/91	12/1/01	1821/ 1600-1800[§]	

[†] MeteoSuisse

[§] Schwab et al. (2001)





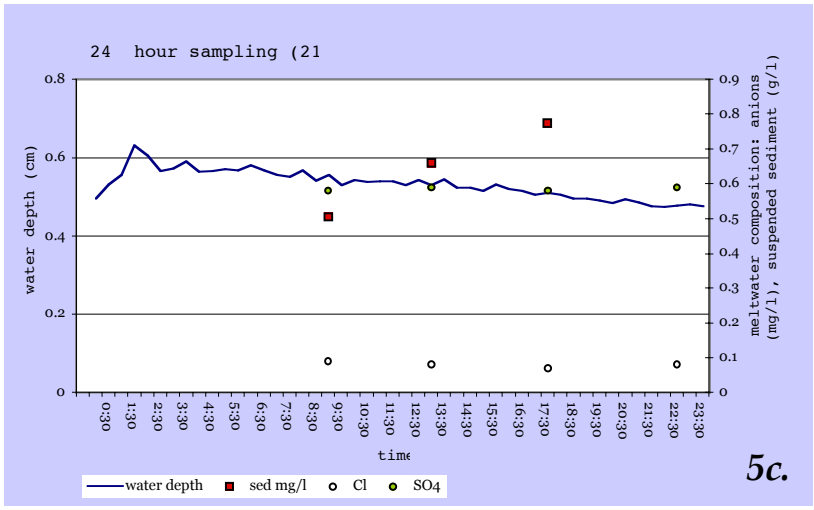


Fig. 5: *24 hour studies of the composition of the Rhône meltwaters.*

5a. *shows an early season flushing event linked to 2 rain storms whose timing is indicated by the arrows.*

5b. *shows the typical diurnal meltwater signature reported by Gurnell et al. (1988).*

5c. *Shows a major flushing event recorded at the end of the ablation period after two months (August and September) when rain storms had not caused suspended sediment to be flushed from the subglacial environment in such quantities. Perhaps the magnitude of this flushing event reflects the fact that the subglacial hydrolic regime had been reordered to favour a distributed system by the end of September (Neinow et al., 1996; Appendix 1 shows that discharges had been declining prior to this date suggesting that the ablation period was waining)*

(Figs. 2 & 3). It was included in the study since it contains an overburden of sediments derived from the crystalline Aar massif (i.e. from the Central Aar Granite and the Grimsel Granodiorite). These sediments were mainly deposited by the retreating Rhône Younger Dryas (YD) ice mass. 3/4 of the Rhône Tributary sediments have not been ice covered since the breakdown of the Younger Dryas ice mass and a thin podzolic pedosphere has subsequently evolved (Egli et al., 2001; this study, *Chapter 6*). This makes the sediments in the catchment 11.6 kyr old (Zumbühl, 1988; Alley et al., 1993; Hormes et al 2001). Therefore there are interactions between the biomass, ions in aqueous solution and the bedrock in this catchment (Fig. 1). The vegetation (alpine meadow) is described by Körner (1999). P1 and D1 are assumed to be the same as in the main Rhône catchment, and R1 is estimated from runoff samples taken monthly during the 2000 ablation period and average discharges measured by Bernath (1991) over a 3 year study period. Comparing R1 from the two catchments, specifically with regard to phosphorus, gives an insight into how the weathering of glacial sediments evolves over an 11.6 kyr time frame (a solute version of a chronosequence; *chapter 5*).

The Rhône and Oberaar forefields.

To assess the long-term weathering rates in these alpine catchments we compared glacial sediments of different ages: In each catchment a chronosequence comprised of recent outwash and suspended sediments, as well as samples taken from profiles dug in Little Ice Age, LIA, moraines and glacial tills dating from the YD was collected (Fig 8; see *chapter 4* for references.). A study of the progressive weathering of apatite grains, changes P forms in the profiles and detrial P weathering rates forms the central third of this thesis (*chapter 4*). This is may not be directly comparable with the R1 results for phosphorus (*chapter 5*), since the Tributary catchment

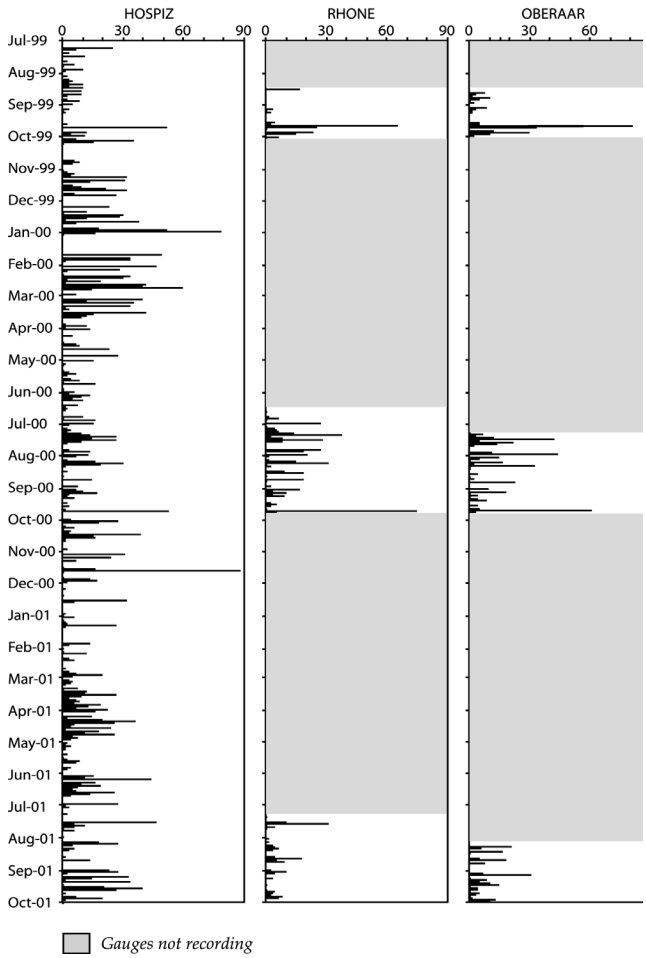


Fig. 6: *Precipitation (mm day^{-1}) measured at the Grimsel Hospiz and in the Rhône, and Oberaar catchments. (Hospitz data from Metosuisse. Rhône and Oberaar data recorded using automatic gauges, see text for a full description).*

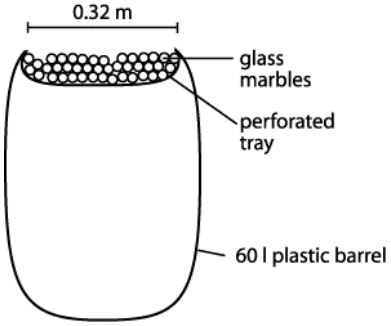


Fig 7: *Dust collector, adapted from Martin Reis, (personal communication)*

** All components were preleached in 10 % ultra pure HNO_3^- and washed 3 times with deionised water before use.*

drains a slope > 25° where the surface runoff component will be large relative to through flow. The profiles used to derive detrital P weathering rates were dug in the valley bottom, where the slope is < 10 ° and therefore the through flow will be greater and more leaching may occur.

Water Analyses

On the Spot Field Analyses

- pH, conductivity and alkalinity were determined in the field on filtered samples (Appendix. 2: Field sampling procedure).
- 500 ml of water was filtered through pre-weighed 0.45 μm cellulose acetate papers to measure suspended sediment concentrations (Slatt, 1972). Weight loss by leaching of the filters is negligible.

The automated station - A continuous assessment of meltwater parameters

A set of probes measuring conductivity (WTW LF-191 - probe LA 1/T) water depth, (Keller PR-46) water temperature and turbidity were installed above the Mutt Tributary, (Fig. 3 & Pict. -plates-1). They were programmed to turn on and record a value ever 5 minutes and a half hourly mean for each parameter was saved on to a multichannel data logger. (`Data Taker DT 500`)

This allowed us to check the quality of our meltwater fluxes, as we could insure that missed major flushing events, where large quantities of sediment and concentrated meltwaters are discharged from the subglacial system, were not missed.

The daily discharge (Q) recorded at Gletsch during the 1999, 2000 and 2001 ablation periods was compared with the daily mean variations in hydraulic head (H), measured using a pressure transducer, in order to assess the hydraulic relationship between the two sites. A logarithmic least squares regression best describes the correlation (Fig. 9a; n = 222 days). H was also measured manually twice a day at the same site using a rule. The correlation between manual and automatic H is good (R^2, 0.94), although the results are unreliable from periods when the air temperature was subzero and, or when the water depth was below 10 cm.

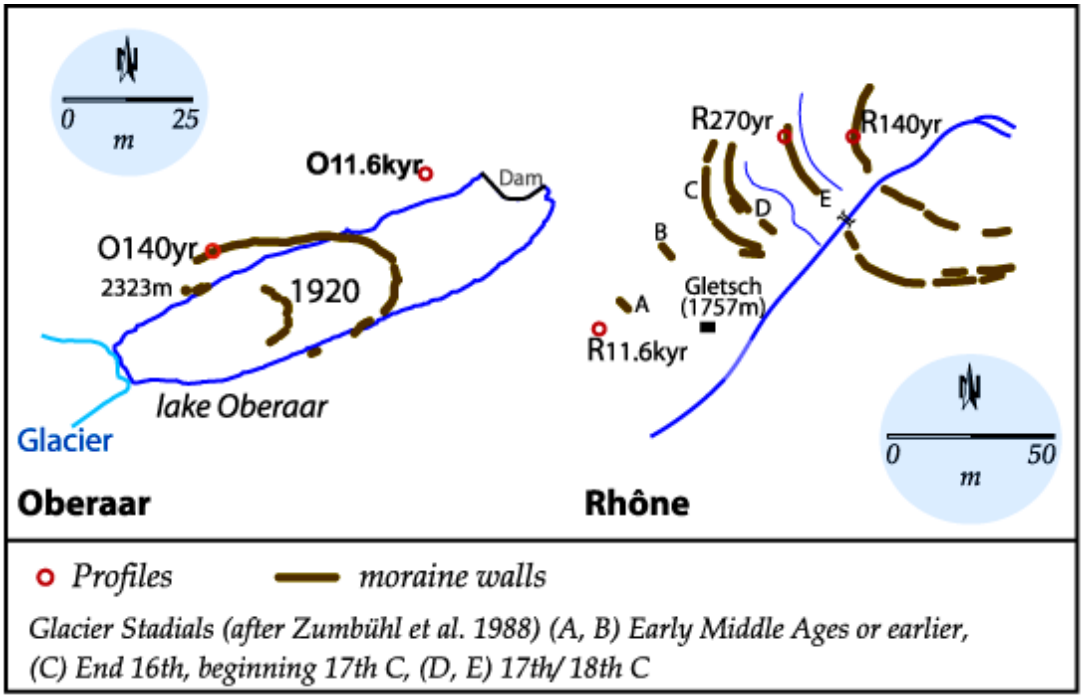


Fig. 8. *Siting of the profiles in the proglacial areas of the Rhône and Oberaar glaciers*

The continuous measurement of conductivity correlates well with manual conductivity readings (R^2, 0.85). Moreover the continuous conductivity record from 2000, together with the corresponding H record indicates that no major flushing events were missed during August and September of 2000, when samples were taken less frequently than in the same months in 1999 (Fig. 9b). Therefore the mean annual fluxes of ions eroded from the presently glaciated Rhône catchment over the 1999-2001 period are representative values. Conductivity is not a good proxy for individual cation concentrations, and the best regressions are obtained between Cl^- and conductivity values and NO_3^- and conductivity values, suggesting that the chemical composition of the Rhône meltwaters is highly sensitive to atmospheric inputs.

The measurement of turbidity is a powerful tool, allowing suspended sediment fluxes to be calculated remotely. Continuous automated measurements can be coupled with spot sampling of suspended sediment concentrations in meltwaters in order to calibrate the probe (Fig. 9c). The mean suspended sediment flux for August and September 2001 is 0.16 g l^{-1}, this compares well with the mean flux that was measured manual for the same months in 1999 and 2000; 0.12 g l^{-1}. Technical problems meant that automatic turbidity data could not be recovered for the 2000 field season, so automatic and manual readings cannot be compared over the same period. Automatic turbidity data can be coupled with measurements of mineral composition to calculate mechanical denudation rates of different minerals. This is particularly useful to estimate erosion and weathering of elements such as phosphorus, which are

confined to the (suspended) particulate load in the glacier covered catchments we studied.

Meltwater Analyses

(GEA lab, Institut de Géologie, Université de Neuchâtel)

Analyses on filtered water samples:

- Major anions (Cl^-, NO^{3-}, SO_4^{2-}) and cations (Ca^{2+}, Mg^{2+}, Na^+, K^+) were each measured on 3-4 ml of solution using a Dionex DX-500 ion chromatograph and IonPak AG/AS-11HC and CG/CS-12 columns respectively. The samples were injected automatically (100 μl anions; 50 μl, cations) and were conveyed through the columns by 20 mM KOH (potassium hydroxide; anions) and 20 mM MSA (metasulfonic acid; cations) at flow rates of 1.5 and 1.0 ml min^{-1} for the anions and cations respectively. Ions were detected by auto suppressed conductivity: The relative error is 5 % for concentrations of < 100 ppb and ≈ 2 % for concentrations > 100 ppb.
- Silicic acid was measured colorimetrically at 695 nm (molybdate blue method, modified from Mullin and Riley, 1955) by FIA (flow injected adsorbtion) using a tecator 5017. The relative error is 5% or better.
- Soluble reactive phosphorus (SRP; PO_4^{3-}) was measured at 880 nm using the molybdenum blue method and a Perkin Elmer UV/VIS Lambda 10 spectrophotometer (Murphy and Riley; 1964; Appendix 3)
- Total dissolved phosphorus (TDP) was oxidised to orthophosphate by microwaving with ammonium peroxodisulphate at 120 °C for 1/2 an hour. The samples were then measured using the molybdenum blue method (Murphy and Riley; 1964; Appendix 4)
- Al, Fe were measured using graphite furnace AAS (atomic adsorption spectrophotometer) and platform tubes. The samples were first

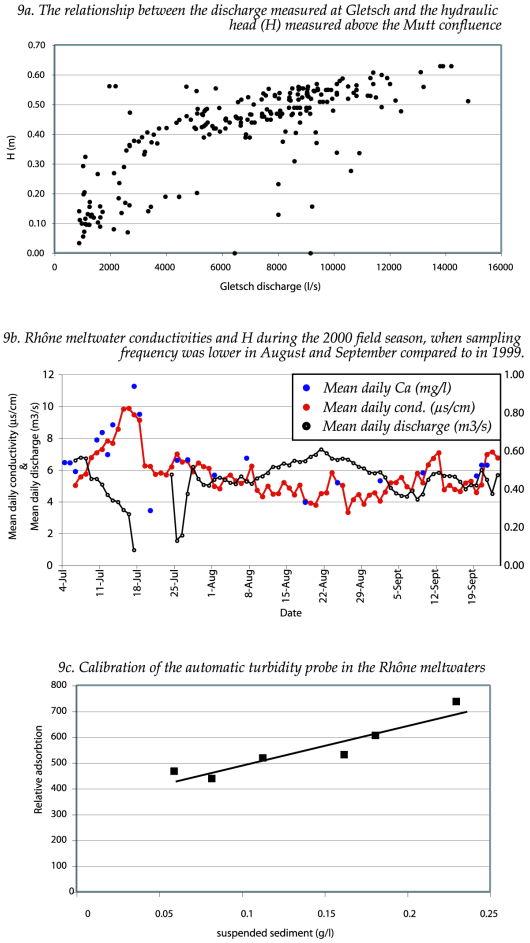


Fig. 9: *Automated measurements made by the water depth, conductivitiy and turbidity probes in the Rhône catchment*

evaporated then calcinated and finally atomised (at 110, 1400 and 2400 °C, Fe and 110, 1700 and 2500 °C Al). Iron is measured at 248 nm and Al at 309 nm.

The relative error for Fe^{3+} was 10 % for concentrations of < 15 ppb and 5 % for concentrations of > 15 ppb. The error for Al^{3+} was 20 % for concentrations of < 15 ppb, 10 % for concentrations of 15–50 ppb, and 3 % for concentrations of > 50 ppb.

- Sr analysis and Sr isotope ratios were measured as part of the thesis of Kaspar Arn and the methods are detailed in his paper (*chapter 7*).

On unfiltered samples

- Total phosphorus (TP) was oxidised to orthophosphate by microwaving with ammonium peroxodisulphate at 120 °C for 1/2 an hour. The samples were then measured using the molybdenum blue method (Murphy and Riley; 1964; Appendix 4)

Sediment Preparations and Analyses

(GEA lab, Institut de Géologie, Université de Neuchâtel, unless stated otherwise)

- The potential for ion exchange X1 in the meltwaters was assessed following Lorrain and Suchez (1972). The filters were washed three times with 10ml 1N ammonium acetate (pH 7), pumping each aliquot through a Nalgene filter unit. The resultant combined leachate was filtered and analysed for Mg^{2+}, Ca^{2+}, Na^{+} and K^{+} using flame atomic absorption (Perkin Elmer 5100 PC). The blanks were 10 times lower than samples in each series, apart from the Rhône Ca^{2+} values and all the Na^{+} values, which were the same as the blanks.
- The granulometry of proglacial sediments was measured by sieving 500 g of sediment through a Retsch VS 1000 sieving column, with the following mesh sizes; 16, 8, 4, 2 and 1 mm; 500, 250, 125 and 63 μm. A sample of the < 63 μm fraction was also retained. Each fraction was dried at 40 °C and reweighed.
- The granulometry of the suspended sediments, dust and the < 63 μm fraction of the proglacial sediments was measured using a Galai CIS 1 Laser Orial granulometer. The relative error is 10 %.
- Proglacial sediments were ground for 3 minutes in an agate mill for further analyses:
- The mineralogy of partially orientated suspended sediments mounted on cellulose acetate filter papers, dust partially orientated on silver filters and pressed proglacial sediments was measured by X-ray diffraction (XRD), using a Scintag XDS 2000. The bulk mineralogies of the suspended sediments were determined by semi-quantitative analysis using external standards (Adatte et al., 1996). The limit of detection for calcite is 0.2 %. Un-orientated powder samples have a relative error of 5 % and we estimate that our partially orientated powder samples have an error of < 10 %.

- The chemistry of suspended and crushed proglacial sediments was determined by XRF, at the University of Fribourg, using a sequential X-ray spectrophotometer (PW-2400), with a relative error of 0.2 - 1 % for major elements.
- The total organic content of 100 mg of the powdered sediments was measured using a Rock Eval 6 with the standard bulk rock pyrolysis method (Espitalié et al., 1986 and Lafargue et al., 1996).
- The pH of sediments was measured with a glass electrode on 1:1 deionized water: soil suspension
- Apatite grains in the 125 –250 μm fraction of samples from the top, middle and bottom of the LIA and YD profiles were concentrated as a function of their density using heavy liquids (grains sink in bromoform; density, 3.13-3.22 g cm^{-3}). They were subsequently separated from most of the other heavy minerals due to their very low magnetic susceptibility when passed through a Frantz Isodynamic Magnetic Separator (residue at 1.7 amps; Flinter, 1959). Their composition was confirmed by energy dispersive X-ray spectroscopy (EDS) and their surface morphologies were imaged by ESEM; Philips XL30 FEG EDS.
- Phosphorus forms were extracted sequentially (SEDEX, Ruttenberg, 1992; detailed method Tamburini, 2001; Appendix 5).and analysed colorimetrically using the molybdenum blue (organic and detrital P; method Perkin Elmer UV/VIS Lambda 10 spectrophotometer) and by mass spectrometer (ironbound; SCPE-laboratory, Neuchâtel; ICP-AES Perkin Elmer Optima 3000).

Acknowledgments:

Oberaar field data: Kaspar Arn, with help from Daniel Arn, Marlen Schaller and others.

Field assistance in the Rhône catchment: Kaspar Arn, Martin Burkhard, Urs Eichenberger, Ray Flynn, Sandra Knispel, David and Katharine Nisbet, Mark Ryle and Philipp Steinmann.

Technical support: François Bourret.

Laboratory analyses: Giulio Galetti (University of Fribourg, XRF). Philipp Steinmann, Khaoula Hamila and Sebastian Ryser (GEA; Major ions; dissolved silica and TOC). Kaspar Arn (Fe* and Al*; granulometry; Soil pH & 50 % of SRP, TDP and TP), Thierry Adatte and Kaspar Arn (XRD), J. Ondrus and S. Pierrehumbert (SCPE-laboratory, Neuchâtel; ICP-AES analysis for ironbound P), Massoud Dadras and Mireille Leboeuf (both Institut de Microtechnologie, Neuchâtel; ESEM). Barbera Seth (formerly of Bern University; help with apatite concentration with heavy liquids and magnetic separation), Bill Higginson, (University of Glasgow; apatite concentration with heavy liquids and magnetic separation). Federica Tamburini (GEA, help with SEDEX analysis).

References

Adatte T., Stinnesbeck W. and Keller G., (1996) Lithostratigraphic and mineralogical correlations of near K/T boundary clastic sediments. in northeastern Mexico: Implications for origins and nature of deposition. *In* Ryder G., Fastovsky D. and Gartner S. (Eds) *The Cretaceous-Tertiary Event and Other Catastrophes in Earth History*: Boulder, Colorado. *Geological Society of America Special* Paper **307**.

Alley R. B., Meese D., Shuman C.A., Gow A.J., Taylor, K.C., Grootes, P.M., White, J.W.C., Ram, M., Waddingtion, E.D., Mayewski P.A., Zielinski, G.A., 1993, Abrupt increase in Greenland snow accumulation at the end of the Younger Dryas event. *Nature* **362**: 527-529.

Amman K. (1977) Der Oberaargletscher im 18., 19. und 20. Jahrhundert. *Zeitschrift für Gletscherkunde und Glazialgeologie* **XII**: 253-291.

Bernath A. (1991) Zum Wasserhaushalt im Einzugsgebiet der Rhône bis Gletsch. (Ed D. Grebner). *Züricher Geographische Schriften* **43**: pp 383.

Carlen M.W. (1997) The Rhône Glacier and its Ice Grotto. *Touristische Betriebe am Rhônegletscher CH-3999 Belvedere, Furkapass-Switzerland*: **pp** 59.

Degueldre C. (1994) Colloid Properties in Groundwaters from Crystalline Formations. *Nagra Technical Report* **92-05**: pp 96.

Egli M., Fitze P., and Mirabella A. (2001) Weathering and evolution of soils formed on granitic, glacial deposits: results from chronosequences of Swiss alpine environments. *Catena* **45**: p. 19-47.

Espitalié J., Deroo G. and Marquis F. (1986) La pyrolyse Rock-Eval et ses applications – III partie. *Rev. Inst. Fr. Pet.* **41**: 73-89.

Flinter B.H. (1959) The magnetic separation of some alluvial minerals in Malaya. *American Mineralogist* **44**: 738-751.

Gurnell A.M., Brown G.H. and Tranter M. (1994) Sampling strategy to describe the temporal hydrochemical characteristics of an alpine proglacial stream. *Hydrological Processes* **8**: 1-25.

Hormes A., Mueller B.U. and Schluechter C., 2001, The Alps with little ice: evidence for eight Holocene phases of reduced glacier extent in the Central Swiss Alps. *The Holocene* **11**: 255-265.

Lafargue E., Espitalié J., Marquis F. and Pillot D. (1996) Rock Eval 6 applications in hydrocarbon exploration, production and in soil contamination studies. *Latin America Congress on Organic Geochemistry, Cancum.*

Lorrain R.D. and Souchez R.A. (1972) Sorption as a factor of in the transport of major cations by meltwaters from an Alpine glacier. *Quaternary Research* **2**: 253-256.

Mercanton P.L. (1916) Vermessungen am Rhônegletscher 1874-1915. *Neue Denkschrift. Schweiz. Naturforschung Ges., Bd* **LII**.

Moldan B. and Cern J. (1994) Small Catchment research. *In Scope **51***

Mullin J.B. and Riley J.P. (1955) The colorimetric determination of silicate with special reference to

sea and natural waters. *Analytica Chimica Acta* **12**: 162-176.

Murphy J. and Riley J.P. (1962) A modified single solution method for the determination of phosphate in natural waters. *Analytica Chimica Acta* **27**: 31-36

Keusen HR., Ganguin J., Schuler P., Buletti M. (1989) *NAGRA technischer Bericht* **87-14**. p

Körner C. (1999) Alpine plant life: Functional plant ecology of high mountain ecosystems: Springer, Germany. **pp** 338.

Oberhänsli R. and F. Schenker. (1988) Indications of Variscan nappe teconics in the Aar Massif. *Scheizerische Mineralogisch Petrographische Mitteilungen* **68**: 509-520.

Otz M.H. (1998) Die hydrologischen Verhältnisse im oberen Valle Santa Maria, Lucomagno, Ticino. [Diplomarbeit]: Bern Universität, Switzerland.

Paces T. (1986) Weathering rates of gneiss and depletion of exchangeable cations in soils under environmental acidification. *Journal Geological Society* **143**: 673-677.

Ruttenberg K.C. (1992) Development of a sequential extraction method for different forms of phosphorus in marine sediments: *Limnology and Oceanography* **37**: p 1460-1482.

Schaer J.P. (2000) Agassiz et les glaciers. Sa conduite de la recherce et ses mérites. *Eclogae geol. Helv*. **93**: 231-256.

Schwab M., Frei C., Schär C. and Daly C. (2001) Mean annual precipitation throughout the European Alps 1971-1990. *In* Landeshydrologie, Bundesamt für Wasser und Geologie. (Ed.) *The Hydrological Atlas of Switzerland*. Bundesamt für Landestopographie, Bern, Switzerland.

Slatt R.M. (1972) Geochemistry of meltwater streams from nine Alaskan glaciers. *Geological Society of America Bulletin*. **83**: 1125-1132.

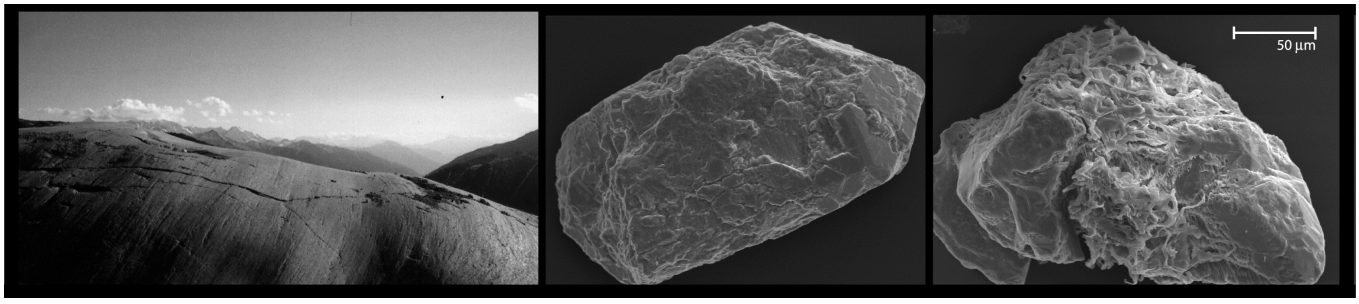
Tamburini F., 2001, *Phosphorus in marine sediments during the last 150,000 years: exploring relationships between continental weathering, productivity, and climate* [Ph.D. thesis]: University of Neuchâtel, Switzerland. **pp**. 219.

The Swiss Glaciers 1997/1998 report No 119/120 (Eds Herren E.R., Hoelzle M. and Maisch M,) Glaciological Commision of the Swiss Academy of Science Zürich, Switzerland. **pp** 46

Wächter H.P. (1981) *Eisdickenmessungen auf dem Rhônegletscher, Ein Versuch mit Radio-Echo-Sounding*. [Diplomarbeit]: Geographisches Insititue ETHZ, Zürich, Switzerland.

Zumbühl H. J. (1988) 129-322. *In:* Zumbühl, H.J., & Holzhauser H. (Eds.) Alpengletscher in Kleinen Eiszeit, Die Alpen. *Zeitschrift der Schweizen Alpen-Clubs*.

CHAPTER 2
appendices



Mean daily discharge from the Rhône catchment 1999-2001 (l/s)*§

Day	7_99	8_99	9_99	10_99	10_99	10_99	1_00	2_00	3_00	4_00	5_00	6_00	7_00	8_00	9_00	10_00	11_00	12_00	1_01	2_01	3_01	4_01
1	7285	8160	6834	4641	201	91	55	37	55	164	626	2864	6588	5704	5576	3383	201	91	55	37	55	164
2	7684	8067	6860	4199	201	91	55	37	55	164	706	4030	7344	6086	4590	2015	201	91	55	37	55	164
3	9605	7659	5993	5075	201	91	55	37	55	164	916	5357	8925	5789	3239	1539	201	91	55	37	55	164
4	9945	7472	4701	4318	201	91	55	37	55	164	1075	7560	9435	5202	2805	1488	201	91	55	37	55	164
5	9945	8288	5024	3307	201	91	55	37	55	164	1155	9102	9010	5117	2635	1522	201	91	55	37	55	164
6	11560	10115	5194	2899	201	91	55	37	55	164	1004	6537	8415	6460	2635	1479	201	91	55	37	55	164
7	8670	11815	5653	2746	201	91	55	37	55	164	865	5882	9095	5440	3060	1284	201	91	55	37	55	164
8	7480	12070	5865	2695	201	91	55	37	55	164	937	5984	8840	5330	2499	1114	201	91	55	37	55	164
9	7166	11135	6367	2703	201	91	55	37	55	164	1109	6673	6154	6052	3409	1046	201	91	55	37	55	164
10	7319	11730	6307	2754	201	91	55	37	55	164	1596	7072	6205	6443	4327	1003	201	91	55	37	55	164
11	7633	9690	6579	2652	201	91	55	37	55	164	2155	8925	5066	6860	5126	978	201	91	55	37	55	164
12	7829	7752	6579	2414	201	91	55	37	55	164	1961	7897	3587	7455	5211	1148	201	91	55	37	55	164
13	8177	6919	6307	2176	201	91	55	37	55	164	1865	8092	3145	7480	4905	3145	201	91	55	37	55	164
14	9095	6571	6316	2006	201	91	55	37	55	164	2129	9180	3120	7897	5041	6783	201	91	55	37	55	164
15	8118	6860	5661	1811	201	91	55	37	55	164	2276	10370	2474	7769	5058	9945	201	91	55	37	55	164
16	7820	7659	4896	1581	201	91	55	37	55	164	2268	8432	2108	8152	4242	5593	201	91	55	37	55	164
17	7693	7242	5321	1411	201	91	55	37	55	164	2264	7013	2091	7897	3485	4080	201	91	55	37	55	164
18	7956	6078	4845	1250	201	91	55	37	55	164	2113	6936	2474	8058	3902	3128	201	91	55	37	55	164
19	7591	6460	4531	1071	201	91	55	37	55	164	2474	7438	2984	8152	3638	2202	201	91	55	37	55	164
20	7837	7463	11220	935	201	91	55	37	55	164	2474	8084	3290	8670	6511	1938	201	91	55	37	55	164
21	8160	7123	9605	1836	201	91	55	37	55	164	1970	8390	3791	9520	4667	1743	201	91	55	37	55	164
22	8245	7285	7463	1165	201	91	55	37	55	164	1558	8050	4429	8755	2950	1607	201	91	55	37	55	164
23	6979	7378	5933	2023	201	91	55	37	55	164	1499	8840	5134	7897	2661	1496	201	91	55	37	55	164
24	6426	8585	5814	1037	201	91	55	37	55	164	1390	7489	7004	7888	2831	1462	201	91	55	37	55	164
25	7055	9605	5806	3120	201	91	55	37	55	164	1445	6248	7200	7650	2924	1386	201	91	55	37	55	164
26	7769	8585	8296	1156	201	91	55	37	55	164	1558	5916	8050	7497	2856	1250	201	91	55	37	55	164
27	8925	9945	7140	816	201	91	55	37	55	164	1583	6044	7302	6834	3128	1233	201	91	55	37	55	164
28	10200	8254	6154	799	201	91	55	37	55	164	1592	6885	7710	6188	2746	1173	201	91	55	37	55	164
29	9095	7795	4913	969	201	91	55	37	55	164	2986	6367	5797	6095	3060	1122	201	91	55		55	164
30	9180	6758	5423	944	201	91	55		55	164	3402	5797	4837	4956	5194	1046	201	91	55		55	164
31	8441	8466		918			55		55		3146		4828	5202		1165		91	55		55	
m	8286	8354	6253	2175	201	91	55	37	55	164	1745	7115	5691	6919	3830	2242	201	91	55	37	55	164

* Daily means are calculated as 85% of the daily discharge measured at Geltsch by the BWG (Bernarth, 1981) for values from May to October.

§ Daily means are taken from a model by the BWG for values from November to April

FIELD SAMPLING PROCEDURE

A. Preparation of 120 ml polypropylene sample bottles.

Soak cation bottles for 12 hours in 10 % HNO_3, then rinse 3 times with de-ionised water.
Soak anion bottles for 12 hours in deionised water and then rinse 3 times with deionised water.
Soak phosphate bottles for 12 hours in deionised water, rinse 3 times with deionised water, add a crystal of iodine and place in an oven for 30 minutes. When bottles are coated with a pink film of iodine rinse three times with deionised water and autoclave at 120° C.

B. Rinse equipment

Rinse 1 l polypropylene bottle 3 times in flowing meltwater, touching all surfaces with water.
Fill bottle to the top leaving as little air as possible.
Put a 0.45 μm cellulose acetate filter on the Nalgene filter equipment
Add 30 ml of sample to the top chamber (measured using a graduated plastic goblet) and rinse the sample around to touch all sides.
Filter to the bottom chamber and repeat rinsing procedure.
Repeat cleaning with a 20 ml and then a 50 ml meltwater sample.

C. Calibrate WTW multiline meter

Calibrate the pH probe once a week, using pH 7 and pH 4 solutions pre-cooled to 4° C.
Calibrate the conductivity probe once every two months using 0.1 M KCl.

D. Measure Alkalinity, Conductivity & pH

Add 400 ml of meltwater to the upper chamber of the filter equipment.
After 150 ml have passed through rinse a 120 ml polypropylene bottle 3 times using 50 ml of filtered meltwater touching all surfaces of the bottle (alkalinity bottle).
Add 80 ml of meltwater to the alkalinity bottle.
Measure the pH and conductivity (in that order).
Add 1 drop of 0.1M HCl acid to sample from the burette.
Insert the pH probe, stir well and measure the pH. Continue, recording the acid volume at approximately pH 4.7, 4.5, 4.2 and 3.7.

E. Meltwater samples

Rinse cation bottle 3 times with 50 ml of filtered meltwater and fill the bottle then add 4 drops of 65 % supra-pure HNO_3 acid using a disposable pipette.
Rinse anion and phosphate bottles with 50 ml of filtered meltwater and fill.

F. Suspended Sediment

Store each sediment laiden filter in a plastic box and dry at 45 °C.

SOLUBLE REACTIVE PHOSPHORUS (SRP)

(modified after Murphy and Riley, 1962)

Reagents, of analytical quality:

A. Sulphuric acid, H_2SO_4; 70 ml of concentrated acid made up to 500 ml in a volumetric flask.

B. Potassium antimony tartrate, $K(SbO)C_4H_4O_6.1/2H_2O$; 1.3715g made up to 500 ml in a volumetric flask.

C. Ammonium molybdate, $(NH_4)_6Mo_7O_24.4H_2O$; 20 g made up to 500 ml in a volumetric flask.

D. Ascorbic acid, $C_6H_8O_6$; 1.76 g made up to 100 ml in a volumetric flask.

Reagents A., B. and C. can be stored in a cool room at 2° C for several months and reagent D. can be stored for up to 1 week.

Glassware: *soak in 10% deconex/ ultrapure water for > 24h, rinse 3 x with ultra pure deionised water, dry at 80° C.*

Standards: *Merck KH_2PO_4 standard solution, 1000 mg l^{-1}, diluted first to 1mg l^{-1} 3µg/l , 10 µg/l, 30 µg/l, 100 µg/l*

Blank: 20 ml ultra pure deionised water

1. Prepare 20 ml filtered samples (0.45 μm cellulose acetate filter papers[1]) and standards in 30 ml graduated plastic goblets.
2. To make the colour developing solution: Mix 50 ml of A, 5 ml of B, 15 ml of C, and 30 ml D in a 100 ml volumetric flask (stable for up to 4 hours).
3. Add 3.2 ml of reactive solution using a disposable pipette.
4. Leave to react for 10-20 minutes.
5. Analyse first standards, then the blank and samples within an hour, using a spectrophotometer at 880 nm wavelength and a 5 cm glass cuvette, pre-rinsed with deionised water and one washing of the sample, three readings of each sample and standard should be made.

[1] Philbert, F.J. (1973) The effect of sample preservation by freezing prior to chemical analysis of Great Lakes waters. Proceedings of the 16th conference of Great Lakes Research 1973, 282-293. International association of Great Lakes Research.

TOTAL PHOSPHORUS (TP; unfiltered samples) AND TOTAL DISSOLVED PHOSPHORUS (TDP; samples filtered through 0.45 µm cellulose acetate filters)

(From the Neuchâtel cantonal laboratory, method 005 0)

Reagents, of analytical quality:

A. Sulphuric acid, H_2SO_4; add 192 ml of concentrated acid to approx. 500 ml of deionised water in a 1000ml flask

B. Potassium antimonyl tartrate, $K(SbO)C_4H_4O_6.{}^1/_2\,H_2O$; dissolve 0.4571 g in approx. 100 ml deionised water.

C. Ammonium molybdate $(NH_4)_6Mo_7O_24.4H_2O$; dissolve 16 g in approx. 200 ml deionised water.

A'. Add B. and C. to the 1000 ml flask containing reagent A. and make up to the mark with deionised water. A' can be kept in a cool room at 2° C for several months.

D. Ascorbic acid, $C_6H_8O_6$; 3.3g made up to 50 ml with deionised water in a volumetric flask.

E. Ammonium peroxodisulphate = 4g : 100ml

Glassware: *soak in 10% deconex/ ultrapur water for > 24h, rinse 3 x with ultra pure deionised water, dry at 80° C.*

Standards: *Merck KH_2PO_4 soln, 1000 mg l^{-1}, diluted 1st to 1mg l^{-1}: 3µg/l, 30 µg/l, 100 µg/l, 500 µg/l, 1000 µg/l*

Blank: 20 ml ultra pure deionised water

1. Prepare 20 ml samples and standards in graduated, 30 ml plastic goblets.
2. Transfer to glass tubes.
3. Add 1.2 ml ofreagent E. to each tube.
4. Close caps on tubes tightly and microwave for 1/2 an hour at 120 °C.
5. Return samples to their plastic goblets and when cool add 1.2 ml of reagent A' and 0.6 ml of reagent D.
6. Leave to react for 10-20 minutes..
7. Analyse first standards, then the blank and samples within an hour, using a spectrophotometer with a wavelength of 650 nm and a 5 cm glass cuvette, pre-rinsed with deionised water and one washing of the sample, three readings of each sample and standard should be made.

SEDEX,
SEQUENTIAL EXTRACTION OF PHOSPHORUS PHASES

Part A. Phosphorus extraction method (Ruttenberg, 1992)

1. Chemicals Formulae

Sodium citrate $C_6H_5Na_3O_7 \cdot 2H_2O$

Sodium bicarbonate $NaHCO_3$

Sodium dithionite $Na_2O_4S_2$

Magnesium chloride $MgCl_2$

Na-acetate $CH_3COONa \cdot 3H_2O$

Magnesium nitrate $Mg(NO_3)_2 \cdot 6H_2O$

Acetic acid $C_2H_4O_2$

Chloridric acid HCl (5N)

2. Extraction Outline

Step I (Reductible Mn & Fe-bound P phase)

Reduction of Fe by dithionite and subsequent complexation by citrate

Step II (Weak acid extractable P, including reactive detrital P)

Acid dissolution at moderately low pH and chelation of Ca by acetate.

Step III (Detrital apatite)

Acid dissolution at pH 1.

Step IV (Organic-bound P)

Dry oxidation of organics and acid dissolution of ashed residue.

3. General points

- After each extraction and wash substep centrifuge samples for 12 minutes at 3000 rpm and pour off the supernatant into the same 30 ml/ 50 ml polypropylene collecting bottle, to obtain one sample per extraction, leaving the sediment in the Falcon tube for the next step.
- Include a reagent blank for each step.
- Measure P concentrations in step I using ICP-AES and is steps II, III and VI using spectrophotometer.

4. Solutions

A. CBD solution (0.5 l)

Mix sodium citrate (32.35 g) and sodium bicarbonate (4.62 g) and add deionised water.

Add the sodium dithionite 11.31 g just before use, (oxidises rapidly).

B. $MgCl_2$ solution (0.5 l)

Add MgCl2 (101.65 g) to 0.5 l deionised water and shake well.

C. Na-acetate solution (0.5 l)

Add Na-acetate (68.04 g) to 0.3 l deionised water, mix well to dissolve solute.

Add 80 ml acetic acid and adjust with the remaining water for 0.5 l of pH 4 final solution.

D. 1 N HCl (1 l)

To obtain 1 l of solution, add 200 ml HCl (5N) to 600 ml of deionized water and make up to 1 l.

E. 50% weight/volume MgNO3 solution

(100 g of solute in 100 ml of deionized water).

5. Procedure

Step I

1) Add 10 ml CBD solution to each 0.1 g sample in a Falcon tube, seal tubes, agitate by hand releasing gas if necessary and shake for 6 hours.
2) Wash the sediment with 10 ml $MgCl_2$ per tube, agitating the samples by hand before shaking for 2 hours.
3) Add 10 ml of deionized water into each tube, agitating the samples by hand before shaking for 2 hours.

Step II

1) Add 10 ml of Na-acetate solution to each 0.1 g sample, shake for 5 hours.
2) Wash with 10 ml of the $MgCl_2$ solution in, agitating the samples by hand before shaking for 2 hours.
3) Repeat $MgCl_2$ wash.
4) Add 10 ml of deionized water into each tube, agitating the samples by hand before shaking for 2 hours.

Step III

1) Add 10 ml of HCl solution to each sample agitating the samples by hand before shaking for 16 hours (overnight).

Step IV

1) Transfer the solid samples from the Falcon tubes to porcelain cups, using deionized water.
2) Evaporate the water overnight in oven at 80°C.
3) Add 1 ml of the $MgNO_3$ solution to each sample and ash at 550°C for 2 hours.
4) Transfer ashed samples back into their respective Falcon tubes same tubes using a plastic spatula and 1N HCl and make up to 10 ml HCl per tube, agitating the samples by hand before shaking for 24 hours.

Part B. Spectrophotometeric analysis of steps II, III & VI (Eaton et al., 1995)

Hardware

Perkin-Elmer UV/Vis spectrophotometer Lambda 10 with computer interface (UV WinLab software package for Windows).

4-cm quartz cuvette.

Chemicals Formulae

Ammonium molybdate $(NH_4)_6Mo_7O_{24}\cdot 4H_2O$

Antimony K tartrate $K(SbO)C_4H_4O_6\cdot 1/2H_2O$

Ascorbic acid $C_6H_3O_6$

Sulphuric acid H_2SO_4 (5N)

Deionized water

Mixing reagent solution (0.75 l)

A. Add 6 g ammonium molybdate to 250 ml deionized water.

B. Make up 5N H_2SO_4 (74 ml H_2SO_4 in 426 ml deionised water).

Add 0.1454 g antimony K tartrate to H_2SO_4

Mix A. and B. (stable for about 2 months).

Colour-developing reagent

C. Add the ascorbic acid to the mixing reagent (0.053 g each 10 ml of solution;

stable for about 1 hour)

Procedure

1) Dilute samples and standards by a factor of 10 (1 ml of solution: 9 ml of deionised water).
2) Add 1 ml of the colour-developing reagent and place samples in the dark.
3) Analyse with the spectrophotometer after 15 minutes.

Detection Limit of Phosphorus (Tamburini, 2001)

Step I	0.03 mg/g
Step II	0.025 mg/g
Step III	0.003 mg/g
Step IV	0.004 mg/g

The 1 sigma error on the sum of steps II and III, weak and strong acid extractable P is < 0.03 mg/g, according to glacial samples remeasured on different extraction runs (n = 5).
The 1 sigma error on step VI is < 0.01 mg/g (n = 4).

References

Eaton, A. D., Clesceri, L. S., Greenberg, A. E. (1995) - Standard methods for the examination of water and wastewater, 19th edition.

Ruttenberg, K. C. (1992) – Development of a sequential extraction method for different forms of phosphorus in marine sediments. Limnol. Oceanogr., 37 (7): 1460 - 1482.

Tamburini, F., (2001) Phosphorus in marine sediments during the last 150,000 years: Explorine relationships between continental weathering, productivity and climate, Ph.D thesis, University of Neuchâtel.





1. *Cumulative rain gauge*
2. *Automatie rain gauge*
3. *Dust collector*
4. *Automatic sample station*





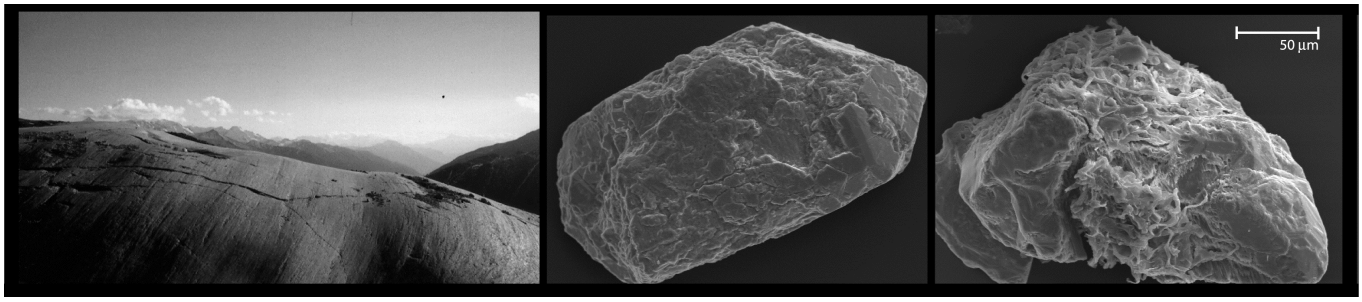
CHAPTER 3

Conversation with a Stone (I)

I knock at the stone's front door
"It's only me, let me come in.
I want to enter your insides
have a look around,
breath my fill of you".

"Go away" says the stone
"I'm shut tight
Even it you break me to pieces
we'll all still be closed
you can grind us to sand,
we still won't let you in".

Wistawa Szymborska, in Nothing Twice



CARBONATE AND SILICATE WEATHERING IN TWO PRESENTLY GLACIATED, CRYSTALLINE CATCHMENTS IN THE SWISS ALPS.

R. Hosein, K. Arn, P. Steinmann, T. Adatte and K.B. Föllmi.

Insititut de Géologie, Université de Neuchâtel, Rue Emile Argand 11, CH-2007, Neuchâtel, Switzerland.

Abstract

We present a weathering mass balance of the presently glaciated Rhône and Oberaar catchments located within the crystalline Aar massif, central Switzerland. The centre of the Oberaar catchment is underlain by a strongly foliated gneissic zone containing up to 9 % calcite, which is more erodable than the granitic and granodioritic bedrock of the Rhône catchment that contains less than 1 % calcite. Annual weathering fluxes are calculated as the weighted mean of monthly accumulation period and twice daily ablation period meltwater samples collected from July, 1999 to May, 2001, and corrected for precipitation inputs. They are dominated by calcium, which represents 81 % and 55 % of the total cation flux in the Oberaar and Rhône catchments respectively (i.e. 555 and 82-96 keq km^{-2} yr^{-1}). An increase of 460 % in the calcite content of Oberaar suspended sediments compared to the Rhône suspended sediments, coupled with the increased erodability and higher sulphide content of the Oberaar bedrock, increases the Ca^{2+} flux by an order of magnitude. This demonstrates the extreme sensitivity of glacial systems to changes in the calcite and sulphide content of crystalline bedrock and suggests that short-term CO_2 sequestration associated with the carbonation driven hydrolysis of carbonate may be locally variable. Silica fluxes from the two catchments are comparable with each other and the cation fluxes derived from silicate weathering in these two presently glaciated catchments are comparable with (Oberaar) and slighltly lower than (Rhône) fluxes from other catchments with crystalline bedrock and similar runoff located at similar latitudes, irrespective of whether they are glacier-covered.

Introduction

Glaciers and periods of glaciation may have a significant impact on global weathering, changing the interplay between physical and chemical weathering processes by putting large volumes of dilute meltwaters and fine-grained sediment in contact with each other. Glaciers are significant agents of physical erosion, for example glaciated valleys in Alaska and Norway have an order of magnitude greater mechanical denudation than equivalent non-glaciated basins (Hallet al., 1996). Hay (1998) suggests that today's global, glacially derived yield of detrital sediments is about half the fluvial detrital yield, but that the two systems' yields were possibly equal before the advent of man. Furthermore the nature of glacially derived sediments may also pre-dispose them to greater rates of chemical weathering compared to sediments derived from fluvial erosion processes. Abrasion and

This chapter has been accepted for publication in Geochimica et Cosmochimica Acta

Table 1: A comparison of the catchments

	Oberaar	Rhone
Geographical position	46° 32' N 8° 14' E	46° 35' N 8° 23' E
Surface of catchment	11.03 km²	26.2 km²
Altitude	2310 - 3631 m a.s.l.	1757 - 3630 m a.s.l.
Glacier cover today (%)	57%	73%
Annual mean temperature *	- 1° C †	+ 1.2° C †
Annual mean precipitation *	2100 mm	2200 mm
Geology of field areas:		
Central Aar Granite	38%	90%
Grimsel Granodiorite	7%	10%
Variscan gneisses	42%	–
Ultramafic Inclusions	1%	–
Southern Aar Granite	12%	–

* Schwab et al. (2001)

† within proglacial area; 2300 m at Oberaar, 1757 m at Rhone

quarrying at the glacier sole generates large volumes of silt-sized grains (Boulton, 1979; Dreimanis & Vagners, 1969, 1971; Drewry, 1986) which are heavily indented and fractured (Mahaney, 1995 and references therein) leading to greater surface areas in comparison to volume, complicated microtopographies and so increased chemical reactivities (White and Brantley, 1995 and references therein). Reaction of this sediment with dilute, close to neutral meltwaters leads to solute fluxes from glacial catchments that are three times Summerfield's (1991) estimated global average denudation rate of 14.8 t km^{-2} yr^{-1} (Sharp et al., 1995), although this may be strongly influenced by the large runoff volumes draining presently glaciated basins. The characteristic chemical signature of glacial meltwaters is strongly linked to the susceptibility of minerals to comminutation and the temperature dependence of mineral dissolution rates (White et al., 1999a). Catchment studies by numerous authors (e.g. Eyles et al., 1982; Drever and Hurcomb, 1986; Sharp et al., 1995; Anderson et al., 1997, 2000) find glacial meltwaters elevated in dissolved Ca^{2+} and K^+ relative to non-glacial runoff, but depressed with respect to silica (e.g. Anderson et al., 1997, 2000; West et al., 2002) due to the temperature dependent nature of silicate weathering (White et al., 1999a). It is widely concluded that the predominant reactions in glacial meltwaters are calcite dissolution and the nonstoichimetric dissolution of K^+ from micas (e.g. Drever and Hurcomb, 1986).

Calcite is highly reactive in dilute glacial meltwaters because its softness (3 on Moh's scale) causes it to be easily milled into ultra-fine particles, (e.g. Fairchild et al., 1999). Also at near neutral pH the dissolution rate of calcite (10^{-5} mol m^{-2} s^{-1}; Plummer et al., 1978) is approximately 11 orders of magnitude faster than the dissolution rate of albite ($\approx 10^{-16}$ mol m^{-2} s^{-1}; Chou and Wollast, 1985). Calcite is not confined to catchments with carbonate or metasedimentary geology, but is also present as an accessory phase in crystalline rocks and as a secondary mineral deposited in hydrothermal veins in areas which have undergone internal deformation (such as the Aar massif in our study). White et al. (1999b) observed that calcite provides up to 98% of the calcium flux from freshly ground granitoid rocks in laboratory leaching experiments. Glacial weathering may optimise carbonate dissolution in catchments with crystalline bedrock, firstly as calcite and quartz are abraded more effectively when ground together, rather than separately (Fairchild et al., 1999) and secondly because crystalline bedrock generally has a lower permeability than carbonate bedrock. This may have implications for weathering on the icesheet scale, whereby ice underlain by crystalline rock may have higher basal water pressures, facilitating increased basal slip and erosion during glacial maxima compared to areas of ice

underlain by carbonate formations (Sugden, 1978). Crystalline rocks form over 20 % of the continental area (granites = 10.4 %, gneisses = 10.4 %; Meybeck, 1987) and predominate over carbonate rocks at latitudes which were ice-covered at the last glacial maximum (Gibbs and Kump, 1994 and references therein). Therefore defining the relative contribution of calcite to weathering fluxes in presently glacier-covered, monolithological crystalline catchments is an important goal in assessing the potential feedbacks between glaciation, weathering of continental rocks and atmospheric CO_2 (e.g. Berner, 1991; Ludwig et al., 1998).

In this study we measure the influence of calcite on meltwater chemistries draining two small, presently glaciated, crystalline catchments in central Switzerland, containing the Rhône and Oberaar glaciers. These geographically and glaciologically comparable watersheds are seated in the Aar massif, comprised of Hercynian aged granites and granodiorites, which contain detactable amounts of calcite (< 1% of which is interstitial calcite; Keusen et al., 1989). The Rhône catchment sits squarely on these two lithologies. The Oberaar watershed, on the other hand, is centred on a strongly foliated gneissic zone, which represents 42% of the catchment area and contains up to 9% calcite (Arn, 2002). We assess weathering intensity by measuring the concentrations of dissolved ions and suspended sediment in the meltwaters. The annual variation in meltwater composition for the catchments is presented, including samples taken during two accumulation periods, when discharge is minimal

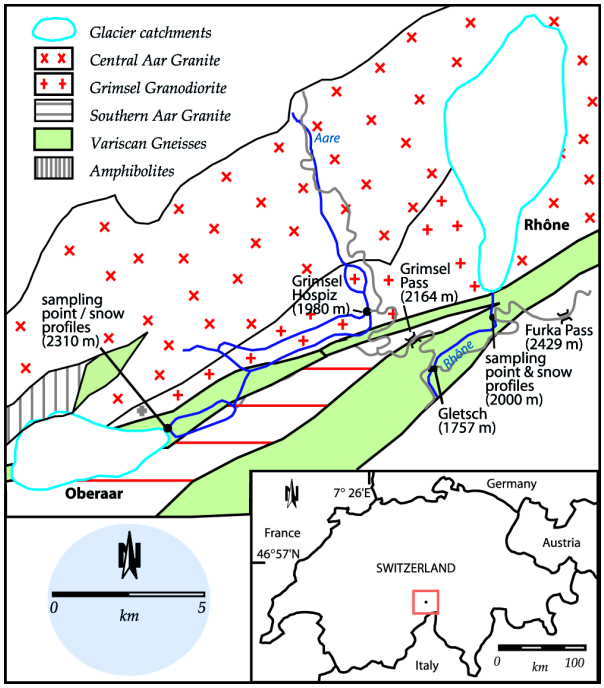


Fig. 1: *The location of the catchments and their geology, from Oberhänsli and Schenker (1988)*

and sediment-water interaction times should therefore be of longer duration. Silica fluxes from the two catchments are comparable with each other and with other catchments with crystalline bedrock and similar runoff, irrespective of whether they are glacier covered. In contrast the total cation flux from the Rhône glacier (147-175 keq km^{-2} yr^{-1}) is significantly below Livingstone's global average (390 keq km^{-2} yr^{-1}; 1963), whereas the Oberaar's total cation flux (681 keq km^{-2} yr^{-1}) is significantly higher (fluxes are corrected for precipitation inputs). Since the specific runoff from the Oberaar basin (2.4 m yr^{-1}) is lower than the runoff from the Rhône basin (3.1 m yr^{-1}) we attribute the elevated cation flux from the Oberaar watershed primarily to the dissolution of approximately 6-7 times more calcium in this catchment (555 keq km^{-2} yr^{-1}, and 82-96 keq km^{-2} yr^{-1} of dissolved calcium are exported from the Oberaar

and Rhône catchments respectively; i.e. 81 % 55 % of the total cation flux). We attribute this difference in calcium flux to the higher sediment yield from the Oberaar catchment (773 t km^{-2} yr^{-1} compared to 388-491 t km^{-2} yr^{-1} from the Rhône) and calcite concentrations which are on average 1.8 %, or 4.6 times higher in the Oberaar meltwaters. This result underlines the extremely reactive nature of calcite in presently glaciated environments.

Methods

Field Areas and Field Methods

This study focuses on the catchments of the Rhône and Oberaar glaciers, in central Switzerland (Fig. 1). The present-day ice cover of Rhône catchment is 73% and the Oberaar catchment is 57 %. The catchments are of comparable size, altitude, and climate (Table 1) and have a simple geometry with one focussed meltwater outlet. The geology of the catchments is similar as they are both situated on the crystalline Aar massif. The bulk mineralogical content of the Central Aar Granite and the Grimsel Granodiorite on which the Rhône glacier sits were documented using optical microscope by Keusen et al. (1989; Table 2). The Oberaar catchments geology is more complex. The central part of the catchment (42% of the catchment area) is strongly foliated and is referred to by Stalder (1964) as the "Gneiss-Schiefer-Zwischenzone". The sides of the catchment are made up of 38 % Central Aar granite, 12 % Southern Aar granite and 8 % Grimsel granodiorite (Oberhänsli & Schenker, 1988; Stalder, 1964; see Fig. 1 for a geological map).

Meltwater samples from the glaciers' outwash streams were collected on a daily basis during the 1999 and 2000 ablation periods. Samples were taken at 10:00 and 17:00 hours, when the daily minimum and maximum discharge occurs (Gurnell et al., 1994). In 1999 sampling commenced on the 6th of July 1999, due to the late clearance of snow from the mountain passes. But discharge started to rise at the hydrographic station at Gletsch (Fig. 1) on the 1st of May 1999 and we interpret this as the start of the ablation period. We estimate that the ablation period ended on the 1st of November 1999. The discharge dropped below 1 m^3 s^{-1} at Gletsch on this date and continued to fall, with the first snowfall lying on the 7th of November 1999. In 2000 the discharge began to rise on the 20th of April 2000. Discharge dropped below 1 m^3 s^{-1} on the 8th of November 2000 and the regression continued from this date. The last of the winter's snow fell on the 25th of April 2000. We therefore consider the months May to October inclusively as the ablation period. Throughout the winters of 1999-2000 and 2000-2001 samples were taken on a monthly basis from October until April. On each sampling 500 ml of meltwater was filtered immediately in the field, as recommended by Slatt (1972) using 0.45μm cellulose nitrate filters and a Nalgene filter unit and hand pump. Conductivity and pH were immediately determined on the filtered samples in the field, using a WTW Multiline P4 meter. In the Rhône catchment alkalinity was measured within 15 minutes of sampling during the 1999 ablation season, measurements were made on filtered meltwaters by titration with 0.1 M, Titrisol

Table 2: Mineralogical composition of the glacial suspended sediments and the bedrock (Central Aar Granite and Grimsel Granodiorite)

	n	Quartz	K-Feldspar (Microcline)	Plagioclase (Albite)	Calcite	Phyllo-silicates[%]	Unquant-ifiable[*]	Epidote	Titantite
Rhône suspended sediment [$]	23	21.8 ± 6.9	17.2 ± 11.1	27.9 ± 16.7	0.5 ± 0.4	14.2 ± 10.8	23.7 ± 27.7		
Oberaar suspended sediment [$]	23	24.3 ± 13.5	6.5 ± 5.7	25.4 ± 11.5	2.3 ± 1.8	13.7 ± 5.5	28.5 ± 17.9		
Central Aar Granite [†]		32.4	33.0	20.9	<1	9.7 [#]		2.9	0.8
Grimsel Granodiorite [†]		28.3	24.4	29.1	<1	16.0 [#]		2.5	1.3

[*] Minerals cannot be quantified due to differences in chemical composition between the samples and the reference standard used, e.g. different Na: Ca ratios in the plagioclase feldspars. Calcite is not contained within the un-quantifiable minerals.

[†] Microscopical quantification after Keusen (1989) converted to weight % using approximate mineral densities. Apatite is reported at < 1 % in both lithologies

[#] Including biotite, chlorite, and white mica

[%] Individual phyllosilicates, e.g. phengite, biotite etc cannot be quantified in the bulk mineralogy nor can amphibole which was identified in some of the Oberaar samples (Adatte et al., 1996). This is due to the fact that differences in the chemical composition of minerals affects their unit cell parameters.

[$] Amphibole did not enter the calculation

HCl. HCO_3^- concentrations were also calculated as the difference between each sample's summed cation and anion concentrations. This calculation is performed on both uncorrected and precipitation corrected meltwater chemistries. In both field areas sample manipulations were performed in tents to limit contamination by dust or precipitation.

Snow samples were taken from 40-80 cm deep sample pits, dug in fresh snow in the proglacial areas of the two catchments during the accumulation periods. Rainwater samples were taken during the ablation periods: A polypropylene bottle was connected to a plastic funnel via a polypropylene tube and the bottle was left for a maximum of 24 hours before the rainwater was filtered and stored. The funnel was protected from dust between samples by covering it with a plastic bag. All filtered samples were bottled in duplicate, kept in the dark at 2°C and analysed within 2 months. Samples intended for anion analysis were stored in polypropylene bottles, pre-leached with ultra-pure deionised water. Samples intended for cation analysis were stored in polypropylene bottles that had been pre-leached with 10 % super-pure HNO_3 and then rinsed 3 times with ultra-pure deionised water. The sediment-laden filters were stored in individual perspex boxes.

The atmospheric dust flux entering the Rhône catchment during the 1999 and 2000 ablation periods was measured using two 0.32 m diameter, 60 l plastic barrels, which had been preleached with 10 % super pure HNO_3 and thoroughly rinsed. The barrels were mounted in open, elevated positions, to avoid collecting saltating grains; a large flat topped erratic boulder approximately half way up the glacier (the up glacier barrel) and a flat grassy step to the right of the glacier snout (the down glacier barrel). Dust was prevented from being blown back out of the barrels by placing a 5 cm deep slatted container holding glass marbles at the mouth of the barrel (the marbles were also cleaned in the same way as the barrel; Marith Reheis U.S. Geological Survey, personal communication). The barrels were left for 48 days in 1999 and 107 days in 2000 and then the

contents were siphoned off and filtered through 0.45 μm filter papers, the barrels were thoroughly rinsed out with several washings of ultra-pure deionised water, which were also filtered.

Laboratory Methods

The major cations and anions Mg^{2+}, Ca^{2+}, K^{+}, Na^{+} and SO_4^{2-}, NO_3^{-}, Cl^{-} were measured using ion chromatography (Dionex DX-500 equipped with C6/CS-12 and AG/AS-11HC columns respectively). The error is 5 % for concentrations of < 100 ppb and ≈ 2 % for concentrations > 100 ppb. Relative Fe and Al were measured using a graphite furnace AAS. The error for Fe^{3+} was 10 % for concentrations of < 15 ppb and 5 % for concentrations of > 15 ppb. The error for Al^{3+} was 20 % for concentrations of < 15 ppb, 10 % for concentrations of 15–50 ppb, and 3 % for concentrations of > 50 ppb. Adsorbed cation concentrations were measured following Lorrain and Suchez (1972). The filters were washed three times with 10ml 1N ammonium acetate (pH 7), pumping each aliquot through a Nalgene filter unit. The resultant combined leachate was filtered and analysed for Mg^{2+}, Ca^{2+}, Na^{+} and K^{+} using flame atomic absorption (Perkin Elmer 5100 PC). The blanks were 10 times lower than samples in each series, apart from the Rhône Ca^{2+} values and all the Na^{+} values, which were the same as the blanks. Dissolved silicon was measured colorimetrically (molybdate blue) by FIA (tecator 5017) (modified from Mullin and Riley, 1955) The relative error for these two methods is 5% or better.

Filters were dried at 40° C, weighed and corrected for the original filter weight to calculate the mass of suspended sediment. The mineral content of the suspended sediment was determined by X-ray diffraction (XRD), while the sediment was still on the filter papers (partial orientation), using a Scintag XDS 2000. The dust samples were passed under the X-ray on silver coated stubs. The bulk mineralogy of the suspended sediments was determined by semi-quantitative analysis using external standards (Adatte et al., 1996). The limit of detection for calcite is 0.2 %. Un-orientated powder samples have an error of 5 % and we estimate that our partially orientated powder samples have an error of < 10 %. The granulometry of the suspended sediment and dust samples was determined using a Laser Oriel granulometer. The chemistry of the suspended sediment was determined by XRF, at the University of Fribourg, using a sequential X-ray spectrophotometer (PW-2400), with a relative error of 0.2-1 % for major elements.

Precipitation Input Corrections

We calculate the input flux for wet precipitation in two ways: Firstly by correcting each meltwater sample for precipitation inputs in proportion to its chloride concentration and secondly based on the estimated volumes of rain and snow falling in the catchments.

In the first approach the concentration of ions in each meltwater sample, X_m are corrected, to give the weathering derived concentrations in the meltwaters, X_m^*. The relative input of ions by wet precipitation is calculated by multiplying the chloride concentration

in the meltwaters Cl_m by a factor, where X_p is the mean concentration of each ion in precipitation and Cl_p is the mean chloride concentration of the precipitation:

$$X_m^* = X_m - Cl_m \cdot X_p/Cl_p$$

Between August 1999 and September 2001, 17 rain and 5 snow samples were collected and used to determine the mean rain and snow concentrations (Table 3). These means are weighted according to the relative proportions of rain and snowfall (in water equivalents) recorded at the Grimsel Hospiz during the study period (60 % snow: 40 % rain; MeteoSuisse; station 5010), yielding a mean annual precipitation composition (Table 3). The Hospiz is located at 1980 m, on the northerly side of the Grimsel Pass, approximately 4 km from the Rhône and 8 km from the Oberaar glacier snouts (Fig. 1.) and provides a daily record of precipitation volumes. Regarding the second, volumetric approach mean annual precipitation data at the Hospiz for 1997, 1999 and 2000 average 2040 mm per year, slightly higher than the average precipitation rate from 1988-2000:1990 mm. Precipitation was assumed to fall as snow from November to April yielding an average snow / total precipitation ratio of 0.68 for September 1999-2000 and 0.53 for September 2000-2001. In the Rhône catchment Bernath (1991) recorded annual inputs ranging between 2108-2845 mm for the period 1979-1983, based on a detailed net of climatological stations. Estimates based on a 20-year local climate record (1971-1990) give an average of 2050 mm of precipitation (Schwab et al., 2001). Because a slightly higher than average precipitation volume is recorded at the Hospiz during our study period we estimate an annual precipitation input of 2200 mm in the Rhône catchment with 60 % of this volume falling as snow. In the Oberaar catchment an annual mean precipitation of 2020 mm has been observed (Schwab et al., 2001). Again, to reflect the elevated precipitation volume recorded at the Hospiz, we use a slightly higher value: 2100 mm, with snowfall representing 60 % of this volume. These rain and snow volumes are multiplied by the mean rain and snow composition to calculate the wet precipitation input to each catchment, which is subtracted from the meltwater fluxes to obtain a denudation rate.

Table 3: Precipitation compositions in µeq l^{-1}.

Sample	Date(s)	Na^+	K^+	Mg^{2+}	Ca^{2+}	Fe^{3+}	Al^{3+}	Cl^-	SO_4^{2-}	NO_3^-	NH_4	Si
Rain												
Rh	28-Aug-99	8.70	7.16	5.76	43.91	n.a.	n.a.	5.64	54.76	15.64	n.a.	n.a
Rh	7-Sep-99	10.87	6.14	4.11	33.43	1.51	1.68	3.67	33.31	28.22	n.a.	6.6
Rh	22-Sep-99	4.78	2.05	1.65	2.50	1.99	2.36	1.41	5.41	5.32	n.a.	n.a
Rh	31-May-00	2.15	1.52	0.00	5.17	0.09	1.01	1.69	7.29	9.84	n.a.	0.5
Rh	7-Jun-00	4.03	6.16	1.31	23.29	0.05	0.61	4.23	28.11	32.42	n.a.	8.2
Rh	28-Jun-00	5.96	5.19	4.62	21.41			4.23	24.36	23.39		
Ob	11-Jul-00	16.96	3.58	10.70	134.23	0.12	0.38	3.10	12.91	10.97	n.a.	52.7
Ob	13-Jul-00	2.75	1.28	0.00	8.37	0.56	0.79	2.26	50.59	5.00	n.a.	64.0
Rh	15-Jul-01	n.a.	2.30	2.47	10.98	0.14	0.86	4.22	29.72	17.61	n.a.	n.a
Rh	27-Jul-00	3.57	1.84	1.56	5.25	0.62	0.87	3.10	20.40	16.93	n.a.	n.a
Rh	1-Aug-00	3.09	2.27	0.59	3.10	0.60	0.61	5.36	16.24	13.22	n.a.	1.8
Rh	7-Aug-00	2.47	1.51	1.37	16.76			1.68	19.57	17.10		
Rh	3-Aug-01	2.61	3.07	1.65	7.49	0.33	n.a.	1.94	12.59	6.44	n.a.	n.a
Ob	3-Aug-01	3.04	4.35	2.47	17.47	0.18	n.a.	3.80	38.18	21.58	n.a.	n.a
Ob	8-Aug-01	2.61	7.67	1.65	11.48	0.05	0.77	3.74	15.84	14.18	n.a.	n.a
Rh	17-Aug-01	4.35	9.21	4.11	25.95	0.14	1.11	6.21	19.52	18.01	n.a.	n.a
Rh	30-Aug-01	6.09	8.18	6.58	53.39	n.a.	0.88	8.46	17.08	19.97	n.a.	n.a
Snow (sample depth)												
Rh (0-85 cm)	18-Jan-01	6.52	2.30	0.82	2.00	0.28	1.05	n.a.	n.a.	n.a.	n.a.	2.8
Ob (0-5 cm)	18-Jan-01	5.22	8.16	0.38	4.00	0.30	1.27	9.87	2.58	3.85	n.a.	0.4
Ob (0-40 cm)	6-Mar-01	2.75	2.57	0.47	16.96	n.a.	n.a.	5.36	2.07	3.60	n.a.	n.a
Ob (0-5cm)	6-Mar-01	2.45	1.88	0.29	14.31	b.d.	0.80	2.81	2.30	2.94	n.a.	n.a
Rh (0-5 cm)	7-Mar-01	0.29	0.99	0.00	1.42	n.a.	n.a.	n.a.	n.a.	n.a.	n.a.	
Mean Rain	1999-2001	4.47	4.37	2.49	18.12	0.52	1.05	3.85	24.56	16.55		11.6
Mean Snow	1999-2001	3.45	3.18	0.39	7.74	0.19	1.04	5.14	2.54	4.87		0.8
Average (ratio40:60)		**3.86**	**3.65**	**1.23**	**11.89**	**0.33**	**1.04**	**4.63**	**11.35**	**9.54**		**5.1**
Other swiss sites												
Alptal (annual mean) †		5.65	1.28	1.65	12.48	0.59	0.56	4.51	6.25	4.19	0.01	7.1
Haut Glacier d'Arolla #	1993-1995	0.40	1.10	0.70	3.80			3.80	3.30	5.80		<0.

n.a.: not analysed

b.d.: below detection

* Rain collected during Saharan red dust event and not included in the mean

† non glaciated; average annual precipitation 2300 mm

mean snowpack winters 93-95, Tranter et al. (2002)

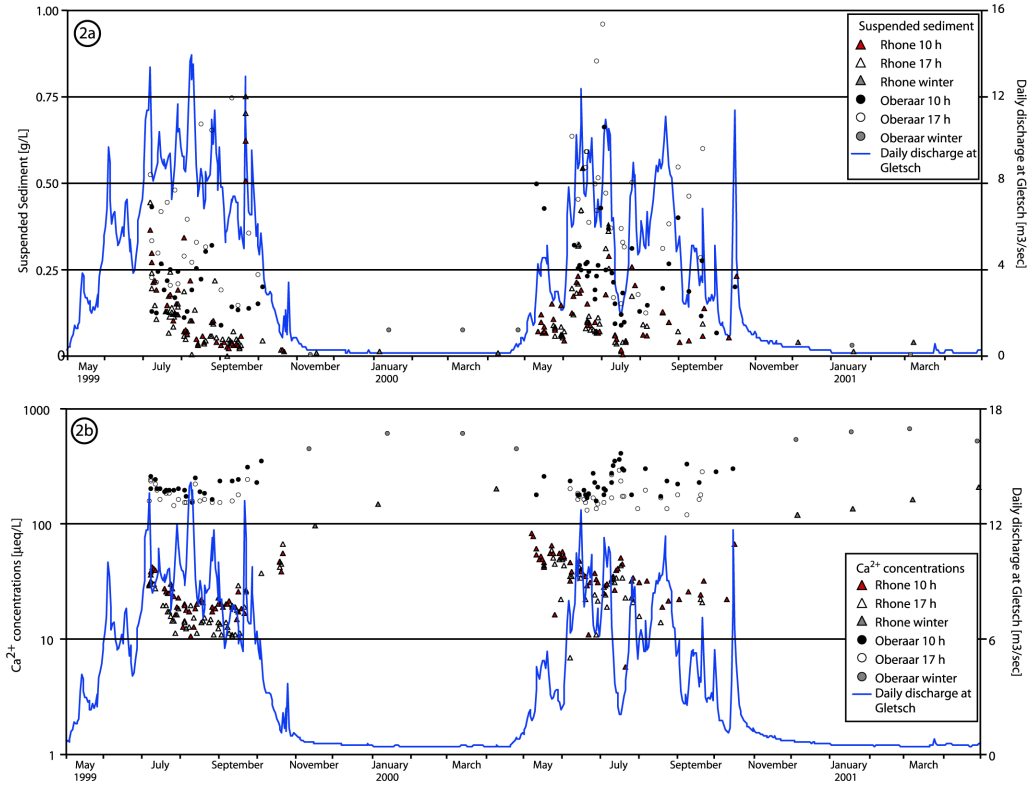


Fig. 2: Ca^{2+} and suspended sediment concentrations.

All ion corrections are subject to some error, firstly because we use mean rain and snow composition, whereas ion concentrations vary significantly during individual rain events (Table 3) and secondly because ions are eluted at different rates from the snow pack, leading to a non-linear relationship between Cl^- and other ions at the start of the ablation season. Both correction methods fail to remove approximately half the NO_3^- flux (Table 4), but correction for NO_3^- may be especially difficult, for example because NO_3^- maybe influenced by subglacial microbial activity (Sharp et al., 1999) and NH_4^+ in rain. The volumetric correction overestimates the total precipitation volume, as negative Cl^- fluxes are calculated (Table 4). We therefore use precipitation ratio values in the discussion section of this paper, and point out that this approach is certainly more robust than using sea salt ratios for catchments located in the continental interior (Table 5).

Flux Calculations

Rhône daily discharges for the 1999 and 2000 ablation periods were recalculated from Swiss National Hydrological Survey data (Federal Office for Water and Geology) from the Gletsch gauging station (no. 2268) . The gauging station is 2.75 km downstream from the glacier snout and receives water from a 38.9 km^2 catchment. Bernath (1991) made a detailed 5-year hydrological study of the Gletsch catchment and calculated that between 14 % and 18% of the discharge measured at Gletsch comes from outside the Rhône glacier catchment. W e

calculate all our ablation period daily fluxes based on the Gletsch daily discharge measurements corrected by 14% and 18% and mean daily meltwater concentrations in order to show the discharge related error on our values. Accumulation period discharges are based on visual estimates and agree well with those proposed by Bernath (1991).

Oberaar discharges were estimated visually to the nearest 0.5 m^3 s^{-1} each time a meltwater sample was taken, based on estimated water velocity and channel geometry. The meltwater channel was relatively stable and the accuracy of these estimates was compared to the discharge calculated using the salt dilution method (Federal Office for Water and Geology, 1994). Discharge estimates of 1.5 m^3 s^{-1} were calculated as 1.64, 1.58 and 1.41 m^3 s^{-1} on three separate occasions using salt dilution. The calculated mean monthly discharges for the Oberaar stream, based on these regular estimates agrees well with the mean monthly discharge estimates produced using a model designed by the Swiss National Hydrological Survey, Federal Office for Water and Geology. Fluxes are calculated for each sample as the product of the ion or suspended sediment concentration and the discharge volume. The mean of the 10:00 and the 17:00 hour fluxes are taken to represent the daily flux, and in both catchments the daily fluxes are used to calculate monthly fluxes which are summed to give yearly fluxes. Fluxes are normalised by catchment area allowing comparison between catchments. Linear regressions between discharges measured at Gletsch at 10:00 and 17:00 and corresponding ion concentrations (Sharp et al., 1995) show no significant correlation, therefore we do not calculate hourly fluxes based on regression models.

Table 5: Seawater and precipitation compositions normalised by chloride.

	Precipitation		Sea salt
Ion	**µeq l^{-1}**	**Ion / Cl^-**	**Ion / Cl^-**
Cl^-	4.63	1	1
Na^+	3.86	0.83	0.56
Mg^{2+}	1.23	0.27	0.07
Ca^{2+}	11.89	2.57	0.02
K^+	3.65	0.79	0.02
SO_4^{2-}	11.35	2.45	0.14
NO_3^-	9.54	2.06	-
Fe^{3+}	0.33	0.07	-
Al^{3+}	1.04	0.23	-
Si	5.15	1.11	-

To calculate adsorbed cation fluxes the adsorbed cation concentrations from 10:00 and 17:00 hour samples for each day were averaged to calculate a daily mean adsorbed concentrations (mg g^{-1}). Weighted monthly concentrations were averaged to calculate a mean annual adsorbed cation concentration (mg g^{-1}) which was multiplied by the annual sediment flux to obtain annual adsorbed cation fluxes.

Results

Atmospheric Dust Flux

In 1999 the up glacier barrel recorded a daily dust input of 0.0011 g day^{-1}, unfortunately the second barrel was lost. In 2000 the up glacier barrel recorded a daily dust input of 0.0013 g day^{-1} and the down

glacier barrel recorded 0.0015 g day^{-1}. This implies that the dust falling over the glacier is evenly spread and the mean dust input is of the order of 5900 kg km^{-2} yr^{-1} or 1 % of the suspended sediment flux (see below). The dust samples contain quartz, mica, chlorite, potassium and plagioclase feldspars, goethite, calcite, smectite and kaolinite. In 1999 5 filters were the same grey colour as the suspended sediment samples, but one filter was covered in red dust. Red coloured dust was also collected during a rain event in 2000. The red colour of some of the dust and the presence of kaolinite suggest that a component of the dust is not local, it maybe of Saharan provenance (Lenaz et al., 1986; Kübler et al., 1990), although dolomite, another mineral typical of peridesertic environments is not observed in our samples, it may have dissolved in the barrels before the sediment was filtered.

Suspended Sediment

The annual variation in the 10:00 and 17:00 hour suspended sediment concentrations in the meltwaters of the two catchments and the daily mean discharge recorded at Gletsch are plotted (Fig. 2a). Suspended sediment concentrations in the Oberaar meltwaters are consistently higher than the Rhône meltwaters. The Rhône ablation period concentration is 0.11 g l^{-1} (± 0.05; n=196) and the Oberaar mean concentration is 0.33 g l^{-1} (± 0.10; n=107). The average winter suspended sediment concentrations are lower, 0.03 g l^{-1} (± 0.02; n=6) for the Rhône and 0.04 g l^{-1} (± 0.03; n=6) for the Oberaar meltwaters. The figure also shows that high discharges, associated with the rapid melting of snow and heavy rain events provoke the evacuation of large volumes of sediment. In both catchments rain events coinciding with the snow melt period mobilise large volumes of sediment, for example 3% of the annual sediment yield was discharged from each catchment during the rainstorm on the 6th of July 1999. The highest Rhône suspended sediment concentrations were associated with a two day rain event on the 20th and 21st of September 1999. The event was of a magnitude that only occurs once ever 2.3 years according to the MeteoSuisse and the sediment exported on these two days represented 9 % of the annual suspended sediment flux. This event was not recorded in the Oberaar catchment. The main flushing events in both catchments occur at times in the ablation period when a distributed drainage system is thought to be in place which creates more contact between subglacial sediment and meltwaters than channelised systems (e.g Nienow et al., 1996).

Table 4: Annual dissolved fluxes from the catchments (keq km^{-2} $year^{-1}$) and suspended sediment fluxes (kg km^{-2} $year^{-1}$).

	Ca^{2+}	K^{+}	Na^{+}	Mg^{2+}	Fe^{3+}	Al^{3+}	Cl^{-}	SO_4^{2-}	NO_3^{-}	HCO_3^{-}	Si	Suspended Sediment
Uncorrected fluxes												
Rhone	96.4-116.2	29-35.4	28.3-34.1	14.9-18.1	5.4-6.5	11.0-13.3	6.6-8.2	49.9-60.0	34.2-42.5	99.9-120.6	152.3-183.2	388274-490771
Oberaar	589.5	59.7	32.4	37.0	4.8	10.4	5.9	226.8	23.8	467.2	182.2	773076
Corrected by precipitation volume												
Rhone	70.2-90.0	21.0-27.4	19.8-25.6	12.2-15.4	4.7-5.8	8.7-11.0	-2, - -3.6	24.9-35.0	13.2-21.5		141.0-171.9	
Oberaar	564.5	52.0	24.3	34.4	4.1	8.2	-3.8	203.0	3.7		171.4	
Corrected by precipitation ratios												
Rhone	81.5-96.4	24.5-29.3	23.1-27.3	13.6-16.4	2.2-2.7	2.1-2.6	0	33.7-39.3	20.5-24.7	93.2-109.7	145.3-173.2	
Oberaar	554.6	53.3	26.1	33.9	4.4	8.9	0	204.5	11.8	467.6	176.4	

Table 6: Daily mean concentrations in µeq l $^{-1}$; conductivities in µS cm $^{-1}$; modelled and measured discharges in l s $^{-1}$.

	n	Na^+	±	K^+	±	Mg^{2+}	±	Ca^{2+}	±	Fe^{3+}	±	Al^{3+}	±	Cl^-	±	SO_4^{2-}	±	NO_3^-	±	$^{\dagger}HCO_3^-$	±	Si	±	Cond.	±	D
Rhone																										
January	1-2	47.4	4.4	33.2	0.8	19.9	1.3	142.2	7.8	2.9	–	5.9	–	5.2	1.7	89.8	12.3	21.4	1.2	137.6	3.2	263.3	–	25.5	1.4	
March	1	47.8	–	35.0	–	20.6	–	163.2	–	1.4	–	3.0	–	n.a.	–	n.a.	–	n.a.	–	n.a.	–	n.a.	–	15.0	–	
April	2	40.2	4.0	33.1	1.7	19.3	2.9	206.3	7.5	0.7	0.4	1.6	0.7	2.3	0.02	79.0	64.9	10.3	0.5	135.0	33.8	230.7	18.8	16.3	–	
May	16	15.4	4.0	15.2	3.5	7.4	3.5	53.6	13.1	1.2	0.2	1.7	0.5	3.7	0.8	26.1	13.0	19.9	2.8	53.8	10.5	57.0	19.1	12.5	5.146	
June	11	9.8	2.9	11.4	4.8	4.9	1.9	33.4	8.3	1.1	0.4	1.3	0.4	2.4	0.4	15.8	3.3	14.2	2.6	31.3	11.8	34.8	16.7	8.7	1.868	
July	26-29	7.9	2.8	8.3	2.1	4.1	1.7	27.6	8.1	1.0	0.4	1.2	0.5	2.3	0.6	14.1	3.9	12.6	3.2	25.2	10.0	33.5	8.7	8.1	2.3	
August	20	5.1	0.8	5.8	1.2	3.1	3.4	17.5	2.9	0.6	0.4	0.6	0.5	1.7	0.6	8.9	1.9	8.0	1.9	14.8	3.8	22.1	7.4	7.2	4.9	
September	20	5.7	3.7	7.1	3.8	3.3	1.1	18.8	5.6	0.9	0.6	1.2	0.7	1.6	0.5	8.7	2.5	6.4	1.3	25.8	13.9	25.5	13.7	5.3	1.6	
October	7	12.1	3.7	12.2	3.7	5.5	2.6	45.7	15.0	1.5	0.3	2.4	0.4	2.0	0.9	19.2	8.7	11.3	4.9	43.6	25.1	103.8	65.8	9.9	1.4	
November	1	26.2	–	20.8	–	12.7	–	96.0	–	1.2	–	2.4	–	3.4	–	45.4	–	17.6	–	98.0	–	147.9	–	18.0	–	
December	1	35.2	–	26.6	–	16.5	–	120.8	–	0.6	–	1.3	–	5.0	–	59.6	–	20.0	–	123.7	–	250.7	–	47.0	–	
Oberaar																										
January	1-2	42.5	3.2	64.1	1.6	36.6	2.9	616.9	13.9	0.7	0.0	3.9	0.9	2.7	1.0	395.1	26.9	10.6	5.6	356.6	42.7	180.8	–	86.3	1.2	
March	2	47.1	1.1	61.6	6.5	39.9	6.4	645.2	38.8	0.5	0.1	3.0	0.2	3.0	0.2	300.8	33.0	11.7	3.1	481.9	88.6	n.a.	–	90.0	2.8	
April	2	39.0	7.6	48.1	5.5	30.9	5.1	484.5	50.1	1.3	0.9	3.5	1.0	4.4	1.7	140.3	149.2	21.2	4.7	441.4	76.3	193.7	18	67.5	7.7	
May	2	16.0	0.2	26.2	4.9	16.1	3.6	218.0	55.8	2.4	2.2	4.3	3.1	3.4	1.2	54.5	38.3	17.5	6.7	282.6	66.7	113.6	16	29.0	5.7	
June	11-12	9.1	1.6	16.7	1.9	10.9	2.2	179.9	23.9	2.3	0.6	3.9	0.7	2.2	0.2	63.7	10.3	10.5	2.6	147.1	17.4	55.8	8.8	23.3	2.3	
July	19-21	10.9	4.0	21.1	5.3	14.0	3.4	216.1	50.1	1.9	0.9	4.1	1.3	2.2	0.4	87.0	27.6	10.6	3.2	166.6	51.2	62.5	24.7	29.4	6.9	
August	10-11	7.3	1.8	16.9	3.5	11.3	2.0	179.0	34.6	2.2	0.9	4.5	1.4	2.0	0.1	66.4	14.6	6.5	1.7	148.5	20.2	62.0	39.3	25.2	4.6	
September	9-10	7.8	3.2	19.9	6.3	14.1	4.6	188.6	57.1	2.1	0.8	4.6	1.2	2.5	0.7	83.2	16.8	6.6	2.2	194.0	30.1	56.4	15.6	30.0	5.4	
October	3	16.8	0.6	33.4	2.3	19.6	4.6	313.3	39.3	2.2	2.1	5.3	3.2	3.0	0.8	113.0	51.7	12.6	3.2	262.0	33.4	74.9	52.3	39.9	10.2	
November	1	31.2	–	54.6	–	31.2	–	456.4	–	3.1	–	6.6	–	2.3	–	252.6	–	14.0	–	314.8	–	n.a.	–	64.7	–	
December	1	33.9	–	60.8	–	33.7	–	547.9	–	0.9	–	3.1	–	3.2	–	312.8	–	15.0	–	349.4	–	n.a.	–	76.6	–	

n.a. not analysed

* Modelled discharge for areas from Swiss National Hydrological Survey (Federal Office for Water and Geology), see text.

† Calculated HCO_3^-

Discharge Rhone measured at Gletsch, Oberaar estimated, see text.

The suspended sediments of the two catchments both contain quartz, plagioclase, alkali feldspar, phyllosilicates and calcite (XRD values). In addition some of the Oberaar samples contain amphibole. The bulk mineralogical analysis shows that quartz, plagioclase feldspar and phyllosilicate content of suspended sediments in the two catchments are similar, but that the Oberaar suspension contains less potassium feldspar than the Rhône suspension. The phyllosilicates have been identified as biotite, phengite and chlorite (Keusen, 1989). The mean calcite concentration is 4.6 times higher in the Oberaar suspension than the Rhône (2.3% and 0.5% respectively, Table 2) although the 1 σ standard deviation around the Oberaar mean is ± 1.8. The mean Na_2O and SiO_2 concentrations of the suspended sediments are similar (XRF, Rhône and Oberaar Na_2O 3.8 & 3.0 % respectively; Rhône and Oberaar SiO_2 68 % & 63 % respectively). The mean CaO content of the Rhône suspended sediments is approximately half that of the Oberaar suspended sediments (0.9 % & 2.0 %, respectively). The strontium and barium concentrations are observed to be elevated in the Oberaar suspended sediments (Ba: 982 ppm, Sr: 238 ppm) with respect to the Rhône (Ba: 524 ppm Sr: 102). The oxides of Ti and P which are found in granitic rocks associated with minerals that contain calcium (sphene and apatite respectively) are also more prevelant in the Oberaar catchment (TiO_2 = 0.66 %, Oberaar & 0.4 %, Rhône; P_2O_5 = 0.18%, Oberaar & 0.1 % Rhône). Finally ferric iron concentrations are also elevated in the Rhône sediments (Oberaar = 3.2 %; Rhône = 1.8 %) indicating a higher concentration of iron sulphides in the Oberaar catchment.

In the two catchments the suspended sediment has a modal grain size in the 4-8 μm range, with 33% of the sediment in this size fraction. The suspended sediment flux from the Oberaar catchment is 773 t km^{-2} yr^{-1} and the suspended sediment flux from the Rhône catchment is 388-490 t km^{-2} yr^{-1}.

Wet Precipitation Composition

Mean rain and snow chemistries are listed in table 3; we also list average annual precipitation concentrations for the Alptal (P Schleppi, personal communication). This non-glaciated valley lies at the northern edge of the Swiss Alps, approximately 80 km from our field areas, between 1100 and 1600 m altitude. Our average annual concentrations agree well with the Alptal dataset, i.e. within 2-3 μeq l^{-1}, the exceptions being the SO_4^{2-} and NO_3^- concentrations, which are approximately twice as high in our glacial catchments. SO_4^{2-} and NO_3^- concentrations in snow agree well with the data for the Haut Glacier d'Arolla (Tranter et al., 2002).

Meltwater Composition

Calcium dominates the meltwater chemistry of the Oberaar watershed and is the second most important ion after silica in the Rhône watershed (Table 6). Fig. 2b shows meltwater samples taken at 10:00 hours have higher Ca^{2+} concentrations than the corresponding samples taken at 17:00 hours. Mean Ca^{2+} concentrations are higher during the accumulation period (Rhône Ca^{2+} concentrations = 4.5 x higher and Oberaar Ca^{2+} concentrations = 2.6 x

higher; see table 6), when discharge is 0.1- 0.3 l s^{-1}, than during the ablation period, when average monthly discharge ranges from 1000- 10'000 l s^{-1}. The trends in Ca^{2+} concentrations are representative for the other dissolved ions. Oberaar meltwater Ca^{2+} concentrations are an order of magnitude higher than Rhône meltwater ones during the 1999 and 2000 ablation periods (Fig. 2b) and Oberaar accumulation period samples contain approximately four times as much Ca^{2+} as equivalent Rhône samples. This is reflected in the higher mean annual pH of the Oberaar meltwaters (7.40) compared to the Rhône meltwaters (pH 5.97). The Oberaar meltwaters also have higher K^+, Mg^{2+}, SO_4^{2-} and calculated HCO_3^- concentrations than the Rhône meltwaters whereas the Na^+, Cl^-, NO_3^- and Si concentrations are comparable between the two areas (Table 6).

Two ternary diagrams show that the Oberaar meltwater compositions plot as a discrete population relative to the Rhône meltwater composition: In the Ca^{2+}-K^+-Na^+ ternary diagram the Oberaar samples are tightly grouped and plot much closer to the Ca^{2+} pole than the Rhône samples (Fig. 3a). Similarly in the Si-calculated-HCO_3^--Ca^{2+} diagram the Oberaar samples plot closer to the Ca-HCO_3 boundary, whereas silica dominantes over HCO_3^- and Ca^{2+} in most of the the Rhône meltwater samples (Fig. 3b).

Fluxes

The Ca^{2+}, K^+, Mg^{2+}, calculated HCO_3^- and SO_4^{2-} fluxes calculated for the Oberaar catchment are elevated compared to those calculated for the Rhône (Ca^{2+} by 5-6 times; K^+ by 1.7-2 times; Mg^{2+} by 2-2.5 times; HCO_3^- by 4-4.6 times and SO_4^{2-} by 3.8-4.5 times; Table 4). The ranges reflect the possible errors in the Rhône fluxes due to the calculated discharge. The Na^+, Cl^- and Si fluxes from the two watersheds are comparable. The trend in the mean monthly Ca^{2+} flux is representative for all the dissolved ionic fluxes (Fig. 4). Note ablation period Ca^{2+} fluxes are 3-4 times higher than accumulation period Ca^{2+} fluxes. The Rhône calculated and measured HCO_3^- fluxes agree well, (measured = 113610 keq km^{-2} yr^{-1}, using late October values to approximate winter values; calculated = 108638 keq km^{-2} yr^{-1}; both fluxes use Gletsch discharge corrected by 14 %). This would suggest that the error in our lab measurements is small and the calculated HCO_3^- values are robust.

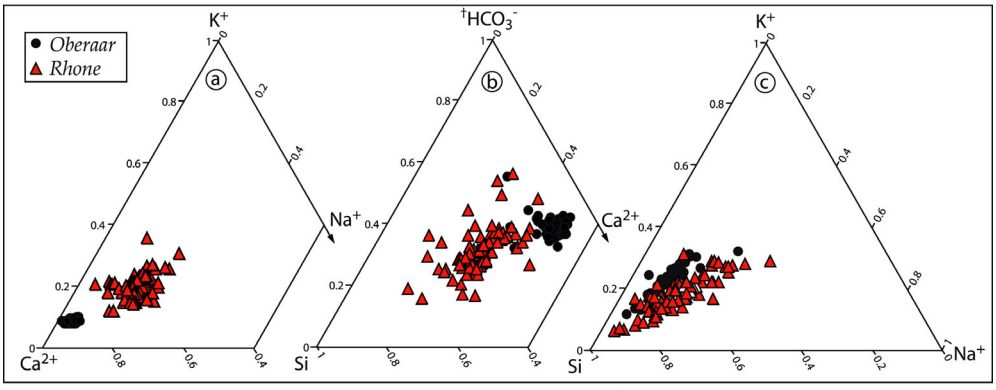


Fig. 3: Ternary diagrams of ions dissolved in meltwaters. *†HCO_3^- = calculated HCO_3^-.*

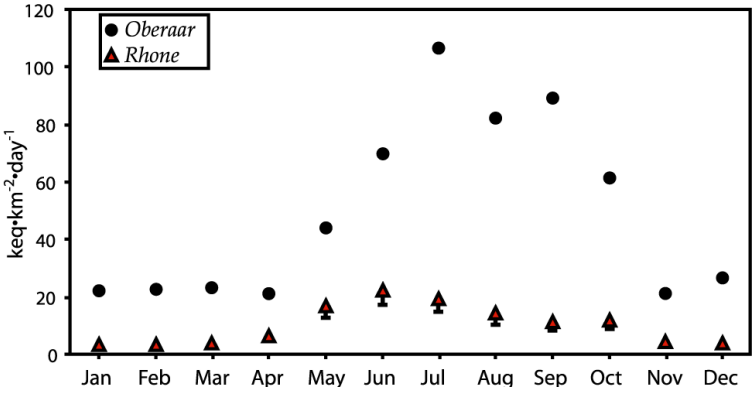


***Fig 4**: Mean daily Ca^{2+} fluxes from the two glaciers (1999 – 2001)*

Adsorbed cations

Average summer and winter adsorbed cation concentrations and annual adsorbed fluxes are shown in table 7. Summer concentrations are higher than winter concentrations and the Oberaar annual adsorbed Ca flux is at least 4 times higher than the Rhône's. The adsorbed fluxes represent between 2 and 10 % of the dissolved flux. These values are comparable with those of Lorrain and Souchez (1972), who measured adsorbed fluxes from the Moiry glacier catchment, Switzerland, which is also underlain by crystalline bedrock.

Discussion

Carbonate Weathering

Calcium denudation appears to be much more important in the Oberaar catchment than the Rhône catchment. Ca^{2+} concentrations in the Oberaar meltwaters are consistently elevated with respect to the Rhône meltwaters and consequently have a higher mean pH and mean calculated HCO_3^- concentrations (Figures 3a and 3b). During the accumulation season the Oberaar Ca^{2+} concentrations are approximately 4 times greater than the Rhône's and in July, at the height of the ablation period, the mean Ca^{2+} concentration in the Oberaar meltwaters is 8 times greater than in the Rhône's (Fig. 2b). This translates to an annual precipitation corrected Ca^{2+} flux from the Oberaar catchment which is approximately 6-7 times higher than from Rhône catchment (Table 4). The Oberaar's elevated Ca^{2+} flux cannot be due to increased plagioclase weathering, given that the suspended sediment from the two catchments contain very similar concentrations of albite (Table 2; XRF measurements) and the Na^+ fluxes from the two catchments are comparable (Table 4). Therefore other calcium bearing minerals are responsible for the elevated Ca^{2+}: Na^+ molar ratio in the Oberaar (11) relative to the Rhône meltwaters (2). The candidate minerals in intrusive alkaline rocks are amphibole, apatite, epidote, sphene and calcite, all of these have been minerals have been detected optically in the rocks in our field areas by Keusen (1989), but we believe calcite is the most important as we explain below. Amphibole was identified in some of the Oberaar suspended sediment samples and Stalder

(1964) describes amphibolite lenses at the borders of the Oberaar catchment. An actinolite composistion is likely (O. Müntener Neuchâtel, pers. comm.). Amphibole was not detected in the Rhône suspended sediment, and therefore may be a potential source of additional calcium in the Oberaar glacier's subglacial environment. However, we assume that the weathering flux of calcium derived from amphibole is negligible in the Oberaar catchment because the peak amplitude (XRD) is less than that of calcite, showing that actinolite is present at concentrations of < 1%, although exact quantification is not possible using this method and b) its weathering rate ($\approx 10^{-15}$ mol cm^{-2} s^{-1}; Brantley and Chen, 1995) is ten orders of magnitude lower than that of calcite at near neutral pH. Apatite dissolution is unlikely to augment the Oberaar Ca^{2+} flux, because orthophosphate concentrations are similar in the meltwaters of the two catchments and apatite weathering is minimal at near neutral pH (Stumm and Morgan, 1996). It is harder to assess the contribution of the accessory minerals sphene and epidote to the calcium flux, as laboratory studies of their weathering rates have not been undertaken and we have not detected these minerals using XRD. Epidote in the Aar massif results from the saussuritization of oligoclase during the alpine orogeny (Keusen et al., 1989) and since plagioclase concentrations are comparable in the two field areas we assume that the epidote concentrations are also similar. Regarding sphene as the weight percent of TiO_2 is 1.65 greater in the Oberaar catchment this suggests that sphene may be more concentrated here. However we suggest that the most likely cause of the elevated Oberaar Ca^{2+} flux is the greater mass of finely ground calcite in contact with meltwaters in the subglacial environment of the Oberaar catchment (both suspended and immobile sediments). As the modal grain size of the suspended sediment in the two catchments is 4-8 μm and calcite tends to be concentrated in the finer size fractions (Fairchild et al., 1999) it is highly reactive when is contact with dilute meltwaters, especially as laboratory experiments show that the dissolution rate of calcite at neutral pH is $\approx 10^{-5}$ mol m^{-2} s^{-1} (Plummer et al., 1978). XRD bulk mineralogy shows that approximately 4.6 times as much calcite is present in the suspended sediment exported from the Oberaar as from the Rhône catchment (Table 2). This observation is supported by our XRF observations, which show that there is twice as much CaO in the Oberaar suspended sediments (the discrepancy is probably due to differences between the methods). In addition the average concentration of sediment in the Oberaar meltwaters is 0.31 g l^{-1} (the mean of accumulation and ablation period average concentrations), whereas the average concentration of sediment in the Rhône meltwaters is 0.07 g l^{-1}. So averaged over a year 7.1 mg l^{-1} of calcite may be

Table 7: Adsorbed composition and fluxes

	Ca^{2+}	K^{+}	Mg^{2+}
Oberaar			
mean ablation (μeq g^{-1})	82.34 (±45.91)	2.05 (±1.79)	2.47 (±0.82)
mean accumulation (μeq g^{-1})	27.49	1.46	0.95
keq km^{-2} yr^{-1}	40	1	1
Rhône			
mean ablation (μeq g^{-1})	< 23.95 (±19.96)*	5.88 (± 8.44)	2.47 (± 0.82)
mean accumulation (μeq g^{-1})	< 16.97	3.36	1.25
keq km^{-2} yr^{-1}	< 8-10	2	1

* Although the blank was as high as the Rhône samples we show the calculated values to indicate the maximum possible fluxes.

suspended in meltwaters in the Oberaar catchment, compared to 0.4 mg l^{-1} in the Rhône catchment, asssuming 2.3 % and 0.5 % of the sediment is calcite. Consequently the total mass of calcite transported by the Oberaar meltwaters on an annual basis is much higher (of the order of 17.7 t km^{-2} yr^{-1}) than that transported by the Rhône meltwaters (2.5 t km^{-2} yr^{-1}). We infer that the volume of immobile calcite in contact with meltwaters in the subglacial environment of the Oberaar glacier will be similarly elevated relative to the calcite under the Rhône glacier. Many authors have underlined the dominant influence of calcite weathering on the chemical signature of glacial meltwaters draining crystalline catchments (e.g. Eyles et al., 1982; Drever and Hurcomb, 1986; Anderson et al., 1997, 2000; West et al., 2002). We would like to stress the extreme sensitivity of glacial systems to changes in calcite concentrations, even in areas of crystalline bedrock. A 4.6 factor difference in the calcite content of the suspended sediments (and by inference subglacial sediments) of these two catchments, coupled with the increased erodability of bedrock in the Oberaar watershed, appears to increase Ca^{2+} fluxes by an order of magnitude, from 10's of keq km^{-2} yr^{-1} to 100's of keq km^{-2} yr^{-1}. Fig. 5 compares the Ca/Na ratios in runoff from presently glacier-covered and non-glacier covered catchments with granitoid bedrock. The Rhône catchment, with its low calcite content plots within the scatter of non-glaciated catchments, whereas the Oberaar catchment plots with other glacierised catchments whose bedrock geologies contain more calcic minerals.

CO_2 Draw Down

Total CO_2 drawdown ($CO_{2\ dd}$) in the catchments is calculated, based on the chloride normalised fluxes (mol km^{-2} yr^{-1}), as the difference between the total dissolved inorganic carbon flux (calculated HCO_3^-; DIC_{tot}; Rhône = 109'792; Oberaar = 467'997 mol km^{-2} yr^{-1}) and the HCO_3^- flux from calcite dissolution (DIC_{cc}).

$$CO_{2\ dd} = DIC_{tot} - (DIC_{cc} + (Na * 0.1))$$

We assume that DIC_{cc} is equal to the Ca flux (Ca; Rhône = 48'291; Oberaar = 277'774 mol km^{-2} yr^{-1}), once it has been corrected for the Ca component from the weathering of plagioclase (Ca_{plag}). To simplify our calculation we assume that the Ca input from the weathering of amphibole, epidote, titanite and apatite is 0. Our plagioclase feldspar is of albitic composition (Keusen et al., 1989) therefore we assume stoichiometric dissolution and calculate Ca_{plag} as 10 % of the Na flux (Ca_{plag} ; Rhône = 2'727; Oberaar = 2'605). Therefore 25'564 and 275'169 moles of HCO_3^- comes from the calcite mineral itself:

$$CaCO_3 + H_2O + CO_2 = Ca^{2+} + 2HCO_3^-$$

So $CO_{2\ dd}$ is 192'828 mol km^{-2} yr^{-1} in the Oberaar catchment and 64'299 mol km^{-2} yr^{-1} in the Rhône catchment. The Oberaar value is comparable with CO_2 drawdown calculated for the Haut Glacier d'Arolla catchment, which has a schistose bedrock geology (1989 = 166'660 mol km^{-2} yr^{-1}; 1990 = 206'410 mol km^{-2} yr^{-1}; Sharp et al., 1995). Determining what portion of this drawdown is long-

term (LT) i.e. used in the acid hydrolysis of silicate minerals is more complex judging from the literature. Raiswell (1984) demonstrated that acid hydrolysis reactions are largely driven by protons derived by carbonation and sulphide oxidation in the subglacial environment. Tranter et al. (1993) observed an inverse relationship beween sulphate mass fraction (SO_4^{2-}/(SO_4^{2-} + HCO_3^-; working in eq l^{-1})) and discharge at the Haut Glacier d'Arolla. They interpreted this as evidence that sulphide oxidation is the dominant proton source for subglacial acid hydrolysis reactions within distributed drainage systems and argued therefore that sulphide oxidation and carbonate dissolution reactions are coupled (SO-CD). The observation that silica concentrations are low in such distributed systems is used to bolster their argument (Tranter et al., 2002). But, in this study silica concentrations are observed to increase by an order of magnitude during the accumulation season, implying that silicate weathering is on-going when a distributed drainage system prevails. Furthermore a significant correlation between the sulphate mass fraction and discharge is lacking in the Oberaar and Rhône catchments (using precipitation corrected meltwater compositions). Moreover the mean sulphate mass fractions for the Oberaar and the Rhône basins (0.3 and 0.26 respectively), demonstrate that weathering reactions are driven by both protons released by carbonation and sulphide oxidation reactions in the meltwaters (Tranter et al., 1993). Hodson et al. (2002) point out that assuming SO-CD leads to maximum estimates of LT CO_2 drawdown (e.g. Sharp et al., 1995). In order to estimate more realistic LT CO_2 drawdown we presume that protons randomly hydrolyse carbonate and silicate minerals without preference. As such 32 % and 64 % of the CO_2 drawdown is LT in the Oberaar and Rhône catchments respectively (Oberaar = 61'705 mol km^{-2} yr^{-1}; Rhône = 41'151 mol km^{-2} yr^{-1}).

Silicate Weathering

Silicate weathering is temperature dependant (Vebel,

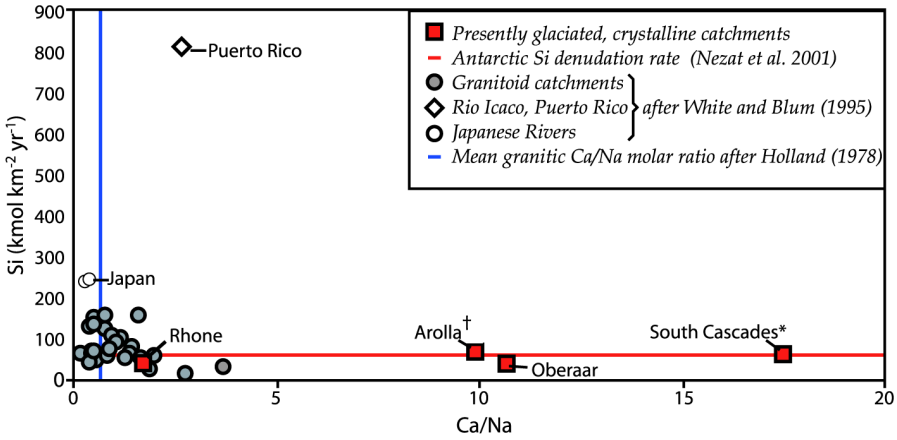


Fig. 5: Silicate and carbonate weathering in presently glaciated and non-glaciated granitoid catchments (All fluxes are corrected for precipitation inputs)

† *Sharp et al. (1995) & * Axtmann and Stallard (1995), cyclical salt corrections; White and Blum (1995), volumetric correction.*

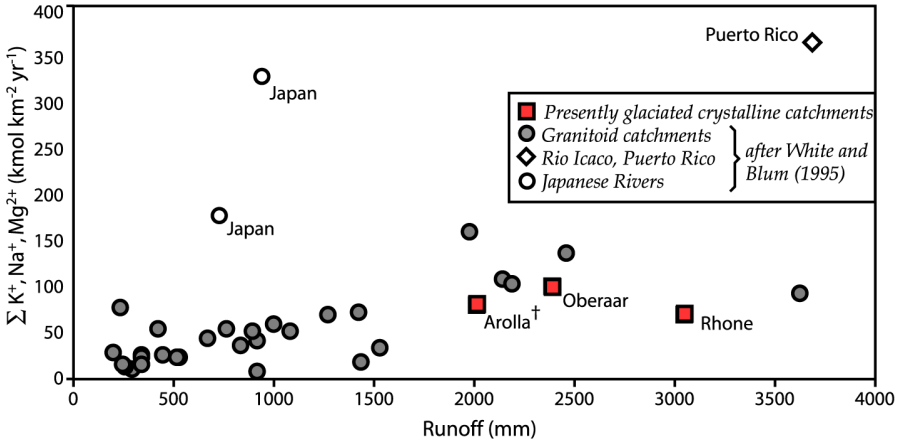


Fig. 6: Molar fluxes of cations derived from silicate weathering against runoff in presently glaciated and non-glaciated granitoid catchments (All fluxes are corrected for precipitation inputs).
† Sharp et al. (1995), cyclical salt corrections; White and Blum (1995), volumetric correction.

1993; White and Blum, 1995). Replotting the values of White and Blum (1995) to include glacial catchments with granitoid bedrock (Fig. 5) shows that the silica fluxes from the Rhône and Oberaar catchments are similar to each other, and to other presently glaciated mountain basins and icesheets underlain by granitoid rocks. The silicate fluxes from the presently glaciated catchments plot amongst the lowest from the non-glaciated granitoid catchments, but they do not form a separate population (Table 4; Figure 5). Our two catchments therefore fit into the scheme proposed by Anderson et al. (1997), who used a very similar data set.

Cations derived from silicate weathering (kmol km^{-2} yr^{-1}; $\sum K^+$, Mg^{2+}, Na^+ and Ca_{plag}) are 1/3 greater from the Oberaar catchment than the Rhône (Oberaar = 99; Rhône = 65). The higher sulphide content of the Oberaar catchment's bedrock contributes to the increased chemical weathering of both carbonates and silicates in the Oberaar catchment. The Oberaar's higher sulphate flux (approximately 5 times greater than the Rhône's when corrected for wet precipitation inputs) points towards a higher concentration of metal sulphides in the Oberaar catchment, which are probably associated with the strongly foliated gneissic zone. Elevated iron concentrations in the Oberaar suspended sediment (XRF data) also give an indirect indication of a higher sulphide content in the Oberaar suspended sediment compared to the Rhône. The approximately doubled Oberaar sediment flux may also be the cause of increased weathering of cations from silicate minerals and greater CO_2 drawdown within this catchment. We note the Oberaar K^+ flux is double the Rhône K^+ flux (Table 4; Fig. 3c; the proportion of phyllosilicates in the suspended sediments from both catchments is the same). The vermiculatisation of micas leads to the preferential release of K^+ ions in glacial waters (Drever and Hurcomb, 1986; Anderson et al., 1997). Our data indicates that the K^+ flux may be directly proportional to the mass of phyllosilicates in suspension. The silicate derived cation fluxes ($\sum K^+$,

Mg^{2+}, Na^{+}) from this study plot in the same range as those from non-glacial catchments with similar runoff, located at similar latitudes (Fig. 6; Ca_{plag} is not included, as is not known for the published data compiled in White and Blum, 1995).

Conclusions

The strongly foliated gneissic zone running down the central third of the Oberaar catchment has a major impact on physical and chemical erosion rates measured within this watershed compared to those of the Rhône catchment, which lies on granitic and granodioritic rocks. Approximately twice as much suspended sediment is exported by the Oberaar meltwaters compared to the Rhône meltwaters during the study period (1999-2001), due to the greater erodability of the Oberaar catchment. This greater erodability, coupled with the larger mean calcite content of the Oberaar sediments (2.3 % compared to 0.5 % for the Rhône suspension), and 5 times more sulphide derived sulphate in the Oberaar catchment, leads to 6-7 times more dissolved calcium being denuded from the Oberaar watershed, most of which comes from carbonate dissolution. Calcite weathering is more important in this glacial catchment than in non-glaciated catchments underlain by granitoid rocks (judging by the Ca/Na molar ratios; Fig. 5). Yet the silicate weathering rates we observe in our presently glaciated alpine catchments and those which are published for other glaciated alpine and Antarctic catchments fall within the range of temperate, non-glaciated granitoid catchments with the same runoff implying that silicate weathering is not accelerated in the subglacial environment.

Acknowledgments

We thank Daniel Arn, David Nisbet, Katharine Nisbet, and Marlen Schaller for field support and Giulio Galetti, Khaoula Hamila and Sebastian Ryser for laboratory assistance. This study was supported by Swiss NF grants 21-53991.98. and 20-61485.00.

References

Adatte T., Stinnesbeck W. and Keller G. (1996) Lithostratigraphic and mineralogical correlations of near K/T boundary clastic sediments. in northeastern Mexico: Implications for origins and nature of deposition. *In*: The Cretaceous-Tertiary Event and Other Catastrophes in Earth History. Ryder G., Fastovsky D., and Gartner S. (Eds.) *Geological Society of America Special Paper* **307**. Boulder, Colorado.

Anderson S.P., Drever J.I. and Humphery N.F. (1997) Chemical weathering in glacial environments. *Geology* **25**: 399-402.

Anderson S.P., Drever J.I., Frost C.D. and Holden P. (2000) Chemical weathering in the foreland of a retreating glacier. *Geochimica Cosmochimica Acta* **64**: 1173-1189.

Arn K. (2002) *Geochemical weathering in the sub- and proglacial zones of two crystalline catchments in the Swiss Alps (Oberaar – Rhône glaciers)*. PhD thesis, Univertité de Neuchâtel.

Axtmann E.V. and Stallard R.F. (1995) Chemical weathering in the South Cascade Glacier basin, comparison of subglacial and extra-glacial

weathering. *In*: *Geochemistry of Seasonally Snow-Covered Catchments (Proceedings of a Boulder Symposium, July 1995)* IAHS **228**: 431-439.

Bernath A. (1991) Zum Wasserhaushalt im Einzugsgebiet der Rhône bis Gletsch. (Ed D. Grebner). *Züricher Geographische Schriften* **43**.

Boulton G.S. (1979) Processes of glacier erosion on different substrata. *Journal of glaciology* **23**: 15-38.

Brantley S. L. & Chen Y. (1995) Chemical weathering rates of pyroxenes and amphiboles. *In*: White A.F. and Brantley S.L. (Eds) Chemical weathering rates of silicate minerals. *Reviews in Mineralogy* **31**: 119-172.

Chou L. and Wollast R. (1985) Steady state kinetics and dissolution mechanisms of albite. *American Journal of Science* **285**: 963-993.

Dreimanis A. and Vagners U. J. (1969) Characteristics of the composition of till derived from the basal and the englacial drift. *The Geological Society of America* **6**: 1-12.

Dreimanis A. and Vagners U.J. (1971) The dependence of the composition of till upon the rule of bimodal distribution, Etudes sur le Quaternaire dans le Monde, **2**, *Bulletin de l'Association Francaise pour l'Etude du Quaternaire* **4**: p. 787-789.

Drever J.I. and Hurcomb D.R. (1986) Neutralization of atmospheric acidity by chemical weathering in an alpine drainage basin in the North Cascade Mountains. *Geology* **14**: 221-224.

Drewry D. (1986) *Glacial Geological Processes.* Edward Arnold, London, England. **pp** 276.

Eyles N., Sassevilee D.R., Slatt R.M. and Rogerson R.J. (1982) Geochemical denudation rates and solute transport mechanisms in a maritime temperate glacier basin. *Canadian Journal of Earth Sci*ence **19**: 1570-1581.

Fairchild I.J., Bradby L., Sharp M. and Tison J-L. (1994) Hydrochemistry of carbonate terrains in Alpine glacial settings. *Earth Surface Processes and Landforms* **19**: 33-54.

Fairchild I.J., Killawee J.A., Hubbard B. and Derybrodt P. (1999) Interactions of calcareous suspended sediment with glacial meltwater: a field test of dissolution behaviour. *Chemical Geology* **155**: 243-263.

Federal Office for Water and Geology (1994) Technischer Bericht: Manual für die Abflussmessung nach dem Salzverdünnungsverfahren.

Gibbs M.T. and Kump L.R. (1994) Global chemical erosion during the last glacial maximum and the present: Sensitivity to changes in lithology and hydrology. *Paleoceanography* **9**: 529-543.

Gurnell A.M., Brown G.H. and Tranter M. (1994) Sampling strategy to describe the temporal hydrochemical characteristics of an alpine proglacial stream. *Hydrological Processes* **8**: 1-25.

Hallet B., Hunter L. and Bogen J. (1996) Rates of erosion and sediment evacuation by glaciers: A review of field data and their implications. *Global and Planetary Change* **12**: 213-235.

Hay W.W. (1998) Detrital sediment fluxes from continents to oceans. *Chemical Geology* **145**: 287-323.

Hoch A.R., Reddy M.J. and Drever J.I. (1999) Importance of mechanical disaggregation in chemical weathering in a cold alpine environment. *GSA Bulletin* **2**: 304-314.

Hodson A., Tranter M., and Vatne G. (2000) Contemporary rates of chemical denudation and atmospheric CO_2 sequestration in glacier basins: an Arctic perspective. *Earth Surface Processes and Landforms* **25**: 1447-1471.

Holland D.H (1978) The chemistry of the Atmosphere and the Oceans. Wiley-Interscience, New York. **pp** 351.

Keusen HR., Ganguin J., Schuler P., Buletti M. (1989) *NAGRA technischer Bericht* **87-14**

Kübler B., Jantschik R. and Huon S. (1990) Minérologie et granulométrie des poussières éoliennes, dites "Sahariennes", du 24 avril 1989 à Neuchâtel. Leur importance pour l'environnment, les sols et les sédiments. *Bulletin de la Société neuchâteloise des Sciences naturelles* **113**: 75-98.

Lenaz R., Landuzzi V. and Tomadin L. (1986) Apports et concentration des masses de poussières éoliennes sur le bassin oriental et occidental de al Méditerranée. *Mem. Soc. Geol. It.* **36**: 189-200.

Lorrain R.D. and Souchez R.A. (1972) Sorption as a factor of in the transport of major cations by meltwaters from an Alpine glacier, *Quaternary Research* **2**: 253-256.

Livingstone D.A. (1963) Chemical compositions of rivers and lakes. *U.S. Geological Survey Professional Paper* **440-G**. **pp** 64.

Ludwig W., Amiotte-Suchet P., Munhoven G. and Probst J-L. (1998) Atmospheric CO_2 consumption by continental erosion: present-day controls and implications for the last glacial maximum. *Global and Planetary Change* **16**: 107-120.

Meybeck M. (1987) Global chemical weathering of surficial rocks estimated from river dissolved loads. *Am. Journal of Sci.* **287**: 401-428.

Mahaney W.C. (1995) Glacial crushing, weathering and diagenetic histories of quartz grains inferred from scanning electron microscopy. In: Menzies J. (Ed.) *Modern glacial environments. Processes, dynamics and sediments, Glacial Environments: Volume 1*. Butterworth-Heinemann, Oxford: **pp** 621.

Mullin J.B. and Riley J.P., (1955) The colorimetric determination of silicate with special reference to sea and natural waters. *Analytica chimica Acta* **12**: 162-176.

Nezat C.A, Lyons B.W. and Welch K.A. (2001) Chemical weathering in streams of a polar desert (Taylor Valley, Antarctica) *GSA Bulletin* **113**: 1401-1408.

Nienow P., Sharp M. and Willis I. (1996) Temporal switching between englacial and subglacial drainage pathways: Dye tracer evidence from the Haut glacier d'Arrola, Switzerland. *Geografiska Annaler* **78**: 51-59.

Oberhänsli R. and F. Schenker. (1988) Indications of Variscan nappe teconics in the Aar Massif. *Scheizerische Mineralogisch Petrographische Mitteilungen* **68**: 509-520.

Plummer L. N., Wigley T. M. L., and Parkhurst D.L. (1978) The kinetics of calcite dissolution in CO_2-water systems at 5-60°C and 0.0-1.0 atm CO_2. *American Journal of Science* **278**: 179-216.

Raiswell R. (1984) Chemical models of solute aquisition in glacial meltwaters. *Journal of Glaciology* **30**: 49-57.

Schwab M., Frei C., Schär C. and Daly C. (2001) Mean annual precipitation throughout the European Alps 1971-1990. *In*: Landeshydrologie, Bundesamt für Wasser und Geologie. (Ed.) *The Hydrological Atlas of Switzerland*. Bundesamt für Landestopographie, Bern.

Summerfield M. (1991) *Global geomorphology:* Harlow, United Kingdom, Longman **pp** 537.

Slatt R.M. (1972) Geochemistry of meltwater streams from nine Alaskan glaciers. *Geological Society of America Bulletin*. **83**: 1125-1132.

Souchez R.A. and Lemmens M.M. (1987) Solutes: 285-303. *In:* Gurnell A.M., and M.J. Clark (Eds.). *Glacio-fluvial sediment transfer: An alpine perspective*. New York, John Wiley & Sons.

Sharp M., Tranter M., Brown G.H. and Skidmore M. (1995) Rates of chemical denudation and CO_2 draw down in a glacier-covered alpine catchment. *Geology* **23**: 61-64.

Sharp M., Parkes J., Cragg B., Fairchild I.J., Lamb H. and Tranter M. (1999) Widespread bacterial populations at glacier beds and their relationship to rock weathering and carbon cycling. *Geology* **27**: 107-110.

Stadler H. A. (1964) Petrographische und mineralogische Untersuchungen im Grimselgebiet (Mittleres Aarmassiv). *Schweizerische Mineralogische und Petrographische Mitteilungen* **44,** 187-389

Stumm W. and Morgan J.J. (1996) Aquatic Chemistry. (Eds Schnoor J.L. & Zehnder A.) John Wiley & Sons. **pp** 1022.

Sugden D.E. (1978) Glacial erosion by the Laurentide ice sheet. *Journal of Glaciology* **20**: 367-394.

Tranter M., Brown G., Raiswell R., Sharp M. and Gurnell A. (1993) A conceptual model of solute acquisition by Alpine glacial meltwaters. *Journal of Glaciology* **39**: 573-581.

Tranter M., Sharp M.J., Lamb H.R., Brown G.H., Hubbard B.P. and Willis I.C. (2002) Geochemical weathering at the bed of Haut Glacier d'Arolla, Switzerland – a new model. *Hydrological Processes* **16**: 959-993.

Vebel M.A. (1993) Temperature dependence of silicate weathering in nature: How strong a negative feedback on longterm accumulation of atmospheric CO_2 and global greenhouse warming? *Geology* **21**: 1059-1062.

West J.A., Bickle M.J., Collins R. and Brasington J. (2002) Small-catchment perspective on Himalayan weathering fluxes. *Geology* **30**: 355-358.

White A.F. and Blum A.E. (1995) Effects of climate on chemical weathering in watersheds. *Geochimica Cosmochimica Acta* **59**: 1729-1747.

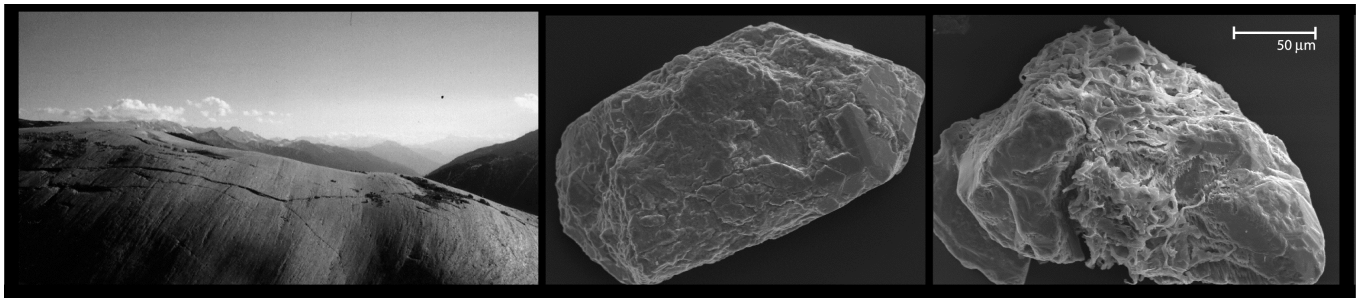
White A.F., Blum A.E., Bullen T.D., Vivit, D.V., Schulz, M.S. and Fitzpatrick J. (1999a) The effect of temperature on experimental and natural

chemical weathering rates of granitoid rocks. *Geochimica Cosmochimica Acta* **63**: 3277-3291.

White A.F., Bullen T.D., Vivit, D.V., Schulz, M.S. and Clow, D.W., (1999b) The role of disseminated calcite in the chemical weathering of granitoid rocks. *Geochimica Cosmochimica Acta* **63**: 1939-1953.

White A.F. and Brantley S.L. (1995) Chemical weathering rates of silicate minerals: An overview. *In*: White A.F. and Brantley S.L. (Eds) *Chemical weathering of Silicate Minerals* Mineralogical Society of America. Washington DC. **pp** 58

CHAPTER 3
appendices



Ablation period Ca^{2+} (mg/l) at maximum and minimum discharge in the Rhône meltwaters (1999-2001)

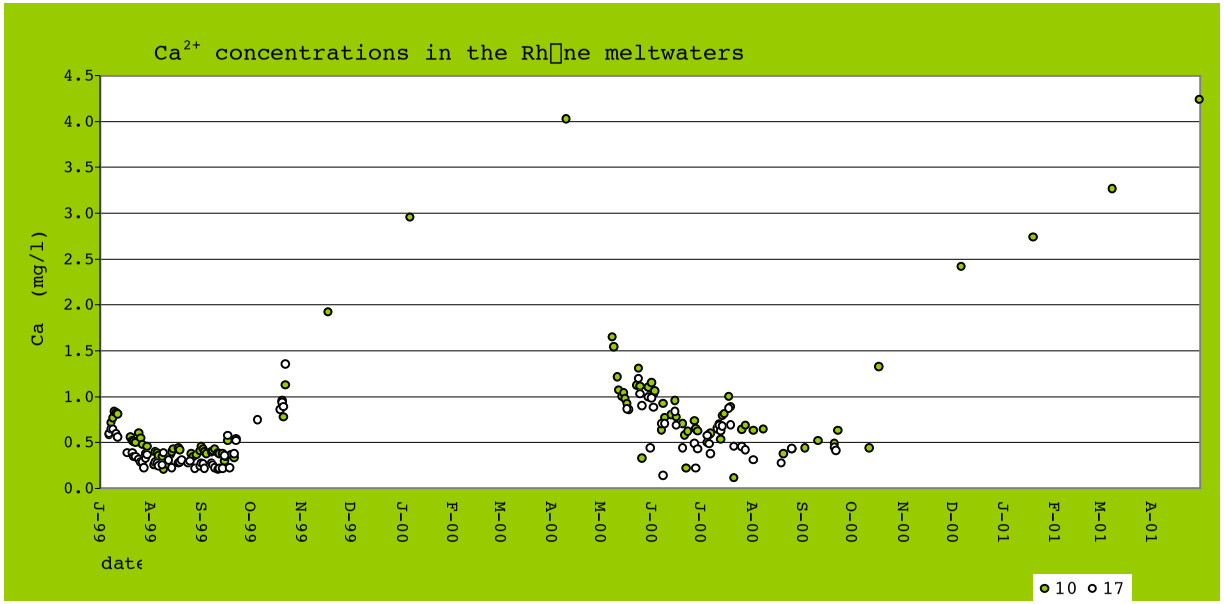
	07_99			08_99			09_99			10_99			05_00			06_00			07_00			08_00			09_00			10_00		
Day	10	17	daily	10	17	daily	10	17	daily	10	17	daily	10	17	daily	10	17	daily	10	17	daily	10	17	daily	10	17	daily	10	17	daily
1							0.43	0.27	0.35							1.03	0.89	0.96				0.63	0.31	0.47	0.44			0.44		
2				0.26		0.23	0.40	0.22	0.31							1.06														
3				0.40	0.29	0.35	0.38		0.30																					
4				0.39	0.28	0.34					0.75								0.50	0.58	0.54									
5				0.36	0.25	0.31													0.59	0.49	0.54									
6	0.59	0.60	0.60				0.40	0.28	0.34							0.64	0.71	0.67	0.60	0.38	0.49									
7	0.72	0.65	0.69	0.35	0.26	0.31	0.41	0.26	0.34				1.65		1.65	0.93	0.14	0.53				0.65								
8	0.77	0.65	0.71	0.21	0.39	0.30	0.43	0.23	0.33				1.55		1.55	0.78	0.71	0.74												
9	0.84		0.72																						0.52					
10	0.83	0.60	0.72				0.39	0.21	0.30				1.22		1.22				0.66	0.65	0.66							0.44		0.44
11	0.81	0.56	0.69	0.26	0.31	0.29	0.38	0.22	0.30				1.07		1.07				0.70	0.69	0.70									
12				0.37		0.29										0.81			0.54	0.63	0.58									
13				0.40	0.23	0.32	0.38	0.22	0.30				1.00		1.00				0.79	0.68	0.74									
14				0.43		0.33	0.30	0.36	0.33				1.04		1.04	0.96	0.84	0.90	0.82											
15							0.35		0.19				0.98		0.98	0.78	0.69	0.74												
16							0.52	0.58	0.55				0.93	0.87	0.90													1.33		1.33
17		0.39	0.46	0.44	0.28	0.36		0.23	0.12				0.86		0.86				1.00	0.87	0.94									
18				0.42	0.29	0.36	0.37		0.30		0.86	0.86							0.89	0.69	0.79		0.28	0.33						
19	0.56		0.48		0.31	0.38				0.96	0.94	0.95				0.71	0.44	0.58				0.38			0.49	0.45	0.47			
20	0.52	0.39	0.46				0.34	0.38	0.36	0.78	0.89	0.84				0.58			0.12	0.46	0.29					0.42	0.53			
21	0.51	0.35	0.43				0.54	0.52	0.53	1.13	1.36	1.25				0.22									0.63					
22	0.50	0.35	0.43										1.13		1.13	0.62														
23					0.28								1.31	1.20	1.26															
24	0.61	0.32	0.47		0.30								1.11	1.03	1.07							0.43	0.44	0.43						
25	0.55	0.29	0.42	0.38									0.33	0.90	0.62				0.64	0.46	0.55									
26	0.48	0.29	0.39	0.35												0.74	0.49	0.61												
27	0.33	0.23	0.28		0.22											0.65	0.22	0.44	0.69	0.42	0.55									
28	0.38	0.33	0.36	0.37												0.63	0.43	0.53												
29	0.46	0.37	0.42										1.11	1.00	1.05															
30				0.41	0.25	0.33							1.01	0.44	0.73															
31				0.46	0.28	0.37							1.16	0.99	1.07															
m			0.51			0.32			0.33			0.97			1.07			0.67			0.61			0.41			0.50			0.88

Accumulation period daily Ca^{2+} concentrations in the Rhône meltwaters (1999-2001)

Date	(mg/l)
16/11/99	1.92
5/12/00	2.42
5/1/00	2.96
18/1/01	2.74
7/3/01	3.27
9/4/00	4.03
29/4/01	4.24
m	3.08

Mean daily Ca concentrations

Month	n	mg/l	± (1 sigma)
January	2	2.90	
February	0		
March	1	3.30	
April	2	4.14	
May	16	1.07	0.26
June	10	0.67	0.17
July	29	0.55	0.16
August	18	0.34	0.06
September	18	0.35	0.11
October	8	0.87	0.33
November	1	1.92	
December	1	2.42	
	Abl.	**Abl.**	**Accu.**
	10:00	17:00	
Mean	0.64	0.49	3.08
±	0.30	0.26	0.84
n	106	82	7



Ablation period Ca^{2+} (mg/l) at minimum and maximum discharge in the Oberaar meltwaters (1999-2001

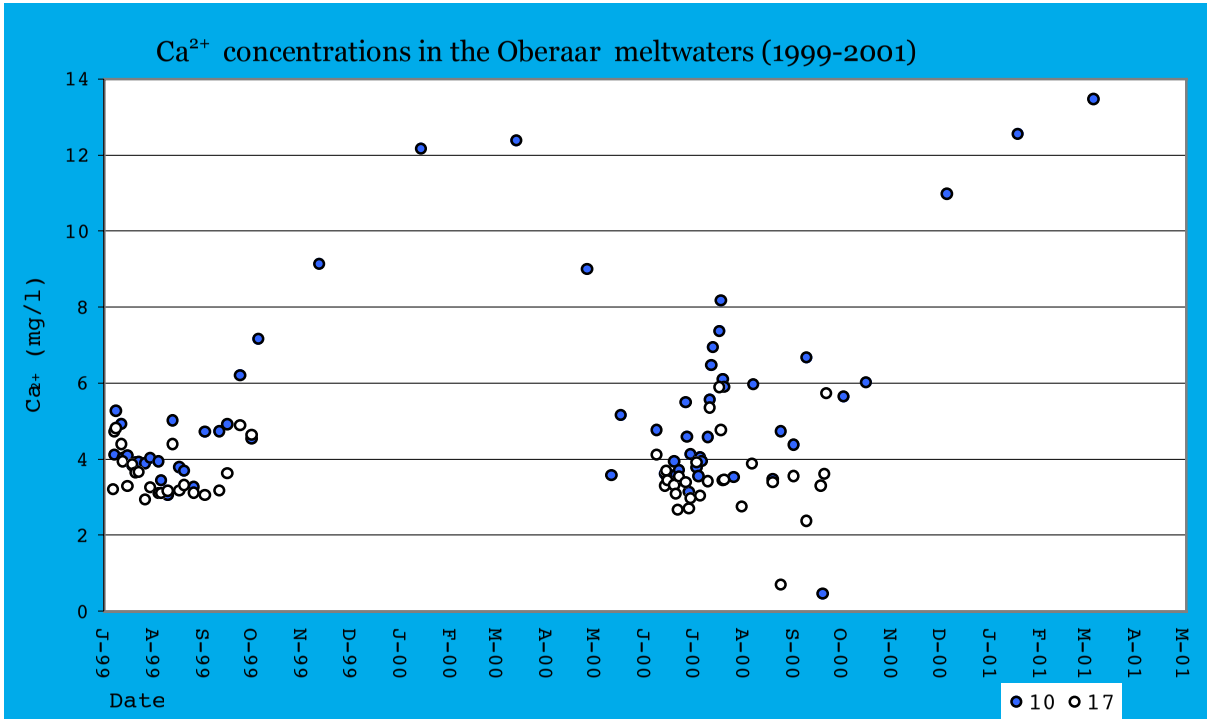
	07_99			08_99			09_99			10_99			05_00			06_00			07_00			08_00			09_00			10_00		
Date	10	17	daily	10	17	daily	10	17	daily	10	17	daily	10	17	daily	10	17	daily	10	17	daily	10	17	daily	10	17	daily	10	17	daily
1							4.72	3.05	3.89																4.39	3.55	3.97			
2																												5.65		5.65
3				3.94	3.10	3.52													3.78	3.9	3.9									
4										7.16		7.16							3.56											
5				3.44	3.10	3.27													4.06	3.05	3.55									
6		3.21	3.21																3.95				3.88	4.93						
7	4.12	4.72	4.42																			5.97								
8	5.27	4.82	5.05													4.77	4.12	4.45												
9				3.05	3.17	3.11																			6.68	2.38	4.53			
10							4.73	3.18	3.96				3.58		3.58				4.58	3.41	4.00									
11	4.93	4.39	4.66																5.57	5.36	5.47									
12	4.03	3.95	3.99	5.02	4.39	4.71													6.48											
13																3.62	3.31	3.47	6.95											
14																3.58	3.69	3.63												
15	4.10	3.29	3.70				4.92	3.63	4.28							3.62	3.44	3.53												
16				3.79	3.18	3.49							5.16		5.16													6.03		6.03
17																			7.37	5.90	6.63									
18	3.85	3.87	3.86																8.17	4.78	6.48					3.31				
19				3.70	3.32	3.51										3.95	3.32	3.63	6.12	3.45	4.78	3.48	3.39	3.44	0.46					
20	3.92	3.65	3.79													3.59	3.09	3.34	5.92	3.47	4.69					3.62				
21																3.43	2.66	3.05								5.74				
22	3.93	3.67	3.80													3.72	3.55	3.64												
23							6.21	4.90	5.56																					
24																						4.73	0.70	2.72						
25				3.27	3.12	3.20																								
26	3.89	2.94	3.42													5.50	3.39	4.45	3.54											
27																4.60		4.60												
28																3.15	2.71	2.93												
29	4.03	3.26	3.65													4.13	2.98	3.56												
30							4.55	4.65	4.60																					
31																				2.75										
m			3.96			3.54			4.45			7.16			4.37			3.69			4.93			3.69			4.25			5.84

Accumulation period daily Ca^{2+} concentrations in the Oberaar meltwaters (1999-2001)

Date	mg/l
11/11/99	9.15
13/1/00	12.17
12/3/00	12.38
25/4/00	9.00
5/12/00	10.98
18/1/01	12.56
6/3/01	13.48
1/5/01	10.42
m	11.27

Mean daily Ca concentrations

Month	n	mg/l	± (1 sigma)
January	2	12.40	
February	0		
March	2	12.90	
April	1	9.00	
May	3	6.39	3.58
June	12	3.69	0.54
July	19	4.37	0.97
August	10	3.59	0.69
September	7	4.40	0.59
October	3	6.28	0.79
November	1	9.15	
December	1	10.98	
	Abl. 10:00	**Abl.** 17:00	**Accu.**
Mean	4.56	3.79	11.27
±	1.31	1.23	1.74
n	58	58	7



Ablation period Mg^{2+} (mg/l) at maximum and minimum discharge in the Rhône meltwaters (1999-2001)

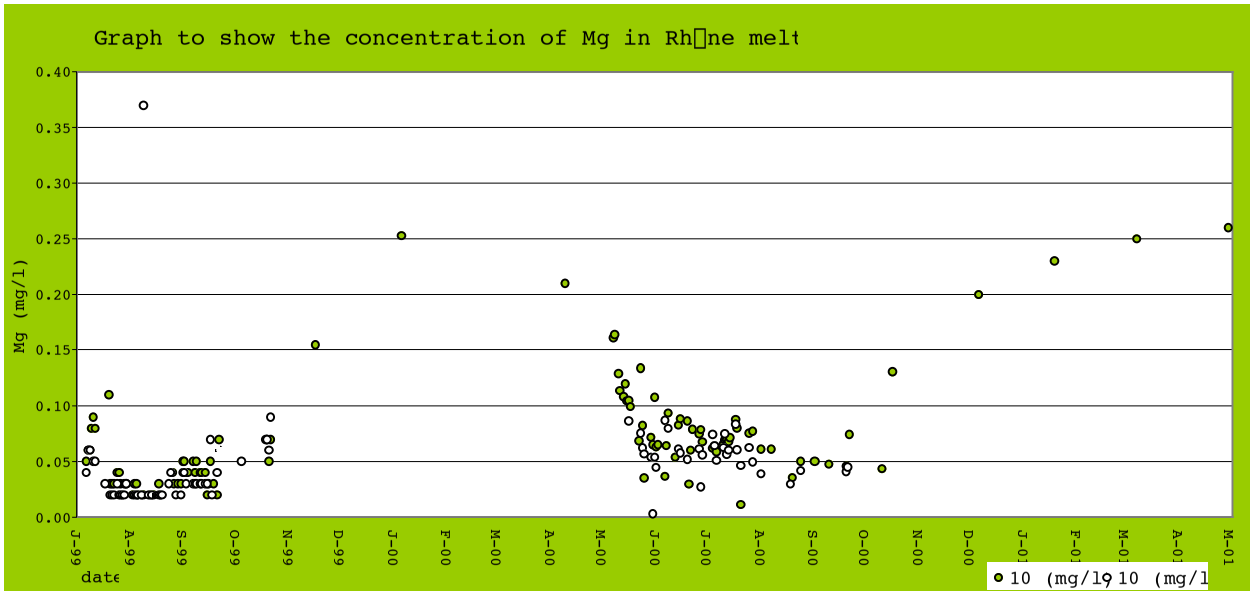
	07_99			08_99			09_99			10_99			05_00			06_00			07_00			08_00			09_00			10_00		
Date	10	17	daily	10	17	daily	10	17	daily	10	17	daily	10	17	daily	10	17	daily	10	17	daily	10	17	daily	10	17	daily	10	17	daily
1							0.05	0.04	0.05							0.06	0.04	0.05				0.06	0.04	0.05	0.05					
2				0.02		0.02	0.04	0.03	0.04							0.07														
3				0.03	0.02	0.03	0.04		0.04																					
4				0.03	0.02	0.03					0.05								0.06	0.07	0.07									
5				0.02	0.02	0.02													0.06	0.06	0.06									
6	0.05	0.04	0.05				0.05	0.03	0.04							0.04	0.09	0.06	0.06	0.05	0.06									
7	0.06	0.06	0.06	0.02	0.02	0.02	0.04	0.03	0.04				0.16		0.16	0.06		0.06				0.06								
8	0.06	0.06	0.06	0.02	0.37	0.20	0.05	0.03	0.04				0.16		0.16	0.09	0.08	0.09												
9	0.08		0.07																						0.05					
10	0.09	0.05	0.07				0.04	0.03	0.04				0.13		0.13				0.07	0.06	0.06							0.04		0.04
11	0.08	0.05	0.07		0.02	0.02	0.04	0.03	0.04				0.11		0.11				0.07	0.07	0.07									
12				0.02		0.02										0.05			0.07	0.06	0.06									
13				0.02	0.02	0.02	0.04	0.03	0.04				0.11		0.11				0.07	0.06	0.06									
14				0.02		0.02	0.02	0.03	0.03				0.12		0.12	0.08	0.06	0.07	0.07											
15							0.03		0.03				0.10		0.10	0.09	0.06	0.07												
16							0.05	0.07	0.06				0.10	0.09	0.10													0.13		0.13
17		0.03	0.04	0.03	0.02	0.03		0.02	0.01				0.10		0.10				0.09	0.08	0.09									
18				0.02	0.02	0.02	0.03		0.03		0.07	0.07							0.08	0.06	0.07		0.03	0.03						
19	0.11		0.09		0.02	0.02				0.07	0.07	0.07				0.09	0.05	0.07				0.04			0.05	0.04	0.04			
20	0.03	0.02	0.03				0.02	0.04	0.03	0.05	0.06	0.06				0.03			0.01	0.05	0.03					0.05	0.06			
21	0.03	0.02	0.03				0.07	0.06	0.07	0.07	0.09	0.08				0.06									0.07					
22	0.03	0.02	0.03										0.07		0.07	0.08														
23					0.03								0.13	0.08	0.10															
24	0.04	0.03	0.04		0.04								0.08	0.06	0.07							0.05	0.04	0.05						
25	0.04	0.02	0.03	0.04									0.04	0.06	0.05				0.08	0.06	0.07									
26	0.03	0.02	0.03	0.03												0.07	0.06	0.07												
27	0.02	0.02	0.02		0.02											0.08	0.03	0.05	0.08	0.05	0.06									
28	0.03	0.02	0.03	0.03												0.07	0.06	0.06												
29	0.03	0.03	0.03										0.07	0.05	0.06															
30				0.03	0.02	0.03							0.07	0.00	0.03															
31				0.05	0.04	0.05							0.11	0.05	0.08															
m			0.04			0.03			0.04			0.07			0.10			0.07			0.06			0.04			0.05			0.09

Accumulation period daily Mg^{2+} concentrations in the Rhône meltwaters (1999-2001)

Date	(mg/l)
16/11/99	0.15
5/12/00	0.20
5/1/00	0.25
18/1/01	0.23
7/3/01	0.25
9/4/00	0.21
29/4/01	0.26
m	0.22

Mean daily Mg concentrations

Month	n	mg/l	± (1 sigma)
January	2	0.20	
February	0		
March	1	0.30	
April	2	0.24	
May	16	0.10	0.04
June	10	0.07	0.01
July	29	0.05	0.02
August	18	0.04	0.04
September	18	0.04	0.01
October	7	0.07	0.03
November	1	0.15	
December	1	0.20	
	Abl. 10:00	**Abl.** 17:00	**Accu.**
Mean	0.06	0.05	11.27
±	0.03	0.04	0.04
n	104	81	7



Ablation period Mg^{2+} (mg/l) at minimum and maximum discharge in the Oberaar meltwaters (1999-2001)

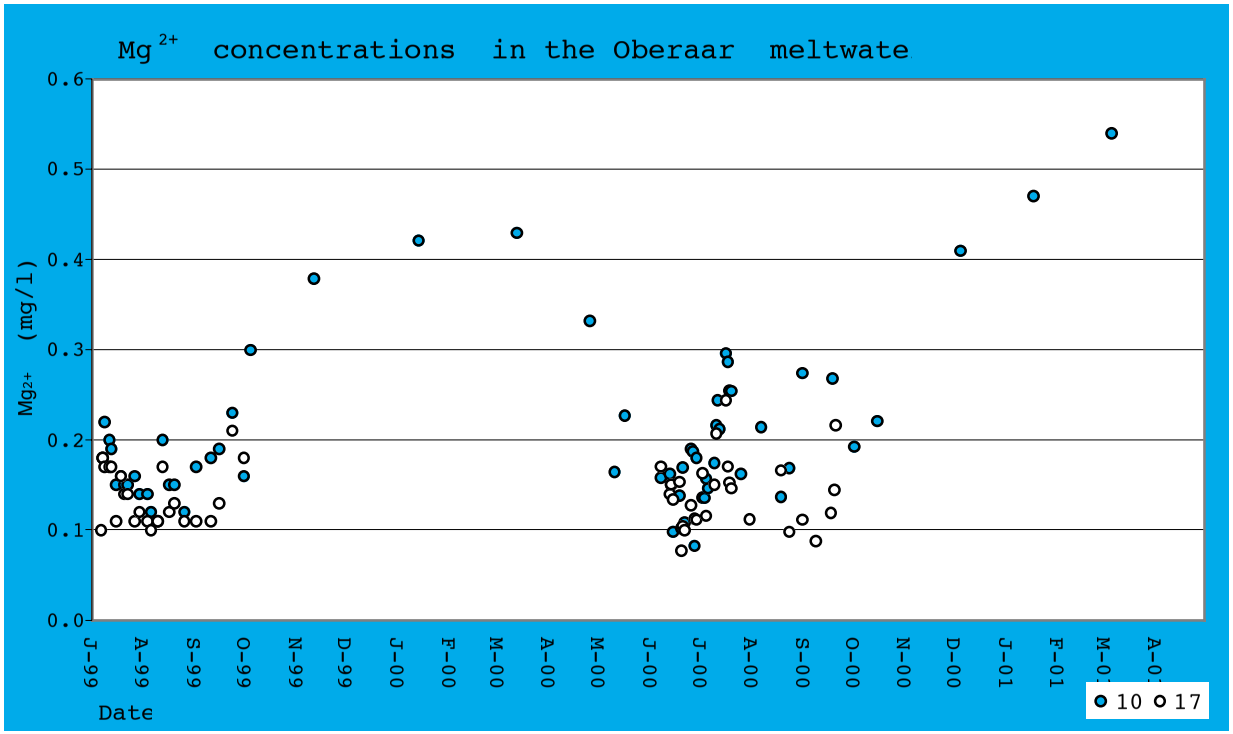
	07_99			08_99			09_99			10_99			05_00			06_00			07_00			08_00			09_00			10_00		
Date	10	17	daily	10	17	daily	10	17	daily	10	17	daily	10	17	daily	10	17	daily	10	17	daily	10	17	daily	10	17	daily	10	17	daily
1							0.17	0.11	0.14																0.27	0.11	0.19			
2																												0.19		0.19
3				0.14	0.11	0.13													0.14	0.16	0.15									
4										0.30		0.30							0.14											
5				0.12	0.10	0.11													0.16	0.12	0.14									
6		0.10	0.10																0.15		0.15									
7	0.18	0.18	0.18																			0.21								
8	0.22	0.17	0.20													0.16	0.17	0.16												
9				0.11	0.11	0.11																				0.09	0.09			
10							0.18	0.11	0.15				0.16		0.16				0.17	0.15	0.16									
11	0.20	0.17	0.19																0.22	0.21	0.21									
12	0.19	0.17	0.18	0.20	*0.17*	0.19													0.24											
13																0.16	0.14	0.15	0.21											
14																0.15	0.15	0.15												
15	0.15	0.11	0.13				0.19	0.13	0.16							0.10	0.13	0.12												
16				0.15	0.12	0.14							0.23		0.23													0.22		0.22
17																			0.30	0.24	0.27									
18	0.16	0.16	0.16																0.29	0.17	0.23					0.12				
19				0.15	0.13	0.14										0.14	0.15	0.15	0.25	0.15	0.20	0.14	0.17	0.15	0.27					
20	0.15	0.14	0.15													0.10	0.08	0.09	0.25	0.15	0.20					0.14				
21																0.17	0.10	0.14								0.22				
22	0.15	0.14	0.15													0.11	0.10	0.10												
23							0.23	0.21	0.22																					
24																						0.17	0.10	0.13						
25				0.12	0.11	0.12																								
26	0.16	0.11	0.14													0.19	0.13	0.16	0.16											
27																0.19														
28																0.08	0.11	0.10												
29	0.14	0.12	0.13													0.18	0.11	0.15												
30							0.16	0.18	0.17																					
31																				0.11										
m			0.15			0.13			0.17			0.30			0.20			0.13			0.19			0.14			0.14			0.21

Accumulation period daily Mg^{2+} concentrations in the Oberaar meltwaters (1999-2001)

Date	(mg/l)
11/11/99	0.38
13/1/00	0.42
12/3/00	0.43
25/4/00	0.33
5/12/00	0.41
18/1/01	0.47
6/3/01	0.54
1/5/01	0.42
m	0.43

Mean daily Mg concentrations

Month	n	mg/l	± (1 sigma)
January	2	0.45	
February	0		
March	2	0.49	
April	1	0.33	
May	3	0.27	0.13
June	11	0.13	0.03
July	20	0.17	0.04
August	9	0.13	0.02
September	7	0.16	0.04
October	3	0.24	0.06
November	1	0.38	
December	1	0.41	
	Abl. 10:00	**Abl.** 17:00	**Accu.**
Mean	0.18	0.2	0.43
±	0.05	0.39	0.07
n	57	55	7



Ablation period Na^+ (mg/l) at maximum and minimum discharge in the Rhône meltwaters (1999-2001)

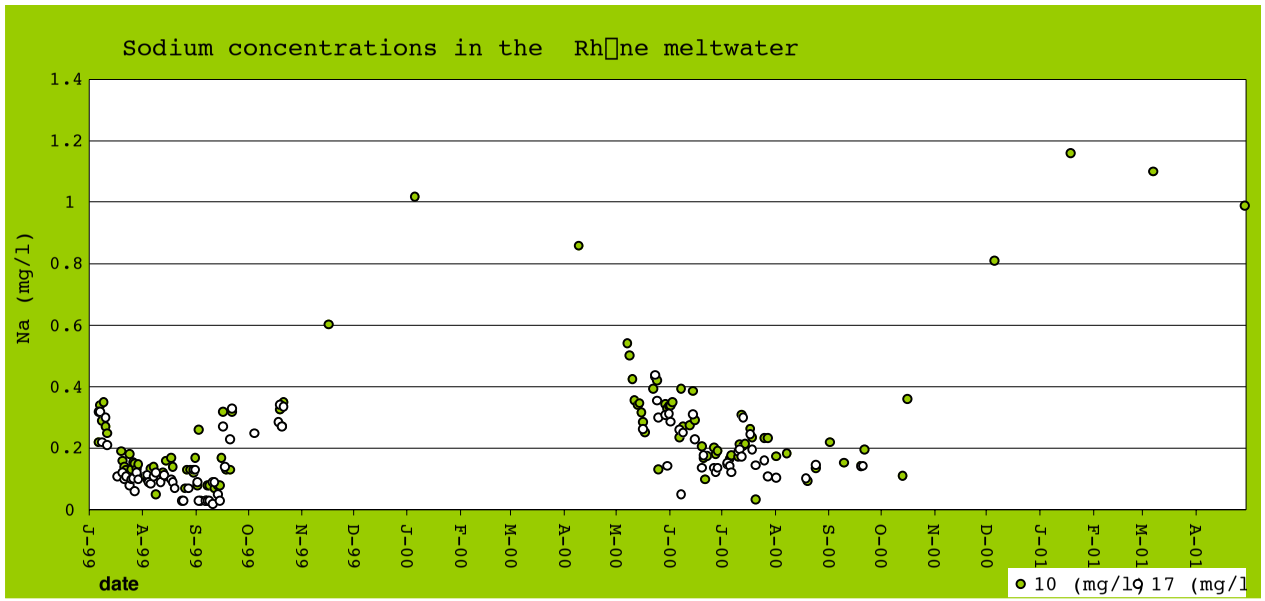
	07_99			08_99			09_99			10_99			05_00			06_00			07_00			08_00			09_00			10_00		
Date	10	17	daily	10	17	daily	10	17	daily	10	17	daily	10	17	daily	10	17	daily	10	17	daily	10	17	daily	10	17	daily	10	17	daily
1							0.08	0.09	0.09							0.34	0.29	0.31				0.17	0.10	0.14	0.22					
2				0.11		0.11	0.26	0.03	0.15							0.35														
3				0.10	0.11	0.11	0.03																							
4				0.10	0.09	0.10					0.25								0.15	0.15	0.15									
5				0.13	0.08	0.11													0.17	0.14	0.15									
6	0.22	0.32	0.27				0.03	0.03	0.03							0.24	0.26	0.25	0.18	0.12	0.15									
7	0.34	0.32	0.33	0.14	0.11	0.12	0.08	0.03	0.06				0.54		0.54	0.39	0.05	0.22				0.18								
8	0.29	0.22	0.26	0.05	0.12	0.09	0.08	0.03	0.06				0.50		0.50	0.27	0.25	0.26												
9	0.35		0.34																						0.15					
10	0.27	0.30	0.29				0.09	0.02	0.06				0.42		0.42				0.17	0.19	0.18							0.11		0.11
11	0.25	0.21	0.23		0.09	0.11	0.07	0.09	0.08				0.36		0.36				0.21	0.20	0.20									
12				0.12		0.12										0.28			0.31	0.17	0.24									
13				0.11	0.11	0.11	0.08	0.05	0.07				0.34		0.34				0.21	0.30	0.25									
14				0.16		0.14	0.08	0.03	0.06				0.35		0.35	0.39	0.31	0.35	0.22											
15							0.17						0.32		0.32	0.29	0.23	0.26												
16							0.32	0.27	0.30				0.28	0.26	0.27													0.36		0.36
17		0.11	0.12	0.17	0.10	0.14		0.14					0.25		0.25				0.26	0.25	0.26									
18				0.14	0.09	0.12	0.13				0.28	0.28							0.24	0.20	0.22		0.10	0.10						
19	0.19		0.15		0.07	0.11				0.33	0.34	0.33				0.21	0.14	0.17				0.09			0.14	0.14	0.14			
20	0.16	0.12	0.14				0.13	0.23	0.18	0.27	0.27	0.27				0.17	0.18	0.17	0.03	0.15	0.09					0.14	0.17			
21	0.14	0.10	0.12				0.32	0.33	0.33	0.35	0.33	0.34				0.10									0.20					
22	0.13	0.11	0.12										0.39		0.39	0.18														
23					0.03								0.43	0.44	0.44															
24	0.18	0.08	0.13		0.03								0.42	0.35	0.39							0.13	0.15	0.14						
25	0.13	0.10	0.12	0.07									0.13	0.30	0.22				0.23	0.16	0.20									
26	0.15	0.10	0.13	0.13												0.20	0.14	0.17												
27	0.15	0.06	0.11		0.07											0.18	0.12	0.15	0.23	0.11	0.17									
28	0.13	0.12	0.13	0.13												0.19	0.14	0.16												
29	0.15	0.10	0.12										0.34	0.31	0.33															
30				0.12	0.13	0.13							0.33	0.14	0.24															
31				0.17	0.13	0.15							0.34	0.31	0.33															
m			0.2			0.1			0.1			0.3			0.36			0.23			0.19			0.13			0.16			0.24

Ablation period daily Na^+ (mg/l) in the Rhône meltwaters (1999-2001)

Date	(mg/l)
16/11/99	0.60
5/12/00	0.81
5/1/00	1.02
18/1/01	1.16
7/3/99	1.10
9/4/00	0.86
29/4/01	0.99
m	0.93

Mean daily Na concentrations

Month	n	mg/l	± (1 sigma)
January	2	1.09	
February	0		
March	1	1.10	
April	2	0.93	
May	16	0.35	0.09
June	11	0.23	0.07
July	29	0.18	0.07
August	18	0.12	0.07
September	14	0.12	0.02
October	8	0.24	0.09
November	1	0.60	0.13
December	1	0.81	
	Abl. 10:00	**Abl.** 17:00	**Accu.**
Mean	0.21	0.16	0.93
±	0.11	0.10	0.19
n	104.00	83.00	7.00



Ablation period Na^+ (mg/l) at maximum and minimum discharge in the Oberaar meltwaters (1999-2001)

	07_99			08_99			09_99			10_99			05_00			06_00			07_00			08_00			09_00			10_00		
Date	10	17	daily	10	17	daily	10	17	daily	10	17	daily	10	17	daily	10	17	daily	10	17	daily	10	17	daily	10	17	daily	10	17	daily
1							0.22	0.12	0.17																0.24	0.18	0.21			
2																												0.39		0.39
3				0.17	0.15	0.16													0.19	0.2	0.2									
4										0.40		0.40							0.23											
5				0.15	0.14	0.15													0.21	0.14	0.17									
6		0.31	0.31																0.20		0.20		0.23	0.26						
7	0.28	0.20	0.24																			0.28								
8	0.29	0.40	0.35													0.24	0.25	0.24												
9				0.15	0.13	0.14																			0.02	0.13	0.07			
10							0.24	0.15	0.20				0.37		0.37				0.24	0.21	0.23									
11	0.36	0.38	0.37																0.29	0.29	0.29									
12	0.33	0.23	0.28	0.23	0.20	0.22													0.35											
13																0.22	0.27	0.24	0.36											
14																0.22	0.22	0.22												
15	0.06	0.11	0.09				0.22	0.17	0.20							0.19	0.19	0.19												
16				0.20	0.17	0.19							0.37		0.37													0.37		0.37
17																			0.40	0.34	0.37									
18	0.19	0.19	0.19																0.53	0.39	0.46					0.16				
19				0.18	0.16	0.17										0.24	0.20	0.22	0.34	0.19	0.26	0.15	0.15	0.15	0.04					
20	0.17	0.17	0.17													0.20	0.16	0.18	0.34	0.18	0.26					0.22				
21																0.20	0.17	0.19								0.27				
22	0.18	0.17	0.18													0.18	0.17	0.18												
23							0.36	0.27	0.32																					
24																						0.20	0.06	0.13						
25				0.13	0.12	0.13																								
26	0.32	0.14	0.23													0.40	0.17	0.28	0.18											
27																0.23														
28																0.15	0.17	0.16												
29	0.17	0.16	0.17													0.24	0.14	0.19												
30							0.29	0.24	0.27																					
31																				0.15										
m			0.2			0.2			0.2			0.4			0.37			0.21			0.27			0.18			0.14			0.38

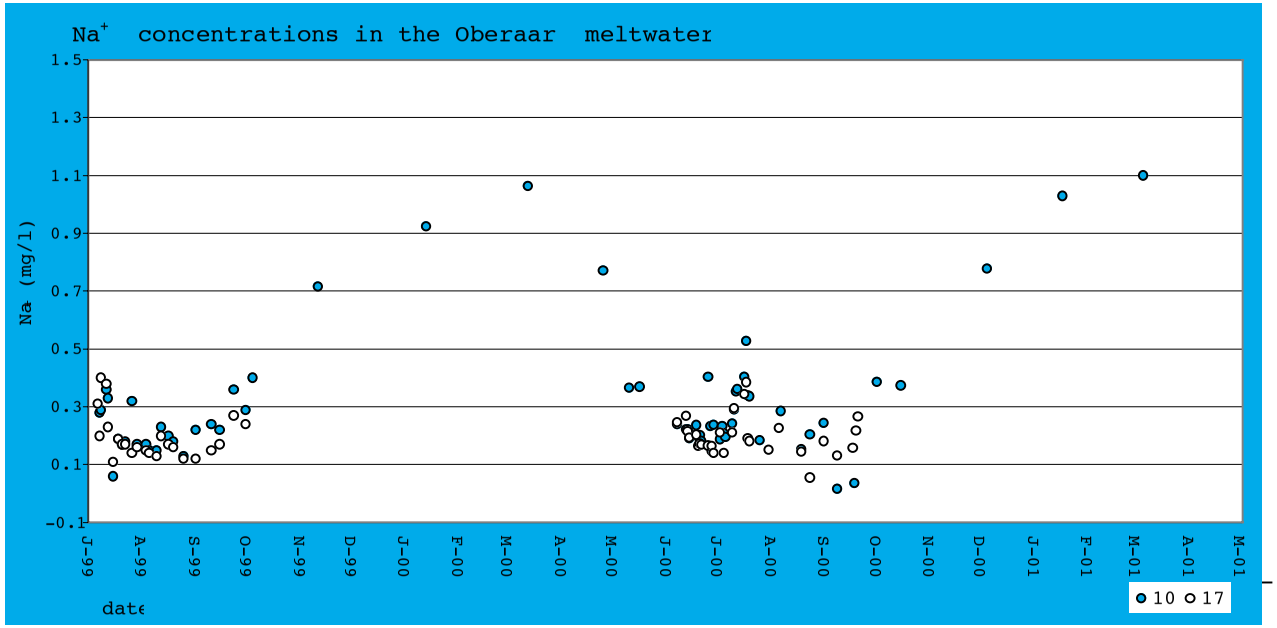
Accumulation period daily Na^+ concentrations in the Oberaar meltwaters (1999-2001)

Date	(mg/l)
11/11/99	0.72
13/1/00	0.93
12/3/00	1.06
25/4/00	0.77
5/12/00	0.78
18/1/01	1.03
6/3/01	1.10
1/5/01	1.02
m	0.93

Mean daily Na concentrations

Month	n	mg/l	± (1 sigma)
January	2	0.98	
February	0		
March	2	1.08	
April	1	0.33	
May	3	0.59	0.38
June	11	0.21	0.04
July	20	0.25	0.09
August	10	0.17	0.04
September	7	0.20	0.08
October	3	0.39	0.01
November	1	0.38	
December	1	0.41	

	Abl. 10:00	**Abl.** 17:00	**Accu.**
Mean	0.25	0.26	0.93
±	0.10	0.38	0.16
n	58	56	7



Ablation period K^+ (mg/l) at maximum and minimum discharge in the Rhône meltwaters (99-01)

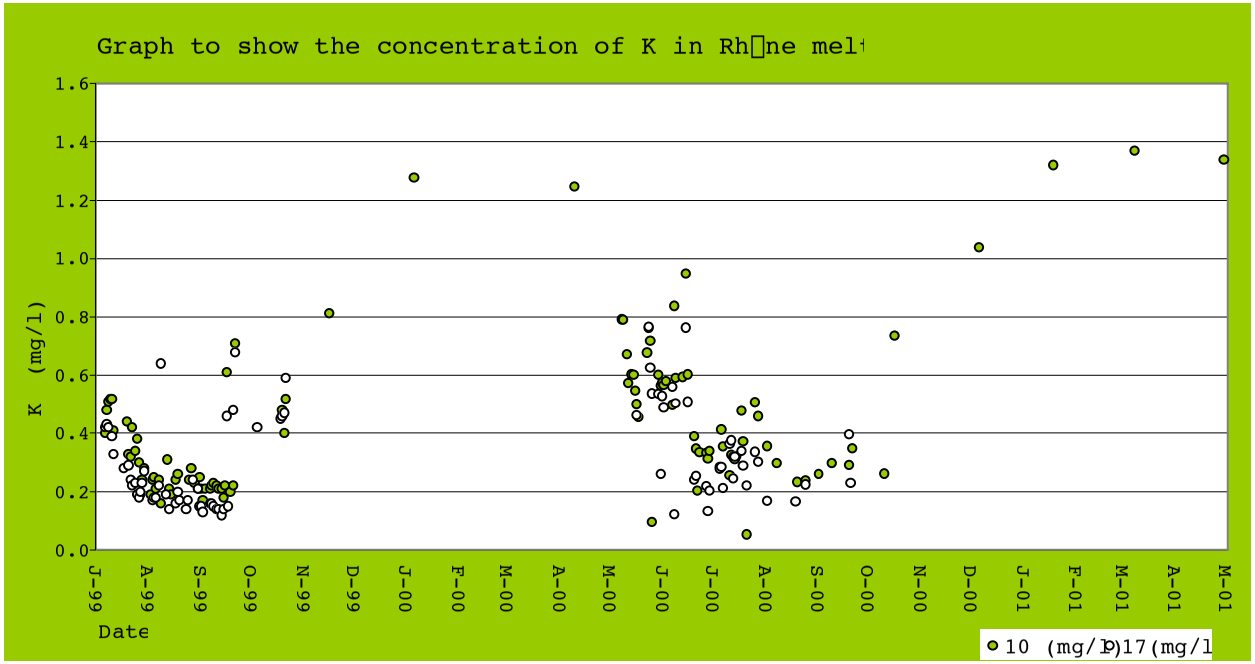
	07_99			08_99			09_99			10_99			05_00			06_00			07_00			08_00			09_00			10_00		
Date	10	17	daily	10	17	daily	10	17	daily	10	17	daily	10	17	daily	10	17	daily	10	17	daily	10	17	daily	10	17	daily	10	17	daily
1							0.21	0.15	0.18							0.57	0.49	0.53				0.36	0.17	0.26	0.26					
2				0.19		0.19	0.17	0.13	0.15							0.58														
3				0.24	0.17	0.21	0.21																							
4				0.25	0.18	0.22					0.42	0.42							0.28	0.28	0.28									
5				0.21	0.18	0.20													0.41	0.28	0.35									
6	0.40	0.42	0.27				0.21	0.16	0.19							0.50	0.56	0.53	0.35	0.21	0.28									
7	0.48	0.43	0.33	0.24	0.22	0.23	0.22	0.16	0.19				0.79		0.79	0.84	0.12	0.48				0.30								
8	0.51	0.42	0.26	0.16	0.64	0.40	0.23	0.15	0.19				0.79		0.79	0.59	0.50	0.55												
9	0.52		0.34																						0.30					
10	0.52	0.39	0.29				0.22	0.14	0.18				0.67		0.42				0.26	0.36	0.31							0.26		0.26
11	0.41	0.33	0.23		0.19	0.26	0.21	0.14	0.18				0.57		0.57				0.33	0.37	0.35									
12				0.31		0.24										0.59			0.32	0.25	0.28									
13				0.21	0.14	0.18	0.21	0.12	0.17				0.60		0.60				0.31	0.32	0.32									
14				0.19		0.15	0.18	0.14	0.16				0.60		0.60	0.95	0.76	0.86	0.32											
15							0.22						0.55		0.55	0.60	0.51	0.56												
16							0.61	0.46	0.54				0.50	0.46	0.48													0.74		0.74
17		0.28	0.12	0.24	0.16	0.20		0.15					0.45		0.45				0.48	0.34	0.41									
18				0.26	0.20	0.23	0.20				0.45	0.45							0.37	0.29	0.33		0.17	0.20						
19	0.44		0.15		0.17					0.48	0.46	0.47				0.39	0.24	0.32				0.23			0.29	0.40	0.34			
20	0.33	0.29	0.14				0.22	0.48	0.35	0.40	0.47	0.44				0.35	0.25	0.30	0.05	0.22	0.14					0.23	0.29			
21	0.32	0.24	0.12				0.71	0.68	0.70	0.52	0.59	0.56				0.20									0.35					
22	0.42	0.22	0.12										0.68		0.68	0.33														
23					0.14								0.76	0.77	0.76															
24	0.34	0.23	0.13		0.17								0.72	0.63	0.67							0.24	0.22	0.23						
25	0.38	0.19	0.12	0.24									0.10	0.54	0.32				0.51	0.34	0.42									
26	0.30	0.18	0.13	0.28												0.33	0.22	0.28												
27	0.19	0.20	0.11		0.24											0.31	0.13	0.22	0.46	0.30	0.38									
28	0.24	0.23	0.13	0.23												0.34	0.20	0.27												
29	0.28	0.27	0.12										0.60	0.53	0.57															
30				0.21	0.21	0.21							0.56	0.26	0.41															
31				0.25	0.15	0.20							0.57	0.53	0.55															
m			0.18			0.22			0.26			0.47			0.58			0.44			0.32			0.23			0.32			0.50

Accumulation period daily K^+ concentrations in the Rhône meltwaters (1999-2001)

Date	(mg/l)
16/11/99	0.81
5/12/00	1.04
5/1/00	1.28
18/1/01	1.32
7/3/01	1.37
9/4/00	1.25
29/4/01	1.34
m	1.20

Mean daily K concentrations

Month	n	mg/l	± (1 sigma)
January	2	1.30	
February	0		
March	1	1.40	
April	2	1.30	
May	16	0.58	0.14
June	11	0.44	0.19
July	29	0.24	0.10
August	17	0.22	0.05
September	14	0.27	0.16
October	8	0.42	0.21
November	1	0.81	
December	1	1.04	
	Abl. 10:00	**Abl.** 17:00	**Accu.**
Mean	0.38	0.31	1.20
±	0.18	0.16	0.20
n	104	83	7



Ablation period K^+ (mg/l) at minimum and maximum discharge in the Oberaar meltwaters (1999-2001)

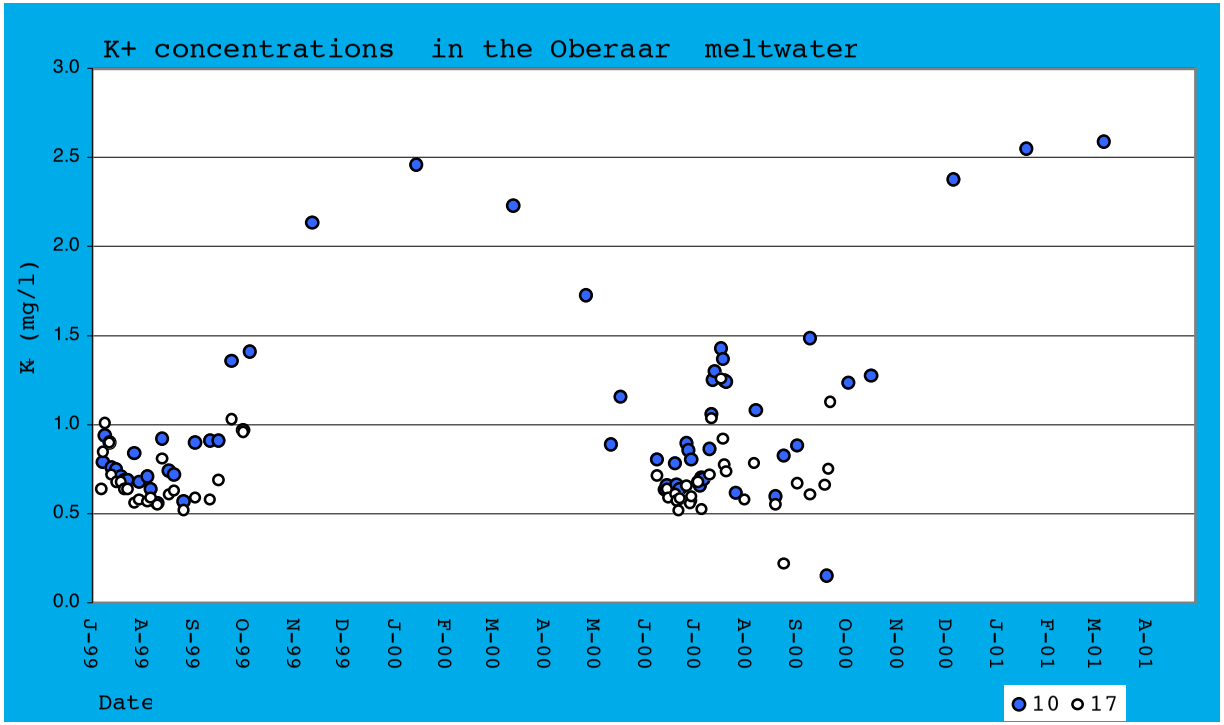
	07_99			08_99			09_99			10_99			05_00			06_00			07_00			08_00			09_00			10_00		
Date	10	17	daily	10	17	daily	10	17	daily	10	17	daily	10	17	daily	10	17	daily	10	17	daily	10	17	daily	10	17	daily	10	17	daily
1							0.90	0.59	0.75																0.88	0.67	0.78			
2																												1.23		1.23
3				0.71	0.57	0.64													0.68	0.68	0.68									
4										1.41		1.41							0.66											
5				0.64	0.59	0.62													0.70	0.53	0.62									
6		0.64	0.64																0.69		0.69		0.78	0.93						
7	0.79	0.85	0.82																			1.08								
8	0.94	1.01	0.98													0.81	0.71	0.76												
9				0.56	0.55	0.56																			1.49	0.61	1.05			
10							0.91	0.58	0.75				0.89		0.89				0.86	0.72	0.79									
11	0.90	0.90	0.90																1.06	1.04	1.05									
12	0.76	0.72	0.74	0.92	*0.81*	0.87													1.25											
13																0.64	0.63	0.63	1.30											
14																0.66	0.64	0.65												
15	0.75	0.68	0.72				0.91	0.69	0.80							0.63	0.59	0.61												
16				0.74	0.61	0.68							1.16		1.16													1.28		1.28
17																			1.43	1.26	1.34									
18	0.71	0.68	0.70																1.37	0.92	1.14					0.66				
19				0.72	0.63	0.68										0.78	0.61	0.70	1.25	0.78	1.01	0.60	0.55	0.58	0.15					
20	0.69	0.64	0.67													0.66	0.58	0.62	1.24	0.74	0.99					0.75				
21																0.59	0.52	0.55								1.13				
22	0.69	0.64	0.67													0.64	0.59	0.61												
23							1.36	1.03	1.20																					
24																						0.83	0.22	0.52						
25				0.57	0.52	0.55																								
26	0.84	0.56	0.70													0.90	0.66	0.78	0.62											
27																0.86														
28																0.57	0.56	0.57												
29	0.68	0.58	0.63													0.80	0.60	0.70												
30							0.97	0.96	0.97																					
31																				0.58										
m			0.74			0.65			0.89			1.41			1.02			0.65			0.92			0.68			0.91			1.26

Accumulation period daily K^+ concentrations in the Oberaar meltwaters (1999-2001)

Date	(mg/l)
11/11/99	2.14
13/1/00	2.46
12/3/00	2.23
25/4/00	1.73
5/12/00	2.38
18/1/01	2.55
6/3/01	2.59
1/5/01	2.03
m	2.26

Mean daily K concentrations

Month	n	mg/l	± (1 sigma)
January	2	2.51	
February	0		
March	2	2.41	
April	1	1.73	
May	3	1.36	0.60
June	11	0.65	0.07
July	20	0.82	0.20
August	10	0.66	0.14
September	7	0.90	0.18
October	3	1.31	0.09
November	1	2.14	
December	1	2.38	
	Abl. 10:00	**Abl.** 17:00	**Accu.**
Mean	0.87	0.76	2.30
±	0.27	0.39	0.30
n	58	56	7



Date	Ca^{2+} (mg/g)	K^{+} (mg/g)	Mg^{2+} (mg/g)	Date	Ca^{2+} (mg/g)	K^{+} (mg/g)	Mg^{2+} (mg/g)
1999				2000			
07-Jul-99	0.06	0.09	0.03	6-Jan-00	0.34	0.13	0.02
07-Jul-99	0.18	0.02	0.01	17-May-00	0.54	0.23	0.03
07-Jul-99	0.08	0.07	0.03	17-May-00	0.18	0.06	0.01
07-Jul-99	0.19	0.02	0.01	25-May-00	0.83	0.42	0.05
12-Jul-99	0.17	0.08	0.05	1-Jun-00	0.68	0.28	0.03
12-Jul-99	0.58	0.15	0.02	2-Jun-00	0.90	0.32	0.04
22-Jul-99	0.09	0.08	0.03	2-Jun-00	0.63	0.21	0.02
22-Jul-99	0.23	0.02	0.01	9-Jun-00	0.50	0.19	0.02
22-Jul-99	0.73	0.12	0.03	9-Jun-00	0.56	0.21	0.03
25-Jul-99	0.19	0.02	0.01	13-Jun-00	0.30	0.23	0.02
25-Jul-99	0.40	0.11	0.02	13-Jun-00	0.38	0.12	0.02
28-Jul-99	0.05	0.06	0.02	22-Jun-00	0.54	0.16	0.02
28-Jul-99	0.04	0.05	0.02	22-Jun-00	0.26	0.08	0.01
28-Jul-99	0.23	0.04	0.01	27-Jun-00	0.59	0.18	0.03
28-Jul-99	0.16	0.03	0.01	27-Jun-00	0.81	0.51	0.02
29-Jul-99	0.16	0.04	0.01	6-Jul-00	0.29	0.07	0.01
29-Jul-99	0.07	0.07	0.02	6-Jul-00	0.22	0.06	0.01
12-Aug-99	0.24	0.02	0.02	13-Jul-00	0.53	0.63	0.02
12-Aug-99	0.51	0.16	0.07	18-Jul-00	1.38	0.22	0.04
20-Aug-99	0.39	0.04	0.02	18-Jul-00	1.05	1.06	0.05
25-Aug-99	0.09	0.08	0.05	19-Aug-00	0.30	0.07	0.01
26-Aug-99	0.35	0.06	0.03	1-Sep-00	0.40	0.43	0.02
31-Aug-99	0.43	0.12	0.03	2-Sep-00	0.97	0.30	0.02
9-Sep-99	0.67	0.34	0.03				
09-Sep-99	0.50	0.12	0.04				
16-Sep-99	0.57	0.15	0.03				
17-Sep-99	1.39	1.74	0.02				
22-Sep-99	0.08	0.44	0.01				
22-Sep-99	0.69	0.30	0.05				
20-Oct-99	0.24	0.72	0.12				
21-Oct-99	1.85	1.91	0.01				
21-Oct-99	1.13	0.05	0.04				
21-Oct-99	1.14	0.13	0.03				
22-Oct-99	1.97	0.87	0.08				
22-Oct-99	2.16	2.21	0.01				

Date	Ca^{2+} (mg/g)	K^{+} (mg/g)	Mg^{2+} (mg/g)	Date	Ca^{2+} (mg/g)	K^{+} (mg/g)	Mg^{2+} (mg/g)
1999				2000			
7-Jul-99	1.31	0.05	0.01	11-May-00	0.55	0.06	0.01
8-Jul-99	14.41	0.64	0.11	14-Jun-00	1.55	0.05	0.01
12-Jul-99	2.22	0.02	0.04	14-Jun-00	1.06	0.07	0.01
15-Jul-99	0.65	0.01	0.01	29-Jun-00	1.26	0.07	0.02
15-Jul-99	1.78	0.01	0.04	29-Jun-00	0.86	0.05	0.01
22-Jul-99	2.03	0.02	0.06	29-Jun-00	0.65	0.03	0.00
30-Jul-99	1.72	0.12	0.03	29-Jun-00	0.22	0.03	0.00
30-Jul-99	2.18	0.37	0.04	29-Jun-00	1.49	0.08	0.01
5-Aug-99	2.61	0.02	0.11	29-Jun-00	1.23	0.09	0.02
5-Aug-99	1.89	0.00	0.02	30-Jun-00	1.49	0.12	0.02
12-Aug-99	1.22	0.02	0.03	30-Jun-00	1.60	0.10	0.03
12-Aug-99	2.34	0.02	0.04	30-Jun-00	1.45	0.07	0.02
19-Aug-99	1.16	0.03	0.03	30-Jun-00	0.87	0.07	0.01
25-Aug-99	1.31	0.02	0.03	30-Jun-00	1.03	0.07	0.01
25-Aug-99	1.62	0.01	0.02	30-Jun-00	0.53	0.04	0.01
1-Sep-99	3.07		0.08	7-Jul-00	1.31	0.05	0.01
1-Sep-99	2.54		0.05	8-Jul-00	14.41	0.64	0.11
10-Sep-99	3.08		0.07	18-Jul-00	0.93	0.24	0.01
11-Sep-99	1.04	0.04	0.01	18-Jul-00	1.43	0.40	0.02
11-Sep-99	1.04	0.04	0.01	20-Jul-00	0.81	0.05	0.01
15-Sep-99	2.15		0.06	30-Jul-00	1.72	0.12	0.03
15-Sep-99	2.60		0.06	30-Jul-00	2.18	0.37	0.04
15-Sep-99	1.43		0.03	20-Aug-00	1.65	0.08	0.02
23-Sep-99	2.41		0.04	20-Aug-00	1.14	0.04	0.01
30-Sep-99	1.70		0.04	10-Sep-00	1.43	0.08	0.02
30-Sep-99	1.61		0.04	10-Sep-00	0.73	0.03	0.01
1-Oct-99	0.83		0.03	21-Sep-00	0.79	0.07	0.01
4-Oct-99	2.30		0.02				

Ablation period Cl^- (mg/l) at minimum and maximum discharge in the Rhône meltwaters (1999-2001)

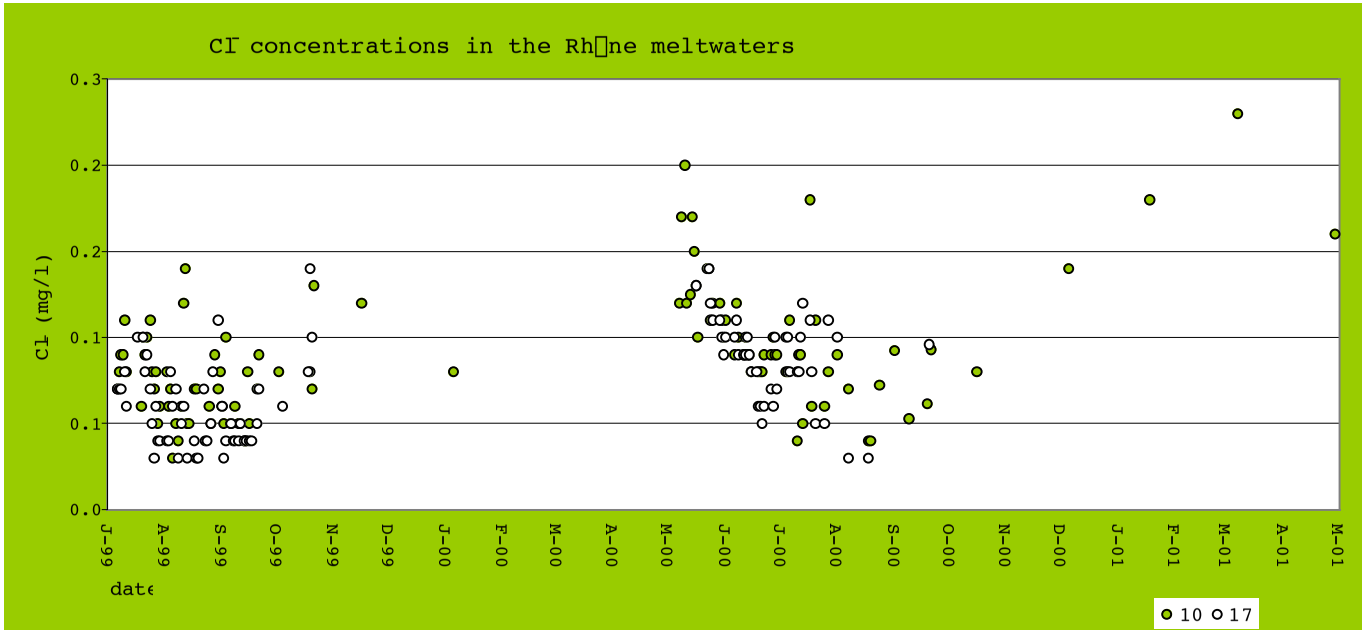
	07_99			08_99			09_99			10_99			05_00			06_00			07_00			08_00			09_00			10_00		
Date	10	17	daily	10	17	daily	10	17	daily	10	17	daily	10	17	daily	10	17	daily	10	17	daily	10	17	daily	10	17	daily	10	17	daily
1							0.06	0.06	0.06							0.11	0.10	0.11				0.09	0.10	0.10	0.09					
2				0.08	0.04	0.06	0.05	0.03	0.04	0.08		0.08																		
3				0.06	0.04	0.05	0.10	0.04	0.07																					
4				0.07	0.08	0.08					0.06	0.06							0.08	0.10	0.09									
5				0.03	0.06	0.05													0.08	0.10	0.09									
6	0.07	0.07	0.07				0.05	0.05	0.05							0.09	0.10	0.10	0.11	0.08	0.10									
7	0.08	0.07	0.08	0.05	0.07	0.06		0.04					0.12		0.12	0.12	0.11	0.12				0.07	0.03	0.05						
8	0.09	0.07	0.08	0.04	0.03	0.04	0.06	0.04	0.05				0.17		0.17	0.10	0.09	0.10												
9	0.09																								0.05					
10	0.11	0.08	0.10	0.06	0.05	0.06	0.05	0.04	0.05				0.20		0.20				0.04	0.08	0.06									
11	0.08	0.06	0.07	0.12	0.06	0.09	0.05	0.05	0.05				0.12		0.12	0.09	0.09	0.09	0.09	0.08	0.09									
12				0.14												0.10	0.09	0.10	0.09	0.10	0.10									
13				0.05	0.03	0.04	0.04	0.04	0.04				0.13		0.13	0.09	0.10	0.10	0.05	0.12	0.09									
14				0.05			0.04	0.04	0.04				0.17		0.17	0.09	0.09	0.09												
15							0.08						0.15		0.15	0.08	0.08	0.08												
16							0.05	0.04	0.05				0.13	0.13	0.13													0.08		0.08
17		0.10		0.07	0.04	0.06		0.04					0.10		0.10				0.18	0.11	0.15									
18				0.07	0.03	0.05					0.08	0.08					0.08		0.06	0.08	0.07	0.04	0.03	0.04						
19	0.06				0.03					0.08	0.14	0.11				0.08	0.06	0.07				0.04			0.06					
20	0.10	0.10	0.10				0.07	0.05	0.06	0.07	0.10	0.09				0.08	0.06	0.07	0.11	0.05	0.08					0.10	0.08			
21	0.09	0.08	0.09				0.09	0.07	0.08	0.13		0.13				0.08	0.05	0.07							0.09		0.09			
22	0.10	0.09	0.10		0.07								0.14		0.14	0.09	0.06	0.08												
23					0.04								0.14	0.14	0.14															
24	0.11	0.07	0.09		0.04								0.11	0.12	0.12							0.07								
25	0.08	0.05	0.07	0.06									0.12	0.11	0.12				0.06	0.05	0.06									
26	0.07	0.03	0.05	0.05	0.05	0.05										0.09	0.07	0.08												
27	0.08	0.06	0.07		0.08	0.09										0.10	0.06	0.08	0.08	0.11	0.10									
28	0.05	0.04	0.05	0.09												0.09	0.10	0.10												
29	0.06	0.04	0.05										0.12	0.11	0.12	0.09	0.07	0.08												
30				0.07	0.11	0.09							0.11	0.10	0.11															
31				0.08									0.10	0.09	0.10															
m			0.07			0.06			0.05			0.09			0.13			0.09			0.09			0.06			0.09			0.08

Accumulation period daily Cl^- concentrations in the Rhône meltwaters (1999-2001)

Date	(mg/l)
16/11/99	0.12
5/12/00	0.14
5/1/00	0.08
18/1/01	0.18
7/3/01	0.23
9/4/00	0.08
29/4/01	0.16
m	0.14

Mean daily Cl concentrations

Month	n	mg/l	± (1 sigma)
January	2	0.20	
February	0		
March	1	0.23	
April	2	0.12	
May	16	0.13	0.03
June	17	0.09	0.01
July	26	0.08	0.02
August	17	0.06	0.02
September	14	0.06	0.02
October	7	0.07	0.03
November	1	0.52	
December	1		
	Abl. 10:00	**Abl. 17:00**	**Accu.**
Mean	0.09	0.07	0.15
±	0.03	0.03	0.05
n	106	92	7



Ablation period Cl^- (mg/l) at minimum and maximum discharge in the Oberaar meltwaters (1999-2001)

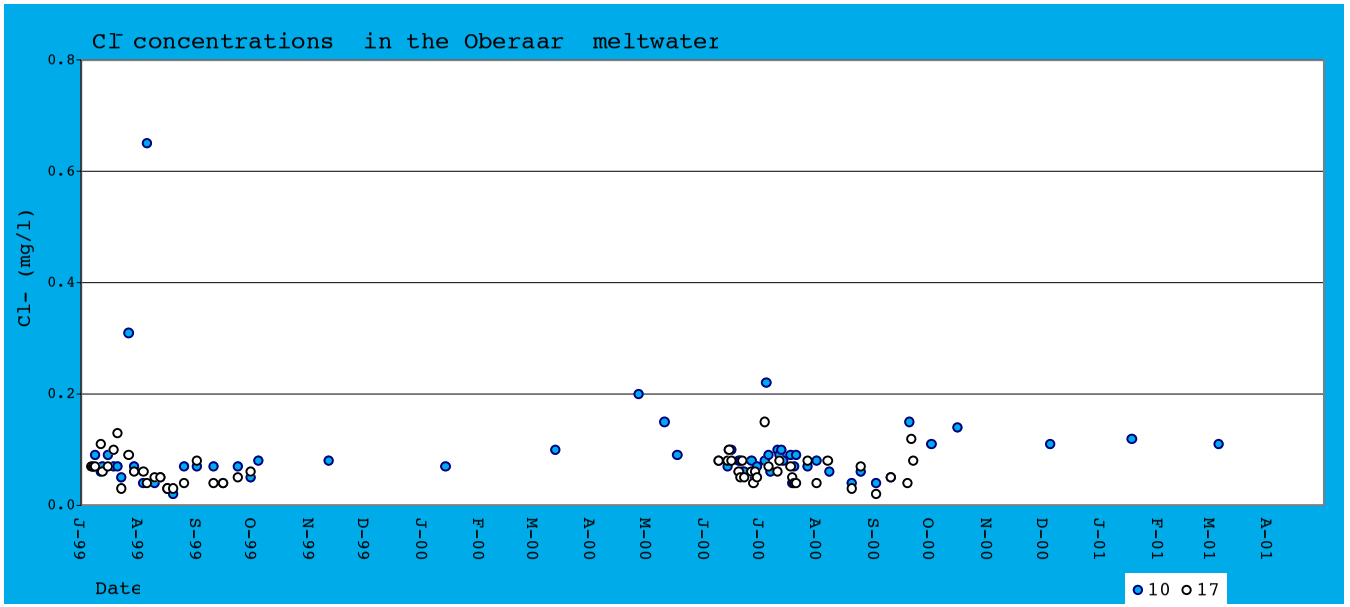
	07_99			08_99			09_99			10_99			05_00			06_00			07_00			08_00			09_00			10_00		
Date	10	17	daily	10	17	daily	10	17	daily	10	17	daily	10	17	daily	10	17	daily	10	17	daily	10	17	daily	10	17	daily	10	17	daily
1							0.07	0.08	0.08																0.04	0.02	0.03	0.11		0.11
2																														
3				0.04	0.06	0.05													0.08	0.2	0.1									
4										0.08		0.08							0.22		0.11									
5				0.65	0.04	0.35													0.09	0.07	0.08									
6		0.07	0.07																0.06		0.06		0.08	0.07						
7	0.07	0.07	0.07																			0.06								
8	0.09	0.07	0.08													0.08	0.08	0.08												
9				0.04	0.05	0.05																			0.05	0.05	0.05			
10							0.07	0.04	0.06				0.15		0.15				0.10	0.06	0.08									
11	0.06	0.11	0.09																0.09	0.08	0.09									
12	0.07	0.06	0.07	0.05	##	0.05													0.10		0.10									
13																0.07	0.08	0.08	0.08		0.08									
14																0.10	0.10	0.10												
15	0.09	0.07	0.08				0.04	0.04	0.04							0.10	0.08	0.09										0.14		0.14
16				0.03	0.03	0.03																								
17													0.09		0.09				0.09	0.07	0.08									
18	0.07	0.10	0.09																0.04	0.05	0.05					0.04	0.10			
19				0.02	0.03	0.03										0.08	0.06	0.07	0.07	0.04	0.06	0.04	0.03	0.04	0.15					
20	0.07	0.13	0.10													0.08	0.05	0.07	0.09	0.04	0.07					0.12	0.12			
21																0.06	0.08	0.07								0.08	0.08			
22	0.05	0.03	0.04													0.06	0.05	0.06												
23							0.07	0.05	0.06																					
24																						0.06	0.07	0.07						
25				0.07	0.04	0.06																								
26	0.31	0.09	0.20													0.08	0.06	0.07	0.07	0.08	0.08									
27																0.06	0.04	0.05												
28																0.05	0.06	0.06												
29	0.07	0.06	0.07													0.07	0.05	0.06												
30							0.05	0.06	0.06																					
31																			0.08	0.04	0.1									
m			0.09			0.09			0.06			0.08			0.12			0.07			0.08			0.06			0.08			0.13

ion period daily Cl^- concentrations in the Oberaar meltwaters (1999-2001)

(mg/l)
0.08
0.07
0.10
0.20
0.11
0.12
0.11
0.11
0.11

Cl^- concentrations

n	mg/l	± (1 sigma)
2	0.10	
0		
2	0.1	
1	0.20	
3	0.12	0.03
12	0.07	0.01
25	0.08	0.03
10	0.08	0.1
10	0.07	0.03
3	0.11	0.03
1	0.08	
1	0.11	
Abl.	**Abl.**	**Accu.**
10:00	17:00	
0.09	0.11	0.14
0.09	0.38	0.05
59	59	7



Ablation period NO_3^- (mg/l) at minimum and maximum discharge in the Rhône meltwaters (1999-2001)

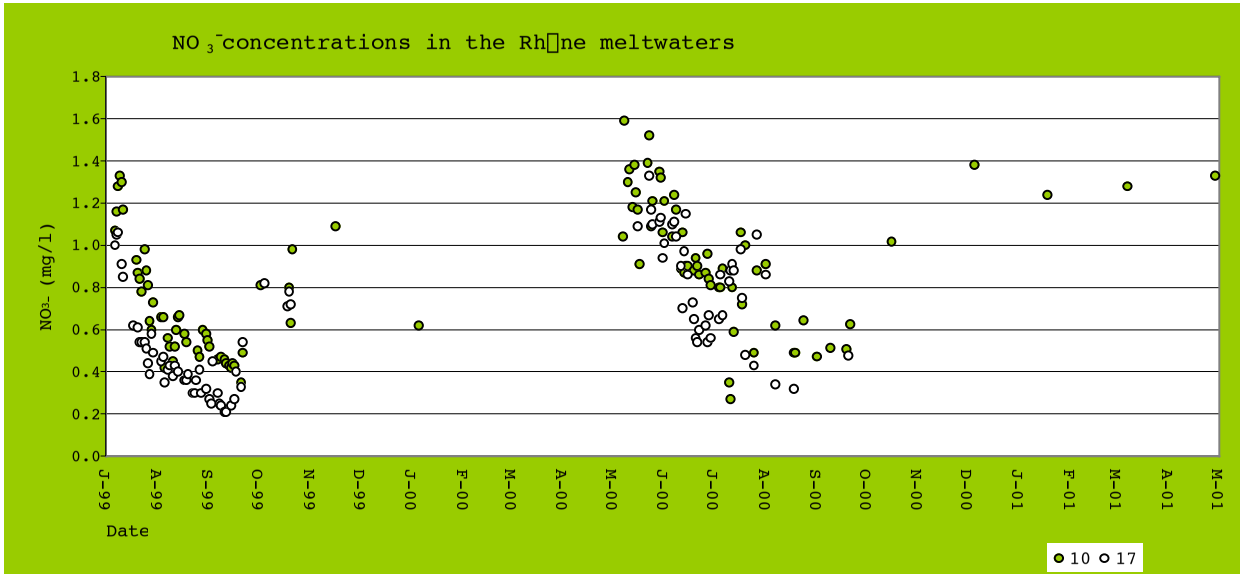
	07_99			08_99			09_99			10_99			05_00			06_00			07_00			08_00			09_00			10_00		
Date	10	17	daily	10	17	daily	10	17	daily	10	17	daily	10	17	daily	10	17	daily	10	17	daily	10	17	daily	10	17	daily	10	17	daily
1							0.52	0.27	0.40							1.21	1.01	1.11				0.91	0.86	0.89	0.47					
2								0.25		0.81		0.81																		
3				0.66	0.45	0.56		0.45																						
4				0.66	0.47	0.57					0.82	0.82							0.80	0.65	0.73									
5				0.42	0.35	0.39													0.80	0.86	0.83									
6	1.07	1.00	1.04				0.46	0.30	0.38							1.04	1.10	1.07	0.89	0.67	0.78									
7	1.16	1.05	1.11	0.56	0.41	0.49		0.25					1.04		1.04	1.24	1.11	1.18				0.62	0.34	0.48						
8	1.28	1.06	1.17	0.52	0.43	0.48	0.47	0.24	0.36				1.59		1.59	1.17	1.04	1.11												
9	1.33																								0.51					
10	1.30	0.91	1.11	0.45	0.38	0.42	0.46	0.21	0.34				1.30		1.30				0.35	0.83	0.59									
11	1.17	0.85	1.01	0.52	0.43	0.48	0.44	0.21	0.33				1.36		1.36	0.89	0.90	0.90	0.27	0.88	0.58									
12				0.60												1.06	0.70	0.88	0.80	0.91	0.86									
13				0.66	0.40	0.53	0.43						1.18		1.18	0.87	0.97	0.92	0.59	0.88	0.74									
14				0.67			0.42	0.24	0.33				1.38		1.38	0.90	1.15	1.03												
15							0.44						1.25		1.25	0.90	0.86	0.88												
16							0.43	0.27	0.35				1.17	1.09	1.13													1.02		1.02
17		0.62		0.58	0.36	0.47		0.40					0.91		0.91				1.06	0.98	1.02									
18				0.54	0.36	0.45					0.71	0.71					0.73		0.72	0.75	0.74	0.49	0.32	0.41						
19	0.93				0.39					0.80	0.78	0.79				0.88	0.65	0.77				0.49			0.51					
20	0.87	0.61	0.74				0.35	0.33	0.34	0.63	0.72	0.68				0.94	0.56	0.75	1.00	0.48	0.74					0.48	0.49			
21	0.84	0.54	0.69				0.49	0.54	0.52	0.98		0.98				0.90	0.54	0.72							0.62		0.55			
22	0.78	0.54	0.66		0.30								1.39		1.39	0.86	0.60	0.73												
23					0.30								1.52	1.33	1.43															
24	0.98	0.54	0.76		0.36								1.09	1.17	1.13							0.64								
25	0.88	0.51	0.70	0.50									1.21	1.10	1.16				0.49	0.43	0.46									
26	0.81	0.44	0.63	0.47	0.41	0.44										0.87	0.62	0.75												
27	0.64	0.39	0.52		0.30	0.45										0.96	0.54	0.75	0.88	1.05	0.97									
28	0.60	0.58	0.59	0.60												0.84	0.67	0.76												
29	0.73	0.49	0.61										1.35	1.11	1.23	0.81	0.56	0.69												
30				0.58	0.32	0.45							1.32	1.13	1.23															
31				0.55									1.06	0.94	1.00															
m			0.81			0.47			0.37			0.80			1.23			0.88			0.75			0.59			0.52			1.02

Ablation period NO_3^- concentrations in the Rhône meltwaters (1999-2001)

Date	mg/l
16/11/99	1.09
5/12/00	1.38
5/1/00	0.62
18/1/01	1.24
7/3/01	1.28
9/4/00	
29/4/01	1.33
m	1.16

Mean daily NO_3 concentrations

Month	n	mg/l	± (1 sigma)
January	2	1.30	
February	0		
March	0		
April	2	0.98	
May	16	1.23	0.17
June	17	0.88	0.16
July	26	0.78	0.20
August	16	0.49	0.12
September	11	0.40	0.08
October	6	0.83	0.14
November	1	1.09	
December	1	1.24	
	Abl. 10:00	**Abl.** 17:00	**Accu.**
Mean	0.82	0.63	1.16
±	0.31	0.29	0.28
n	103	90	6



Ablation period NO_3^- (mg/l) at minimum and maximum discharge in the Oberaar meltwaters (1999-2001)

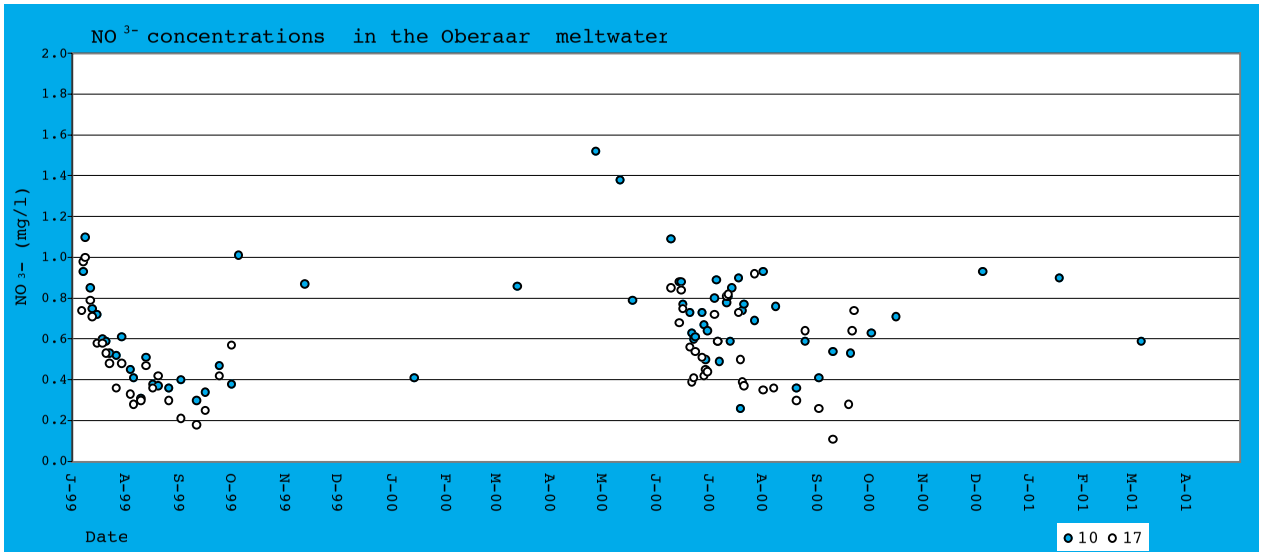
	07_99			08_99			09_99			10_99			05_00			06_00			07_00			08_00			09_00			10_00		
Date	10	17	daily	10	17	daily	10	17	daily	10	17	daily	10	17	daily	10	17	daily	10	17	daily	10	17	daily	10	17	daily	10	17	daily
1							0.40	0.21	0.31																0.41	0.26	0.34	0.63		0.63
2																														
3				0.45	0.33	0.39													0.80	0.72	0.76									
4										1.01		1.01							0.89		0.89									
5				0.41	0.28	0.35													0.59	0.59	0.59									
6		0.74	0.74																0.49		0.49		0.36	0.56						
7	0.93	0.98	0.96																			0.76								
8	1.10	1.00	1.05													1.09	0.85	0.97												
9				0.31	0.30	0.31																			0.54	0.11	0.33				
10							0.30	0.18	0.24				1.38		1.38				0.78	0.81	0.80									
11	0.85	0.79	0.82																0.81	0.82	0.82									
12	0.75	0.71	0.73	0.51	0.47	0.49													0.59		0.59									
13																0.88	0.68	0.78	0.85		0.85									
14																0.88	0.84	0.86												
15	0.72	0.58	0.65				0.34	0.25	0.30							0.77	0.75	0.76										0.71		0.71
16				0.38	0.36	0.37																								
17													0.79		0.79				0.90	0.73	0.82									
18	0.60	0.58	0.59																0.26	0.50	0.38					0.28	0.41			
19				0.37	0.42	0.40										0.73	0.56	0.65	0.74	0.39	0.57	0.36	0.30	0.33	0.53					
20	0.59	0.53	0.56													0.63	0.39	0.51	0.77	0.37	0.57					0.64	0.64			
21																0.60	0.41	0.51								0.74	0.74			
22	0.53	0.48	0.51													0.61	0.54	0.58												
23							0.47	0.42	0.45																					
24																						0.59	0.64	0.62						
25				0.36	0.30	0.33																								
26	0.52	0.36	0.44													0.73	0.51	0.62	0.69	0.92	0.81									
27																0.67	0.42	0.55												
28																0.50	0.45	0.48												
29	0.61	0.48	0.55													0.64	0.44	0.54												
30							0.38	0.57	0.48																					
31																			0.93	0.35	0.64									
m			0.69			0.38			0.35			1.01			1.09			0.65			0.68			0.50			0.49			0.67

Accumulation period daily NO_3^- concentrations in the Oberaar meltwaters (1999-2001)

Date	(mg/l)
11/11/99	0.87
13/1/00	0.41
12/3/00	0.86
25/4/00	1.52
5/12/00	0.93
18/1/01	0.90
6/3/01	0.59
1/5/01	1.11
m	0.90

Mean daily NO_3 concentrations

Month	n	mg/l	± (1 sigma)
January	2	0.70	
February	0		
March	2	0.70	
April	1	1.52	
May	3	1.09	0.30
June	12	0.65	0.16
July	25	0.69	0.17
August	10	0.41	0.11
September	10	0.42	0.16
October	3	0.78	0.20
November	1	0.87	
December	1	0.93	
	Abl.	**Abl.**	**Accu.**
	10:00	17:00	
Mean	0.65	0.56	0.90
±	0.23	0.41	0.33
n	59	60	7



Ablation period SO_4^{2-} (mg/l) at maximum and minimum discharge in the Rhône meltwaters (1999-2001)

	07_99			08_99			09_99			10_99			05_00			06_00			07_00			08_00			09_00			10_00		
Date	10	17	daily	10	17	daily	10	17	daily	10	17	daily	10	17	daily	10	17	daily	10	17	daily	10	17	daily	10	17	daily	10	17	daily
1							0.50	0.26	0.38							1.08	0.92	1.00				0.67	0.80	0.74	0.46					
2				0.58	0.34	0.46		0.24		0.86		0.86																		
3				0.54	0.38	0.46		0.45																						
4				0.54	0.39	0.47					0.98	0.98							0.58	0.62	0.60									
5				0.34	0.29	0.32													0.44	0.88	0.66									
6	0.97	0.84	0.91				0.45	0.30	0.38							0.72	0.77	0.75	0.81	0.65	0.73									
7	0.94	0.86	0.90	0.47	0.36	0.42		0.25					2.86		2.86	0.88	0.84	0.86				0.38	0.33	0.36						
8	1.02	0.85	0.94	0.46	0.37	0.42	0.44	0.21	0.33				1.86		1.86	0.90	0.83	0.87												
9	1.11																								0.54					
10	1.12	0.77	0.95	0.40	0.33	0.37	0.43	0.20	0.32				2.48		2.48				0.50	0.72	0.61									
11	0.92	0.68	0.80	0.45	0.38	0.42	0.39	0.20	0.30				1.47		1.47	0.82	0.81	0.82	0.50	0.84	0.67									
12				0.50												0.94	0.63	0.79	0.69	0.88	0.79									
13				0.53	0.32	0.43	0.41						0.88		0.88	0.82	0.98	0.90	0.50	0.82	0.66									
14				0.58			0.41	0.21	0.31				1.05		1.05	0.90	1.35	1.13												
15							0.43						0.92		0.92	0.90	0.79	0.85												
16							0.44	0.27	0.36				0.85	0.82	0.84													1.43		1.43
17		0.53		0.51	0.31	0.41		0.40					0.62		0.62				1.10	1.02	1.06									
18				0.48	0.33	0.41					0.97	0.97					0.61		0.70	0.71	0.71	0.40	0.27	0.34						
19	0.74				0.35					1.18	1.14	1.16				0.68	0.54	0.61				0.40			0.50					
20	0.69	0.50	0.60				0.50	0.40	0.45	0.90	1.08	0.99				0.73	0.44	0.59	1.03	0.44	0.74					0.61	0.55			
21	0.67	0.45	0.56				0.58	0.58	0.58	1.41		1.41				0.70	0.42	0.56							0.65		0.63			
22	0.62	0.45	0.54		0.28								1.12		1.12	0.67	0.47	0.57												
23					0.27								1.26	1.18	1.22															
24	0.82	0.47	0.65		0.36								0.92	1.02	0.97							0.59								
25	0.70	0.41	0.56	0.48									0.97	0.89	0.93				0.40	0.25	0.33									
26	0.60	0.34	0.47	0.47	0.40	0.44										0.73	0.54	0.64												
27	0.47	0.30	0.39		0.29	0.40										0.82	0.47	0.65	0.79	1.02	0.91									
28	0.44	0.42	0.43	0.50												0.86	0.64	0.75												
29	0.57	0.39	0.48										1.06	0.90	0.98	0.76	0.53	0.65												
30				0.56	0.31	0.44							1.11	0.93	1.02															
31				0.53									0.92	0.83	0.88															
m			0.65			0.42			0.38			1.06			1.26			0.76			0.70			0.48			0.59			1.43

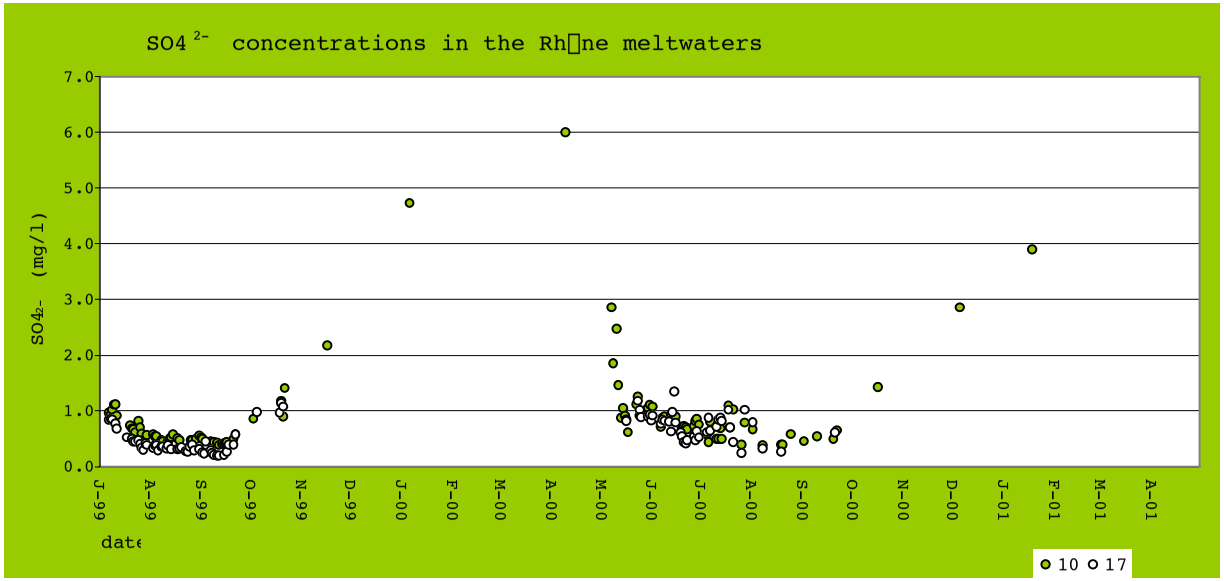
Accumulaiton period daily $SO4^{2-}$ concentrations in the Rhône meltwaters (99-01)

Date	mg/l
16-Nov-99	2.18
05-Jan-00	4.73
09-Apr-00	6.00
05-Dec-00	2.86
18-Jan-01	3.90
07-Mar-01	
29-Apr-01	3.19
m	3.81

Mean daily SO_4 concentrations

Month	n	mg/l	± (1 sigma)
January	2	4.30	
February	0		
March	0		
April	2	4.06	
May	16	1.26	0.62
June	17	0.76	0.16
July	26	0.68	0.19
August	17	0.43	0.09
September	11	0.42	0.12
October	6	1.04	0.24
November	1	2.18	
December	1	2.86	

	Abl. 10:00	**Abl.** 17:00	**Accu.**
Mean	0.76	0.58	3.81
±	0.39	0.28	1.39
n	104	91	6



Ablation period SO_4^{2-} (mg/l) at minimum and maximum discharge in the Oberaar meltwaters (1999-2001)

	07_99			08_99			09_99			10_99			05_00			06_00			07_00			08_00			09_00			10_00		
Date	10	17	daily	10	17	daily	10	17	daily	10	17	daily	10	17	daily	10	17	daily	10	17	daily	10	17	daily	10	17	daily	10	17	daily
1							4.66	2.42	3.54																3.72	2.50	3.11	5.23		5.23
2																														
3				3.87	2.81	3.34													5.87	2.66	4.27									
4										8.00		8.00							2.73		2.73									
5				3.32	2.40	2.86													3.11	3.27	3.19									
6		2.78	2.78																2.12		2.12		2.40	4.13						
7	3.86	4.87	4.37																			5.85								
8	5.80	5.32	5.56													4.18	3.20	3.69												
9				2.81	2.66	2.74																			7.31	1.18	4.25			
10							4.55	2.10	3.33				1.32		1.32				3.47	0.28	1.88									
11	5.90	5.30	5.60																0.79	0.61	0.70									
12	4.40	4.29	4.35	5.02	4.27	4.65													0.53		0.53									
13																3.24	2.44	2.84	7.67		7.67									
14																3.38	3.32	3.35												
15	4.36	3.42	3.89				4.62	3.24	3.93							3.04	3.06	3.05										3.05		3.05
16				3.49	2.43	2.96																								
17													3.92		3.92				8.70	6.84	7.77									
18	4.30	4.29	4.30																2.19	4.22	3.21					2.24	3.33			
19				3.31	3.03	3.17										3.92	2.63	3.28	6.82	3.19	5.01	2.70	2.28	2.49	4.41					
20	4.15	3.61	3.88													3.25	1.78	2.52	6.62	3.15	4.89					2.83	2.83			
21																2.90	1.91	2.41								5.63	5.63			
22	4.03	3.68	3.86													3.25	2.78	3.02												
23							6.30	4.86	5.58																					
24																						5.31	0.60	2.96						
25				2.71	2.21	2.46																								
26	3.85	2.59	3.22													4.78	2.87	3.83	0.40	0.79	0.60									
27																4.49	2.47	3.48												
28																2.63	1.89	2.26												
29	3.73	2.95	3.34													3.74	2.30	3.02												
30							3.13	3.67	3.40																					
31																			0.77	0.30	0.54									
m			4.10			3.17			11.34			8.00			2.62			3.06			3.22			3.19			3.83			4.14

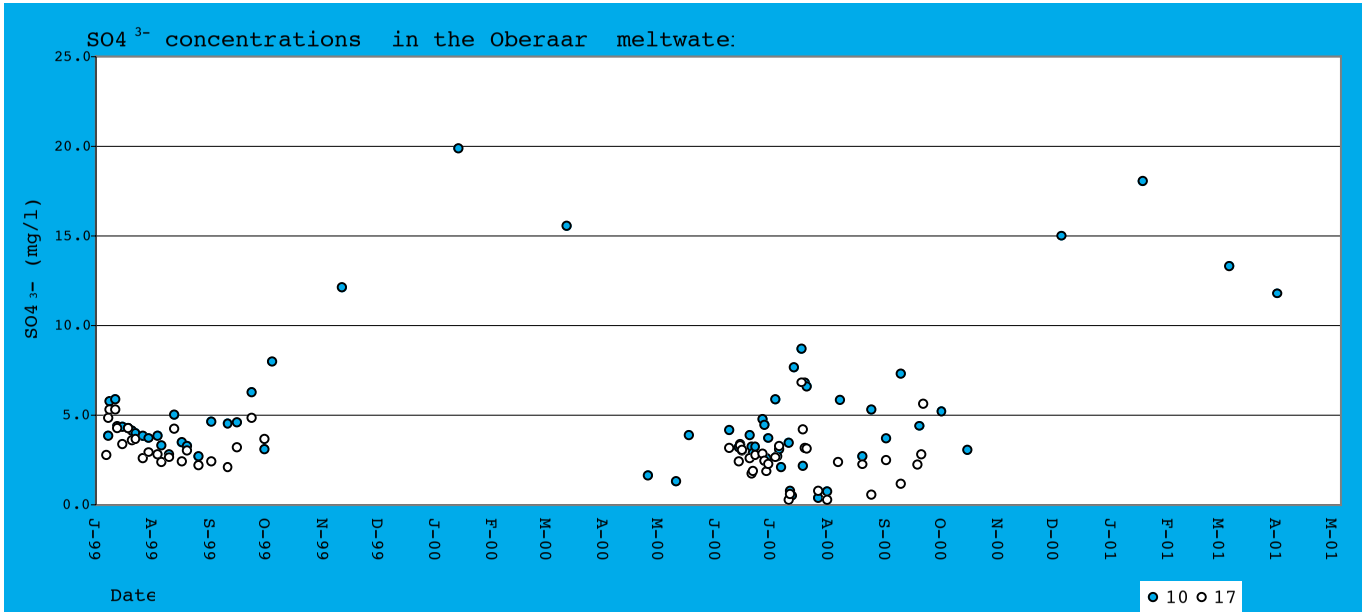
Accumulation period daily SO_4^{2-} concentrations in the Oberaar meltwaters (1999-2001)

Date	(mg/l)
11/11/99	12.13
13/1/00	19.89
12/3/00	15.57
25/4/00	1.67
5/12/00	15.02
18/1/01	18.06
6/3/01	13.33
1/5/01	11.80
m	13.43

Mean daily SO_4 concentrations

Month	n	mg/l	± (1 sigma)
January	2	19.00	
February	0		
March	2	14.50	
April	1	1.67	
May	3	6.39	3.58
June	12	3.69	0.54
July	25	3.61	1.95
August	10	3.17	0.70
September	10	3.89	0.99
October	3	5.43	2.48
November	1	12.13	
December	1	15.02	

	Abl. 10:00	**Abl.** 17:00	**Accu.**
Mean	4.03	3.03	13.67
±	1.76	1.68	5.91
n	59	60	7



Ablation period HCO_3^- (mg/l) at maximum and minimum discharge in the Rhône meltwaters (1999-2001)

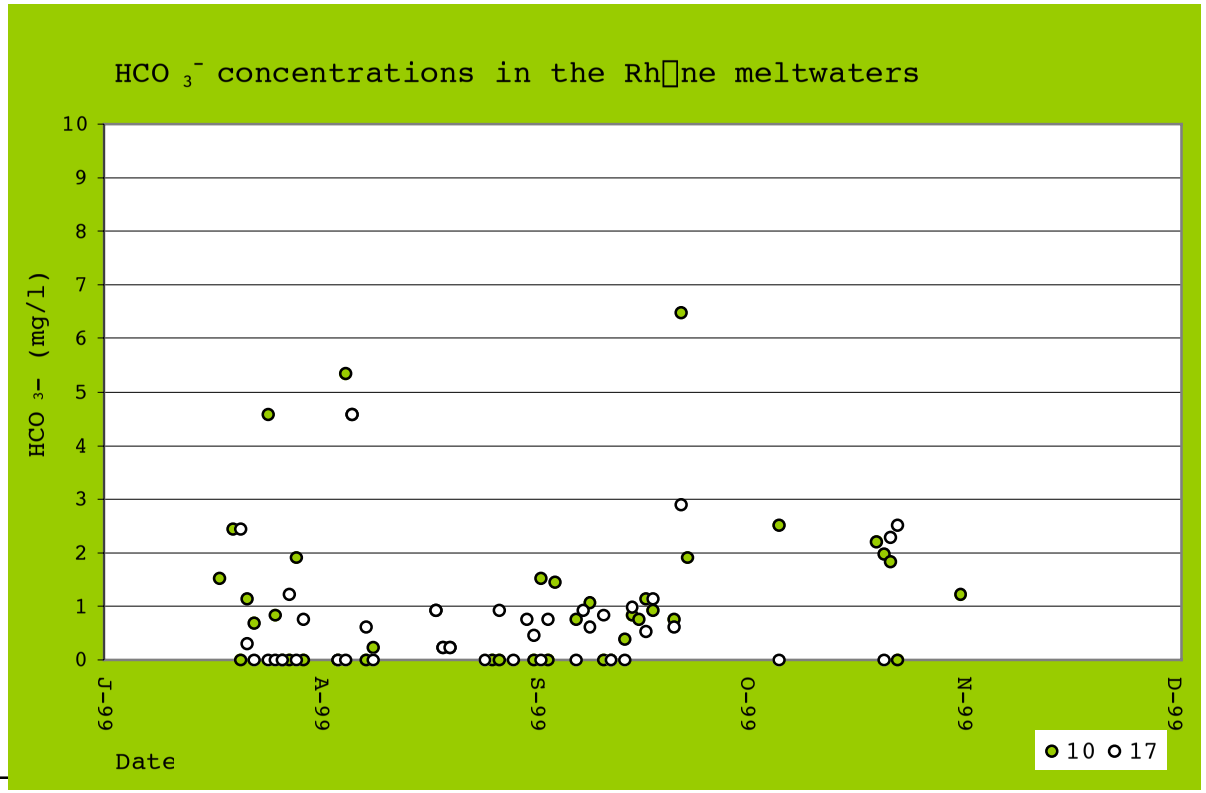
	07_99			08_99			09_99			10_99		
Date	10	17	daily	10	17	daily	10	17	daily	10	17	daily
1							0.00	0.76	0.38			
2				0.00	0.00	0.00	1.45		1.45			
3				5.34	0.00	2.67						
4				4.58	4.58	4.58				2.52	0.00	1.26
5							0.76	0.00	0.38			
6				0.00	0.61	0.31		0.92	0.92			
7				0.23	0.00	0.12	1.07	0.61	0.84			
8												
9							0.00	0.84	0.42			
10							0.00	0.00	0.00			
11												
12							0.38	0.00	0.19			
13							0.84	0.99	0.92			
14							0.76		0.76			
15							1.14	0.53	0.84			
16	1.53		1.53	0.92	0.92	0.92	0.92	1.14	1.03			
17				0.23	0.23	0.23						
18	2.44		2.44	0.23	0.23	0.23				2.21		2.21
19	0.00	2.44	1.22				0.76	0.61	0.69	1.98	0.00	0.99
20	1.14	0.31	0.73				6.48	2.90	4.69	1.83	2.29	2.06
21	0.69	0.00	0.35				1.91		1.91	0.00	2.52	1.26
22												
23	4.58	0.00	2.29		0.00	0.00						
24	0.84	0.00	0.42	0.00		0.00						
25	0.00	0.00	0.00	0.00	0.92	0.46						
26	0.00	1.22	0.61									
27	1.91	0.00	0.96		0.00	0.00						
28	0.00	0.76	0.38									
29					0.76	0.76						
30				0.00	0.46	0.23						
31				1.53	0.00	0.77						
m			0.99			0.75			1.03			1.56

Accumulation period daily HCO3- concentrations in the Rhône meltwaters (1999-2001)

Date	(mg/l)
16/11/99	1.22
m	1.22

Mean daily HCO_3^- concentrations

Month	n	mg/l	± (1 sigma)
January	0		
February	0		
March	0		
April	0		
May	0		
June	0		
July	11	0.99	0.80
August	15	0.75	1.26
September	15	1.03	1.12
October	5	1.56	0.54
November	0		
December	0		
	Abl.	**Abl.**	**Accu.**
Mean	10:00	17:00	
±	1.22	0.71	3.81
n	1.98	2.73	
	44	40	1



Ablation period *HCO_3^- (mg/l) at minimum and maximum discharge in the Rhône meltwaters (1999-2001)

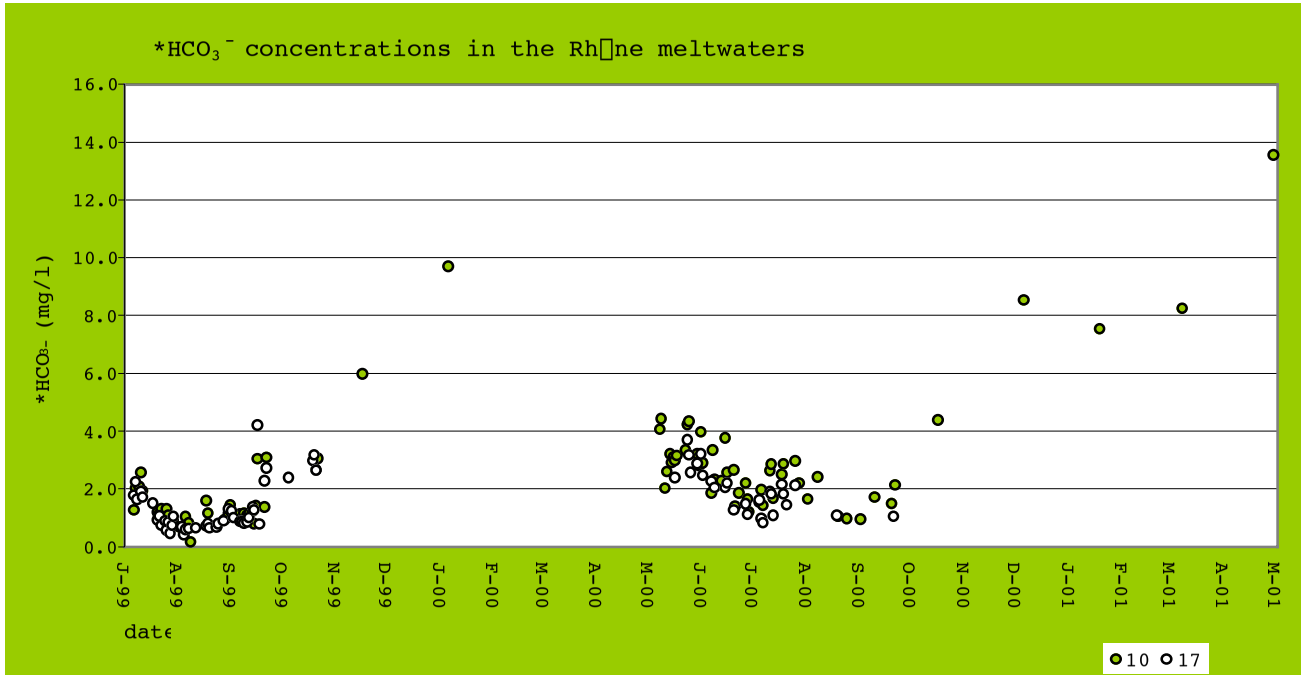
	07_99			08_99			09_99			10_99			05_00			06_00			07_00			08_00			09_00			10_00		
Date	10	17	daily	10	17	daily	10	17	daily	10	17	daily	10	17	daily	10	17	daily	10	17	daily	10	17	daily	10	17	daily	10	17	daily
1							1.18	1.24	1.21							2.91	2.48	2.69				1.65			0.96					
2				0.68				1.01																						
3				0.70	0.69	0.70																								
4				0.62	0.43	0.53					2.40								1.54	1.63	1.59									
5				1.04	0.60	0.82													1.97	0.98	1.47									
6	1.27	1.78	1.53				1.13	0.89	1.01							1.86	2.28	2.07	1.44	0.83	1.13									
7	2.03	2.26	2.15	0.81	0.63	0.72		0.89					4.08		4.08	3.35						2.41								
8	1.76	1.64	1.70	0.18			1.17	0.83	1.00				4.44		4.44	2.33	2.05	2.19												
9	2.10																								1.71					
10	2.57	1.92	2.25				1.10	0.86	0.98				2.03		2.03				2.64	1.91	2.28									
11	1.94	1.73	1.83		0.66		1.14	1.01	1.07				2.60		2.60				2.85	1.83	2.34									
12																2.28			1.69	1.08	1.39									
13							1.23	1.37	1.30				3.21		3.21															
14							0.80	1.27	1.04				2.93		2.93	3.77	2.06	2.91												
15							1.42						3.11		3.11	2.57	2.21	2.39												
16							3.04	4.22	3.63				2.99	2.40	2.70													4.38		4.38
17		1.51		1.59	0.73	1.16		0.79					3.16		3.16				2.51	2.15	2.33									
18				1.16	0.80	0.98					2.99	2.99							2.87	1.83	2.35		1.09	1.08						
19					0.66					2.99	3.19	3.09				2.67	1.28	1.98				1.06			1.50					
20	1.19	0.93	1.06				1.37	2.29	1.83	2.67	2.65	2.66				1.40		0.70		1.46						1.06	1.28			
21	1.14	1.08	1.11				3.09	2.74	2.91	3.05		3.05													2.14		1.60			
22	1.32	0.74	1.03										3.35		3.35	1.86		0.93												
23					0.68								4.23	3.71	3.97															
24	1.02	0.90	0.96		0.80								4.33	3.19	3.76							0.97								
25	1.32	0.59	0.95											2.58					2.97	2.14	2.55									
26	1.08	0.86	0.97													2.21	1.49	1.85												
27	0.60	0.47	0.54		0.90	0.93										1.66	1.12	1.39	2.21											
28	0.89	0.75	0.82	0.95												1.22														
29	0.93	1.05	0.99										3.23	2.89	3.06															
30				1.15	1.31	1.23							2.80																	
31				1.45									3.98	3.22	3.60															
m			1.28			0.88			1.60			2.95			3.29			1.91			1.94			1.08			1.44			4.38

Accumulation period daily *HCO_3^- concentrations in the Rhône meltwaters (99-01)

Date	(mg/l)
16/11/99	5.98
5/12/00	8.53
5/1/00	9.70
18/1/01	7.55
7/3/01	8.26
9/4/00	
29/4/01	13.56
m	8.93

Mean daily HCO_3^- concentrations

Month	n	mg/l	± (1 sigma)
January	2	8.40	
February	0		
March	1		
April	2	11.63	
May	14	3.29	0.64
June	10	1.91	0.72
July	23	1.54	0.61
August	9	0.90	0.23
September	12	1.57	0.85
October	5	3.10	0.76
November	1	5.98	
December	1	7.55	
	Abl. 10:00	**Abl.** 17:00	**Accu.**
Mean	2.03	1.55	8.93
±	1.03	0.87	2.58
n	87	70	6



Ablation period HCO_3^- (mg/l) at minimum and maximum discharge in the Oberaar meltwaters (1999-2001)

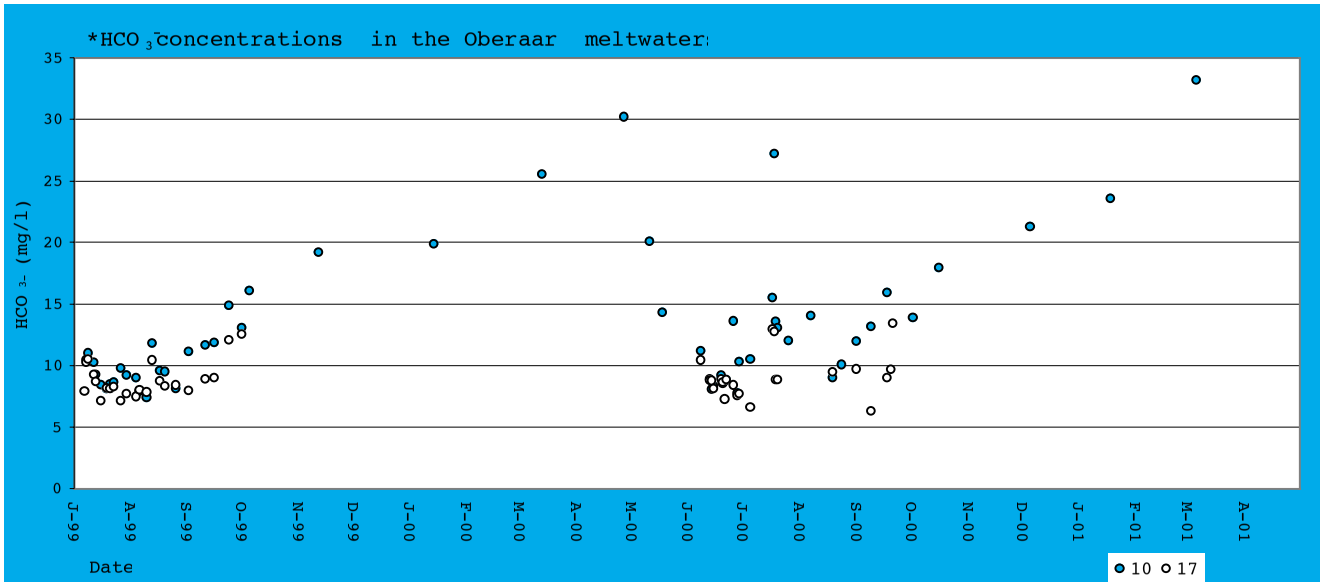
	07_99			08_99			09_99			10_99			05_00			06_00			07_00			08_00			09_00			10_00		
Date	10	17	daily	10	17	daily	10	17	daily	10	17	daily	10	17	daily	10	17	daily	10	17	daily	10	17	daily	10	17	daily	10	17	daily
1							11.16	8.02	9.59																			13.89		13.89
2																														
3				9.02	7.49	8.25																								
4										16.11		16.11							10.55	6.63	8.59									
5				7.91	8.05	7.98																								
6		7.93	7.93																			14.07								
7	10.48	10.27	10.38													11.21	10.46	10.84												
8	11.03	10.55	10.79																						13.22	6.30	9.76			
9				7.40	7.86	7.63																								
10							11.69	8.95	10.32				20.13		20.13															
11	10.26	9.30	9.78																											
12	9.28	8.72	9.00	11.83	10.47	11.15										8.93	8.82	8.87												
13																8.11	8.79	8.45												
14																8.36	8.14	8.25												
15	8.45	7.16	7.80				11.89	9.04	10.47																			17.96		17.96
16				9.60	8.76	9.18													15.53	12.98	14.25									
17													14.37		14.37				27.24	12.77	20.00				15.97	9.05	12.51			
18	8.12	8.19	8.15													9.21	8.90	9.06	13.60	8.88	11.24	9.03	9.50	9.26						
19				9.52	8.37	8.94										8.58	8.67	8.62	13.09	8.89	10.99					9.70	12.83			
20	8.52	8.14	8.33													8.80	7.30	8.05								13.45	14.71			
21																8.82	8.85	8.83												
22	8.66	8.29	8.47																											
23							14.92	12.10	13.51													10.08								
24																														
25				8.16	8.43	8.30										13.64	8.43	11.03	12.03											
26	9.79	7.16	8.48																											
27																7.81	7.55	7.68												
28																10.33	7.71	9.02												
29	9.24	7.70	8.47																											
30							13.09	12.57	12.83																					
31																						11.99	9.73	10.86						
m			8.87			8.78			11.34			16.11			17.25			8.97			13.02			10.06			12.45			15.93

Accumulation period daily $^*HCO_3^-$ concentrations in the Oberaar meltwaters (1999-2001)

Date	(mg/l)
11/11/99	19.21
13/1/00	19.91
12/3/00	25.58
25/4/00	30.22
5/12/00	21.32
18/1/01	23.60
6/3/01	33.23
1/5/01	23.64
m	24.59

Mean daily HCO_3^- concentrations

Month	n	mg/l	± (1 sigma)
January	2	21.80	
February	0		
March	2	29.4	
April	1	30.22	
May	3	19.32	4.68
June	11	8.97	1.06
July	16	10.17	3.12
August	9	9.06	1.23
September	9	11.84	1.84
October	3	15.99	2.04
November	1	19.21	
December	1	21.32	
	Abl.	**Abl.**	**Accu.**
	10:00	17:00	
Mean	11.45	8.99	24.72
±	3.67	2.95	5.32
n	50	51	7



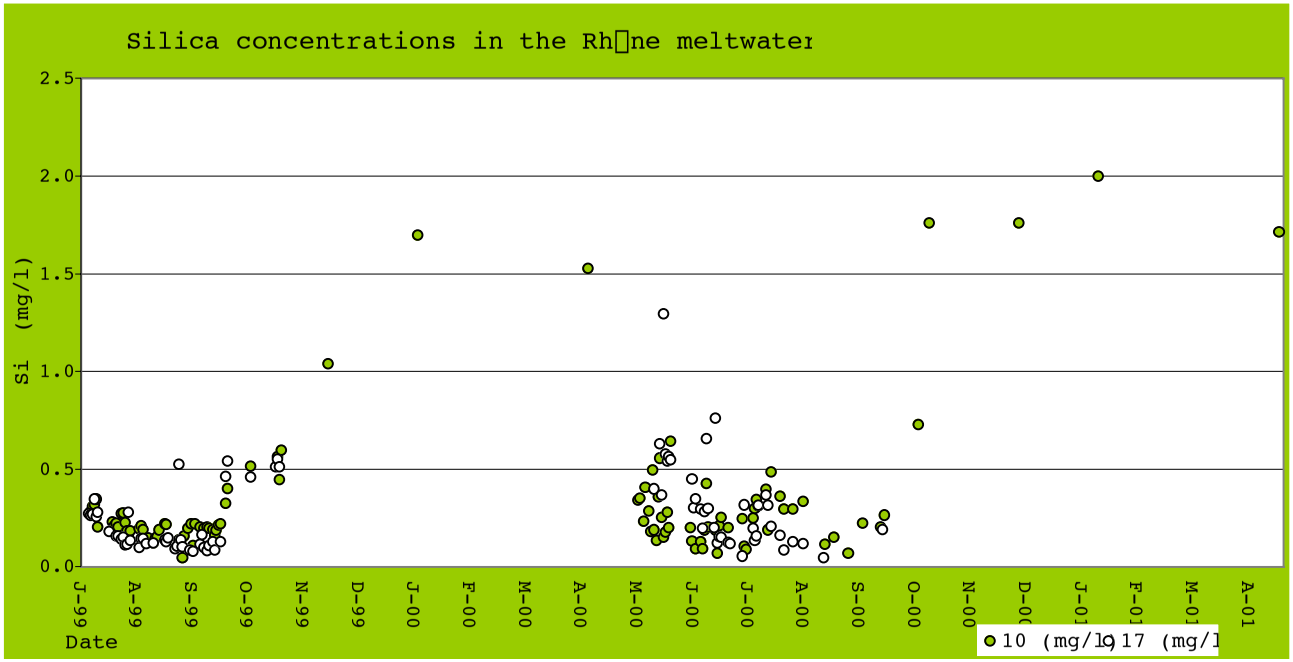
Ablation period Si (mg/l) at the times of maximum and minimum discharge in the Rhône meltwaters (99-01)

	07_99			08_99			09_99			10_99			05_00			06_00			07_00			08_00			09_00			10_00		
Day	10	17	daily	10	17	daily	10	17	daily	10	17	daily	10	17	daily	10	17	daily	10	17	daily	10	17	daily	10	17	daily	10	17	daily
1							0.22															0.30	0.13	0.21	0.07					
2							0.11	0.08	0.09																					
3				0.19	0.10	0.15	0.22																							
4				0.21	0.15	0.18				0.51	0.46	0.49							0.25	0.05	0.15									
5				0.19	0.14	0.17										0.20			0.10	0.32	0.21									
6		0.27	0.27				0.20	0.11	0.16							0.13	0.45	0.29	0.09											
7	0.28	0.26	0.27	0.15	0.12	0.13		0.16					0.34		0.34		0.30					0.33	0.12	0.23						
8	0.31	0.27	0.29	0.15			0.20	0.10	0.15				0.35		0.35	0.09	0.35	0.22												
9	0.32	0.35	0.33																						0.22					
10	0.35	0.26	0.30				0.20	0.08	0.14				0.23		0.23				0.25	0.20	0.22							0.73		0.73
11	0.21	0.28	0.24	0.12	0.12	0.12	0.20	0.11	0.15				0.41		0.41	0.13	0.30	0.21	0.30	0.13	0.22									
12				0.15												0.09	0.20	0.15	0.34	0.16	0.25									
13				0.15			0.19	0.13	0.16				0.29		0.29	0.19	0.28	0.24	0.31	0.31	0.31									
14				0.19			0.16	0.09	0.12				0.18		0.18	0.43	0.66	0.54												
15							0.19						0.50		0.50	0.20	0.30	0.25												
16							0.21						0.19	0.40	0.29													1.76		1.76
17		0.18		0.22	0.14	0.18	0.22	0.13	0.17				0.13		0.13				0.40	0.37	0.38									
18				0.22	0.13	0.17					0.51		0.36		0.36		0.20		0.19	0.31	0.25		0.05	0.08						
19	0.23				0.15					0.56	0.55	0.56	0.56	0.63	0.59	0.19	0.76	0.48				0.12			0.20		0.20			
20	0.21						0.32	0.46	0.39	0.45	0.51	0.48	0.25	0.37	0.31	0.07	0.12	0.10	0.49	0.21	0.35					0.19	0.20			
21	0.22	0.16	0.19				0.40	0.54	0.47	0.60			0.15	1.30	0.72	0.21	0.15	0.18							0.26		0.20			
22	0.20	0.16	0.18										0.18	0.58	0.38	0.25	0.15	0.20												
23					0.09								0.28	0.54	0.41															
24	0.27	0.14	0.21		0.11								0.20	0.57	0.38							0.15								
25	0.27	0.15	0.21	0.14	0.53	0.33							0.64	0.55	0.59				0.36	0.16	0.26									
26	0.23	0.11	0.17	0.14	0.14	0.14										0.20	0.13	0.16												
27	0.19	0.12	0.15	0.05	0.10	0.07											0.12		0.30	0.09	0.19									
28	0.16	0.28	0.22	0.16																										
29	0.18	0.14	0.16																											
30				0.20																										
31					0.09																									
m			0.23			0.16			0.20			0.51			0.38			0.25			0.25			0.17			0.20			1.24

Accumulation period daily Si (mg/l) in the Rhône meltwaters (99-01)	
Date	(mg/l)
16/11/99	1.0387
5/12/00	1.7600
5/1/00	1.6977
18/1/01	2.0000
9/4/00	1.5267
29/4/01	1.7130
m	1.6227

Mean daily Si concentrations

Month	n	mg/l	± (1 sigma)
January	2	1.85	
February	0		
March	0		
April	2	1.85	
May	17	0.38	0.15
June	12	0.25	0.13
July	25	0.24	0.06
August	13	0.17	0.07
September	13	0.20	0.11
October	5	0.80	0.54
November	1	1.04	
December	0		
	Abl. 10:00	**Abl.** 17:00	**Accu.**
Mean	0.26	0.28	1.62
±	0.20	0.26	0.32
n	101	84	6



Ablation period Si (mg/l) at minimum and maximum discharge in the Oberaar meltwaters (1999-2001)

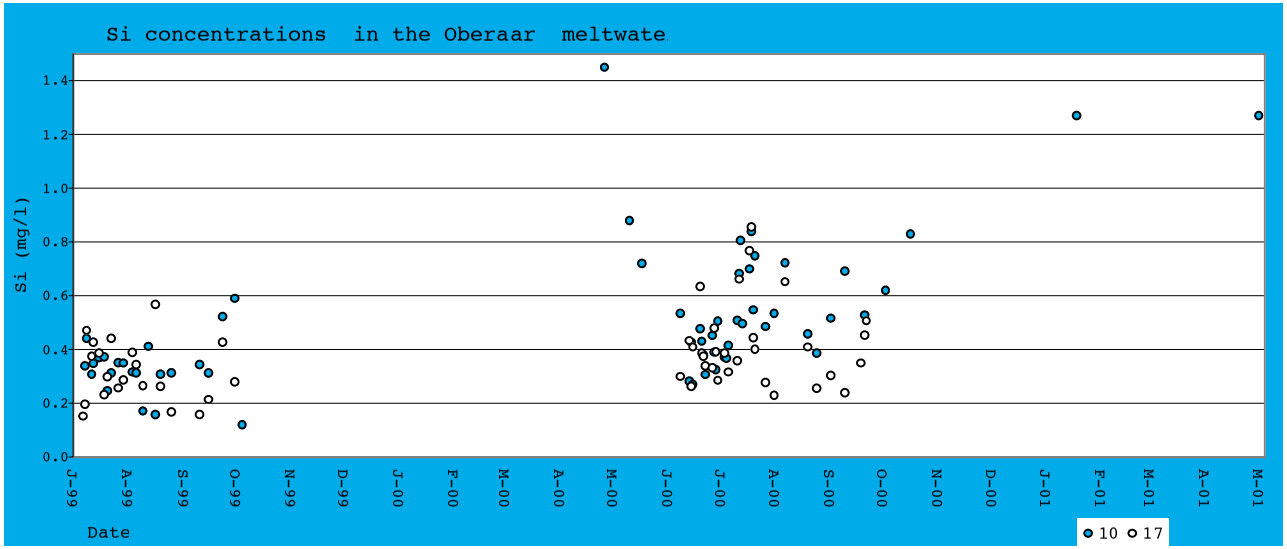
	07_99			08_99			09_99			10_99			05_00			06_00			07_00			08_00			09_00			10_00		
Date	10	17	daily	10	17	daily	10	17	daily	10	17	daily	10	17	daily	10	17	daily	10	17	daily	10	17	daily	10	17	daily	10	17	daily
1																									0.52	0.30	0.41			
2																												0.62		0.62
3				0.32	0.39	0.35													0.37	0.39	0.38									
4										0.12		0.12							0.37		0.34									
5				0.31	0.34	0.33													0.42	0.32	0.37									
6		0.15	0.15																			0.72	0.65	0.69						
7	0.34	0.20	0.27																											
8	0.44	0.47	0.46													0.53	0.30	0.42												
9				0.17	0.27	0.22																			0.69	0.24	0.47			
10							0.34	0.16	0.25				0.88		0.88				0.51	0.36	0.43									
11	0.31	0.37	0.34																0.68	0.66	0.67									
12	0.35	0.43	0.39	0.41	*1.84*	1.13													0.81		0.73									
13																0.28	0.43	0.36	0.50		0.63									
14																0.43	0.26	0.34												
15	0.37	0.39	0.38				0.31	0.21	0.26							0.27	0.41	0.34												
16				0.16	0.57	0.36																						0.83		0.83
17													0.72		0.72				0.70	0.77	0.73									
18	0.37	0.23	0.30																0.84	0.86	0.85					0.35	0.52			
19				0.31	0.26	0.29										0.48	0.63	0.56	0.55	0.44	0.50	0.46	0.41	0.43						
20	0.25	0.30	0.27													0.43	0.39	0.41	0.75	0.40	0.57				0.53	0.45	0.49			
21																0.38	0.37	0.38								0.51	0.25			
22	0.31	0.44	0.38													0.31	0.34	0.32												
23							0.52	0.43	0.47																					
24																						0.39	0.26	0.32						
25				0.31	0.17	0.24																								
26	0.35	0.26	0.30													0.45	0.33	0.39	0.49	0.28	0.38									
27																0.39	0.48	0.44												
28																0.33	0.39	0.36												
29	0.35	0.29	0.32													0.51	0.29	0.40												
30							0.59	0.28	0.44																					
31																			0.53	0.23	0.38									
m			0.32			0.42			0.36			0.12			0.80			0.39			0.54			0.48			0.43			0.73

Accumulation period daily Si concentrations in the Oberaar meltwaters (1999-2001)	
Date	(mg/l)
11/11/99	
13/1/00	
12/3/00	
25/4/00	1.45
5/12/00	1.27
18/1/01	
6/3/01	
1/5/01	1.27
m	1.33

Mean daily Si concentrations

Month	n	mg/l	± (1 sigma)
January	1	1.30	
February	0		
March	0		
April	1	1.45	
May	3	0.96	0.28
June	12	0.39	0.06
July	24	0.44	0.17
August	10	0.44	0.28
September	9	0.40	0.11
October	3	0.52	0.36
November	0		
December	0		

	Abl. 10:00	**Abl.** 17:00	**Accu.**
Mean	0.47	0.40	1.33
±	0.21	0.25	0.10
n	58	52	3



Ablation period suspended sediment (g/l) at minimum and maximum discharge in the Rhône meltwaters (1999-2001)

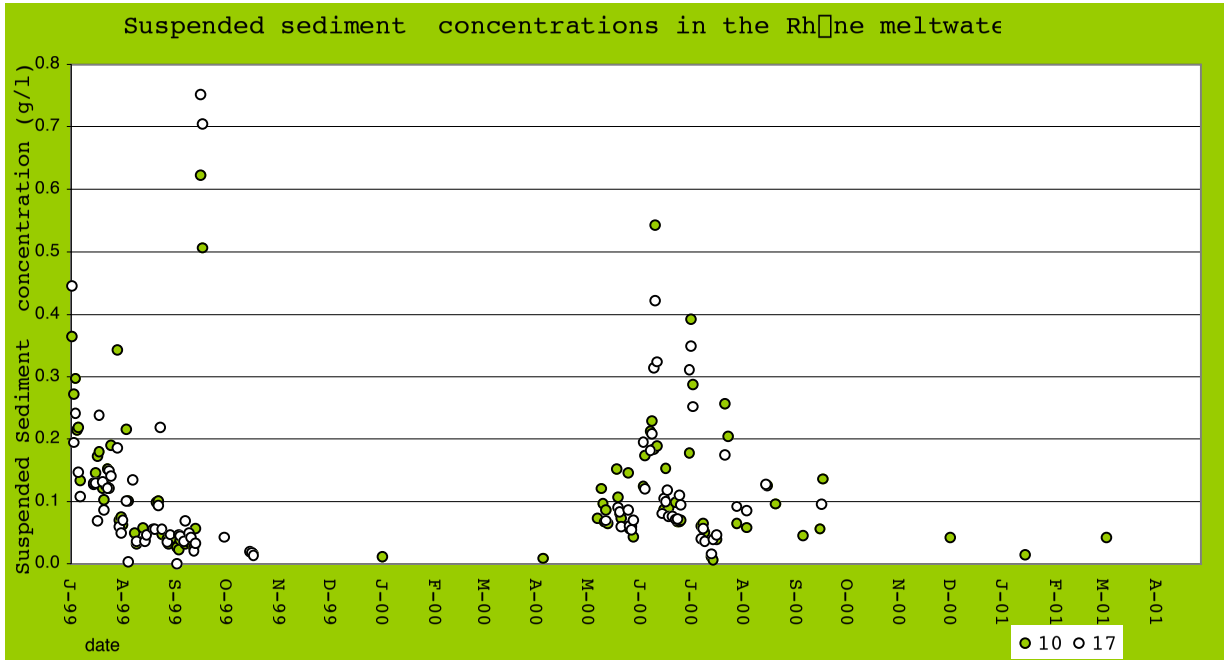
	07_99			08_99			09_99			10_99			05_00			06_00			07_00			08_00			09_00			10_00		
Date	10	17	daily	10	17	daily	10	17	daily	10	17	daily	10	17	daily	10	17	daily	10	17	daily	10	17	daily	10	17	daily	10	17	daily
1							0.03									0.04	0.07	0.06				0.06	0.09	0.08	0.04			0.05		0.05
2				0.34	0.19	0.26		0.05																						
3				0.07	0.06	0.06	0.04																							
4				0.07	0.05	0.06				0.04	0.04								0.18	0.31	0.24									
5				0.06	0.07	0.07													0.39	0.35	0.37									
6	0.36	0.45	0.45				0.03	0.00											0.29	0.25	0.27									
7	0.27	0.19	0.23	0.22	0.10	0.16	0.02	0.05	0.04							0.12	0.20	0.16				0.06	0.09	0.07						
8	0.30	0.24	0.27	0.10	0.00	0.05	0.04	0.05	0.04							0.17	0.12	0.15												
9	0.21																								0.05		0.05			
10	0.22	0.15	0.18				0.04	0.04	0.04																					
11	0.19	0.11	0.15		0.13		0.03	0.07	0.05				0.07		0.07	0.21	0.18	0.20	0.06	0.04	0.05									
12				0.05		0.18										0.23	0.21	0.22	0.06	0.06	0.06									
13				0.03	0.04	0.03	0.04	0.05	0.04				0.12		0.12	0.18	0.31	0.25	0.05	0.04	0.04									
14							0.03	0.04	0.04				0.10		0.10	0.54	0.42	0.48												
15							0.03						0.07		0.07	0.19	0.32	0.26										0.23		0.23
16							0.03	0.02	0.02				0.09	0.07	0.08															
17				0.06			0.06	0.03	0.04				0.06		0.06				0.01	0.02	0.01									
18				0.04	0.04	0.04											0.08	0.04	0.01	0.04	0.02		0.13	0.13						
19	0.13	0.13	0.13		0.05	0.04				0.02	0.02					0.09	0.10	0.10				0.13			0.06		0.08			
20	0.15	0.13	0.14				0.62	0.75	0.69	0.02	0.02	0.02				0.15	0.10	0.13	0.04	0.05	0.04					0.10	0.08			
21	0.17	0.07	0.12				0.51	0.70	0.61	0.02	0.01	0.01				0.10	0.12	0.11							0.14		0.12			
22	0.18	0.24	0.21										0.15			0.09	0.08	0.08												
23					0.06	0.06							0.11	0.09	0.10															
24	0.12	0.13	0.13		0.06	0.06							0.08	0.08	0.08		0.08	0.04				0.10								
25	0.10	0.09	0.09	0.10		0.10							0.07	0.06	0.07				0.26	0.17	0.22									
26	0.13		0.11	0.10	0.09	0.10										0.10	0.07	0.09												
27	0.15	0.12	0.14		0.22	0.22										0.07	0.07	0.07	0.20											
28	0.12	0.15	0.14	0.04	*0.06*	0.05										0.07	0.11	0.09												
29	0.19	0.14	0.17										0.15	0.09	0.12	0.07	0.09	0.08												
30													0.06	0.06	0.06															
31				0.04	0.04	0.04							0.06	0.05	0.06								0.07							0.14
m			0.18			0.09			0.16			0.02			0.08			0.14			0.13			0.09			0.08			0.73

Accumulation period daily suspended sediment concentrations in the Rhône meltwaters (1999-2001)

Date	(g/l)
16/11/99	0.0078
5/1/00	0.0115
9/4/00	0.0092
5/12/00	0.0420
18/1/00	0.0144
7/3/00	0.0420
m	0.0212

Mean daily Suspended sediment concentrations

Month	n	g/l	± (1 sigma)
January	2	0.0130	
February	0		
March	1	0.0420	
April	1	0.0092	
May	12	0.0817	0.0216
June	18	0.1437	0.1085
July	25	0.1590	0.1061
August	20	0.0929	0.0652
September	14	0.1371	0.2175
October	6	0.0633	0.0841
November	1	0.0078	
December	1	0.0420	
	Abl. 10:00	**Abl.** 17:00	**Accu.**
Mean	0.125	0.12	0.02
±	0.11	0.13	0.02
n	96	86	6



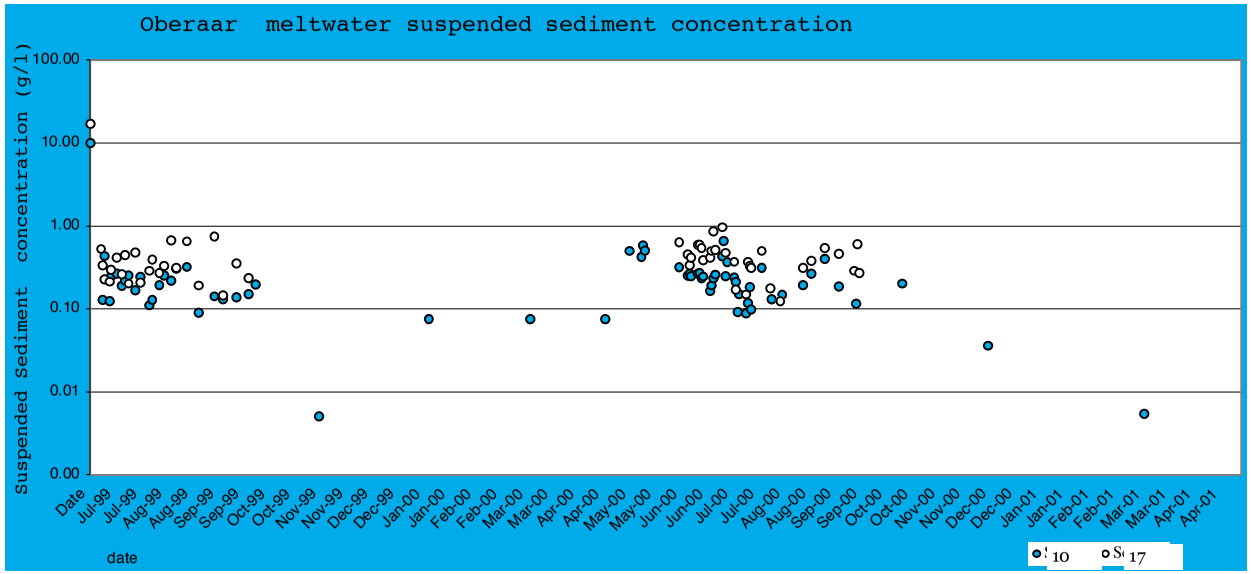
Ablation period suspended sediment (g/l) at minimum and maximum discharge in the Oberaar meltwaters (1999-2001)

	07_99			08_99			09_99			10_99			05_00			06_00			07_00			08_00			09_00			10_00		
Date	10	17	daily	10	17	daily	10	17	daily	10	17	daily	10	17	daily	10	17	daily	10	17	daily	10	17	daily	10	17	daily	10	17	daily
1							0.09	0.19	0.14													0.13		0.15	0.40	0.55	0.47			
2																														
3				0.11	0.29	0.20													0.43	0.96	0.70									
4										0.20		0.20							0.66											
5				0.13	0.40	0.26													0.25	0.47	0.36									
6		0.53	0.53																0.36				0.12	0.21						
7	0.13	0.33	0.23																			0.15								
8	0.43	0.23	0.33													0.32	0.63	0.48												
9				0.19	0.27	0.23																			0.19	0.46	0.32			
10							0.14	0.75	0.45				0.50		0.50				0.24	0.37	0.30									
11	0.12	0.21	0.17																0.21	0.17	0.19									
12	0.24	0.30	0.27	0.25	0.33	0.29													0.09											
13																0.25	0.45	0.35	0.15											
14																0.26	0.33	0.30												
15	0.27	0.42	0.34				0.13	0.15	0.14							0.25	0.42	0.33												
16				0.22	0.67	0.45																						0.20		0.20
17													0.42		0.42				0.09	0.15	0.12									
18	0.19	0.26	0.23										0.58		0.58				0.12	0.37	0.24					0.29	0.20			
19				0.30	0.32	0.31							0.50		0.50	0.27	0.59	0.43	0.18	0.33	0.26	0.19	0.31	0.25	0.12					
20	0.22	0.45	0.33													0.27	0.59	0.43	0.10	0.32	0.21					0.60				
21																0.23	0.55	0.39								0.27				
22	0.25	0.20	0.23													0.25	0.38	0.31												
23							0.14	0.36	0.25																					
24																						0.27	0.38	0.32						
25				0.32	0.65	0.49																								
26	0.17	0.48	0.32													0.16	0.42	0.29	0.31	0.50	0.41									
27																0.19	0.50	0.35												
28																0.23	0.86	0.54												
29	0.24	0.21	0.23													0.26	0.52	0.39												
30							0.15	0.23	0.19																					
31																				0.18										
m			0.29			0.32			0.23			0.20			0.50			0.38			0.31			0.24			0.33			0.20

Accumulation period daily Ca concentrations in the Rhône meltwaters (1999-2001)	
Date	g/l
11/11/99	0.0051
13/1/00	0.0763
13/3/00	0.0750
26/4/00	0.0750
5/12/00	0.0361
6/3/01	0.0054
m	0.05

Mean daily Ca concentrations

Month	n	mg/l	± (1 sigma)
January	2	0.0579	
February	0		
March	2	0.0402	
April	1	0.0750	
May	4	0.5025	0.0643
June	12	0.3829	0.0763
July	20	0.2995	0.1308
August	11	0.2880	0.1014
September	8	0.2707	0.1307
October	2	0.2002	
November	1	0.0051	
December	1	0.0361	
	Abl.	**Abl.**	**Accu.**
	10:00	17:00	
Mean	0.2590	0.3950	0.0450
±	0.1460	0.1830	0.0320
n	64	55	7



Ablation periodpH at minimum and maximum discharge in the Rhône meltwaters (1999-2001)

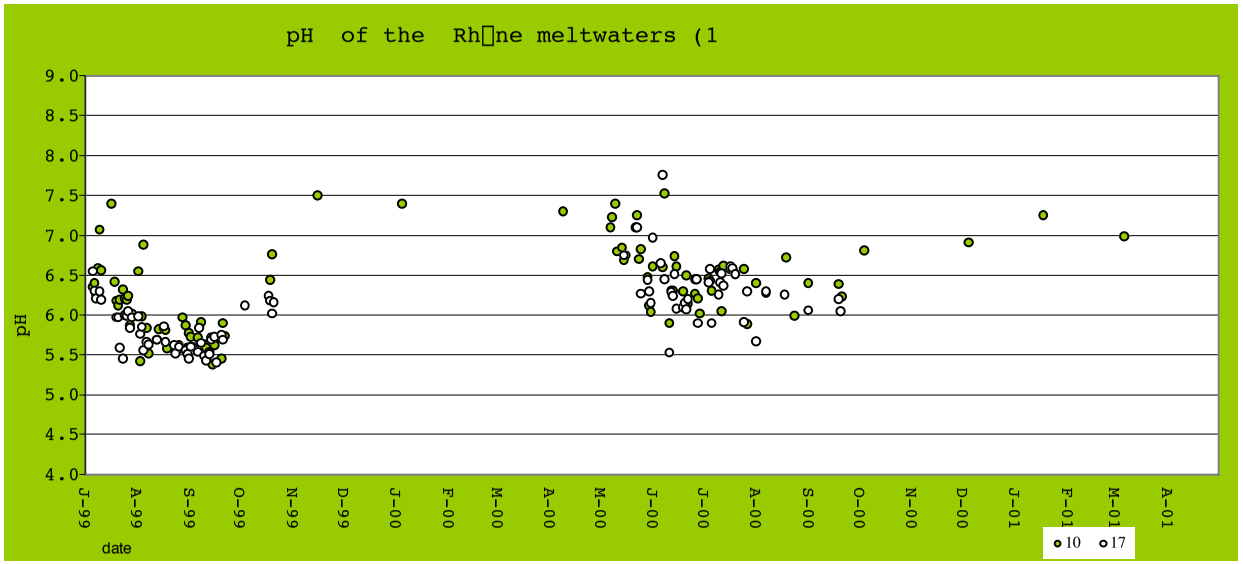
	07_99			08_99			09_99			10_99			05_00			06_00			07_00			08_00			09_00			10_00		
Date	10	17	daily	10	17	daily	10	17	daily	10	17	daily	10	17	daily	10	17	daily	10	17	daily	10	17	daily	10	17	daily	10	17	daily
1							5.77	5.45	5.58							6.61	6.97	6.75				6.40	5.67	5.90	6.40	6.06	6.20			
2				6.55	5.98	6.18	5.73	5.60	5.66																					
3				5.42	5.76	5.56	5.60		5.60																					
4				5.98	5.85	5.91					6.12	6.12							6.46	6.41	6.43									
5				6.88	5.56	5.84													6.43	6.58	6.50									
6	6.35	6.55	6.44				5.72	5.54	5.62								6.65	6.65	6.31	5.90	6.06									
7	6.40	6.31	6.35	5.84	5.66	5.74		5.84	5.84				7.10		7.10	6.60	7.76	6.87				6.28	6.30	6.29						
8	6.27	6.21	6.24	5.52	5.63	5.57	5.91	5.65	5.76				7.23		7.23	6.60	6.45	6.52												
9	6.59		6.59																											
10	7.07	6.30	6.53				5.63	5.49	5.55				7.40		7.40				6.57	6.26	6.39							6.81		6.81
11	6.56	6.19	6.34				5.59	5.43	5.50				6.80		6.80	5.90	5.53	5.68	6.54	6.41	6.47									
12																6.31	6.29	6.30	6.05	6.52	6.22									
13				5.69	5.69	5.69	5.54	5.51	5.52							6.31	6.24	6.27	6.62	6.37	6.48									
14				5.82		5.82	5.72	5.69	5.70				6.85		6.85	6.74	6.51	6.61												
15							5.38		5.38				6.69	6.75	6.72	6.61	6.08	6.27												
16							5.62	5.73	5.67				6.75		6.75															
17	7.40		7.40	5.84	5.86	5.85		5.40	5.40										6.58	6.61	6.59									
18				5.81	5.66	5.73					6.24	6.24							6.57	6.59	6.58		6.26	6.43						
19	6.42		6.42	5.58		5.58				6.44	6.18	6.29				6.30	6.10	6.19				6.72			6.39	6.20	6.28			
20	6.18	5.97	6.06				5.45	5.75	5.57	6.76	6.02	6.25				6.14	6.15	6.14	6.51	6.51	6.51					6.05	6.13			
21	6.12	5.97	6.04				5.90	5.69	5.78		6.16	6.16				6.50	6.07	6.23							6.23					
22	6.19	5.59	5.79				5.74		5.74				7.10		7.10	6.14	6.20	6.17												
23					5.62	5.62							7.25	7.10	7.17															
24	6.32	5.45	5.70		5.52	5.54							6.70		6.70							5.99		5.99						
25	6.21	6.00	6.09	5.57									6.83	6.27	6.47				6.58	5.91	6.13									
26	6.19	5.99	6.08	5.62	5.60	5.61										6.27	6.45	6.35												
27	6.24	6.05	6.13													6.45	6.45	6.45	5.89	6.30	6.05									
28	5.87	5.84	5.85	5.97		5.97										6.21	5.90	6.03												
29	6.02	5.97	5.99										6.48	6.44	6.46	6.02	0.52	6.02												
30				5.87	5.56	5.69							6.12	6.30	6.20															
31				5.59	5.51	5.55							6.04	6.15	6.09					0.18										
m			6.12			5.70			5.60			6.21			6.62			6.23			0.31			6.10			6.20			0.20

Accumulation period daily pH in the Rhône meltwaters (1999-2001)

Date	pH
16/11/99	1.92
5/12/00	2.42
9/4/00	2.96
5/12/00	2.74
18/1/01	3.27
7/3/01	4.03
m	2.89

Mean daily pH concentrations

Month	n	pH	± (1 sigma)
January	2	7.32	
February	0		
March	1	7.40	
April	1	7.86	
May	11	6.58	
June	15	6.23	
July	26	6.16	
August	15	5.77	
September	14	5.70	
October	3	6.39	
November	1	7.50	
December	1	6.91	
	Abl.		**Accu.**
Mean	5.97		7.17
±	0.46		0.84
n	106		6



Ablation period pH at minimum and maximum discharge in the Oberaar meltwaters (1999-2001)

	07_99			08_99			09_99			10_99			05_00			06_00			07_00			08_00			09_00			10_00		
Date	10	17	daily	10	17	daily	10	17	daily	10	17	daily	10	17	daily	10	17	daily	10	17	daily	10	17	daily	10	17	daily	10	17	daily
1							7.1	7.5	7.3													7.4		7.3	7.1	7.4	7.2			
2																												7.1		7.1
3				7.6	7.6	7.6													7.5	7.5	7.5									
4										7.1	7.1	7.1							7.5											
5				7.3	8.0	7.5													7.6	7.5	7.6									
6																			7.5				7.0	7.1						
7	7.5	8.2	7.7																			7.2								
8	7.7	8.1	7.9													7.0														
9				7.6	8.2	7.8																			7.2	7.7	7.4				
10							8.1	8.5	8.2				7.4		7.4															
11	7.2	7.5	7.3																7.6	7.6	7.6									
12	7.2	7.6	7.4	7.2	8.1	7.4													7.1											
13																7.6	7.4	7.5	7.5											
14																7.4	7.4	7.4												
15	7.5	7.5	7.5				7.5	7.9	7.6							7.5														
16				7.2	7.3	7.2																								
17													8.5		8.5				7.5	7.4	7.5									
18	7.3	7.3	7.3																7.5	7.7	7.6					7.1		0.0		
19																7.2	7.6	7.3	7.5	7.5	7.5	7.2	7.3	7.2	7.3		7.3			
20																7.6	7.4	7.5	7.5	7.3	7.4					7.3	7.3			
21																7.2	7.0	7.1								7.7	7.7			
22																7.4	7.3	7.3												
23							7.8	7.8	7.8																			0.0		
24																						7.9	7.6	7.7						
25				8.1	8.9	8.3																								
26	7.0															7.7	7.5	7.6	7.2	7.4	7.3									
27																7.6	7.2	7.3												
28																7.3	7.3	7.3												
29																7.5	7.5	7.5												
30							7.1	7.1	7.1																					
31																				7.2										
m			7.5			7.5			7.4			7.1		**7.1**	7.7			7.4			7.5			7.3			7.3			7.1

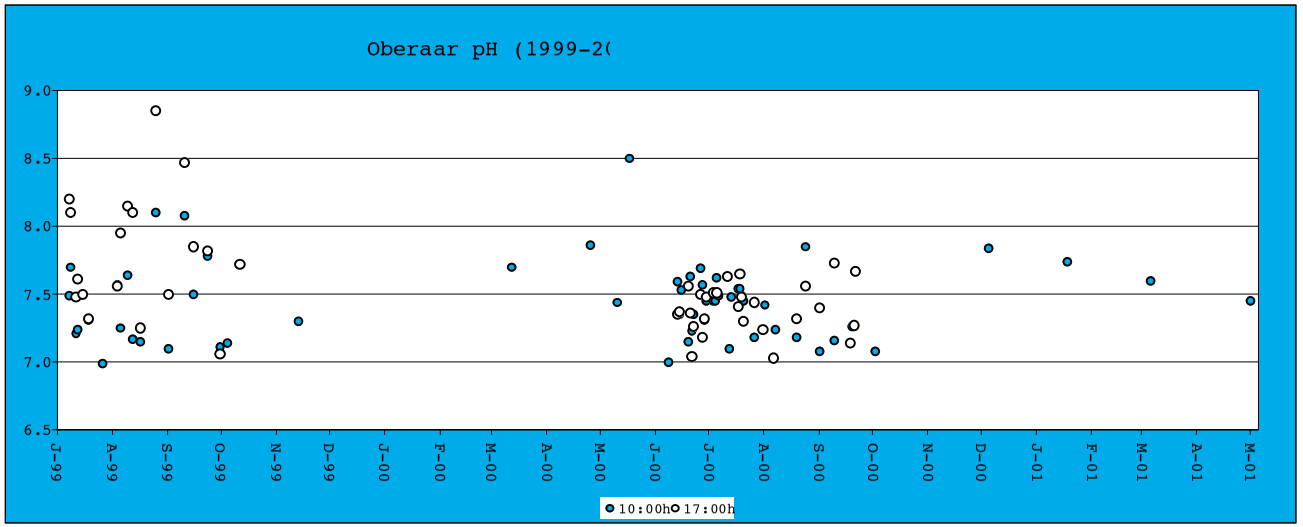
Accumulation period daily pH in the Oberaar meltwaters (1999-2001)

Date	pH
11/11/99	7.72
13/1/00	7.30
12/3/00	7.70
25/4/00	7.86
5/12/00	7.84
18/1/01	7.74
6/3/01	7.60
m	7.68

Mean daily pH

Month	n	mg/l
January	2	7.47
February	0	
March	2	7.65
April	1	7.86
May	3	7.60
June	10	7.35
July	14	7.47
August	11	7.42
September	10	7.40
October	3	7.11
November	1	7.72
December	1	7.84

	Abl. 10:00	**Accu.**
Mean	7.4	7.64
±	0.30	0.19
n	49	7



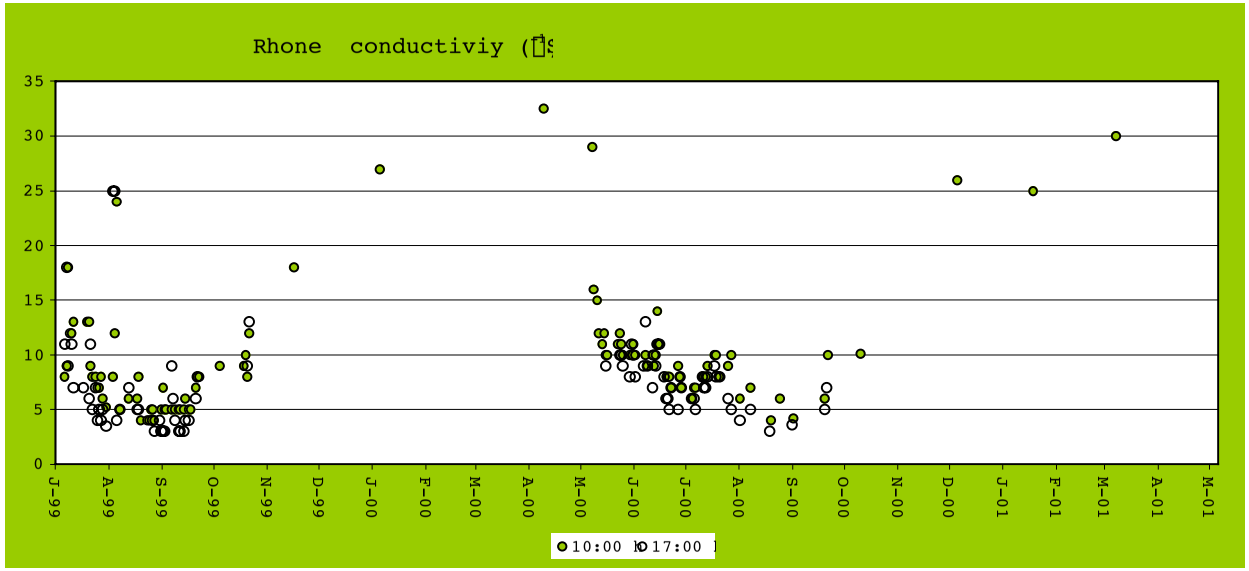
Ablation period conductivity (µs/cm) at minimum and maximum discharge in the Rhône meltwaters (1999-2001)

	07_99			08_99			09_99			10_99			05_00			06_00			07_00			08_00			09_00			10_00		
Date	10	17	daily	10	17	daily	10	17	daily	10	17	daily	10	17	daily	10	17	daily	10	17	daily	10	17	daily	10	17	daily	10	17	daily
1							7.0	3.0	4.0							10.0	8.0	9.0				6.0	4.0	5.0	4.2					
2							5.0	3.0	4.0																					
3				8.0	25.0	16.5	5.0																							
4				12.0	25.0	18.5				9.0		9.0							6.0	6.0	6.0									
5				24.0	4.0	14.0													7.0	6.0	6.5									
6	8.0	11.0	9.5				5.0	9.0	7.0								9.0		7.0	5.0	6.0									
7	9.0	18.0	13.5	5.0	5.0	5.0		6.0					29.0		29.0	10.0	13.0	11.5				7.0	5.0	6.0						
8	18.0	9.0	13.5				5.0	4.0	4.5				16.0		16.0	9.0	9.0	9.0												
9	12.0																													
10	12.0	11.0	11.5				5.0	3.0	4.0				15.0		15.0				8.0	8.0	8.0							10.1		10.1
11	13.0	7.0	10.0				5.0	3.0	4.0				12.0		12.0	10.0	7.0	8.5	8.0	7.0	7.5									
12				6.0	7.0	6.5										9.0	10.0	9.5	8.0	7.0	7.5									
13							5.0	3.0	4.0				11.0		11.0	10.0	9.0	9.5	9.0	8.0	8.5									
14							6.0	4.0	5.0				12.0		12.0	14.0	11.0	12.5												
15													10.0	9.0	9.5	11.0	11.0	11.0												
16							5.0	4.0	4.5				10.0		10.0															
17		7.0		6.0	5.0	5.5	5.0												10.0	9.0	9.5									
18				8.0	5.0	6.5				9.0		9.0					8.0		10.0	8.0	9.0		3.0	3.5						
19	13.0			4.0						10.0		10.0				8.0	6.0	7.0				4.0			6.0	5.0	5.5			
20	13.0	6.0	9.5				7.0	6.0	6.5	8.0	9.0	8.5				8.0	6.0	7.0	8.0	8.0	8.0					7.0	8.5			
21	9.0	11.0	10.0				8.0	8.0	8.0	12.0	13.0	12.5				8.0	5.0	6.5							10.0					
22	8.0	5.0	6.5				8.0						11.0			7.0	7.0	7.0												
23				4.0									12.0	10.0	11.0															
24	8.0	7.0	7.5	4.0									11.0	10.0	10.5							6.0								
25	7.0	4.0	5.5	5.0									10.0	9.0	9.5				9.0	6.0	7.5									
26	7.0	5.0	6.0	5.0	4.0	4.5										9.0	5.0	7.0												
27	8.0	4.0	6.0	4.0	*3.0*	3.5										8.0	8.0	8.0	10.0	5.0	7.5									
28	6.0	5.0	5.5													7.0	7.0	7.0												
29													10.0	8.0	9.0															
30	5.2	3.5	4.4		4.0	4.5							10.0	11.0	10.5															
31				5.0	3.0	5.0							11.0	10.0	10.5								3.6	3.9						
m			6.1			5.7			5.6			6.2			6.6			6.2			0.3			6.1			6.2			0.2

Accumulation period daily conductivity in the Rhône meltwaters (1999-2001)	
Date	(mg/l)
16/11/99	18.0
7/12/99	
5/1/00	27.0
9/4/00	32.5
5/12/00	26.0
18/1/01	25.0
7/3/01	30.0
m	26.4

Mean daily conductivity

Month	n	mg/l	± (1 sigma)
January	2	26.0	
February	0		
March	1	30.0	
April	1	32.5	
May	14	12.5	5.1
June	15	8.7	1.9
July	26	8.1	2.3
August	15	7.2	4.9
September	13	5.3	1.6
October	6	9.9	1.4
November	1	18.0	
December	1	26.0	
	Abl. 10:00	**Abl.** 17:00	**Accu.**
Mean	8.8	7.3	26.4
±	3.8	4.0	5.0
n	99	82	6



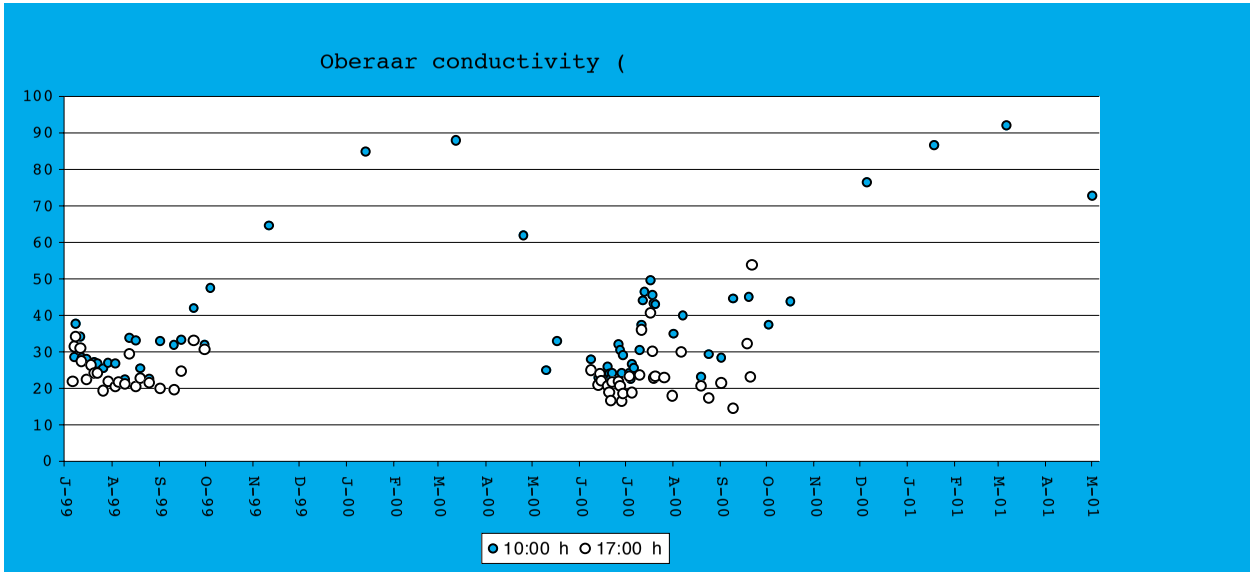
Ablation period conductivity at minimum and maximum discharge in the Oberaar meltwaters (1999-2001)

	07_99			08_99			09_99			10_99			05_00			06_00			07_00			08_00			09_00			10_00		
Date	10	17	daily	10	17	daily	10	17	daily	10	17	daily	10	17	daily	10	17	daily	10	17	daily	10	17	daily	10	17	daily	10	17	daily
1							33.0	20.0	26.5													35.0		26.5	28.4	21.5	25.0			
2																														
3				26.8	20.5	23.7													24.3	23.3	23.8									
4										47.6		47.6							22.6											
5				21.4	21.8	21.6													26.7	18.8	22.8									
6		21.9	21.9																25.6				30.0	35.0						
7	28.6	31.5	30.1																			40.0								
8	37.8	34.3	36.1													28.0	25.0	26.5												
9				22.5	21.2	21.9																			44.7	14.5	29.6			
10							31.9	19.7	25.8				25.0		25.0				30.5	23.6	27.1							10.1		10.1
11	34.2	31.1	32.7																37.5	36.1	36.8									
12	28.5	27.4	28.0	33.8	29.5	31.7													44.2											
13																23.0	21.0	22.0	46.5											
14																24.0	24.0	24.0												
15	28.1	22.4	25.3				33.3	24.7	29.0							24.0	22.0	23.0												
16				33.2	20.5	26.9																								
17													33.0		33.0				49.7	40.6	45.2									
18	26.3	26.4	26.4																45.6	30.2	37.9					32.3	38.7			
19				25.5	22.8	24.2										26.0	20.6	23.3	43.4	22.9	33.2	23.2	20.7	22.0	45.1					
20	27.2	24.2	25.7													24.0	18.9	21.5	43.1	23.3	33.2					23.1	34.1			
21																22.8	16.6	19.7								53.8				
22	26.8	24.2	25.5													24.2	21.8	23.0												
23							42.0	33.2	37.6																					
24																						29.4	17.3	23.4						
25				22.6	21.6	22.1																								
26	25.5	19.4	22.5													32.1	21.9	27.0	23.0	23.0	23.0									
27																30.5	20.6	25.6												
28																24.1	16.5	20.3												
29	27.0	21.9	24.5													29.2	18.5	23.9												
30							32.0	30.7	31.4																					
31																				18.0										
m			27.1			24.6			30.1			47.6			29.0			23.3			31.4			26.7			31.8			0.2

Accumulation period daily conductivity in the Oberaar meltwaters (1999-2001)	
Date	(µs/cm)
11/11/99	64.7
13/1/00	85.0
12/3/00	88.0
25/4/00	62.0
5/12/00	76.6
18/1/01	86.7
6/3/01	92.0
m	79.3

Mean daily conductivity

Month	n	(µs/cm)	± (1 sigma)
January	2	86.3	
February	0		
March	2	90.0	
April	2	67.5	
May	2	29.0	
June	12	23.3	2.3
July	25	29.4	6.9
August	10	25.2	4.6
September	10	30.0	5.4
October	3	39.9	10.2
November	1	64.7	
December	1	76.6	
	Abl. 10:00	**Abl.** 17:00	**Accu.**
Mean	31.9	24.2	79.3
±	9.8	6.8	11.9
n	65	54	7



Estimated discharge from the Oberaar catchment 1999-2001 (m^3/s)

Day	7_99		8_99		9_99		10_99		11_99	12_99	1_00	2_00	3_00	4_00	5_00	6_00		7_00		8_00		9_00		10_00	11_00	12_00	1_01	2_01	3_01
	10	17	10	17	10	17	10	17	10	10	10	10	10	10	10	10	17	10	17	10	17	10	17	10	10	10	10	10	10
1					1	3														2		2	3	1					
2																													
3			2	3														2	3										
4							1											2											
5			2	3														2	3							0.2			
6		5																2			2								0.15
7	3	3																		1									
8	2	3														2	2												
9			2	3																		2	3						
10					2	3									1			2	3										
11	2	3							0.2									1	2										
12	2	3	2	3									0.15					1											
13											0.15					1	2	1											
14																1	2												
15	2	3			2	3										1	2							1					
16			2	3																									
17															1			1	1										
18	3	3																1	2				3				0.15		
19			2	3												1	2	1	2	2	3	2							
20	2	3														2	2	1	2				4						
21																2	2						1						
22	2	3												0.25		2	2												
23					1	2																							
24																				1	2								
25			2	3																									
26	2	3														1	2	3	4										
27																1	2												
28																1	3												
29	2	3														2	2												
30					1	2																							
31																			3										

RHONE	SiO_2 %	TiO_2 %	Al_2O_3 %	Fe_2O_3 %	FeO %	MnO %	MgO %	CaO %	Na_2O %	K_2O %	P_2O_5 %	LOI %	Fe tot %	Ba ppm	Cr ppm	Cu ppm	Nb ppm	Ni ppm	Pb ppm	Rb ppm	Sr ppm	V ppm	Y ppm	Zn ppm	Zr ppm
Suspension																									
R_{oyr}	67.9	0.4	15.3	1.6	1.8	0.1	1.3	0.9	3.9	4.8	0.09	1.8	3.58	515	20	7	38	7	29	335	100	32	73	66	134
R_{oyr}'	67.6	0.4	15.1	1.8	1.9	0.1	1.5	0.9	3.7	4.8	0.1	1.7	3.9	533	15	9	36	5	27	337	103	38	64	76	151
Mean	67.8	0.4	15.2	1.7	1.8	0.1	1.4	0.9	3.8	4.8	0.1	1.8	3.7	524	18	8	37	6	28	336	102	35	69	71	143
Meltout																									
R1	82.6	0.1	9.4	0.3	0.3	0.0	0.2	0.5	3.2	3.0	0.04	0.3	0.60	262	5	2	18	3	9	132	61	7	47	75	374

OBERAAR	SiO_2 %	TiO_2 %	Al_2O_3 %	Fe_2O_3 %	FeO %	MnO %	MgO %	CaO %	Na_2O %	K_2O %	P_2O_5 %	LOI %	Fe tot %	Ba ppm	Cr ppm	Cu ppm	Nb ppm	Ni ppm	Pb ppm	Rb ppm	Sr ppm	V ppm	Y ppm	Zn ppm	Zr ppm
Suspension																									
O_{oyr}	61.7	0.67	16.3	2.31	3.37	0.11	3.1	2	2.81	4.31	0.18	3.04	6.05	1026	99	31	17	42	27	224	238	100	33	118	177
O_{oyr}'	63.7	0.65	15.7	2.11	2.93	0.1	2.54	2	3.1	4.13	0.18	2.54	5.37	938	67	27	19	32	32	221	237	86	38	103	221
Mean	62.7	0.7	16.0	2.2	3.2	0.1	2.8	2.0	3.0	4.2	0.2	2.8	5.7	982	83	29	18	37	30	223	238	93	36	111	199
Meltout																									
O1	72.9	0.3	13.2	0.8	1.2	0.1	1.0	1.9	4.4	2.6	0.17	1.5	2.19	625	26	12	8	12	19	99	317	38	23	105	192
O2	69.8	0.4	14.3	1.4	1.6	0.1	1.4	2.0	4.5	2.9	0.17	1.7	3.15	678	43	19	10	20	32	117	334	56	25	114	205
O3	72.8	0.3	13.7	0.9	0.9	0.0	0.8	1.5	4.7	3.1	0.11	0.9	1.88	563	21	14	9	12	19	104	235	34	26	26	226
O4	72.3	0.4	13.4	1.2	1.2	0.1	1.0	1.9	4.4	2.7	0.17	1.4	2.43	636	28	15	9	12	23	100	327	43	25	103	228
O5	71.4	0.4	14.5	1.0	1.2	0.1	0.9	1.9	4.8	3.2	0.13	1.1	2.25	625	26	12	14	10	16	116	263	37	33	107	249
Mean	71.8	0.3	13.8	1.0	1.2	0.1	1.0	1.8	4.5	2.9	0.2	1.3	2.4	625	29	14	10	13	22	107	295	42	26	91	220

Sample	Phyllosilicates %	Quartz %	K-Feldspar %	Plagioclase %	Calcite %	Unquantified %
6-7-99 (10:00)	9.5	19.8	19.8	77.3	0.5	0.0
6-7-99 (17:00)	19.9	21.4	4.7	8.1	1.2	44.7
6-7-99 (17:00)	8.6	30.5	33.4	39.2	0.8	0.0
11-7-99 (17:00)	55.0	34.8	1.3	10.4	0.0	0.0
21-7-99 (10:00)	10.3	35.1	30.5	38.6	0.9	0.0
22/7/1999 (time unknown)	9.9	33.8	32.0	42.5	0.2	0.0
22-7-99 (10:00)	11.4	34.5	41.5	57.3	0.3	0.0
22-7-99 (17:00)	22.3	21.0	12.9	22.9	0.0	20.9
25-7-99 (10:00)	13.4	16.8	29.5	26.7	0.0	13.5
25-7-99 (17:00)	19.2	26.1	17.4	25.5	0.5	11.2
27-7-99 (11:00)	18.6	24.5	19.0	28.4	0.6	8.9
27-7-99 (17:00)	18.5	14.5	12.1	23.7	0.8	30.3
27-7-99 (11:00)	12.1	31.0	26.1	23.3	1.0	6.5
28-7-99 (22:00)	5.1	34.1	16.7	27.6	0.8	15.7
28-7-99 (04:00)	10.0	29.3	20.4	38.0	0.5	1.9
28-7-99 (09:00)	12.3	19.7	19.7	33.8	1.1	13.5
28-7-99 (17:00)	10.3	22.3	14.2	28.5	0.9	23.7
24-8-99 (10:00)	27.6	17.3	18.3	31.7	0.5	4.7
25-8-99 (11:00)	8.9	12.1	7.9	18.5	0.0	52.6
30-8-99 (17:00)	5.1	9.3	7.1	16.2	0.0	62.3
15-9-99 (10:30)	5.5	3.6	3.1	5.5	0.4	81.8
18-10-99 (13:00)	5.4	7.0	4.2	9.2	0.3	73.8
20-10-99 (12:00)	6.6	2.9	3.1	8.5	0.6	78.3
Meltout	0.0	21.7	3.5	8.3	0.0	66.5
Mean	14.2 (± 10.8)	21.8 (±10.2)	17.2 (± 11.1)	27.9 (± 16.7)	0.5 (± 0.4)	23.7 (±27.7)

Sample	Phyllosilicates %	Quartz %	K-Feldspar %	Plagioclase %	Calcite %	Unquantified %
8-7-99 (17:00)	17.1	13.1	6.2	21.0	1.1	41.5
11-7-99 (10:00)	27.0	11.8	2.8	12.4	0.5	45.5
15-7-99 (10:00)	9.2	28.9	5.1	40.0	2.8	14.0
15-7-99 (17:00)	6.3	28.8	10.4	22.6	0.0	31.8
22-7-99 (17:00)	23.6	13.4	4.6	17.5	3.0	38.0
22-7-99 (17:00)	11.0	29.1	26.8	32.6	2.0	0.0
5-8-99 (10:00)	14.9	19.0	5.4	29.9	2.5	28.3
12-8-99 (17:00)	13.9	15.1	4.5	13.7	8.0	44.7
19-8-99 (10:00)	6.4	30.4	10.5	30.6	4.9	17.2
19-8-99 (17:00)	13.6	38.9	5.4	16.2	1.9	24.0
25-8-99 (17:00)	10.4	25.5	2.5	31.3	0.0	30.3
25-8-99 (17:00)	17.5	25.5	0.0	0.0	0.0	57.0
1-9-99 (10:0c)	13.8	0.0	3.1	16.4	2.4	64.3
1-9-99 (10:0a)	14.8	67.2	2.6	27.8	2.9	0.0
10-9-99 (10:0b	11.9	10.7	2.9	26.8	2.4	45.2
10-9-99 (17:0c)	10.2	23.2	2.4	27.7	5.0	31.5
15-9-99 (10:00)	23.9	10.7	3.1	16.7	2.2	43.5
15-9-99 (17:00)	8.1	25.3	5.1	24.3	1.4	35.7
23-9-99 (10:00)	12.4	42.6	2.6	22.0	1.9	18.5
23-9-99 (17:00)	17.6	26.2	8.2	27.0	2.3	18.6
30-9-99 (10:00)	10.6	29.0	10.7	27.4	1.8	20.5
30-9-99 (17:00)	12.2	22.5	12.6	48.8	1.8	2.1
4-10-99 (12:00)	7.5	22.3	12.7	51.8	1.5	4.1
Mean	13.7 (± 5.5)	24.3 (±13.5)	6.5 (± 5.7)	25.4 (± 11.5)	2.3 (± 1.8)	28.5 (±17.9)

"Unquantified minerals" may be due to a number of factors: the main reason is that the atomic composition of the samples (for minerals with solid solution seies like the feldspars) was different to the atomic composition for the standards which were passed, thereby affecting the unit cell parameters. Calcite only has one atomic composition which is identical to the calcite standard passed on the XRD, therefore it's concentrations are the most accurate.

Samples were partially orientated when they were passed on the x-ray, which means there may be a positive bias in the number of platy phyllosilicated being intercepted by the monochromatic x-rays.

Samples were also passed on cellulose acetate filter papers, and so if the sediment concentration was particiarly low this may have created interference with the beam.
Sample 1-9-99 was not passed twice, but was rather as a split sample, which was poured in two aliquots into the filter equipment, 1-9-99 a was poured just after the sample had been agitated and therefore contains nearly 70 % quartz. On the other hand sample 1-9-99 b was poured latter and may not have been reagitated before pouring, therefore it contains no grains in the 16-32 μm fraction (see appendix 3-3-8b) and no quartz.

RHÒNE SUSPENSION	63 - 125 µm %	32 - 63 µm %	16 - 32 µm %	8 - 16 µm %	4 - 8 µm %	2 - 4 µm %	1 - 2 µm %	0 - 1 µm %
6-7-99 (10:00)	0	0	14.22	17.97	33.48	21.18	9.04	4.11
6-7-99 (10:00)	0	18.66	18.44	16.16	23.73	14.84	5.46	2.7
6-7-99 (17:00)	0	0	2.39	14.01	38.78	28.19	11.14	5.48
6-7-99 (17:00)	0	17.58	19.37	14.66	25.01	15.3	5.58	2.51
11-7-99 (17:00)	0	0	0	9.16	41.83	29.93	12.24	6.84
21-7-99 (10:00)	0	0	12	20.73	33.08	21.21	8.77	4.21
21-7-99 (10:00)	0	4.88	23.12	16.17	28.28	17.34	7.03	3.17
24-7-99 (11:00)	0	10.98	15.03	15.22	27.52	18.99	8.21	4.06
27-7-99 (13:00)	0	0	12.88	17.4	32.66	24.54	8.64	3.88
27-7-99 (17:00)	0	0	11.6	19.22	33.95	23.24	8.39	3.61
27-7-99 (23:00)	0	0	2.39	17.94	34.06	28.59	11.64	5.38
28-7-99 (01:00)	0	10.17	18.64	16.82	25.98	19.38	6.34	2.68
11-8-99 (19:00)	0	5.79	26.58	14.98	25.94	16.42	6.93	3.35
24/8/99 (17:00)	0	0	2.98	15.59	39.72	25.32	10.51	5.88
25/8/99	0	9.97	16.81	13.86	27.84	19.73	8.18	3.61
28-8-99 (9:00)	0	0	7.87	16.01	35.87	24.83	10.37	5.06
28-8-99 (17:00)	0	0	7.18	20.2	36.56	24.4	8.3	3.35
30/8/99	0	0	4.42	14.06	37.94	26.38	11.38	5.82
8/9/99	0	0	0	6.9	41.68	29.15	14.53	7.74
15/9/99	0	0	0	6.74	38.62	31.68	14.93	8.03
19/9/99	0	0	0.02	13.6	37.77	28.82	13	6.78
21-9-99 (17:00)	0	0	17.43	21.83	29.62	19.14	8.03	3.95
18/10/99 (13:00)	0	0	0	4.58	36.41	32.14	16.3	10.57
20/10/99 (12:00)	0	0	0.09	10.82	40.04	28.57	13.01	7.46
mean	**0.00**	**3.25**	**9.73**	**14.78**	**33.60**	**23.72**	**9.91**	**5.01**
	(± 0.00)	(± 5.84)	(± 8.46)	(± 4.44)	(± 5.62)	(± 5.28)	(± 2.99)	(± 2.05)

OBERAAR SUSPENSION	63 - 125 µm %	32 - 63 µm %	16 - 32 µm %	8 - 16 µm %	4 - 8 µm %	2 - 4 µm %	1 - 2 µm %	0 - 1 µm %
8-7-99 (10:00)	0	0	2.56	17.76	42.18	25.41	8.49	3.6
12-7-99 (10:00)	0	0	1.84	16.99	38.63	26.71	10.79	5.04
15-7-99 (10:00)	0	0	0	10.61	39.4	31.32	12.78	5.88
15-7-99 (10:00)	0	15.17	26.26	19.85	19.87	12.24	4.6	2.01
15-7-99 (17:00)	0	0	1.41	24.04	37.55	24.49	8.72	3.79
22-7-99 (10:00)	0	0	0	6.38	39.24	33.52	14.14	6.71
22-7-99 (17:00)	0	0	0.7	16.97	38.07	27.85	10.95	5.74
26-7-99 (17:00)	0	0	0	8	38.37	32.53	14.14	6.95
26-7-99 (17:00)	0	34.59	25.43	13.46	15.13	8.04	2.5	0.84
5-8-99 (10:00)	0	0	0.31	17.3	38.06	28.25	10.86	5.22
5-8-99 (17:00)	0	24.51	14.56	16.17	24.57	14.79	4.04	1.37
12-8-99 (10:00)	0	15.98	19.37	18.32	23.01	14.95	5.73	2.64
12-8-99 (17:00)	0	0	17.21	17.2	30.35	20.68	9.52	5.03
19/8/99 (10:00)	0	0	1.82	14.21	39.22	28.34	10.88	5.53
19/8/99 (17:00)	0	10.26	19.2	18.2	26.99	16.76	6	2.6
25-8-99 (10:00)	0	11.1	25.61	16.44	25.05	13.88	5.3	2.62
25-8-99 (17:00)	1.1	33.8	16.57	12.97	19.11	11.48	3.55	1.41
1/9/99 (10:00)	0	0	0	25.3	35.66	22.74	10.32	5.97
1/9/99 (10:00)	0	0	20.89	17.26	27.97	20.56	8.6	4.72
1/9/99 (17:00)	0	0	2.13	16.29	40.95	26.58	9.82	4.24
10-9-99 (10:00)	0	0	4.71	23.16	33.53	24.94	9.15	4.5
15/9/99 (10:00)	0	3.24	12.94	23.3	30.76	18.99	7.33	3.54
15/9/99 (17:00)	0	0	4.93	19.16	38.36	24.38	8.94	4.23
23-9-99 (10:00)	0	0	4.16	19.57	34.35	25.43	10.8	5.7
23-9-99 (17:00)	0	3.68	6.47	23.95	32.7	21.39	8.14	3.68
30-9-99 (10:00)	0	2.69	32.25	19.01	24.17	14.21	5.2	2.48
30-9-99 (17:00)	0	0	15.25	15.97	31.69	22.95	9.69	4.45
4:10:99 (12:00)	0	14.76	31.22	17.57	19.73	10.88	3.96	1.88
1:10:99 (12:00)	0	0	15.95	14.05	30.43	22.81	10.81	5.94
mean	**0.04**	**5.85**	**11.16**	**17.22**	**31.56**	**21.62**	**8.47**	**4.08**
	(± 0.20)	(± 10.19)	(± 10.58)	(± 4.44)	(± 7.63)	(± 6.87)	(± 3.14)	(± 1.70)

CHAPTER 4

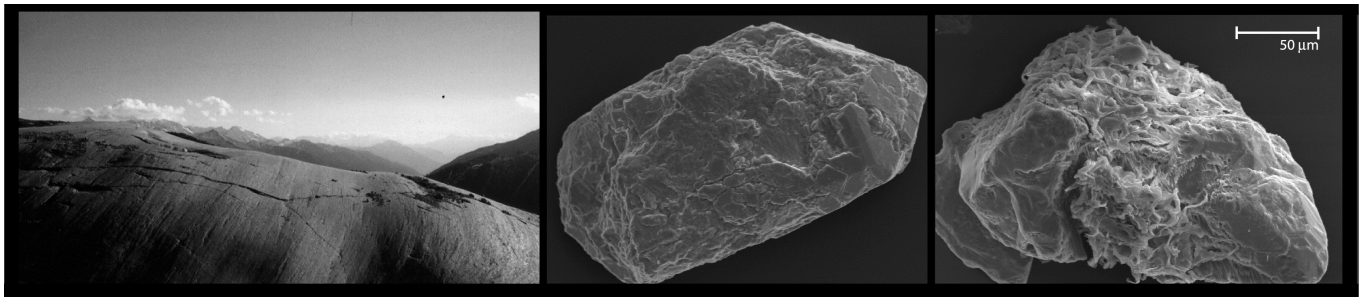
Love, like circum-stellar diamonds

A fire-flash seared on the retinas black canvas
Startled intake of breath at that
Almighty convergence, atomic fusion.
E= mc^2 and boy did it ripple out fast!
A tidal-wave, tsunami, 60KPa.
And zack

Out on the fringes, nuids floating on the tide
Suspended in the circum-stellar envelope
They caught it
No poom! Kebam!

Rather a glassy stillness, rigid crystalline calm
Angstron pricks of diamond chronometry
Never to forget the nanosecond after my star began.

Rachel Hosein: for my family



ELEVATED APATITE WEATHERING RATES IN ALPINE GLACIER FOREFIELDS (RHÔNE AND OBERAAR GLACIERS, CENTRAL SWITZERLAND)

Hosein, R.,[1] Arn, K.,[1] Lee, M.R,[2] Steinmann, P.,[1] and Föllmi, K.B.[1]

Institut de Géologie, Université de Neuchâtel, Neuchâtel 2007, CH[1]
Division of Earth Sciences, Lilybank Gardens, University of Glasgow, Glasgow G12 8QQ, UK[2]

Abstract

Apatite dissolution textures and long-term detrital phosphorus (P) weathering rates were determined from chronosequences in the Oberaar and Rhône glacier forefields, central Switzerland. Apatite grains from present-day outwash sediments, Little Ice Age moraines and Younger Dryas tills were graded (1-4) relative to weathering-induced changes in their surface morphologies. Present-day apatite grains are heavily indented and dissolution rounded (grade 1). Little Ice Age grains from two 0-10 cm depth samples already showed extensive dissolution etching, similar to surface grains from the Younger Dryas profile (mean grades 2.7, 3.5 and 3.5 respectively). The weathering front deepened progressively due to bio-corrosion in the evolving acidic pedosphere, with mechanical indentations on grains acting as sites for preferential dissolution. Ironbound, organic, and detrital P concentrations were measured in the chronosequences: organic and ironbound P in the Younger Dryas profiles replaces detrital P. Detrital P weathering rates are calculated as 0.31 and 0.28 g m^{-2} yr^{-1} for Little Ice Age moraines and 0.01g m^{-2} yr^{-1} for Younger Dryas tills. During the first 300 yrs of glacial sediment exposure P dissolution rates were ≈ 70 times higher than the mean global riverine dissolved P flux from ice-free continents. Over 11.6 kyr the flux is 2.5 times the global mean. These data strengthen the argument for changes in the biolimiting P flux on glacial-interglacial timescales.

Introduction

Phosphorus (P) is an essential nutrient and its supply to the biosphere fosters and may even limit primary productivity (Broecker and Peng, 1982; Haselwandter et al., 1983; Tyrell, 1999). Physical weathering is the first order control on the supply of apatite, the principal P-bearing mineral, to the biosphere (Syers and Walker, 1976; Filippelli and Delaney, 1994). Rates of subsequent biogeochemical weathering of apatite are controlled by its quantity and reactive surface area, the ambient temperature and the supply of weathering solution (Guidry and Mackenzie, 2000). Physical abrasion in the subglacial environment produces large volumes of silt sized sediment grains with complicated microtopographies

This chapter has been submitted to Geology.

and consequently enhanced reactive mineral surface areas (e.g. Mahaney, 1995). Apatite is particularly prone to comminutation, owing to its (weak) cleavage and relatively low hardness. Moreover, although the near-neutral pH of glacial meltwaters probably renders apatite chemically unreactive in the subglacial environment (Stumm and Morgan, 1996), deposition of mechanically preconditioned apatite grains in proglacial sediments and their exposure to pedogenic processes may accererate biogeochemical P weathering rates. Our study of glacial chronosequences in the Rhône and Oberaar forefields, Switzerland, demonstrates elevated apatite weathering rates in their proglacial zones compared to the average global riverine P flux (Meybeck, 1993). Weathering intensities were assessed by observing changes in grain morphologies, quantifying different forms of P (organic, detrital and ironbound; see below) and calculating weathering rates of detrital P over the last 11.6 kyr. We suggest that apatite dissolution rates are enhanced in proglacial settings due to a combination of physical and chemical factors: i.e. the mechanical abrasion of sediment and the percolation of porewaters that are acidified by atmospheric aerosols and pedogenic processes.

Field areas, sampling, soil identifications, and methods

We sampled a chronosequence (present-day, Little Ice Age = LIA and Younger Dryas = YD sediments) in each glacial forefield. The forefields are approximately 10 km apart and are comparable in their present vegetation (alpine flowers, grasses, and shrubs), altitude (Rhône, 1750 m; Oberaar, 2310 m), climate (mean annual temperature and precipitation for Rhône: +1.2°C, 2200 mm; Oberaar: -1°C, 2100 mm; EDI, 1992) and geology (the crystalline rocks of the Aar massif). The Rhône bedrock consists of Variscan granites (≈ 90%) and granodiorites (≈ 10%), whereas the Oberaar bedrock is a mixture of strongly foliated, pre-Variscan gneisses (≈ 40%), Variscan granites (≈ 50%) and granodiorites (≈ 10%). These distributions hold for the LIA ice extent of both glaciers, and the YD ice extent in the Oberaar catchment. But the Rhône YD ice would have also covered the foliated gneissic zone (≈ 20%) and been joined to the adjacent Mutt glacier, which is underlain by metamorphosed Mesozoic sedimentary rocks (≈ 20 %) in addition to the granite and granodiorite (≈ 40 %).

Fresh outwash sediment from the Rhône glacier snout and suspended sediment in the two glaciers' meltwaters were considered as present-day material (Rhône: $\mathbf{R_{0yr\ outwash}}$, $\mathbf{R_{0yr\ susp.}}$; Oberaar: $\mathbf{O_{0yr\ susp.}}$). LIA moraine ridges dated as 140- and 145 yr and 240-270 yr old were sampled (Oberaar: $\mathbf{O_{140yr}}$; Rhône: $\mathbf{R_{145yr}}$ and $\mathbf{R_{270yr}}$; Ammann, 1977; Zumbühl, 1988). We also sampled tills that are interpreted to have been deposited during the rapid, globally synchronous breakdown of the YD glaciers 11.6 kyr ago, and to have remained ice-free after this event (Rhône: $\mathbf{R_{11.6kyr}}$; Oberaar: $\mathbf{O_{11.6\ kyr}}$; Zumbühl, 1988; Alley et al., 1993; Hormes et al., 2001). 1 m profiles were dug in the LIA moraine walls and integrated samples were taken at 10 cm intervals. The YD section $\mathbf{O_{11.6\ kyr}}$ terminated in bedrock at 60 cm and the YD section $\mathbf{R_{11.6\ kyr}}$ was dug to a Bw horizon at 70 cm depth (soil

classification according to USDA, 1998, 1999). An appendix has been placed in the Geology Data Repository containing general soil descriptions; soil pH's; the ratio of the < 2 mm fraction; detrital P and TiO_2 concentrations and the bulk densities (Appendix 1).

Apatite grains were isolated in samples from sites $\mathbf{R}_{0yr\ outwash}$, $\mathbf{O}_{140yr}$, $\mathbf{R}_{270yr}$, and $\mathbf{R}_{11.6kyr}$: Approximately 500 g of sediment sample was wet sieved in order to ascertain the granulometry. Apatite grains from the 125-250 μm fraction (approx. 30-120 g) were concentrated by heavy liquids and magnetic separation; confirmation of their chemical composition was obtained using an energy dispersive X-ray spectroscopy (EDS). The surface morphologies of all the apatite grains found whilst combing each sample for a minimum of 4 hours were assessed with an environmental scanning electronic microscope (ESEM; Philips XL30 FEG EDS). Observations were made with regard to the scale, intensity, and location of biogeochemical weathering features on the individual apatite grains.

We also performed two sets of analyses on the < 2mm fraction of samples from sites $\mathbf{O}_{140yr}$ and $\mathbf{O}_{11.6\ kyr}$, and $\mathbf{R}_{145yr}$, $\mathbf{R}_{270yr}$, and $\mathbf{R}_{11.6kyr}$, which were ground up in an agate mill for 3 minutes. Firstly, we determined TiO_2 concentrations using an X-ray spectrometer (XRF PW 24000), in order to correct for volume change in the profiles. Secondly, we measured ironbound, detrital, and organic P concentrations by sequential extraction (SEDEX; Ruttenberg, 1992; Tamburini, 2001). The SEDEX method was originally designed for use on marine sediments and has applied to lake and river sediments (e.g. Filippelli and Souch, 1999). We interpret the "authigenic" P phase extracted by the sodium acetate step as detrital P, based on a test series of SEDEX analyses on pure apatite grains (Hosein, unpublished data) and on the observation that prolonged grinding enhances dissolution of the detrital analog phase in the sodium acetate extraction step (Ruttenberg, 1992). Furthermore authigenic P does not normally form in acidic soils (Sharpley, 2000) and was not observed on any detrital grains in the ESEM study. A spectrophotometer (Perkin Elmer UV/VIS Lambda 10) was used to determine the detrital and organic P, and an ICP-AES (Perkin Elmer Optima 3000) to quantify the ironbound P.

Calculating detrital P weathering rates

We calculated detrital P weathering rates for the more complete and chemically homogenous Rhône chronosequence using a method analogous to Taylor and Blum (1995): The present-day phosphorus inventory (L) is for a surface of 1 m^2 and a depth of 1m (minimal apatite grain dissolution is observed in the LIA samples at this depth and Egli et al. (2001) define 1m as the BC horizon of the YD profile). L is calculated as the sum of 10 cm thick soil slices (L_j): $L_j = P_j \rho_j F_j V_j$, where P_j is the present-day detrital P concentration. The soil density, ρ_j, is taken from Egli et al., (2001) and F_j is the weight fraction of < 2 mm material of the total mass of the till (Appendix 1; a positive bias may be introduced as large clasts > 4 cm are not included). V_j is the volume of soil slice j.

The mass of P initially present in each soil slice, prior to any weathering, is $S_j = P_j / X_j$, where X_j is the depletion factor. Based on the assumption that titanium is immobile in these granitic soils, the depletion factor can be calculated as $X_j = (P_j / P_0)/(Ti_j / Ti_0)$, where Ti_j is the measured concentration of Ti in the soil slice j and Ti_0 is the Ti concentration of the parent material. The concentration of detrital P (mg/g) in the parent material is P_0.

Subtracting the summed inventories of present-day P from the summed inventory of initial P, gives the amount of P weathered: $W_P = \Sigma S_j - \Sigma L_j$. The long term P weathering rate at each site (R_{LT}), is W_P divided by the soil age.

Results

Biogeochemical weathering and apatite grain surface morphology

From observations of the morphology of apatite grain surfaces we identify four different grades of chemical weathering (Fig. 1):

1 Mechanically and slightly biogeochemically weathered: Whole grains show "fresh", unaltered surfaces, with the exception of the presence of localised mechanical indentations; zooming in the mechanically indentations show dissolution rounding (Fig. 1: 1 and 1a)

2 Mechanically and biogeochemically weathered: Whole grains show rather "fresh" and only slightly altered surfaces, with localised mechanical indentations; zooming in the indentations are locally chemically etched to form a sugary texture and localised denticular margins (Fig. 1: 2 and 2a)

3. Predominantly biogeochemically weathered: Whole grains show a "sugary" surface texture; zooming in, the surface is covered by pervasive initial lenticular etch pits and denticular margins (Fig. 1: 3 and 3a)

4. Pervasively biogeochemically weathered: Whole grains are heavily etched. Individual pits have coalesced to form pervasive acicular or tower block-like structures (Fig. 1: 4 and 4a) and/ or extensive enlargement of pits has generated a secondary porosity in the grain.

Each isolated grain was graded according to this scale and a mean grade was established for each sample (Table 1).

Generally, in grains of grades 1 and 2, mechanically damaged surface areas (e.g., along chatter marks and

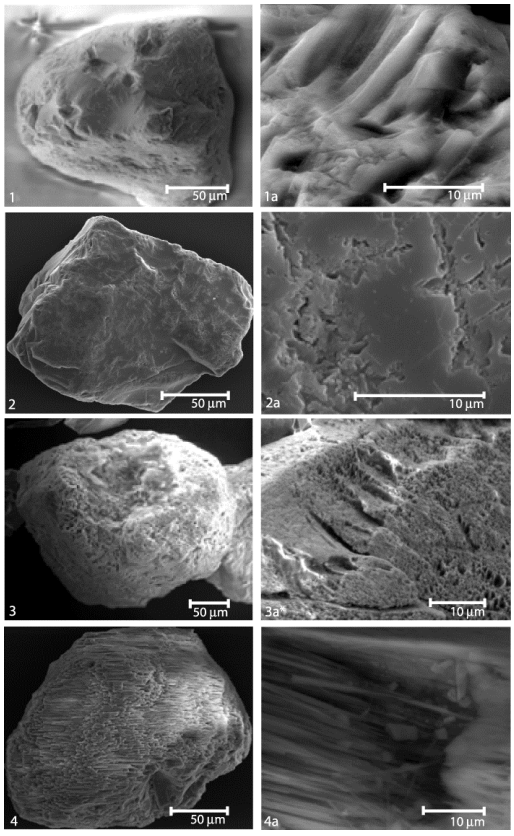


***Fig. 1**: Typical grain morphologies of the four apatite-weathering grades.*

3a, The physical erosion feature allows more pervasive chemical etching*

fractures) are sites of preferential biogeochemical weathering (Fig. 1: 3a). We also observed that the mean weathering grades of surface samples from sites $\mathbf{O_{140yr}}$ and $\mathbf{R_{270yr}}$ (2.7) and (3.5) are higher than samples from the middle of the profiles (1.4 and 1.8 respectively). The mean grades of weathering in the middle and bottom slices of site $\mathbf{R_{11.6kyr}}$ are 2.6 and 2.8 respectively and 68 % fewer apatite grains were observed in these samples compared to those of LIA age, albeit similar amounts of sediment being treated (≈ 30-40 g). In general, the intensity of biogeochemical weathering depends on sample age and depth, with highest weathering grade (4) even observed in grains from the top sample of the 140 yr old moraine. At site $\mathbf{O_{140yr}}$ (0-10cm), we identified two apatite grains where denticular weathering structures were covered in fungal hyphae (Fig. 2).

Table 1: Weathering grades of the apatite grains

Sample	Grains analysed	Grade 1	Grade 2	Grade 3	Grade 4	Mean grade
R_{0yr}						
Meltout sed.	5	5				1.0
O_{140yr}						
(0-10 cm)	11	2	3	2	4	2.7
(40-50 cm)	7	4	3			1.4
(90-100 cm)	9	6	3			1.3
R_{270yr}						
(0-10 cm)	11			6	5	3.5
(40-50 cm)	10	5	2	1	1	1.8
(90-100 cm)	10	7	2	1		1.4
$R_{11.6kyr}$						
(0-10 cm)	6			3	3	3.5
(30-40 cm)	4	1	1	2	1	2.6
(60-70 cm)	4		1	3		2.8

Each sample represents the apatite grains concentrated from ≈ 500 g of sample and was combed for at least 4 hours in order to detect a maximum number of apatite grains

SEDEX P forms

Extraction of different P forms by the SEDEX method shows that the mean detrital P concentrations in $\mathbf{R_{0yr\ susp}}$ and $\mathbf{O_{0yr\ susp}}$ are 0.32 (± 0.05 mg/g) and 0.58 (± 0.08 mg/g), organic P measures 0.09 mg/g and 0.14 mg/g (± 0.005 mg/g) and ironbound P is below detection (< 0.03 mg/g). Detrital P remains the predominant P phase at the LIA sites and ironbound P is still below detection; mean C-horizon detrital P values are almost three times higher in the $\mathbf{O_{140yr}}$ profile (0.63 mg/g) than the $\mathbf{R_{145yr}}$ profile (0.23 ± 0.05 mg/g). Detrital P is reduced in the $\mathbf{R_{270yr}}$ profile (0.15 ± 0.03 mg/g) and again at the YD sites, where ironbound P is dominant (especially in the surface samples). The presence of organic P is almost entirely limited to surface samples (max. depth is 30 cm) and its concentration increases as a function of age, with nearly 4 times as much organic P in $\mathbf{O_{11.6kyr}}$ as $\mathbf{R_{11.6kyr}}$. Whereas total P concentrations remain stable throughout the LIA profiles, total P increases considerably towards the upper part of the YD sections. Total P values in YD surface samples are 5 to 10 times higher than in LIA samples.

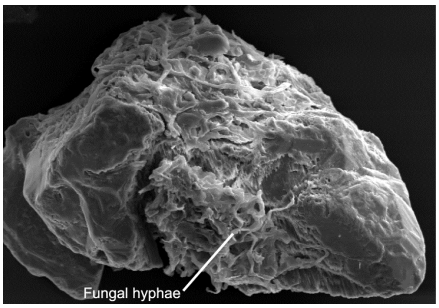


Fig. 2: *Apatite grain showing denticular weathering structures covered in fungal hyphae ($O_{140\ yr}$, 0-10 cm).*

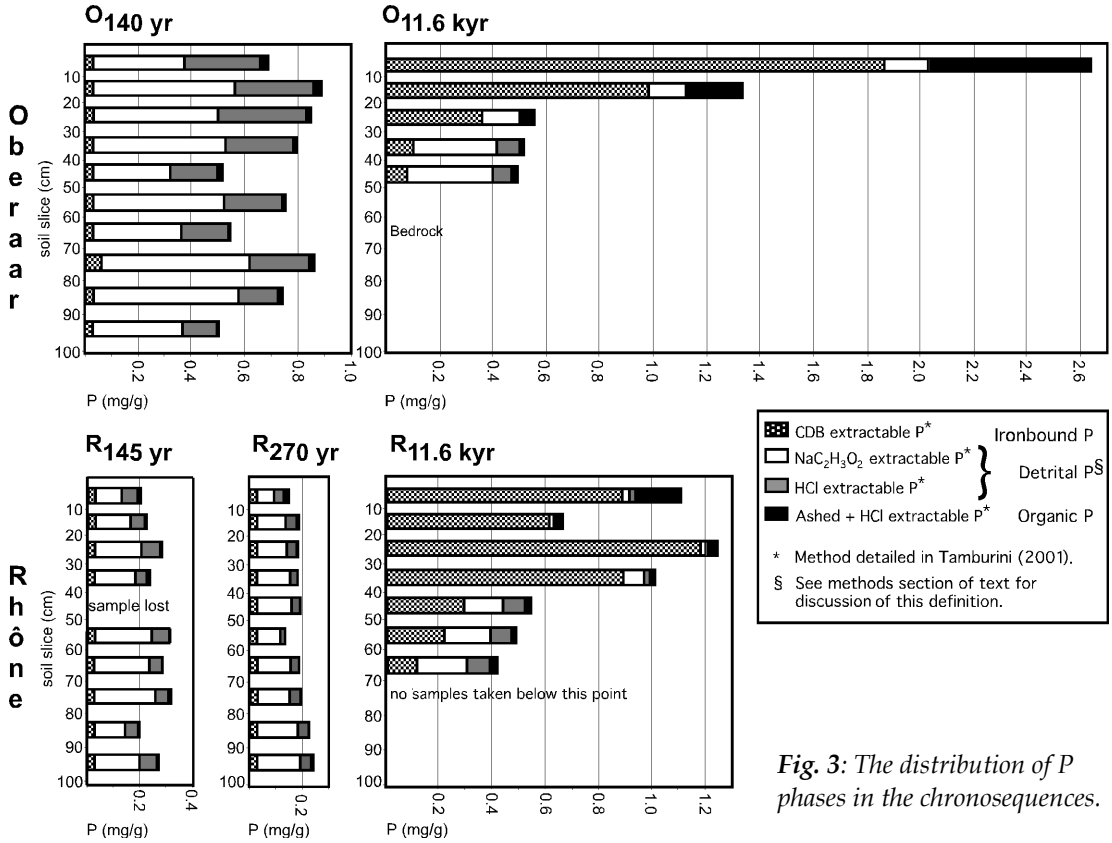


***Fig. 3**: The distribution of P phases in the chronosequences.*

Detrital P weathering rates

We calculate detrital P weathering rates at LIA sites of 0.31 and 0.28 g m^{-2} yr^{-1} (**R_{145yr}; R_{270yr}**). At YD site **$R_{11.6kyr}$** the rate decreases to 0.01 g m^{-2} yr^{-1}. LIA rates are calculated by approximating P_0 as the mean detrital P concentration of present-day suspended sediment and the **R_{145yr}** C-horizon (0.29 mg/g) and Ti_0 as the mean Ti concentration in the **R_{145}** C-horizon (0.21 mg/g). The change in source rock composition of the YD profile may change its P_0 and Ti_0. Because the YD profile C-horizon was not sampled we estimate P_0 by extrapolating the linear increase in detrital P between 40-70 cm down to 100 cm (the BC horizon after Egli, 2001; 0.34 mg/g detrital P) and we assume that the Ti_0 measured at 60 and 70 cm remains constant to 100 cm depth (0.32 mg/g). The use of a P_0 derived from the LIA parent material would double the YD weathering rate.

Discussion and Conclusions

Our observations of the progressive change in surface morphology of whole apatite grains, the systematic shift in the composition of P from detrital to ironbound and organic P forms, and our estimations of the weathering rate of detrital P indicate that apatite is actively biogeochemically weathered in proglacial areas and converted into other P forms. The weathering rates of other soft and chemically reactive minerals, i.e. carbonates and metal sulphides are also higher in arctic and alpine Little Ice Aged proglacial sediments with respect to equivalent fluxes from presently ice-covered areas (30-50 %; Anderson

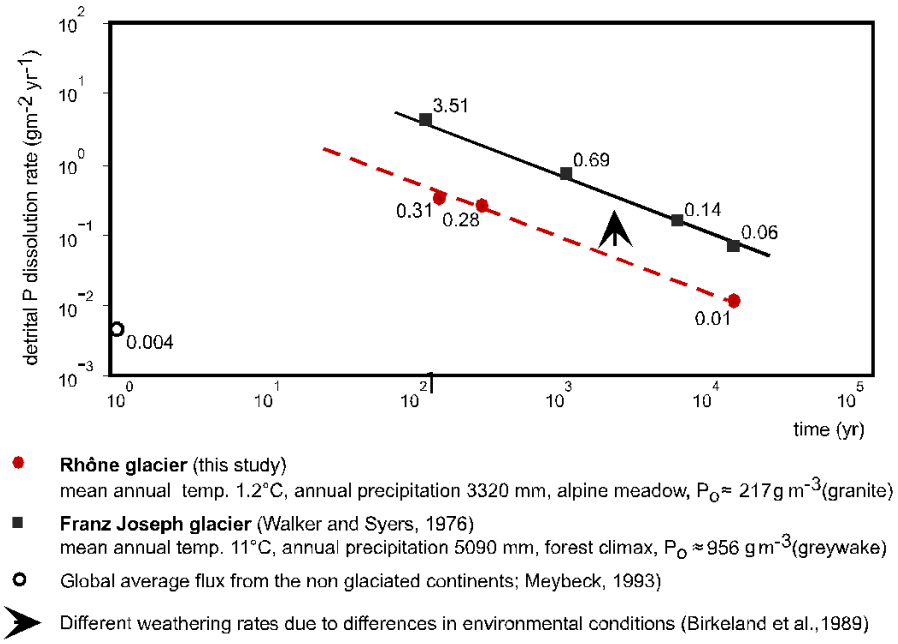


Fig. 4: *Phosphorus weathering rates in two proglacial chronosequences*

et al., 2000; Wadham et al., 2001). Apatite grains are preconditioned for biogeochemical weathering by mechanical abrasion during subglacial transit, facilitated by their (weak) tendency to cleave and fairly low Vickers hardness. Apatite weathering is most intense at the tops of profiles where pedogenic and biological processes are localised and the pH may be as low as 4.6 (Appendix 1). Two major modes of acid hydrolysis can be distinguished on apatite grains. Firstly, diffuse etching is attributed to the acidic soil solution, whose pH is lowered by the rapid oxidation of sulphides in the proglacial environment (e.g. Anderson et al., 2000), acid aerosols and acidifying pedogenic processes. Secondly, intense localised dissolution is interpreted as active biogeochemical weathering (Fig. 2; Frossard et al., 1995). After only 140–270 years of exposure a combination of chemical and active biogeochemical processes probably give rise to surficial apatite grains with the same weathering grade as 11.6 kyr grains from 50-70 cm depth.

The detrital P weathering rates reported here are one order of magnitude lower than those calculated by Walker and Syers (1976), although the decrease in weathering intensity with age is comparable (Fig. 4). We attribute the difference in weathering intensity to the warmer, wetter climate of Walker and Syers' chronosequence, which is located in the Franz Joseph glacier forefield (Fig. 4; see also Birkland et al., 1989).

The P dissolution rates we calculate for the Rhône proglacial area are approximately 70 times higher than the world average dissolved P flux from non-glaciated continents (0.004 g P m^{-2} yr^{-1}; Meybeck, 1993). Filippelli and Souch (1999) postulate that the low P binding capacity of proglacial protosoils may allow an important flux of bioavailable P to leak into aquatic ecosystems and

enhance productivity. The 0.07 mg/g drop in the mean detrital P content of the Rhône sediments over 130 yr ($\mathbf{R_{145yr}} - \mathbf{R_{270yr}}$) with no increase in ironbound or organic P forms may support this hypothesis, but the possibility of initial variability in the detrital P concentrations between profiles can not be discounted. During deglaciation following the last glacial maximum 28 % of the Northern Hemisphere's land surface fell within the proglacial zone, (Gibbs and Kump, 1994). Consequently elevated dissolution of detrital P has a geographically wide-ranging impact on bioproductivity (Föllmi, 1995).

Increased terrestrial productivity may only be achieved in a more evolved, conservative pedosphere with more efficient internal recycling of P (Crews et al., 1995). During pedogenesis a combination of biological and abiological mechanisms gradually sequester labile P from precipitation and weathering inputs, leading to the concentration of P on the continents in increasingly bioavailable (kyr timescales) and subsequently recalcitrant (myr timescales) organic and ironbound P forms (Haselwandter et al., 1983; Birkland et al., 1989; this study, YD tills). In oligotropic tropical soils after millions of years the eolian inputs of detrital P, which limit productivity, are partially derived from glacial sources (Crews et al., 1995; Chadwick et al., 1999 and references therein).

In conclusion, during deglaciation the widespread exposure of reactive proglacial sediment and the rapid dissolution of associated detrital P may increase bioavailable P supply to both terrestrial and aquatic ecosystems on centennial to millennial timescales.

Acknowledgements

Massoud Dadras and Mireille Leboeuf (both Neuchâtel) assisted with the ESEM, Giulio Galetti (Fribourg) provided the XRF data, and J. Ondrus and S. Pierrehumbert (SCPE-laboratory, Neuchâtel) performed the ICP-AES analysis, and Jean-Michel Gobat (Neuchâtel) helped with soil identification. Swiss National Science Foundation grants 21-53997.98 and 20-61485.00 are gratefully acknowledged.

Appendix

Appendix 1: Soil descriptions

References

Alley R. B., Meese D., Shuman C.A., Gow A.J., Taylor K.C., Grootes P.M., White J.W.C., Ram M., Waddingtion E.D., Mayewski P.A. and Zielinski G.A. (1993) Abrupt increase in Greenland snow accumulation at the end of the Younger Dryas event. *Nature* **362**: 527-529.

Ammann K. (1977) Der Oberaargletscher im 18., 19. und 20. Jahrhundert. *Zeitschrift für Gletscherkunde und Glazialgeologie* **Bd XII 2**: 253-291.

Anderson S.P., Drever J.I., Frost C.D. and Holden P. (2000) Chemical weathering in the foreland of a retreating glacier. *Geochimica et Cosmochimica Acta* **64**: 1173-1189.

Birkland P.W., Burke R.M. and Benedict J.B. (1989) Pedogenic gradients for iron and aluminium accumulation and phosphorus depletion in Arctic and Alpine soils as a function of time and climate. *Quaternary Research* **32**: 193-204.

Broecker W. and Peng T.-H. (1982) Tracers in the sea. Lamont-Doherty Geological Observatory, Palisades, N.Y: **pp** 690.

Chadwick O.A., Derry L.A., Vitousek P.M., Huebert B.J. and Hedin L.O. (1999) Changing sources of nutrients during four million years of ecosystem development. *Nature* **397**: 491-497.

Crews T.E., Kitayama K., Fownes J.H., Riley R.H., Herbert D.A. and Mueller-Dombois D. (1995) Changes in soil phosphorus fractions and ecosystem dynamics across a long chronosequence in Hawaii. *Ecology* **76**: 1407-1424.

EDI, (Eidgenössisches Department des Innern), (1992) Hydrologischer Atlas der Schweiz: Bern, Switzerland, Bundesamt für Landeshydrologie-und-Geologie: **pp** 206.

Egli M., Fitze P. and Mirabella A. (2001) Weathering and evolution of soils formed on granitic, glacial deposits: results from chronosequences of Swiss alpine environments. *Catena* **45**: 19-47.

Filippelli G.M. and Delaney M.L. (1994) The oceanic phosphorus cycle and continental weathering during the Neogene. *Paleoceanography* **60**: p. 643-652.

Filippelli G.M. and Souch C. (1999) Effects of climate and landscape development on the terrestrial phosphorus cycle. *Geology* **27**: 171-174.

Föllmi K.B. (1995) 160 m.y. Record of marine sedimentary phosphorus burial: Coupling of climate and continental weathering under greenhouse and icehouse conditions. *Geology* **23**: 859-862.

Frossard E., Brossard M., Hedley M.J. and Metherell A. (1995) Reactions controlling the cycling of P in Soils, *In:* Tiessen H. (Ed) *Phosphorus in the global environment: Transfers, cycles and management*. Scope **54**: 107-137. Wiley.

Gibbs M.T. and Kump L.M. (1994) Global chemical erosion during the last glacial maximum and the present: Sensitivity to changes in lithology and hydrology. *Paleoceanography* **9**: 529-543.

Guidry M.W. and Mackenzie F.T. (2000) Apatite weathering and the Phanerozoic phosphorus cycle. *Geology* **28**: 631-634.

Hay W.W. (1998) Detrital sediment fluxes from continents to oceans. *Chemical Geology* **145**: 287-323.

Haselwandter K., Hofmann A., Holzmann H. -P. and Read D.J. (1983) Availability of nitrogen and phosphorus in the nival zone of the Alps: *Oecologia* **57**: 266-269.

Hormes A., Mueller B.U. and Schluechter C. (2001) The Alps with little ice: evidence for eight Holocene phases of reduced glacier extent in the Central Swiss Alps. *The Holocene* **11**: 255-265.

Körner C. (1999) Alpine plant life: Functional plant ecology of high mountain ecosystems: Germany, Springer: **pp** 338.

Mahaney W.C. (1995) Glacial crushing, weathering and diagenetic histories of quartz grains inferred from scanning electron microscopy: 487-590. *In*: Menzies J. (Ed) *Modern glacial environments. Processes, dynamics and sediments. Glacial Environments* **1** : Butterworth-Heinemann, Oxford: **pp** 621.

Meybeck M. (1993) Natural sources of C, N, P and S: 163-193. *In*: Wollast R. Mackenzie F.T. and Chou L. (Eds.) Interactions of C, N, P and S Biogeochemical Cycles and Global Change. *NATO ASI Series:* **I 4**. Springer-Verlarg, Berlin Heidelberg.

Pennington W. (1981) Records of a lake's life in time: the sediments. *Hydrobiologia* **79***: 197-219.*

Ruttenberg K.C. (1992) Development of a sequential extraction method for different forms of phosphorus in marine sediments. *Limnology and Oceanography* **37**: 1460-1482.

Sharpley A. (2000) Phosphorus Availability: p. D-18-D-36. *In:* Sumner M.E. (Ed) *Handbook of soil science*. CRC Press.

Stumm W. and Morgan J.J. (1996) *Aquatic Chemistry*. Wiley, New York: **pp** 1022.

Tamburini F. (2001) *Phosphorus in marine sediments during the last 150,000 years: exploring relationships between continental weathering, productivity, and climate* [Ph.D. thesis]: University of Neuchâtel, Switzerland: **pp** 219.

Taylor A. and Blum J.D. (1995) Relation between soil age and silicate weathering rates from the chemical evolution of a glacial chronosequence. *Geology*: **23**: 979-982.

Tyrell T. (1999) The relative influences of nitrogen and phosphorus on oceanic primary production. *Nature* **400**: 525-531.

Wadham J.L., Cooper R.J., Tranter M. and Hodgkins R (2001) Enhancement of solute fluxes in the proglacial zone of a polythermal glacier. *Journal of Glaciology* **47**: 378-386.

Walker T.W. and Syers J.K. (1976) The fate of phosphorus during pedogenesis. Geoderma **15**: 1-19.

Zumbühl H. J. (1988) Der Rhônegletscher in den historischen quellen: 129-322. *In*: Zumbühl, H.J., & Holzhauser H. (Eds.) Alpengletscher in Kleinen Eiszeit, Die Alpen, Zeitschrift der Schweizen Alpen-Clubs, Bern.

Appendix 1: chronosequence parameters

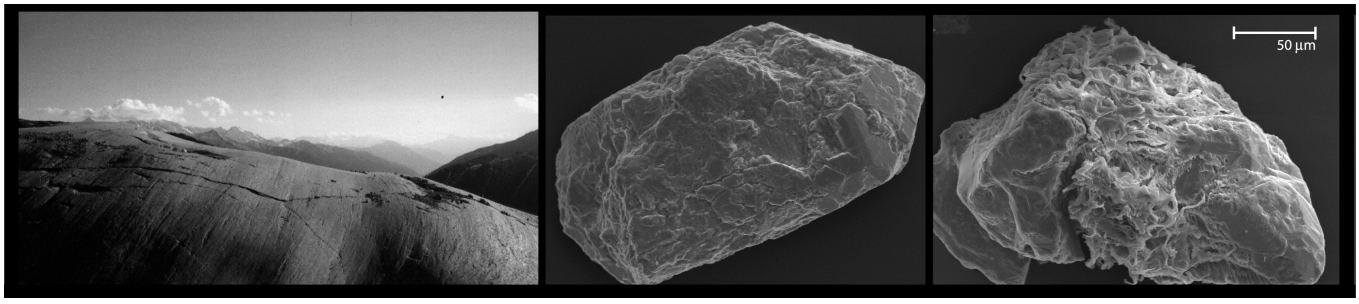
	140/145 yr							270 yr							11.6 kyr						
sample depth (cm)	soil type & horizon	Det_P (mg/g)	TOC %	pH	TiO_2 (mg/g)	bulk density [§]	< 2mm	soil type & horizon	Det_P (mg/g)	TOC %	pH	TiO_2 (mg/g)	bulk density [§]	< 2mm	soil type & horizon	Det_P (mg/g)	TOC %	pH	TiO_2 (mg/g)	bulk density [§] (g/ cm^3)	< 2mm[*]
Rhone	Orthent (Entisol)							Umbrept (Inceptisol)							Humod (Spodosol)						
0-10	Oh-Ah-Ac	0.16	0.24	5.0	0.22	1.02	0.55	Oh-Ah-Bw	0.10	0.67	4.6	0.21	0.91	0.59	Oh-Ah	0.05	5.05	-	0.34	0.60	0.66
10-20	Ac	0.19	0.15	5.2	0.20	1.30	0.56	Bw	0.15	0.37	4.8	0.22	1.22	0.50	E	0.02	1.45	5.4	0.33	1.32	0.39
20-30	Ac	0.24	<0.1	6.0	0.18	1.20	0.67	BwC	0.15	0.19	4.9	0.21	1.24	0.45	Bhs	0.04	1.93	5.4	0.40	1.28	0.46
30-40	C	0.20	<0.1	6.4	0.20	1.30	0.52	(Bw)C	0.15	<0.1	5.9	0.19	1.37	0.47	Bhs[†]	0.10	1.12	5.5	0.43	1.24	0.42
40-50		-	<0.1	6.6	0.19	1.30	0.71	C	0.16	<0.1	6.0	0.20	1.53	0.39	Bw	0.23	1.01	5.5	0.35	1.55	0.63
50-60		0.28	<0.1	6.5	0.22	1.30	0.47		0.11	<0.1	6.1	0.17	1.53	0.39	Bw	0.25	0.68	5.9	0.35	1.56	0.88
60-70		0.25	<0.1	6.4	0.22	1.30	0.62		0.16	<0.1	6.2	0.17	1.53	0.45	Bw	0.27	0.37	5.8	0.32	1.56	0.80
70-80		0.28	<0.1	6.5	0.2	1.30	0.65		0.16	<0.1	6.3	0.2	1.53	0.55							
80-90		0.16	<0.1	6.7	0.21	1.30	0.68		0.19	<0.1	6.5	0.21	1.53	0.55							
90-100		0.24	<0.1	6.9	0.19	1.30	0.78		0.20	<0.1	6.2	0.21	1.53	0.44	BC[§]						
Oberaar	Orthent (Entisol)														Humod (Spodosol)						
0-10	Oh-Ah	0.63	0.11	5.4	0.46										Oh-Ah	0.17	24.09	6.7	0.28		
10-20	AC	0.83	<0.1	6.3	0.41										E	0.14	9.00	6.5	0.33		
20-30	C	0.80	<0.1	6.7	0.40										Bhs	0.13	3.49	6.1	0.42		
30-40		0.75	<0.1	7.1	0.35										Bw	0.40	1.54	5.5	0.43		
40-50		0.47	<0.1	7.2	0.33										Bw	0.39	1.03	5.7	0.39		
50-60		0.71	<0.1	7.2	0.34										Bw		<0.1	5.8	0.39		
60-70		0.51	<0.1	7.7	0.36										R						
70-80		0.79	<0.1	7.9	0.37																
80-90		0.69	<0.1	8.2	0.38																
90-100		0.47	<0.1	8.1	0.38																

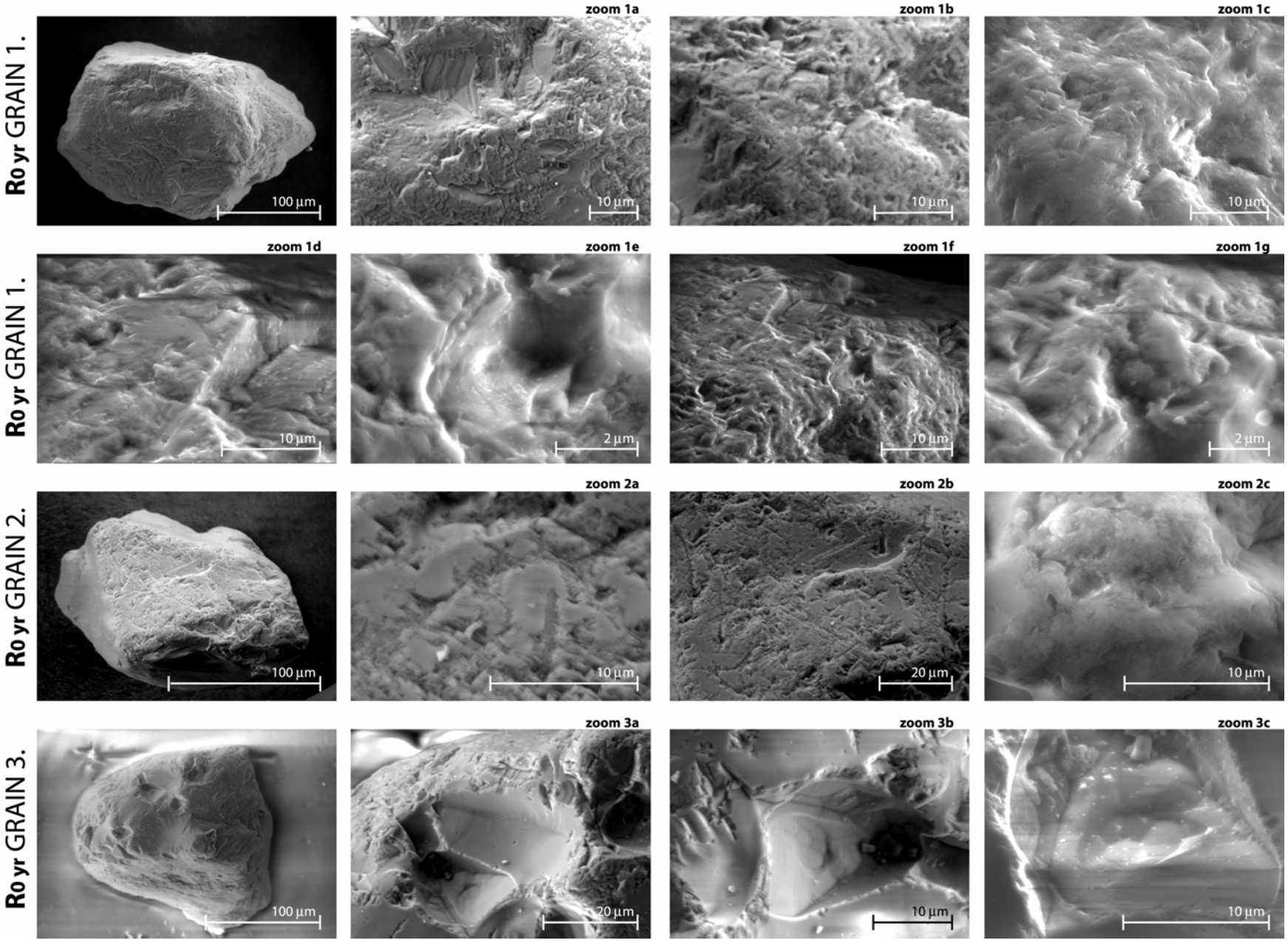
[†] A rust layer was observed in this zone, we interpret it as the presence of a water table.

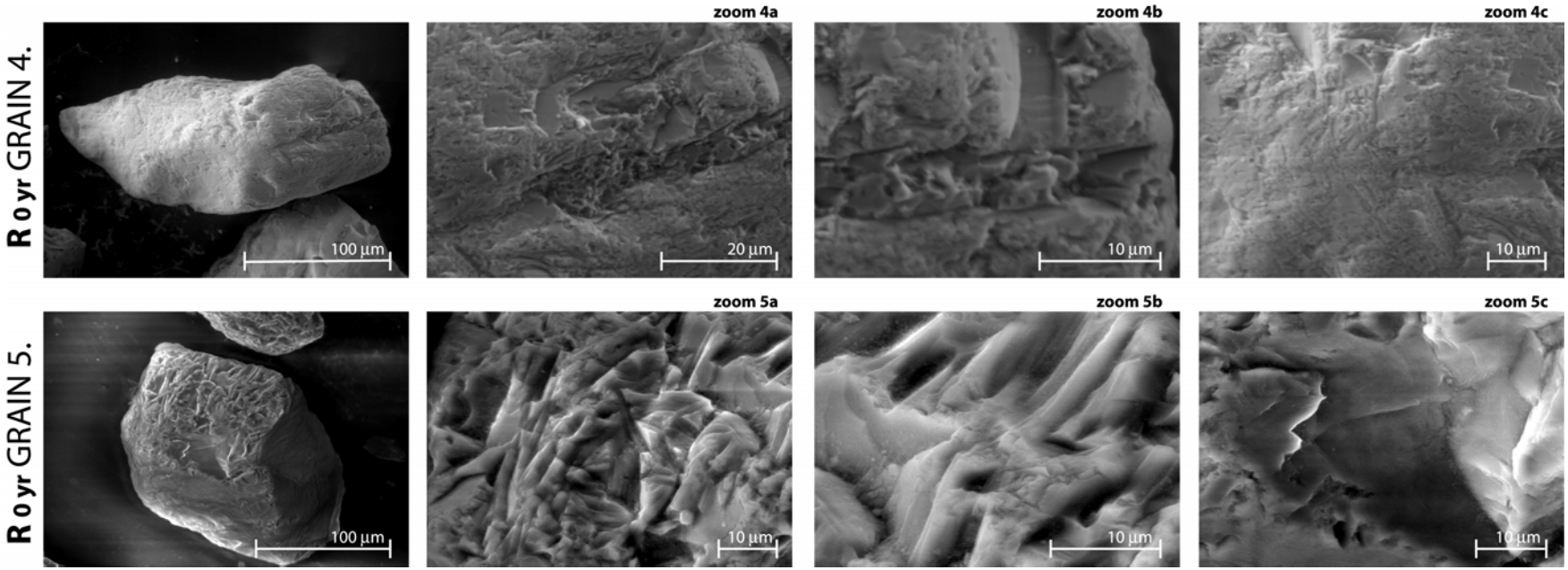
[§](Egli et al. 2001)

[*] Ratio of the < 2 mm fraction

CHAPTER 4
appendicies




Ro yr GRAIN 1.
zoom 1a
zoom 1b
zoom 1c
100 µm
10 µm
10 µm
10 µm
Ro yr GRAIN 1.
zoom 1d
zoom 1e
zoom 1f
zoom 1g
10 µm
2 µm
10 µm
2 µm
Ro yr GRAIN 2.
zoom 2a
zoom 2b
zoom 2c
100 µm
10 µm
20 µm
10 µm
Ro yr GRAIN 3.
zoom 3a
zoom 3b
zoom 3c
100 µm
20 µm
10 µm
10 µm


R oyr GRAIN 4.
zoom 4a
zoom 4b
zoom 4c
100 µm
20 µm
10 µm
10 µm
R oyr GRAIN 5.
zoom 5a
zoom 5b
zoom 5c
100 µm
10 µm
10 µm
10 µm

O140 yr (0-10cm)
GRAIN 1.
O140 yr (0-10cm)
GRAIN 2.
O140 yr (0-10cm)
GRAIN 3.
O140 (0-10cm)
GRAIN 4.
100 µm
zoom 1a
10 µm
zoom 2a
10 µm
zoom 3a
5 µm
zoom 4a
5 µm
zoom 3b
5 µm
zoom 4b
5 µm

O140 yr (0-10cm)
GRAIN 5.

O140 yr (0-10cm)
GRAIN 6.

O140 yr (0-10cm)
GRAIN 7.

O140 yr (0-10cm)
GRAIN 8.

O140 yr (0-10cm) GRAIN 8.

O140 yr (0-10cm) GRAIN 9.

O140 yr (0-10cm) GRAIN 10.

O140 yr (0-10cm) GRAIN 11.

O140 yr (30-40cm)
GRAIN 1.

O140 yr (30-40cm)
GRAIN 2.

O140 yr (30-40cm)
GRAIN 3.

O140 yr (30-40cm)
GRAIN 4.

O140 yr (30-40cm)
GRAIN 5.

O140 yr (30-40cm)
GRAIN 6.

O140 yr (30-40cm)
GRAIN 7.

O140 yr (90-100 cm)
GRAIN 1.
O140 yr (90-100 cm)
GRAIN 2.
O140 yr (90-100 cm)
GRAIN 3.
100 µm
zoom 1a
10 µm
zoom 1b
10 µm
zoom 1c
10 µm
zoom 1d
100 µm
zoom 1e
10 µm
zoom 1f
10 µm
zoom 1g
10 µm
100 µm
zoom 2a
50 µm
zoom 2b
10 µm
100 µm
zoom 3a
50 µm
zoom 3b
20 µm

O140 yr (90-100 cm) GRAIN 4.

O140 yr (90-100 cm) GRAIN 5.

O140 yr (90-100 cm) GRAIN 6.

O140 yr (90-100 cm) GRAIN 7.

$O_{140\,yr}$ (90-100 cm) GRAIN 9.

$O_{140\,yr}$ (90-100 cm) GRAIN 8.

R270 yr (0-10 cm)
GRAIN 1.

R270 yr (0-10 cm)
GRAIN 2.

R270 yr (0-10 cm)
GRAIN 3.

R270 yr (0-10 cm)
GRAIN 4.

R270 yr (0-10 cm)
GRAIN 5.

R270 yr (0-10 cm)
GRAIN 6.

R270 yr (0-10 cm)
GRAIN 7.

R270 yr (0-10 cm)
GRAIN 8.

R270 yr (0-10 cm)
GRAIN 9.

R270 yr (0-10 cm)
GRAIN 10.

R270 yr (0-10 cm)
GRAIN 11.

R270 yr (30-40 cm)
GRAIN 4.

R270 yr (30-40 cm)
GRAIN 5.

R270 yr (30-40 cm)
GRAIN 6.

R270 yr (30-40 cm)
GRAIN 7.

R270 yr (30-40 cm)
GRAIN 8.

R270 yr (30-40 cm)
GRAIN 9.

R270 yr (30-40 cm)
GRAIN 10.

zoom 1c
20 µm
zoom 1b
10 µm
zoom 1a
20 µm
100 µm
R270 yr (90-100 cm)
GRAIN 1.
zoom 1d
100 µm
R270 yr (90-100 cm)
GRAIN 2.
100 µm
R270 yr (90-100 cm)
GRAIN 3.
zoom 4a
50 µm
100 µm
R270 yr (90-100 cm)
GRAIN 4.

R270 yr (90-100 cm)
GRAIN 5.

R270 yr (90-100 cm)
GRAIN 6.

R270 yr (90-100 cm)
GRAIN 7.

R270 yr (90-100 cm)
GRAIN 8.

R270 yr (90-100 cm)
GRAIN 10.

R270 yr (90-100 cm)
GRAIN 9.

R1 1.6 kyr (0-10 cm) GRAIN 1.

R1 1.6 kyr (0-10 cm) GRAIN 2.

R1 1.6 kyr (0-10 cm) GRAIN 3.

R1 1.6 kyr (0-10 cm) **R1 1.6 kyr** (0-10 cm) **R1 1.6 kyr** (0-10 cm)

GRAIN 4. GRAIN 5. GRAIN 6.

R11.6 kyr (20-30 cm) GRAIN 1.

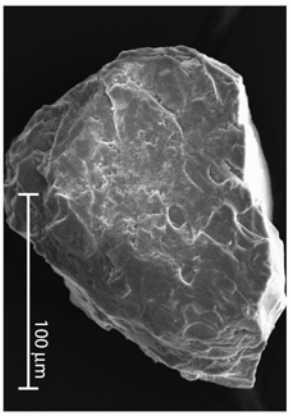
R11.6 kyr (20-30 cm) GRAIN 2.

R11.6 kyr (20-30 cm) GRAIN 3.

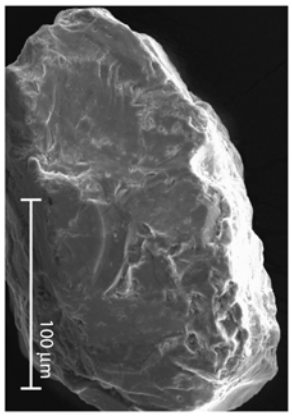
R11.6 kyr (20-30 cm) GRAIN 4.

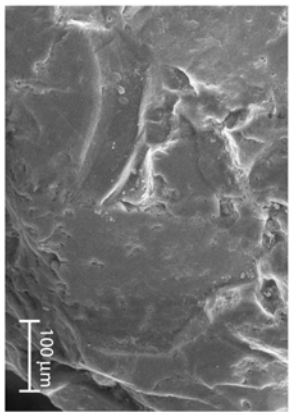
R1 1.6 kyr (20-30 cm)
GRAIN 5.

R11.6 kyr (60-70 cm)
GRAIN 4.

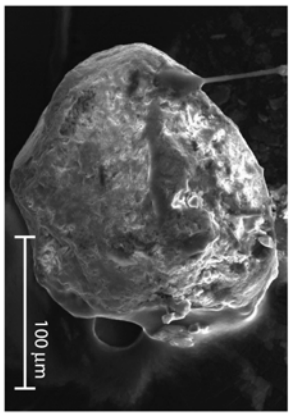


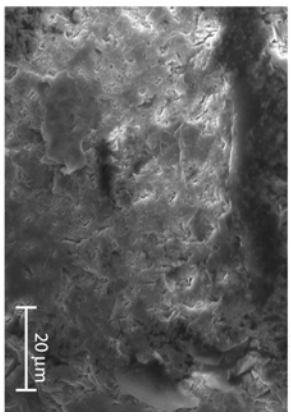
R11.6 kyr (60-70 cm)
GRAIN 3.



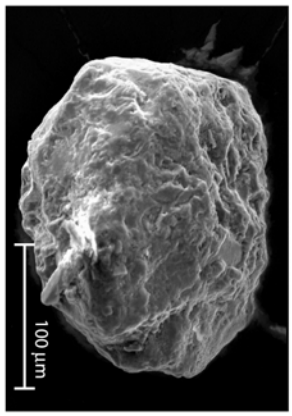


R11.6 kyr (60-70 cm)
GRAIN 2.





R11.6 kyr (60-70 cm)
GRAIN 1.



Grain	crystal habit	grain grade	blind check	comments
RH00				
1	2	1		
2	3	1		All grains look "greasy" and are heavily pitted or mechanically indented. Crystal form is poorly preserved, 4/5 grains show considerable rounding of the grain edges. All indentations are angular, showing that dissolution rounding of individual indentations is minor. Grain 4 has a 10 um long 1 µm wide striation where is has been abraided by a harder particle.
3	4	1		
4	1	1		
5	2	1		
mean grade		**1.0**		
O140, 0-10				
1	3	1	1	Indentations are fresh in grain 1
2	3	1	2	Indentations are fresh in grain 2
3	3	2	2	Indentations on grain 3 look sugary and show evidence of localised dissolution etching
4	3	3	4	The dissolution etching is more extensive on the 001 grain surface forming irregular shaped, denticular features perpendicular to the 001 surface. These are sometimes covered by a local surface coating. A microporosity has developed locally between the towers, but does not permeate the whole grain.
5	3	2	2	Grain 5 is covered by small shallow indentations all of which have sugary, diffuse edges.
6	3	2	2	The crystal habit of grain 6 is pristine, there is no dissolution rounding. Its surface is covered by shallow indentations which are sugary.
7	3	4	4	Grain 7 shows a "towerblock-like structure" which pervades the whole grain interior following the 001 crystal plane. The sides of the towers are up to several µm wide.
8	3	4	4	Grain 8 is covered in randomly orientated denticular structures, which end in rounded points on some parts of the grain: locally 1-2 µm long, orgainic looking "worms" are localised at the ends of these . Elsewhere on the grain irregular tabular crystals, measuring 1-3 µm in width are observed between the more accicular, denticular structures. Some of the denticular structure are covered by a localised surface coating.
9	3	4	4	Grain 9 shows a "towerblock-like structure" which pervades the whole grain, interior following the 001 crystal plane. The ends of the towers are pointed.
10	3?	4	4	The central part of grain 10 is covered with a network of fungal hyphae, several µm wide and up to 40 µm long. The formation of towerblock like structures is localised around the hyphea, the rest of the grain looks fresh.
11	3	3	4	The dissolution etching is more extensive on the 001 grain surface forming irregular shaped, denticular features perpendicular to the 001 surface. A microporosity has developed locally between the towers, but does not permeate the whole grain. The bottom corner of the grain has been protected from etching.
mean grade		**2.7**	**3.0**	

Grain	crystal habit	grain grade	blind check	comments
O140, 30-40 cm				
1	4	1	1	
2	2	1	1	
3	3	1	2	Several 30-40 cm grains have very localised pitting, a tendency towards indentations with sugary textures and localised lenticular etch pits. Grain 5 has a characteristic "flakey" texture.
4	3	2	2	
5	3*	2	2	
6	3	1	1	
7	3	2	2	
mean grade		**1.4**	**1.6**	
O140, 90-100cm				
1	4	2	2	Minor pitting and lenticular structures developing on the grain surface. Grain is coated in Al/Si layer in places.
2	4	2	2	Two bacteria possbily observed on zoom 2a, located to a sub hexagonal form. The flakey texture is observed on one side of the of the grain. The texture is similar to RH00 5b, but the indentations are less sharp, implying further etching in the proglacial environment
3	4	1	3	The morphology of grain 3 appears fresh, and similar to RH00 4c in texture. There are some surface coatings on the grain.
4	4	1	1	A fresh grain.
5	4	1	1	This grain is very smooth and fresh, from glavio-fluvial dissolution rounding. No secondary etching or pitting is observed.
6	4	1	2	The morphology of grain 6 appears fresh, and similar to RH00 4c in texture. There are some surface coatings on the grain.
7	4	1	1	A fresh grain.
8	2	1	1	This grain has the same texture as grain RH00 5.
9	3	2	1	Minor pitting and lenticular structures developing on the grain surface. Grain is coated in Al/Si layer in places.
mean grade		**1.3**	**1.6**	

Grain	crystal habit	grain grade	blind check	comments
R270, 0-10 cm				
1	4	4	3	Grain 1 has a large secondary porosity stemming from the coalescence of pervasive lenticular etch pits. The etchings all have a similar orientation.
2	4	4	3	Grain 2 has a large secondary porosity stemming from the coalescence of pervasive lenticular etch pits to form large cavities in the grain. The etchings all share a common orientation.
3	4	4	3	Grain 3 has a large secondary porosity stemming from the coalescence of pervasive lenticular etch pits to form large cavities in the grain. The etchings all share a common orientation.
4	3	3	4	A third of grain 4 is etched to form the denticular commonly orientated "towerblocks". The remainder of the grain appears fresh, appart from some pitting.
5	4	3	3	The surface of grain 5 is heavily etched forming commonly orientated denticular structures which penetrate the grain most deeply where it is striated.
6	4	4	3	Grain 6 has a large secondary porosity stemming from the coalescence of pervasive lenticular etch pits to form large cavities in the grain. The etchings all share a common orientation.
7	3	3	3	The surface of grain 7 is heavily and deeply pitted, but there has been no coalescence of etch pits. 2 µm raspberry shaped masses, comprised of indivudual " blobs" were observed in a surface depression, this may be a secondary precipiate.
8	4	3	2	The surface of grain 8 is heavily and deeply pitted to give a spongy texture, it is not clear that the porosity is pervasive throughout the grain.
9	4	4	3	Grain 9 has a significant secondary porosity stemming from the coalescence of pervasive lenticular etch pits to form large cavities in the grain. The etchings all share a common orientation.
10	4	3	2	The surface of grain 10 is heavily and deeply pitted to give a spongy texture, it is not clear that the porosity is pervasive throughout the grain. The same precipitate texture as in grain 7 is observed here.
11	4	3	2	The surface of grain 11 is heavily and deeply pitted to give a spongy texture, it is not clear that the porosity is pervasive throughout the grain.
mean grade		**3.5**	**2.8**	
R270 30-40 cm				
1	3	1	2	
2	5	1	1	
3	2	1	2	
4	4	2	2	Etching and the formation of denticular structures is particuarly pronounced around a striation on grain 4.
5	4	3	2	Considerable coalescence of lenticular etch pits is observed on grain 5.
6	5	2	2	Etching and the formation of lenticular structures is particularly pronounced depressions caused by the conchoidal fracture.
7	4	4	4	Grain 7 has the same character as O140, 0-10cm, grain 7. There is a pervasive coalescence of denticular structures to form fine towers and needles. Blocky grains (2-3 µm in length) are observed on the grain (zoom 7a) in a cavity where the needles have broken.
8	4	2	2	There are some deep pits on the surface of grain 8.
9	4	1	2	
10	4	1	1	
mean grade		**1.8**	**2**	

Grain	crystal habit	grain grade	blind check	comments
R270, 90-100 cm				
1	4	3	3	The surface of grain 1 is heavily etched forming deep irregularly- orientated lenticular structures which penetrate the grain most deeply where it is striated.
2	5	2	4	Lenticular structures are observed on the broken edge of grain 2.
3	5	2	1	Initial lenticular structures are observed on grain 3.
4	4	1	1	
5	4	1	2	
6	5	1	2	
7	4	1	1	
8	4	1	1	
9	4	1	1	
10	4	1	1	
mean grade		**1.4**	**1.7**	
R11.6, 0-10 cm				
1	4	3	3	Grain 1 shows no sign of denticular structures, etchings on the grain are in the form of superimposesed subhexagonal forms. Bacteria are observed on the grain in a crack.
2	4	3	4	Grain 2 is deeply etched to form a series of linear, parallel depressions. Sub-mircometer denticular morphologies are observed on the grain (zoom 2d, 2e, 2f) on other parts of the grain the coalesance of 10 µm long lenticular etch pits is observed. Bacteria are observed on this grain surface.
3	4	4	4	Grain 3 is rounded and has a spongy texture due to secondary porosity. There are some secondary coatings in a depression on the grain surface. Zoom 3a shows denticular features.
4	4	3	3	Grain 4 also has denticular features. Chattermarks on the grain surface are also etched, allowing chemical weathering to access more of the grain.
5	4	4	4	Grain 5 is rounded and shows pervasive denticular features which have coalesced throughout the grain.
6	4	4	4	Grain 5 is rounded, with considerable secondary porosity and shows pervasive denticular features which have coalesced throughout the grain. A rootlet is observed on the grain surface.
mean grade		**3.5**	**3.7**	
R11.6, 20-30 cm				
1	4	2	3	Grain 1 has the same flakey texture observed in grain 5, O140, 30-40 and grain 2, O140, 90-100. Surface coatngs are observed.
2	4	4	3	Grain 2 is very deeply etched forming 10 µm wide diamond shaped pits, which generate a high secondary porosity. 50 µm, towerblock-shaped margins are also observed.
3	3	3	3	Grain 3 is crumbling in the middle, and has a sugary texture.
4	2	3	3	Grain 4 shows the coalsence of towerblock shaped etchpits (Zoom 4b)
5	4	1	2	Grain 5 looks fresh.
mean grade		**2.6**	**2.8**	
R11.6, 90-100 cm				
1	1	3	3	Grain 1 has a flakey/ sugary surface texture and has densly spaced, fine etchings which appear randomly orientated.
2	4	3		Grain 2 is rounded with a spongy texture and fine, densly spaced, randomly orienteded etchings.
3	4	2	3	Grain 3 looks fresh and zoom 3a shows that the fine etchings are less densely spaced.
4	4	3	3	Grain 4 has fine, randomly orientated etchings dense etchings and a sugary texture.
mean grade		**2.8**	**3**	

Total number of whole grains: 78

Crystal/ fragment/Crystal habit: 1. Long prismatic habit; 2. Short prismatic; 3. Tabular; 4. Unknown; 5. Fragment with conchoidal fracture; *. Prominent dipyramid

Name grain	Grade	general grain description				description of morphological features						porosity						biological agents of alteration	
		fresh	flakey	sugary	spongy	sugary indentation	fine crack-like etchings	localised (lenticular) pits	coalesced (lenticular) pits	denticular structures	pervasive towers/ kneedles	surface-porosity	pervasive porosity	secondary preciptate	coatings	rounded grain	bacteria	fungal hyphea
O140 0-10 _1	1	1																
O140 0-10 _2	1	1																
O140 30-40 _1	1	1																
O140 30-40 _2	1	1																
O140 30-40 _3	1	1																
O140 30-40 _6	1	1																
O140 90-100 _3	1	1													1			
O140 90-100 _4	1	1																
O140 90-100 _5	1	1																
O140 90-100 _6	1	1													1			
O140 90-100 _7	1	1																
O140 90-100 _8	1	1																
R11600, 20-30_5	1	1																
R270, 30-40_1	1	1																
R270, 30-40_10	1																	
R270, 30-40_2	1	1																
R270, 30-40_3	1	1																
R270, 30-40_9	1																	
R270, 90-100_10	1	1																
R270, 90-100_4	1	1																
R270, 90-100_5	1	1																
R270, 90-100_6	1	1																
R270, 90-100_7	1	1																
R270, 90-100_8	1	1																
R270, 90-100_9	1	1																
RHOO_1	1	1																
RHOO_2	1	1																
RHOO_3	1	1																
RHOO_4	1	1																

Name grain	Grade	general grain description				description of morphological features						porosity					biological agents of alteration	
		fresh	flakey	sugary	spongy	sugary indentation	fine crack-like etchings	localised (lenticular) pits	coalesced (lenticular) pits	denticular structures	pervasive towers/ kneedles	surface-porosity	pervasive porosity	secondary preciptate	coatings	rounded grain	bacteria	fungal hyphea
RHOO_5	1	1																
O140 0-10 _3	2					1		1										
O140 0-10 _5	2					1												
O140 0-10 _6	2					1												
O140 30-40 _4	2					1		1										
O140 30-40 _5	2					1		1										
O140 30-40 _7	2					1		1										
O140 90-100 _1	2					1		1							1			
O140 90-100 _2	2		1														1	
O140 90-100 _9	2							1							1			
R11600, 20-30_1	2		1												1			
R11600, 90-100_3	2	1					1											
R270, 30-40_4	2							1		1								
R270, 30-40_6	2							1										
R270, 30-40_8	2							1										
R270, 90-100_2	2							1										
R270, 90-100_3	2							1										
O140 0-10 _11	**3**									1		1						
O140 0-10 -4	3									1		1			1			
R11600, 0-10_1	3								hexagonal								1	
R11600, 0-10_2	3								1	1							1	
R11600, 0-10_4	3									1								
R11600, 20-30_3	3			1														
R11600, 20-30_4	3								1									
R11600, 90-100_1	3		1	1			1											
R11600, 90-100_2	3				1		1											
R11600, 90-100_4	3			1			1											
R270, 0-10_10	3				1							1		1				
R270, 0-10_11	3				1							1						

Name grain	Grade	general grain description				description of morphological features						porosity						biological agents of alteration	
		fresh	flakey	sugary	spongy	sugary indentation	fine crack-like etchings	localised (lenticular) pits	coalesced (lenticular) pits	denticular structures	pervasive towers/ kneedles	surface-porosity	pervasive porosity	secondary preciptate	coatings	rounded grain	bacteria	fungal hyphea
R270, 0-10_4	3	1*									1							
R270, 0-10_5	3									1								
R270, 0-10_7	3								1			1		1				
R270, 0-10_8	3				1								1					
R270, 30-40_5	3								1									
R270, 90-100_1	3								1									
O140 0-10 _10	4										1							1
O140 0-10 _8	4									1								1
O140 0-10 _9	4										1							
O140 0-10 -7	4										1							
R11600, 0-10_3	4				1					1			1		1	1		
R11600, 0-10_5	4										1							
R11600, 0-10_6	4										1		1					
R11600, 20-30_2	4								1		1		1					
R270, 0-10 _1	4								1				1					
R270, 0-10_2	4								1				1					
R270, 0-10_3	4								1				1					
R270, 0-10_6	4								1				1					
R270, 0-10_9	4								1				1					
R270, 30-40_7	4										1			1				

Sample	Fe-P mg/g	Weak acid mg/g	Strong acid mg/g	Det-P mg/g	Org_P mg/g	PP mg/g
R_{oyr}						
7/7/99 (10:00)	0.04	0.19	0.10	0.28	0.02	0.35
8/7/99 (17:00)	0.05	0.17	0.09	0.26	0.00	0.32
9/7/99 (10:00)	0.06	0.18	0.07	0.25	0.02	0.32
21/7/99 19:00)	0.07	0.19	0.05	0.24	0.01	0.32
29/07/99 (10:00)	0.03	0.21	0.11	0.32	0.01	0.36
2/08/99 (10:00)	0.05	0.14	0.09	0.23	0.00	0.28
4/8/99 (10:00)	0.22	0.22	0.12	0.34	0.01	0.56
21/9/99 (14:00)	0.01	0.18	0.10	0.29	0.01	0.31
21/9/99 (10:00)	0.06	0.23	0.12	0.35	0.00	0.41
21/9/99 (10:00)	0.06	0.22	0.13	0.35	0.00	0.41
13/5/00 (10:00)	0.06	0.26	0.08	0.35	0.01	0.41
23/5/00 (10:00)	0.07	0.22	0.05	0.27	0.01	0.36
6/6/00 (10:00)	0.03	0.23	0.12	0.34	0.01	0.38
15/6/00 (10:00)	0.03	0.20	0.10	0.29	0.01	0.33
19/6/00 (17:00)	0.06	0.21	-	0.21	0.01	0.28
11/6/00 (10:00)	0.03	0.20	0.13	0.33	0.01	0.37
20/6/00 (10:00)	0.06	0.30	0.05	0.35	0.00	0.40
4/7/00 (10:00)	0.03	0.20	0.12	0.32	0.01	0.37
6/7/00 (10:00)	0.04	0.30	0.09	0.39	0.01	0.44
25/7/00 (10:00)	0.03	0.29	0.11	0.40	0.01	0.44
25/7/00 (17:00)	0.03	0.27	0.12	0.38	0.02	0.44
19/8/00 (10:00)	0.02	0.22	0.12	0.33	0.01	0.36
22/08/00 (10:00)	0.04	0.23	0.14	0.36	0.01	0.42
Mean	**0.05** *(± 0.04)*	**0.22** *(± 0.04)*	**0.10** *(± 0.03)*	**0.31** *(± 0.05)*	**0.01** *(± 0.01)*	**0.38** *(± 0.06)*

Sample	Fe-P mg/g	Weak acid mg/g	Strong acid mg/g	Det-P mg/g	Org_P mg/g	PP mg/g
O_{oyr}						
7/7/99 (10:00)	0.02	0.30	0.14	0.45	0.01	0.48
29/7/99 (17:00)	0.03	0.30	0.29	0.58	0.01	0.62
1/9/99 (17:00)	0.03	0.28	0.26	0.54	0.01	0.59
5/8/99 (10:00)	0.05	0.37	0.36	0.73	0.01	0.79
19/8/99 (10:00)	0.04	0.27	0.25	0.52	0.01	0.56
17/5/00 (10:00)	0.02	0.31	0.28	0.59	0.02	0.62
14/6/00 (17:00)	0.02	0.33	0.28	0.61	0.02	0.64
26/6/00 (17:00)	0.02	0.30	0.27	0.57	0.01	0.60
10/7/00 (17:00)	0.02	0.29	0.23	0.51	0.03	0.56
26/7/00 (17:00)	0.02	0.37	0.27	0.64	0.01	0.67
26/7/00 (17:00)	0.03	0.34	0.28	0.62	0.01	0.66
9/8/00 (10:00)	0.02	0.31	0.18	0.49	0.02	0.53
18/9/00 (17:00)	0.02	0.36	0.25	0.61	0.01	0.65
sample name lost	0.05	0.49	0.24	0.73	0.01	0.79
20/9/00 (17:00)	0.02	0.31	0.26	0.57	0.02	0.61
Mean	**0.03** *(± 0.01)*	**0.33** *(± 0.06)*	**0.26** *(± 0.05)*	**0.58** *(± 0.08)*	**0.01** *(± 0.01)*	**0.63** *(± 0.08)*

RHONE PROFILES	Depth cm	Fe-P mg/g	Weak acid mg/g	Strong acid mg/g	Det-P mg/g	Org_P mg/g	PP mg/g	TOC* mg/g	pH*
R_{145yr}									
	0_10	0.03	0.10	0.06	0.16	0.01	0.20	0.24	5.0
	10_20	0.03	0.13	0.06	0.19	0.00	0.22	0.15	5.2
	20_30	0.03	0.17	0.07	0.24	0.01	0.28	0	6.0
	30_40	0.03	0.15	0.05	0.20	0.01	0.24	0	6.4
	40_50							0	6.6
	50_60	0.03	0.21	0.07	0.28	0.00	0.31	0	6.5
	60_70	0.03	0.21	0.05	0.25	0.00	0.29	0	6.4
	70_80	0.03	0.23	0.05	0.28	0.01	0.32	0	6.5
	80_90	0.03	0.11	0.05	0.16	0.00	0.20	0	6.7
	90_100	0.03	0.17	0.07	0.24	0.00	0.27	0	6.9
	mean	**0.03** *(± 0.00)*	**0.16** *(± 0.05)*	**0.06** *(± 0.01)*	**0.22** *(± 0.05)*	**0.01** *(± 0.00)*	**0.26** *(± 0.05)*		
R_{270yr}									
	0_10	0.03	0.06	0.04	0.10	0.02	0.15	0.67 - 1.08	4.6
	10_20	0.03	0.11	0.04	0.15	0.01	0.19	0.37 -	4.8
	20_30	0.03	0.11	0.04	0.15	0.01	0.18	0.19 - 0.13	4.9
	30_40	0.03	0.12	0.03	0.15	b/d	0.18	0	5.9
	40_50	0.03	0.13	0.03	0.16	b/d	0.19	0	6.0
	50_60	0.03	0.09	0.02	0.11	b/d	0.14	0	6.1
	60_70	0.03	0.12	0.04	0.16	b/d	0.19	0	6.2
	70_80	0.03	0.12	0.04	0.16	b/d	0.19	0	6.3
	80_90	0.03	0.15	0.04	0.19	b/d	0.22	0	6.5
	90_100	0.03	0.16	0.04	0.20	0.01	0.24	0	6.2
	mean	**0.03** *(± 0.00)*	**0.12** *(± 0.03)*	**0.03** *(± 0.01)*	**0.15** *(± 0.03)*	**0.01** *(± 0.00)*	**0.19** *(± 0.03)*		
$R_{11.6kyr}$									
	0_10	0.89	0.02	0.03	0.05	0.17	1.11	5.05	n.a.
	10_20	0.61	0.02	0.01	0.02	0.03	0.66	1.45	5.4
	20_30	1.18	0.02	0.01	0.04	0.03	1.24	1.93	5.4
	30_40	0.89	0.08	0.02	0.10	0.02	1.01	0.50	5.5
	40_50	0.29	0.15	0.08	0.23	0.02	0.54	1.12	5.5
	50_60	0.21	0.18	0.08	0.25	0.02	0.49	1.01	5.9
	60_70	0.11	0.19	0.09	0.27	0.03	0.41	0.68	5.8
	mean	**0.60** *(± 0.42)*	**0.09** *(±0.07)*	**0.04** *(±0.03)*	**0.14** *(± 0.01)*	**0.05** *(± 0.05)*	**0.78** *(± 0.37)*		

* Second values refers to profile R_{270yr}'

OBERAAR PROFILES	Depth cm	Fe-P mg/g	Weak acid mg/g	Strong acid mg/g	Det-P mg/g	Org_P mg/g	PP mg/g	TOC* mg/g	pH*
O_{140yr}									
	0_10	0.03	0.35	0.28	0.63	0.03	0.69	0.11 - 0.36	5.4 - 7.6
	10_20	0.03	0.53	0.29	0.83	0.03	0.89	0 - 0.11	6.3 - 6.7
	20_30	0.03	0.47	0.33	0.80	0.02	0.85	0	6.7 - 6.6
	30_40	0.03	0.50	0.25	0.75	0.01	0.79	0	7.1 - 6.6
	40_50	0.03	0.29	0.18	0.47	0.01	0.51	0	7.1 - 6.6
	50_60	0.03	0.49	0.21	0.71	0.02	0.76	0	7.2 - 7.1
	60_70	0.03	0.34	0.17	0.51	0.01	0.55	0	7.7 - 7.5
	70_80	0.06	0.56	0.23	0.79	0.02	0.86	0	7.9 - 7.2
	80_90	0.03	0.54	0.15	0.69	0.02	0.74	0	8.2 - 7.1
	90_100	0.03	0.34	0.13	0.47	0.01	0.51	0	8.1 - 6.9
	mean	**0.03** *(± 0.01)*	**0.44** *(± 0.1)*	**0.22** *(± 0.07)*	**0.66** *(± 0.14)*	**0.02** *(±0.01)*	**0.71** *(± 0.14)*		
$O_{11.6kyr}$									
	0_10	1.87	0.17	0.01	0.17	0.60	2.64	6.7	24.09
	10_20	0.98	0.14	0.00	0.14	0.22	1.34	6.5	9.00
	20_30	0.36	0.14	0.00	0.14	0.06	0.55	6.1	3.49
	30_40	0.10	0.31	0.09	0.40	0.02	0.52	5.5	1.54
	40_50	0.08	0.32	0.07	0.39	0.02	0.49	5.7	1.03
	mean	**0.68** *(± 0.76)*	**0.21** *(± 0.09)*	**0.03** *(± 0.04)*	**0.25** *(± 0.13)*	**0.18** *(± 0.25)*	**1.11** *(± 0.93)*		

* Second values refers to profile O_{140yr} '

RHÒNE PROFILES	Depth cm	Dry Weight g	>32 mm g	>16 mm g	>8 mm g	>4 mm g	>2 mm g	>1 mm g	>0.5 mm g	>250 µm g	>125 µm g	>63 µm g	>32 µm g	>16 µm g	>8 µm g	>4 µm g	>2 µm g	>1 µm g	>0 µm g
R_{145yr}																			
	0_10	488.97		71.21	54.97	50.50	45.38	43.77	37.02	32.28	31.64	28.71	29.34	30.24	16.15	11.61	4.72	1.12	0.31
	10_20	519.17		103.45	50.90	30.35	42.86	49.68	45.07	39.69	39.81	33.52	66.26	13.43	2.11	1.27	0.60	0.14	0.03
	20_30	422.74		29.07	13.09	46.58	49.24	48.33	39.64	33.72	36.13	26.73	22.47	26.73	19.69	18.98	9.48	2.29	0.58
	30_40	456.42		80.74	49.84	47.51	42.38	47.09	41.88	37.36	31.76	26.93	20.13	13.22	7.50	6.15	3.00	0.75	0.18
	40_50	430.86			31.81	44.23	50.25	60.73	55.56	45.10	47.02	34.08	17.90	20.47	9.98	8.31	4.08	1.04	0.30
	50_60	495.35		94.72	71.49	50.43	43.78	45.13	39.04	36.05	32.90	29.03	11.52	17.57	8.70	8.71	4.81	1.17	0.31
	60_70	475.61		39.70	42.55	49.70	47.36	55.77	49.41	44.27	38.27	38.27	49.86	15.52	2.72	1.47	0.58	0.13	0.03
	70_80	464.97			55.80	56.17	50.14	53.13	47.37	41.86	35.02	38.39	1.87	26.17	19.75	22.94	11.95	3.34	1.07
	80_90	457.69			30.05	59.78	57.99	59.12	50.54	46.74	47.06	39.49	14.30	20.75	11.74	11.49	6.15	1.85	0.63
	90_100	463.79			7.46	41.82	54.41	60.70	54.97	51.87	53.65	42.96	23.82	27.60	15.70	17.18	8.83	2.20	0.62
R_{270yr} (a)																			
	0_10	371.62		24.99	40.00	44.58	42.24	37.54	35.31	31.75	31.72	29.33	22.46	16.00	7.27	5.58	2.28	0.47	0.09
	10_20	374.04		25.94	65.61	46.98	49.38	44.30	35.89	28.47	23.82	17.44	7.61	12.00	6.80	6.19	2.82	0.60	0.18
	20_30	394.93		50.26	66.48	45.62	53.61	45.17	34.24	27.84	21.96	17.00	5.25	11.89	6.80	5.76	2.38	0.53	0.14
	30_40	448.81		65.75	56.38	59.01	55.60	48.43	41.77	36.97	33.64	21.41	1.48	11.94	5.88	6.60	3.07	0.70	0.18
	40_50	463.75		113.37	66.17	57.94	47.12	42.21	38.36	32.87	24.99	17.13	4.20	8.20	4.48	3.95	2.08	0.54	0.14
	50_60	483.67		79.41	100.95	58.22	57.32	44.16	38.83	34.54	26.99	17.27	0.87	9.07	5.72	6.22	3.17	0.74	0.19
	60_70	413.96		63.15	44.92	66.50	53.16	44.86	36.59	30.58	24.93	19.01	11.36	8.98	4.25	3.63	1.66	0.31	0.07
	70_80	404.14		32.39	52.31	47.68	49.43	50.60	44.82	38.41	34.71	22.90	7.10	10.26	5.72	4.83	2.22	0.58	0.16
	80_90	367.31		27.92	40.85	46.63	50.05	47.43	39.56	32.15	29.47	22.71	7.00	10.26	5.10	5.27	2.23	0.53	0.15
	90_100	483.84		109.82	58.47	53.95	50.11	44.52	37.28	32.36	32.41	26.18	18.20	10.88	4.49	3.54	1.32	0.26	0.06
R_{270yr} (b)																			
	0_10	368.09			23.31	6.42	59.97	51.77	49.52	44.52	30.39	18.87	46.52	20.80	8.76	5.08	1.73	0.35	0.07
	10_20	375.82		80.60	37.42	34.61	34.89	36.84	37.79	35.76	27.11	19.93	15.38	9.25	3.40	1.97	0.71	0.14	0.03
	20_30	386.44		63.02	44.49	54.51	46.07	42.37	42.68	38.63	22.23	12.08	4.45	6.99	3.58	3.45	1.52	0.31	0.07
	30_40	435.42	49.80	71.19	48.16	47.68	40.93	40.23	36.07	31.64	24.16	17.09	9.02	10.80	4.15	3.07	1.16	0.22	0.05
	40_50	495.26		59.83	74.53	60.36	59.84	61.96	51.10	38.44	31.12	21.80	6.10	13.18	8.03	5.98	2.38	0.48	0.12
	50_60	466.90		93.73	77.97	58.79	53.63	48.78	41.25	29.68	20.32	16.02	4.70	11.65	4.92	3.59	1.48	0.31	0.08
	60_70	477.54		88.54	85.37	76.86	51.96	45.34	36.97	27.22	20.87	16.62	10.74	9.60	3.61	2.55	1.03	0.20	0.05
R11.6kyr																			
	0_10	442.90		7.63	29.89	46.67	66.70	62.15	56.68	49.87	40.74	29.44	31.83	13.68	3.86	2.42	1.02	0.25	0.06
	10_20	783.45	66.28	123.67	116.87	86.29	84.50	69.64	60.37	47.41	37.58	32.90	34.61	12.83	4.59	3.73	1.64	0.41	0.12
	20_30	875.52		120.92	166.86	89.42	93.72	75.86	69.52	57.76	52.85	42.52	56.63	26.71	11.08	7.42	3.18	0.82	0.25
	30_40	622.69		186.02	105.45	35.71	33.12	30.84	33.50	34.35	41.63	41.45	46.03	20.95	7.13	4.28	1.67	0.43	0.13
	40_50	482.89		36.18	55.97	37.41	49.20	37.04	36.33	45.35	52.40	45.88	48.36	24.43	7.62	4.72	1.59	0.32	0.10
	50_60	459.27			12.11	17.76	27.52	34.33	39.20	54.45	75.61	68.53	68.81	38.49	13.59	6.37	2.04	0.39	0.09
	60_70	672.85		40.22	28.75	25.22	39.36	45.84	56.12	71.28	94.72	101.95	107.33	43.89	10.55	5.08	2.02	0.41	0.12

OBERAAR PROFILES	Depth cm	Dry Weight g	>32 mm g	>16 mm g	>8 mm g	>4 mm g	>2 mm g	>1 mm g	>0.5 mm g	>250 µm g	>125 µm g	>63 µm g	>32 µm g	>16 µm g	>8 µm g	>4 µm g	>2 µm g	>1 µm g	>0 µm g
$O_{140yr\ (a)}$																			
	0_10	529.40		79.34	24.58	47.49	68.28	72.09	65.51	59.63	43.13	20.09	17.53	14.93	7.26	5.89	2.79	0.67	0.18
	10_20	557.71		52.41	45.81	48.08	74.43	77.32	70.61	68.37	61.26	26.71	10.10	8.86	5.11	5.48	2.46	0.55	0.14
	20_30	412.32		9.29	18.63	30.03	47.32	55.90	47.28	45.05	45.25	27.50	4.02	27.90	21.79	18.76	9.39	2.93	1.27
	30_40	491.80			15.99	34.25	48.07	61.91	68.17	86.58	86.32	56.75	14.54	9.06	3.64	3.61	2.01	0.67	0.22
	40_50	478.60		19.21	53.93	24.55	39.03	58.06	62.28	73.98	74.57	42.43	5.34	8.36	5.57	6.26	3.41	1.19	0.44
	50_60	500.83		89.92	88.50	56.98	50.13	58.18	45.21	34.10	31.00	20.39	1.93	9.57	5.73	5.40	2.87	0.70	0.21
	60_70	515.50		55.66	95.68	58.98	60.35	62.31	50.47	40.45	34.86	20.37	7.00	10.81	6.51	6.72	3.92	1.07	0.33
	70_80	510.15		97.39	88.99	68.49	53.62	53.97	43.12	28.36	21.41	15.66	5.92	11.73	7.65	7.71	4.50	1.21	0.42
	80_90	536.96		60.64	114.74	65.92	65.93	72.05	50.68	31.49	20.60	15.64	5.40	11.81	7.17	8.56	4.78	1.20	0.36
	90_100	512.03		75.06	140.87	89.15	59.05	51.90	19.54	18.94	9.88	6.79	9.01	13.66	6.50	6.85	3.69	0.89	0.25
$O_{140yr\ (b)}$																			
	0_10	547.71		188.74	118.70	49.39	30.86	15.24	18.92	21.08	14.41	11.31	15.10	20.90	17.81	16.61	6.79	1.47	0.38
	10_20	541.38		196.13	105.09	49.17	27.53	9.65	15.06	32.97	29.31	14.77	16.49	19.64	6.97	11.75	5.14	1.32	0.39
	20_30	423.15		106.33	119.00	55.65	23.44	13.15	9.60	9.27	7.36	3.40	8.95	27.64	15.24	14.90	7.07	1.66	0.49
	30_40	466.68		58.65	101.92	57.01	41.06	34.88	31.45	30.59	24.64	16.27	31.31	16.37	8.01	8.84	4.38	1.03	0.27
	40_50	500.18		24.54	60.70	50.99	52.03	62.28	64.61	69.78	46.01	23.77	0.82	13.57	10.29	11.52	6.44	2.06	0.76
	50_60	495.72		28.28	92.08	60.64	57.36	56.45	54.97	55.82	36.70	21.81	1.53	10.29	6.86	7.19	4.01	1.26	0.48
	60_70	496.67		22.93	58.86	57.00	62.93	63.68	60.93	64.09	43.60	19.71	3.04	12.83	9.19	9.38	5.88	1.89	0.72
	70_80	532.50		46.52	146.35	94.30	59.98	32.86	30.45	36.14	26.85	18.06	3.76	14.25	7.94	8.39	4.65	1.53	0.47
	80_90	535.15		132.20	135.44	76.77	47.49	30.18	28.27	27.43	18.53	11.52	0.37	6.41	6.39	7.99	4.62	1.21	0.34
	90_100	528.56		38.44	100.84	76.63	69.95	59.30	52.10	46.45	27.31	17.21	12.76	10.72	5.86	6.53	3.41	0.85	0.20
$O_{11.6kyr}$																			
	0_10	181.16				7.69	10.54	15.75	30.59	38.29	23.39	20.21	25.51	6.51	1.51	0.74	0.27	0.10	0.05
	10_20	486.20		7.35		5.67	38.07	43.46	36.32	41.39	60.88	48.06	128.47	58.88	11.73	4.14	1.46	0.27	0.06
	20_30	419.79			13.36	17.43	38.64	38.59	32.58	36.31	60.83	71.33	60.63	33.50	10.99	4.06	1.17	0.27	0.08
	30_40	493.99		19.79	47.42	28.92	44.03	40.69	36.55	38.33	78.28	58.33	56.98	27.98	9.48	5.09	1.65	0.36	0.09
	40_50	638.27		62.43	40.62	32.60	50.15	53.00	50.18	50.23	77.14	77.75	77.62	37.33	13.49	10.21	4.35	0.95	0.22
	50_60	660.25		7.48	22.34	47.86	44.54	47.22	46.38	50.53	83.74	80.88	143.60	51.58	13.00	12.70	6.49	1.50	0.41





5. *Meltout sediment*
6., 7., 8. *LIA profiles*





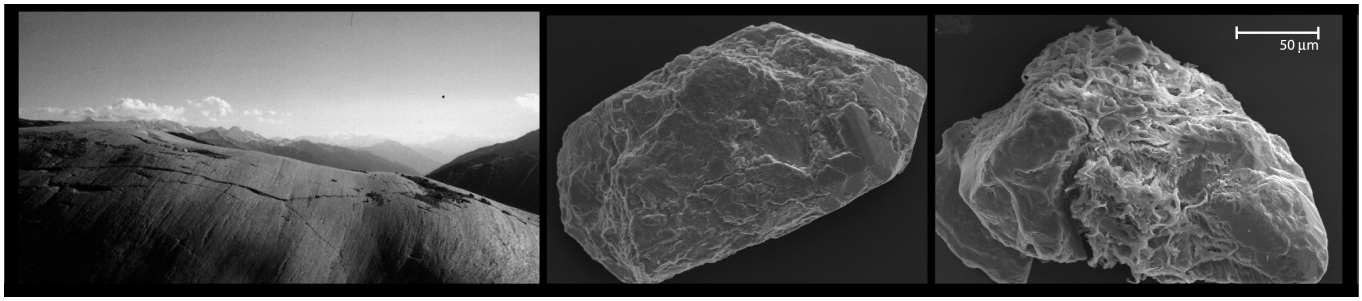
CHAPTER 5

Conversation with a Stone (II)

I knock at the stone's front door-
"It's only me, let me come in
I've come out of pure curiosity.
Only life can quench it.
I mean to stroll through your palace,
then go calling on leaf, a drop of water.
I don't have much time.
My mortality should touch you."

"I'm made of stone" says the stone,
"and must therefore keep a straight face
go away
I don't have the muscles to laugh".

Wistawa Szymborska in Nothing Twice



PHOSPHORUS WEATHERING: FOUR CASE STUDIES FROM THE SWISS ALPS AND VENEZUELA

R. Hosein[1] , K. Arn[1] , P. Steinmann[1] , T. Adatte[1] , S. Huon[2] and K.B. Föllmi[1].

[1]Insititut de Géologie, Université de Neuchâtel, Rue Emile Argand 11, CH-2007, Neuchâtel, Switzerland.

[2]UMR 7618 (UPMC-CNRS-INRA) Biogéochimie Isotopique, Université Pierre & Marie Curie, 4 place Jussieu. 75252 Paris cedex 05. France.

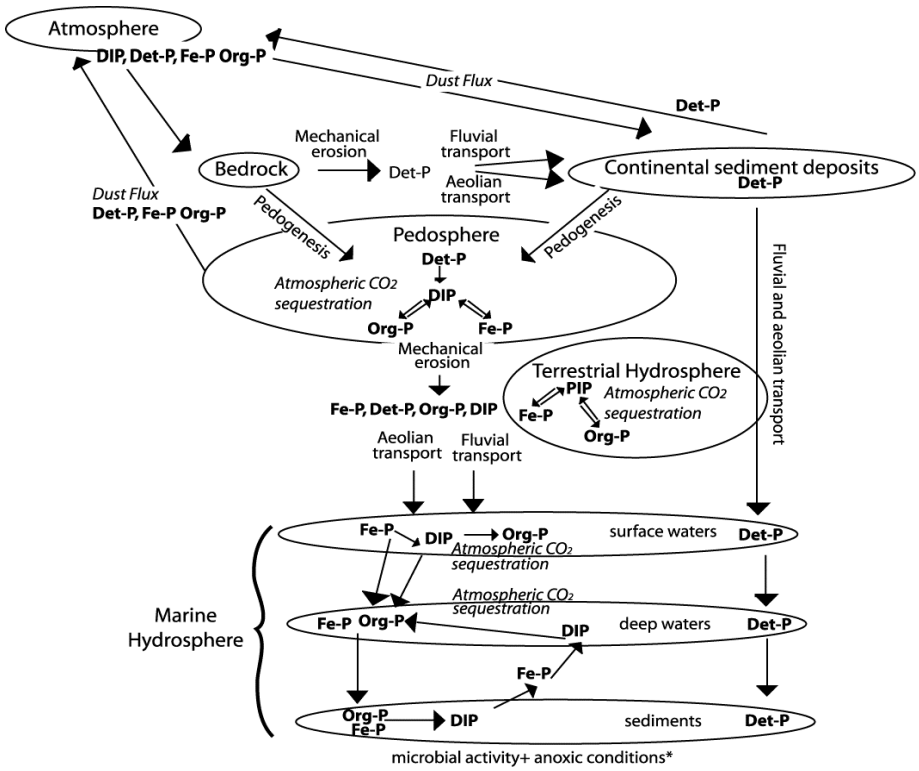
Abstract

The runoff from the Apure watershed contains more conditionally bio-available P (dissolved inorganic and organic P, and particulate ironbound and organic P; 1.97 kmol km^{-2} yr^{-1}) than glacial meltwaters from the Rhône and Oberaar glaciers (0.29 – 0.39 kmol km^{-2} yr^{-1}). But, the eolian input of bio-available P to the Apure watershed by Saharan dust is greater than the output flux of conditionally bio-available P. This implies that soils in our largely transport limited tropical catchment act as a reservoir for P.

In contrast, while runoff from the presently glaciated catchments is dominated by scarcely bio-available detrital P (97 %), the role subglacial erosion and weathering processes play in bringing large volumes of freshly comminuted, detrital P to the biosphere (7 & 11 kmol km^{-2} yr^{-1} in our presently glaciated catchments) may be important in controlling inputs of bio-available P to the oceans on glacial-interglacial timescales: The weathering-derived soluble reactive phosphorus (SRP) flux from the recently deglaciated Rhône Tributary catchment (0.17 kmol km^{-2} yr^{-1}) is elevated compared to the weathering-derived SRP flux from the Rhône and Oberaar subglacial environments (0.04 - 0.05 kmol km^{-2} yr^{-1}) and global mean riverine SRP flux (0.13 kmol km^{-2} yr^{-1}). This indicates that the dissolution of detrital P is accelerated in proglacial sediments and that the low P binding capacity of immature, weathering limited, glacial soils allows the leakage of bio-available P into aquatic ecosystems.

Introduction

Dissolved phosphorus (P) in the form of orthophosphate, is a potentially biolimiting nutrient in terrestrial, freshwater and marine ecosystems (e.g. Schindler, 1977; Cotner, 1997; Chadwick et al., 1999) and may be the ultimate limiting nutrient for oceanic primary productivity on geological timescales (e.g. Broecker, 1982; Tyrell, 1999). The fundamental control on the P flux to the biosphere is the weathering rate of P bearing minerals (Filippelli and Delaney, 1994; Delaney, 1998). Paradoxically detrital P is scarcely bio-available in freshwater and marine environments, and in fact 90-99 % of total P is transported fluvially in solid forms that are either only conditionally or scarcely bio-



* This chain of events can also occur in the bottom sediments of laclustrine environments.

Fig. 1: *The transfer of different P forms from the continents to oceanic sediments*

available (Figs. 1 and 2; Martin and Meybeck, 1979; Froelich et al., 1982; Boström et al., 1988; Reynolds and Davis, 2001). Biologically reactive P is a limited resource under natural conditions (e.g. Hudson et al., 2000) that is often recycled intrabiotically, with algal biomass forming the main source of P in the oceans and organic matter being a principal source of bio-available P in 10'000 year old soils (Crews et al., 1995; Chadwick et al., 1999). Although increased physical erosion rates associated with tectonic uplift and possibly glaciation (Southam and Hay, 1981; Guidry, 2000) augment the flux of apatite (the main P bearing mineral) supplied to the biosphere and physically precondition it for chemical weathering, the timescales and mechanisms by which it becomes bio-available are unclear. Apatite dissolution is limited in rivers, lakes and sea water due to their close to neutral pH's (6-8.4; Skirrow, 1975; Meybeck, 1993) and therefore freshly weathered apatite conveyed directly to ocean reservoirs will not be bioreactive.

Consequently it is vital that detrital P should be retained in terrestrial environments where apatite solubility is enhanced by acidic porewaters (Stumm and Morgan, 1996). Acidic soils increase the dissolution of detrital P through a range of chemical and biogeochemical processes, like acid aerosols, the H^+ pump at root tips and organic acid exudates, such as oxalic acid from rootlets and associated mycorhizal fungi (e.g. Kpomblekou and Tabatabai, 1994). Detrital P is rapidly dissolved in soils, for

instance it is no longer detected in 20'000-year-old glacial (Birkland et al., 1989) and Hawaiian soils (Crews et al., 1995). Furthermore protosoils established on recently deposited sediment have a low P binding capacity due to their low organic matter and iron oxide concentrations and therefore they are often leaky with regard to biologically reactive, dissolved phosphorus, (van der Molen et al., 1997; Filippelli and Souch, 1999) causing an important flux of bio-available P to drain into aquatic ecosystems.

While soils become impoverished in detrital P they become enriched in ironbound and organic P phases (e.g. Walker and Syers, 1976; Birkland et al., 1989; Crews, 1995). The organically bound and ironbound P are conditionally bio-available, i.e., they can become bio-available under specific environmental conditions: Organic P can take many forms in soils and surface waters, with a whole range of bio-reactivities, giving rise to the recycling of P within ecosystems (Newbold et al., 1984; Lucas et al., 1993; Frossard et al., 1995; Crews et al., 1995; Sharpley, 2000). Some phytoplankton can secrete alkaline phosphatases that separate orthophosphate groups from dissolved organic compounds rendering them bio-available (Cembella et al., 1984) and microbial activity in coastal marine and lake sediments also releases orthophosphates from organically bound P (Ruttenberg, 1992). Ironbound P is generally only available to specific microbes in the pedosphere that produce siderophores (Frossard et al., 1995; Sharpley, 2000). But if soils are eroded and transported by rivers ironbound P may become available to phytoplankton through desorbtion processes: Flocs of iron oxide are a significant source of orthophosphate in some river estuaries, where P desorbtion is driven by changes in salinity and pH (Fox, 1986) and below the redoxcline of anoxic water bodies, where iron is reduced to its ferric form (e.g., Golterman, 1984). Berner and Rao (1994) studied the various P forms in Amazon River, estuary and shelf

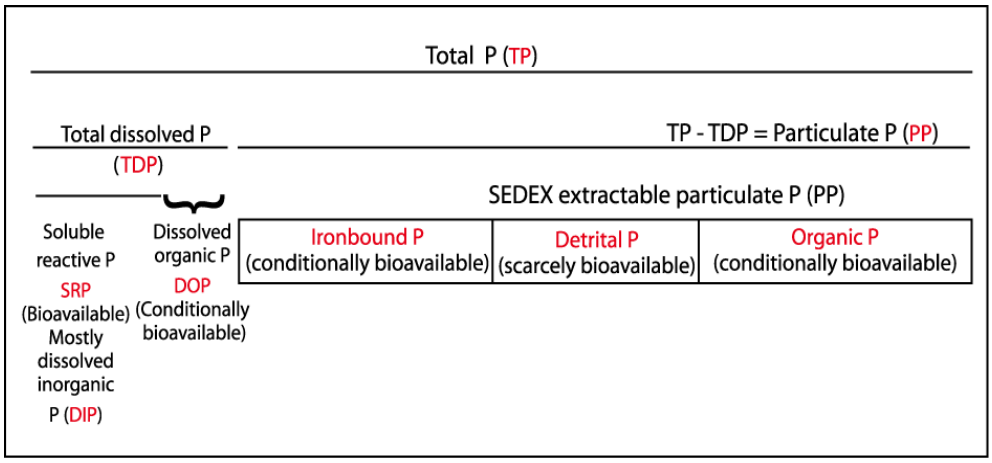


Fig 2: *A schematic diagram showing the P forms measured in this paper and their bioavailabilites (after Boström et al., 1988 & Reynolds and Davis, 2001)*

sediments using Ruttenberg's (1992) sequential extraction technique and observed a marked drop in organic and ironbound P concentrations in the shelf sediments compared to the river sediments. They attributed this decrease to the solubilisation of P in the sediments, which they estimate represents a source of bio-available P that is almost three times larger than the dissolved P flux from the Amazon River (18 x 10^{10} gm P yr^{-1}).

In this paper we present four case studies, we compare P forms in the meltwaters from three presently or recently glaciated alpine catchments in central Switzerland, with P forms in the runoff from the tropical Apure catchment which encompasses an area of the Venezuelan Andes and Llanos. In the presently glaciated Rhône and Oberaar catchments ≈ 97 % of P is in detrital form, i.e. scarcely bio-available and the soluble reactive P (SRP) derived from the weathering of detrital minerals is negligible, (0.05 kmol km^{-2} yr^{-1}). However, in the recently glaciated Rhône Tributary catchment dissolved P is dominant and the weathering-derived-SRP-flux is 0.17 kmol km^{-2} yr^{-1}. In contrast rivers in the tropical Apure watershed contain conditionally bio-available dissolved organic P (0.1 - 0.6 μmol l^{-1}), which is not found in the runoff from the glacial catchments. Also sediments in the Apure waters contain an order of magnitude more organic P than sediments in the glacial meltwaters and scarcely bio-available detrital P is replaced downstream by conditionally bio-available ironbound P. Therefore, not only is terrestrial productivity higher in the tropical catchment compared to glacial catchments (as evinced by the higher concentrations of organic P), but the tropical sediments might also stimulate more productivity in aquatic ecosystems, because of the higher concentrations of conditionally bio-available P. Paradoxically the elevated SRP flux from the Apure catchments (0.52 kmol km^{-2} yr; Saunders and Lewis, 1988) could be largely due to atmospheric inputs of P. 1.36 kmol km^{-2} of SRP are delivered to to the Llanos per year (Montes and José, 1989), and a considerable portion of the regional bio-available P flux is established to of an eolian Saharan source (Reichholf, 1986; Swamp et al., 1992). In contrast the Rhône Tributary's rain corrected SRP flux is comparable with the mean global SRP flux from unpolluted non-glaciated catchments (0.13 kmol km^{-2} yr^{-1}; Meybeck, 1993; this flux is not corrected for atmospheric inputs). Therefore we suggest that

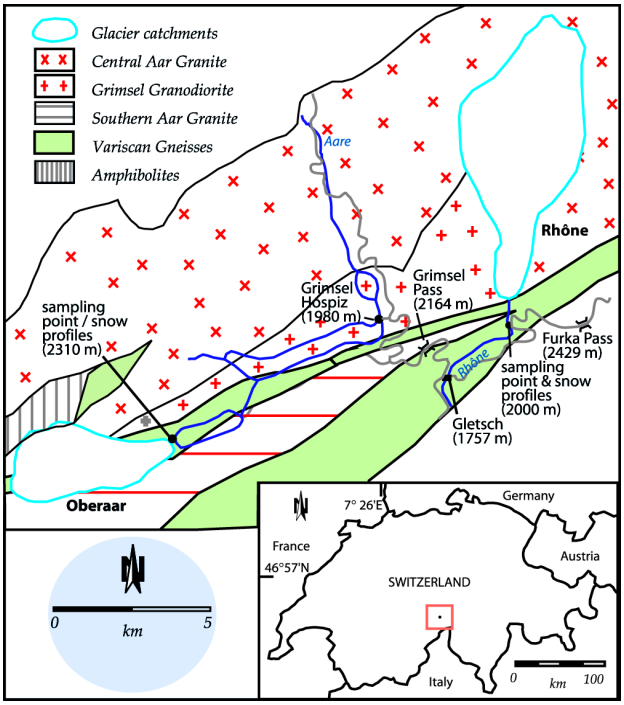


Fig. 3: *The glacial catchments in the Swiss Alps and their crystalline bedrock geology*

periods of glacial retreat may have a positive impact on the SRP flux to the biosphere and that glacial preconditioning of grains, coupled with acidifying pedogenic processes may accelerate the dissolution of detrital P minerals.

The Glacial and Tropical Catchments

The presently glaciated Rhône (Rh) and Oberaar (Ob) catchments and the proglacial Rhône Tributary catchment are located on crystalline bedrock of the Aar massif in central Switzerland (Table 1; Fig. 3). The glacial catchments are both pristine and anthropogenic pollution can only influence precipitation inputs to the catchments. The presently glaciated catchments both have well-defined meltwater streams that were sampled up to 100's of meters from the glacier snouts. The catchments have been part of a detailed three-year study and their major anion and cation chemistries and the fluxes of major ions and suspended sediments from the catchments are presented elsewhere (*chapter 3*). The Rhône Tributary catchments is located on a steep sided slope (> 25 °) adjacent to the Rhône glacier (Fig. 3). Approximately 80 % of the catchment contains glacial drift of Younger Dryas age that is undergoing podzolification and has a vegetation cover of alpine flowers, grasses and shrubs. (Zumbühl, 1988; Egli et al., 2001)

The Apure watershed, a fan shaped array of tributaries draining an area of 167000 km^2, is located in the north-west of Venezuela, with its headwaters beginning at approximately 2000 m in the Venezuelan Andes. We have sampled headwater streams that feed the Bocono River and taken upstream samples of some other important tributaries, Guanare and the Portuguesa. The Bocono joins the Guanare approximately 200 km along its course and the Guanare subsequently joins the Portuguesa after a further 400 km. The Guanare and the Portuguesa are major left bank affluents of the Apure River, which the Portuguesa joins 70 km downstream from its confluence with the Guanare. The Apure joins the

Table 1: The physical parameters of the Oberaar, Rhône and Rhône tributary catchments, Switzerland and the Apure catchment, Venezuela

	Oberaar	Rhone	Rhône Tributary	Apure
Geographical position	46° 32'N 8° 14'E	46° 35'N 8° 23E	46° 35'N 8° 23E	
Geology	granite & strongly foliated gneiss	granite and granodiorite	granodiorite, with granite and granodiorite drift	crystalline and sediments
Catchment area (Km^2)	11.03	26.2	1.5	167000
Glacial cover (%)	57	73	0	0
Temperature (° C)	-1	1.2	1.2	27[†]
Annual precipitation (mm)	2100	2200	2200	1600
Elevation (m)	2310-3631	2050-3630	1770-2600	2000 -50[*]
Sampling elevation (m a.s.l)	2316m (snout)	1840m	1770 m	-

[†] Maximum mean annual temperature (Vegas-Vilarrubia et al., 1993)

[*] Only 15 % of the catchment is > 500 m (Saunders and Lewis, 1988)

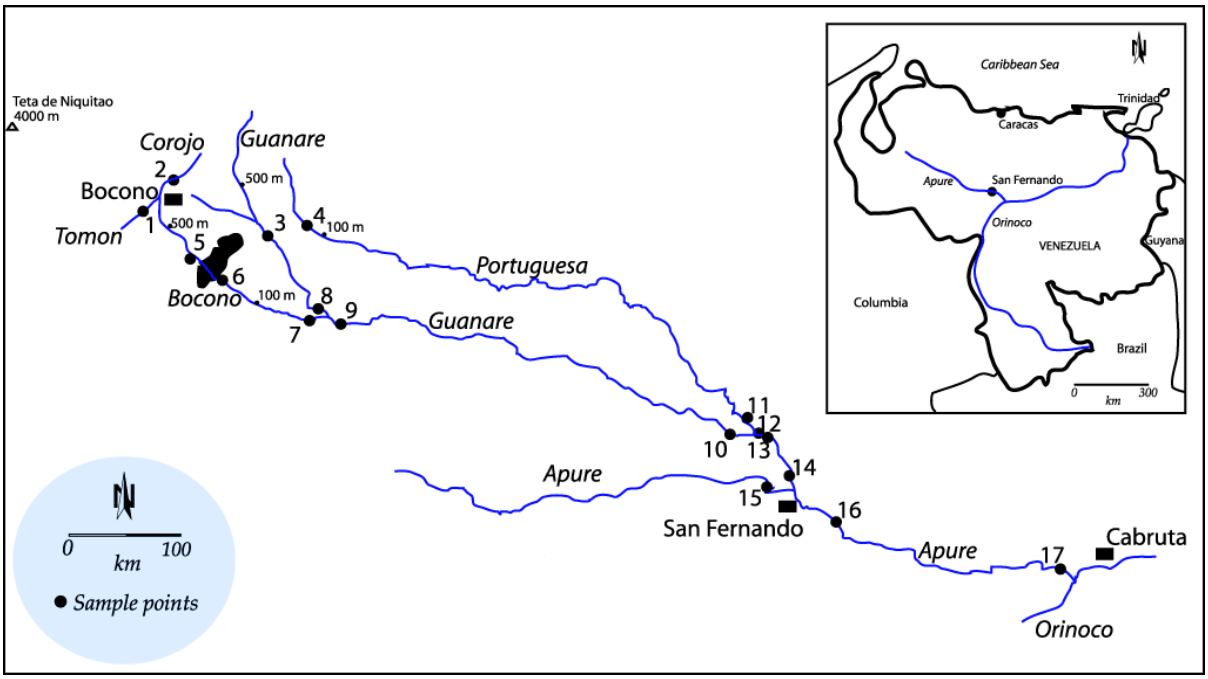


Fig. 4: *The principal rivers sampled in the Apure watershed, Venezuela*

Orinoco River 1500 km from its source, having descended approximately 2000 m (Fig. 4). The Apure watershed drains the eastern slopes of the Cordillera de Merida and the Cordillera de la Costa, composed of ancient basement rocks and associated

metamorphosed sedimentary and volcanic rocks of Mesozoic age which have been thrust southwards onto Paleogene flysch deposits (Edmond et al., 1996). Having left the Andes the Apure and its tributaries subsequently meander over the alluvial plain of the Llanos: The refluxing of water through these porous sediments has weathered them intensely, transforming them from felsic arenites to quartz sands (Johnsson et al., 1988). The summits of the Cordillera are covered by paramo type vegetation, with the lower slopes being used for arable production, for example coffee, peppers and corn. The Llanos plain is used as pasture for cattle, but there are important riparian zones that are flooded each rainy season. The precipitation maximum occurs in June or July and annual rainfall averages 1,600 mm (Lewis and Saunders, 1989)

Methods: Sampling Techniques and Laboratory Analysis.

Weekly meltwater samples were collected from the Rhône and Oberaar catchments during the summers of 1999, 2000 and 2001. In order to calculate daily mean concentrations samples were taken in pairs at the times of minimum and maximum daily discharge (10am and 5pm; Gurnell et al., 1994). Throughout the winter samples were taken on a monthly basis. In

total 70 Rhône meltwater and 50 Oberaar meltwater samples were taken. The Rhône Tributary was sampled six times on a monthly basis between May and September 2000. The Apure river system was sampled in February 1999, September 1999 and November 2000. The 1999 campaign coincided with a year when the El Nino –El Nina effect was particularly pronounced, leading to very dry river beds in February and particularly swollen rivers in September.

Samples for total phosphorus (TP) analysis were bottled without filtration, samples for soluble reactive phosphorus (SRP) and total dissolved phosphorus (TDP) analysis were filtered immediately in the field, as recommended by Slatt (1972) using pre-weighed 0.45μm cellulose acetate filters, a Nalgene filter unit and hand pump (The difference between TSP and SRP is ascribed to dissolved organic phosphorus; DOP). Approximately 125 ml of filtered water was bottled for analysis and stored in the dark at 2°C. In 1999 all samples were stored in polyethylene bottles, pre-leached with deionised water after Edmund et al., (1996). The Venezuelan samples were poisoned with several drops of Na_2N_3 since they were only analysed after 2-3 weeks (GEA laboratory, Neuchâtel). The 1999 glacial samples were poisoned using $MgCl_2$ to prevent SRP uptake by bacteria (Mackereth et al., 1978). We found the $HgCl_2$ made TDP analysis inaccurate. So in 2000 and 2001 all samples were stored in autoclaved, iodine coated polypropylene bottles that were rinsed three times with river water before filling them to leave no airspace (Mackereth et al., 1978).

5 snow samples were taken from profiles dug during the 2000-2001 accumulation season in front of the Rhône and Oberaar glaciers. 17 rain samples were also collected during the 2000 and 2001 ablation periods by connecting a pre-leached 1 liter polypropylene bottle to a funnel via a polypropylene tube. A fine copper mesh was used to limit particles falling into equipment and the bottle was left for a maximum of 24 hours before the rainwater was filtered and bottled.

Sediment-laden-filters were retained from each sampling event, generally representing the sediment in 500 ml of water; the filters were dried at 40°C, weighed and used to calculate suspended sediment concentrations in the meltwaters. Venezuela bedload samples were also taken using a grab sampler; they were dried at 40° C in the GEA laboratory Neuchâtel within 3 weeks.

The TDP and TP samples were dissolved with ammonium peroxide at 120°C and subsequently measured together with the SRP samples using a Perkin Elmer spectrophotometer (molybdenum blue method; Murphy and Riley, 1962). The 4 cm cuvette affords a limit of detection of 0.03 μ mol l^{-1} (± 0.04 μmol l^{-1}).

The ironbound, detrital and organic P concentrations of the suspended and bedload sediments were analysed using a sequential extraction method (SEDEX; Ruttenberg, 1992; Tamburini 2001), which has also been used on river and on lake sediments (Berner and Rao, 1994; Fillipelli and Souch, 1999). The method removes increasingly recalcitrant phosphorus forms in progressive steps. Samples were prepared as follows: Suspended sediment was removed from each filter paper ultrasonically, the sample was immediately centrifuged and the supernatant (deionised water) decanted off. The blank filters were dried and reweighed to calculate the exact mass of sediment transferred (between 0.04 and 0.2 g). Bedload samples were ground for 3 minutes in an agate mill and 0.1 g was used for the extraction. Step 1 of the SEDEX method removes ironbound P using a pH 7.6 citrate-dithionate-bicarbonate solution (CDB). Step 2, an acetic acid-sodium acetate solution buffered at pH 4, was designed to identify marine authigenic phosphorus (Ruttenberg; 1992). We interpret the P extracted by this step as fine detrital P, which can be solublised if sediment grains are not approximately 250 μm in diameter (Ruttenberg; 1992). As the modal grain size of our glacial suspended sediment is approximately 4-8 μm and the bedload samples are equally fine it is highly likely that detrital P dissolution occurs (Hosein et al submitted; Hosein unpublished data, general appendix 1). Step 3 extracts detrital P with a 1 N HCl digestion and step 4 involves ashing the samples with peroxide at 550 °C and redigesting them with 1 N HCl to measure organic P. The solutions obtained from steps 2-4 were analysed within 1 week, using the molybdenum blue method in the GEA laboratory. The relative error of the detrital P measurements is ± 0.64 μmol g^{-1} and the relative

Table 2: Mean precipitation PO_4^{3-}/Cl in the Rhône and Oberaar glacier catchments

Sample	SRP (µeq l^{-1})	TDP (µeq l^{-1})	TP (µeq l^{-1})	Cl (µeq l^{-1})
Rain				
28/8/99				5.64
7/9/99				3.67
22/9/99				1.41
31/5/00	0.52	0.88		1.69
7/6/00				4.23
28/6/00	0.93	1.46		4.20
13/7/00	0.15			2.26
15/7/01				4.22
27/7/00	0.30	1.15		3.10
1/8/00	0.86	1.23		5.36
7/8/00	0.41	0.49		1.68
15/7/01			2.08	4.22
23/7/01			8.13	
3/8/01				3.80
3/8/01		1.00	4.71	1.94
8/8/01		1.16	3.36	3.74
17/8/01			5.18	6.21
30/8/01			3.35	8.46
Snow				
18/1/01 (Rhône)	0.14	0.24	0.23	2.52
18/1/01 (Oberaar)	0.57	0.78	1.09	9.87
6/3/01 (0-5 cm; Oberaar)	0.08	0.39		2.80
6/3/01 (0-40 cm; Oberaar)	0.04	0.39		5.32
6/3/01 (0-5 cm; Rhône)	0.06	0.15	0.30	
mean rain	0.53	1.05	4.47	3.87
mean snow	0.18	0.39	0.54	5.13
weighted average	**0.32**	**0.66**	**2.11**	**4.63**
† Alptal, Switzerland (non glaciated; average annual precipitation)				4.51
# Haut glacier d'Arolla, Switzerland (mean snowpack)				3.80
PO_4^{3-}/Cl	**0.07**	**0.14**	**0.46**	n/a

† Mean annual precip. for a non-glaciated valley on the northern border of the Alps; Average annual precipitation 2300 mm; Schleppi P. Pers. Comm. (Swiss Federal Insititute for Forests Snow and Landscape Research)

Mean winter snowpack 93-95, Tranter et al. (2002)

Values are given in µeq and P concentrations are listed as PO_4^{3-} to show the PO4/Cl ratios used to correct the raw data.
Blank spaces are left where the samples were not analysed

Table 3: P concentrations in glacial runoff and precipitation inputs

	n†	Oberaar µmol l-1	Rhône µmol l-1	Tributary µmol l-1	Precipitation µmol l-1
		Ablation Period Runoff			**Rain**
SRP	48; 64; 6	0.08 (± 0.02)	0.05 (± 0.02)	0.14 (± 0.04)	0.18 (± 0.1)
TDP	41; 54; 5	0.10 (± 0.04)	0.07 (± 0.03)	0.17 (± 0.04)	0.35 (± 0.1)
DOP	-	b/d	b/d	b/d	0.17
TP	24; 30; 2	5.58 (± 3.21)	2.17 (±2.39)	0.29 (± 0.01)	1.52 (± 0.7)
Cl-	111;198; 5	2.23 (± 0.49)	2.23 (±0.88)	2.70 (±0.92)	3.97 (± 1.85)
		Accumulation Period Runoff			**Snow**
SRP	7; 6; 1*	0.11 (± 0.02)	0.09 (± 0.04)	0.09	0.06 (± 0.07)
TDP	4; 4; 1*	0.13 (± 0.03)	0.14 (± 0.06)	0.16	0.13 (± 0.08)
DOP	-	b/d	b/d	0.07	-
TP	3; 3; -	0.26 (± 0.03)	0.23 (± 0.03)	-	0.18 (± 0.16)
Cl-	7; 6; 1*	3.19 (± 1.10)	4.25 (± 0.05)	3.52	5.13 (± 3.40)

† n: Oberaar; Rhône; Tributary

* Winter estimate is based on a sample taken on the 19-Sept-00

b/d = below detection

error of the organic P measurements is ± 0.32 μmol g^{-1}. The samples obtained from step 1 were analysed for iron and P at the Neuchâtel cantonal laboratory " Service cantonale de l'eau et l'environnement" by ICP-AES.

The mineralogy of the powdered Venezuelan bedload sediment samples and the glacial and Venezuelan suspended sediments retained on the 0.45 μm cellulose acetate filters were measured by X-ray diffraction (XRD), using a Scintag XDS 2000.

P fluxes were calculated as the product of the P concentrations and discharge volumes (see chapter 3 for details of how fluxes are calculated in the presently glaciated catchments). In the Rhône Tributary catchment discharges are estimated from Bernath (1991) who recorded the Tributary's discharges over a three-year period (1981-1984; mean discharges are 250, 277, 150 and 66 l s^{-1} for the months of June, July, August and September respectively; ± 48 l s^{-1}). A winter flux is estimated by taking the lowest discharge recorded by Bernath (1991, 7 l s^{-1} and the P concentration measured on the 19th of September as a representative winter value. The annual P fluxes are calculated as the mean of the ablation and accumulation period P fluxes, multiplied by 365. In all three catchments "weathering derived P fluxes" are also calculated, using P concentrations that have been corrected for atmospheric P inputs using the cyclical salts method described in chapter 3; P: Cl ratios are shown in Table 2.

Results

P Concentrations

P concentrations in the glacial catchments: Particulate P (PP), the difference between total dissolved and total P, is the most concentrated P form in the glacial meltwaters (Table 3) and at least 96-

97% of this P is detrital (Rh= 10.00 μmol g^{-1}, ± 1.61; 0.03 %; Ob = 18.72 μmol g^{-1}, ± 2.58). The concentration does not vary as a function of discharge or seasonal evolution of the subglacial hydrological system and the mean detrital P concentration of the Rhône suspension is similar to the detrital P concentration of the catchment's bedrock; the Central Aar granite (0.04 - 0.07 % Keusen et al., 1989). The mean concentrations of ironbound and organic P in the glacial suspended sediments are < 1.61 μmol g^{-1} and 0.32 μmol g^{-1} (± 0.32 μmol g^{-1}) respectively.

The partitioning of P is very different in the runoff from the Rhône Tributary catchment: P is mostly transported in dissolved forms, and the mean SRP and TDP concentrations of the Rhône Tributary waters are approximately double those in the glacial meltwaters (Table 3). Suspended particulate matter in the Rhône Tributary waters is negligible, therefore we have not analysed its solid P composition. One similarity between the three glacial catchments is that the SRP and TDP concentrations are within experimental error of each other (± 0.04 μmol l^{-1}) in the great majority of the Rhône, Oberaar and Rhône Tributary water samples and therefore dissolved inorganic P (DIP) is the predominant dissolved form in the runoff from all three catchments and dissolved organic P (DOP) is below detection.

P concentrations in the rain and snow falling in the glacial catchments: The most important difference between the mean P composition of the glacial runoff and the mean P composition of the precipitation entering the catchments is that the precipitation samples contain DOP. The mean DOP concentration in rain is 0.17 μmol l^{-1}, DOP was also detected in some snow samples (Table 3).

Comparing P concentrations in the runoff from the glacial and tropical catchments: The SRP concentration of the Apure tributaries ranges from 0.1 - 1.6 μmol l^{-1}, i.e. 1 - 2 orders of magnitude higher than the mean SRP concentrations of the glacial meltwaters (Appendix 1; Table 3). Also, in contrast with the glacial meltwaters, DOP is detected in the tropical runoff (0.1 - 0.6 μmol l^{-1}; Appendix 1). In the sediments of the Apure tributaries ironbound, detrital and organic P forms are all detected: ironbound P concentrations are generally higher in the suspension samples (mean suspension = 10.17 μmol g^{-1}; mean bedload = 3.28 μmol g^{-1}) as are organic P concentrations (mean suspension = 4.99 μmol g^{-1}; mean bedload = 2.82 μmol g^{-1}). Detrital P concentrations are generally higher in the bedload samples (mean suspension = 6.80 μmol g^{-1}; mean bedload = 13.34 μmol g^{-1}). We observe a pattern of decreasing detrital P and increasing ironbound P concentrations with distance downriver, whereas organic P concentrations do not appear to change as a function of distance (Fig. 5; Table 4). The mean particulate P concentrations of suspended sediments from these climatically distinct catchments are similar (Rh = 11.93 μmol g^{-1}; Ob = 20.65 μmol g^{-1}; Apure = 21.95 μmol g^{-1}), but whereas detrital P represents 96 – 97 % of the particulate P in the glacial suspensions, it only represents 30 % of the average solid P content in the Apure suspended sediments. This is because ironbound and organic P

Table 4: The detrital, ironbound and organic P compositions of the Rhône Oberaar (glacial) and the Apure and Amazon (tropical) particulate P fluxes (PP)

	Sample Date	Distance from Source	Det-P'	Fe-P	Org-P	PP
		(km)	(µmol/g)	(µmol/g)	(µmol/g)	(µmol/g)
APURE SEDIMENTS[#]						
Bedload						
Head water rivers						
1. Tomon	Mar-99	-	11.31	0.89	0.79	12.98
Vitisy	Sep-99	-	33.05	21.02	25.19	79.26
Tirindi	Sep-99	-	0.00	0.97	1.82	2.79
2. Corojo	Mar-99	-	36.23	0.97	2.91	40.11
2. Corojo	Sep-99	-	48.76	0.97	2.91	52.63
Average (without Vitisy)		20	*17.93*	*0.94*	*1.84*	*20.71*
Intermediate and Llanos Rivers						
5. Bocono entry to lake	Sep-99	100	26.82	1.01	1.14	28.97
3. Guanare, Biscucui	Sep-99	137	12.64	1.97	1.64	16.25
4. Portugesa, Llanos Rd	Sep-99	200	6.61	4.81	4.58	16.01
8. Guanare before Bocono (0-2m)	Sep-99	213	20.77	4.57	3.31	28.66
9. Bocono & Guanare	Sep-99	216	17.81	2.07	2.01	21.89
15. Apure before Portuguesa, San Fernando	Sep-99	950	0.14	1.20	5.11	6.45
17. Mouth Apure	Mar-99	1247	4.02	9.69	2.91	16.61
Average			*13.34*	*3.28*	*2.82*	*19.44*
Suspension						
Intermediate and Llanos Rivers						
5. Bocono entry to lake	Sep-99	100	13.77	5.63	5.57	24.97
3. Guanare, Biscucui	Sep-99	137	8.44	5.50	3.30	17.24
4. Portugesa, Llanos Rd	Sep-99	200	5.93	3.57	4.79	14.29
8. Guanare before Bocono (0-2m)	Sep-99	213	8.73	8.43	6.36	23.52
9. Bocono & Guanare	Sep-99	216	8.97	7.90	5.77	22.64
10. Guanare before Portuguesa (g)	Nov-00	400	7.56	9.69	5.16	22.41
10. Guanare before Portuguesa (s)	Nov-00	400	7.30	10.33	5.22	22.85
12. Portugesa + Guanare 800 m (g)	Nov-00	400	5.80	11.62	6.12	23.55
12. Portugesa + Guanare 800 m (s)	Nov-00	400	4.86	15.18	5.29	25.33
13. Portugesa + Guanare 15 km (s)	Nov-00	415	5.94	11.95	5.70	23.58
14. Portuguesa before Apure, San Fernando (g)	Nov-00	450	6.72	12.92	5.49	25.13
15. Apure before Portuguesa, San Fernando (g)	Sep-99	950	4.20	17.04	3.23	24.47
15. Apure before Portuguesa, San Fernando (g)	Nov-00	950	6.46	8.72	5.17	20.34
15. Apure before Portuguesa, San Fernando (s)	Nov-00	950	6.12	8.72	5.36	20.20
16. Apure Boquerones	Sep-99	1037	4.51	10.91	3.58	19.01
17. Mouth Apure	Sep-99	1247	3.44	14.55	3.73	21.72
Average			*6.80*	*10.17*	*4.99*	*21.95*
AMAZON RIVER SUSPENSION[†]	-		6.78	7.43	7.43	21.63
GLACIAL SEDIMENTS						
Rhône (n=21)	1999-2000	0	10.00 (± 1.16)	< 1.61°	0.32 (±0.32)	11.93
Oberaar (n=15)	1999-2000	0	18.72 (± 2.58)	< 1.61°	0.32 (± 0.32)	20.65

[#] The numbering corresponds to the sample points on Fig. 3

* Value from Nov-00

[†] Berner and Rao (1994)

° We estimate 0.32 µmol/g in bioavailable flux calculation (Table 5)

concentrations are on average > 6 and 15 times higher (respectively) in the suspended sediments of the Apure catchment than in the suspended sediments of the glacial catchments.

Comparing the mineralogy of the glacial and tropical sediments: The sediment suspended in the glacial meltwaters contains quartz (21.8 & 24.3 %); potassic feldspar (17.2 & 6.5 %); plagioclase (27.9 & 25.4 %), phyllosilicates (14.2 & 13.7 %), and calcite (0.5 & 2.3 %), with some additional amphibole in the Oberaar catchment (mean values are given for the Rhône and Oberaar glaciers respectively). The Venezuelan suspended and bedload sediments generally contain kaolinite in addition to the minerals found in the glacial catchments.

Glacial P Fluxes

The dominance of solid P forms in the glacial meltwaters leads to a strong correlation between the TP and suspended sediment concentrations (R^2; Ob = 0.92; Rh = 0.80). This enables us to use least squares regressions to calculate the TP concentrations in 174

Rhône and 117 Oberaar meltwater samples, based on their suspended sediment concentrations. We can thereby calculate a more representative TP flux that includes several flushing events, such as a two day rain event on the 20th and 21st of September 1999 where 9 % of the annual suspended sediment flux was exported from the Rhône glacier (*Chapter 3*; The particulate P concentration and the suspended sediment bulk mineralogy were not observed to change as a function of discharge). We obtain average TP fluxes of 8 and 11 kmol km^{-2} yr^{-1} respectively from the Rhône and Oberaar catchments using this method (precipitation inputs of TP are relatively minor; Table 5). The larger Oberaar TP flux reflects both the elevated detrital P concentration of the Oberaar suspension and the higher suspended sediment concentration of the Oberaar meltwaters

Table 5: Fluxes from the glaciated catchments in kmol km^{-2} yr^{-1}

	Oberaar	Rhône	Tributary
Runoff			
SRP	0.19	0.19	0.29
TP	13.82	8.46	< 2.33
PP	11.18	8.27	-
Rain corrected			
SRP	0.04	0.05	0.17
TP	10.58	7.38	≈ 0.60
PP	10.53	7.33	-

(Hosein et al., submitted). We attribute these differences to the presence of an easily eroded gneissic zone that forms the central part (42 %) of the Oberaar catchment.

The particulate P flux, calculated as the product of the mean particulate P concentration of the suspended sediments (ironbound & detrital & organic P) and the annual suspended sediment fluxes from each glacier, is comparable with the particulate P fluxes calculated as the difference between the TP and SRP fluxes (see Table 6).The SRP fluxes from the presently glaciated Rhône and Oberaar catchments are significantly lower than the SRP fluxes from Rhône Tributary catchment. Moreover, when these fluxes are corrected for precipitation inputs, the glacial catchments' SRP fluxes are approximately 4 times less than the SRP flux from

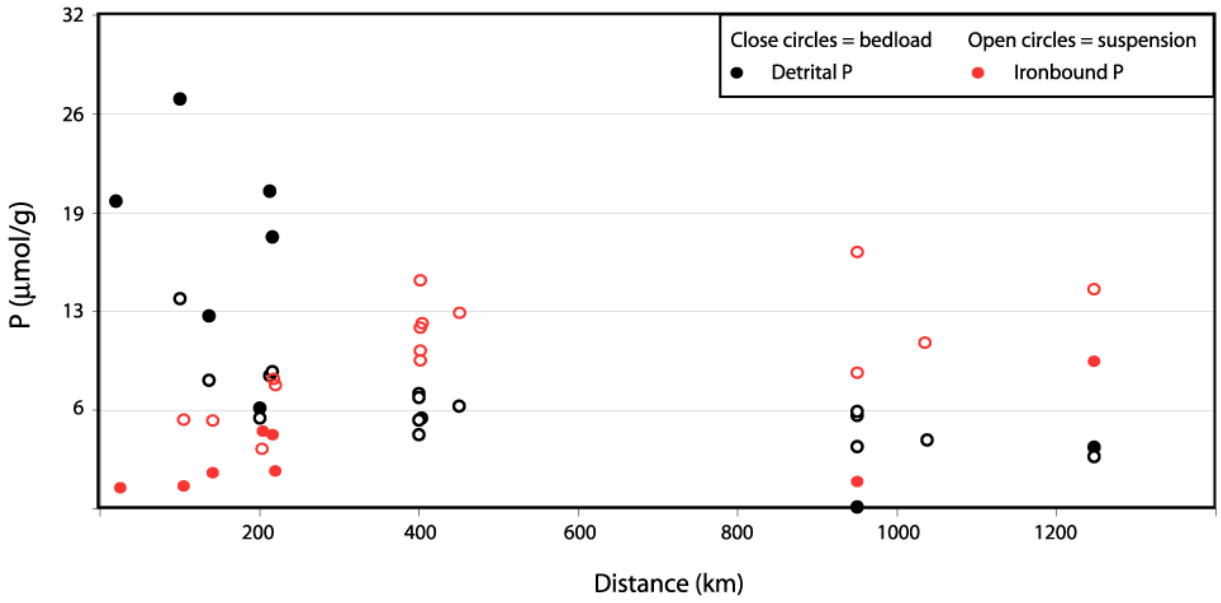


Fig. 5: *Detrital and ironbound P concentrations in the bedload and suspended sediments of the Apure watershed.*

the Rhône Tributary catchment (Table 4). TP fluxes are not calculated for the Rhône Tributary catchment as TP concentrations were only measured on 2 samples, but since the TP concentrations are approximately double the SRP concentrations it would follow that the TP flux should also be approximately double the SRP flux, i.e. ≈ 0.6 kmol km^{-2} yr^{-1}.

Discussion

The annual, precipitation corrected, total phosphorus fluxes in the two presently glaciated catchments are 7 and 11 kmol km^{-2} yr^{-1} and more than 99 % of this flux is in particulate form. Our glacial catchments' particulate P fluxes are the same order of magnitude as catchments in tectonically active areas, such as the Ganges, Amazon and Mekong, which also have high suspended sediment fluxes (see table 6). Rivers draining watersheds located in areas that are less tectonically active, such as the Gambia and Congo have particulate P fluxes that are 2 orders of magnitude lower, as do non-glaciated crystalline catchments that are a similar size to the glacierised ones (table 6). Although glacial erosion may potentially produce similar sediment volumes as fluvial erosion (Hay, 1998) the P forms in the runoff from presently glaciated and tropical catchments are different. The Amazon and the Apure, two of the world's major tropical rivers, have now been shown to carry an important load of particulate P in ironbound and organic P forms (Berner and Rao, 1994; this study). Upstream in the Apure catchment detrital P concentrations are higher than ironbound P concentrations in the suspended sediments, but downstream (over 400 km from the headwaters) ironbound P becomes the dominant P forms in the suspended sediments (Fig. 5). This may suggest that detrital P is deposited up stream and colonised by vegetation and transfered into ironbound and organic

Table 6: A comparison of particulate P (PP), total P (TP) and conditionally bioavailable P fluxes (kmol km^{-2} yr^{-1})

River system	Study	Geology	Catchment	Sediment flux[%]	Altitude	PP	TP	Conditionally bioavailable P [≈]
			(Km^2)	(t km^{-2} yr^{-1})	(m)	(kmol km^{-2} yr^{-1})	(kmol km^{-2} yr^{-1})	(kmol km^{-2} yr^{-1})
Ganges	Martin & Meybeck 1979		3820000	437	>3000	7.90		
Amazon	Martin & Meybeck 1979		6150000	195	>3000	10.40	10.92[$]	7.59
Orinoco	Lewis & Saunders, 1989		990000	212	>3000	2.32	3.10	2.56
Mekong	Martin & Meybeck 1979		790000	203	>3000	13.08		
Apure	Saunders & Lewis, 1988		167000		1000-3000	1.49	2.20	1.95
Vaal 1978-81	Grobler & Silberbauer 1985	sedimentary	16153		1000-3000		0.03	
Limpopo-sub 1980-82	Grobler & Silberbauer 1985	igneous	1171		1000-3000		0.08	
Limpopo-sub 1979-81	Grobler & Silberbauer 1985	igneous	129		1000-3000		0.03	
Rhône	This study	granite-granodiorite	27	491[#]	1000-3000	6*-8°	8.01	0.29
Oberaar	This study	granite, foliated gneisse	11	773[#]	1000-3000	11°-16*	11.66	0.37
Gambia	Lesack et al., 1984		42000		500-1000	0.09	0.25	0.23
Richmond river	McKee & Eyre, 2000	volcanic	6861		500-1000		0.42[§], 1.64[†]	
Congo	Martin & Meybeck 1979		3820000	11	100-500	0.55		
Thi National Park	Stoorvogel et al., 1997		1.17		100-500	4.00	4.62	3.70
Mean export from 25 forested catchments	Dillon and Kirchner, 1975	plutonic	10-100				0.15	
Mean export from 8 forested sedimentary	Dillon and Kirchner, 1975	sedimentary	10-100				0.38	
mean export from 7 volcanic catchments	Dillon and Kirchner, 1975	volcanic	10-100				2.32	

[*] Calculated from SEDEX extraction

[%] Milliman and Meade,1985

[°] Calculated as the difference between SRP and TP

[§]Flux calculated from weathering of bedrock

[†] Total Phosphorus

[#] Hosein et al., (submitted)

[$] After Berner and Rao, (1994) and references therein

[≈] [(]Fe-P +Org-P)[*] + TDP) [*] Estimated as 68% of PP in the Amazon catchment after Berner and Rao, 1994; 83 % of PP in the Apure and Orinoco catchments after the particulate P composition at the mouth of the Apure, Table 5 and 77 % of PP in the other tropical catchments.

P forms. Our data suggest that the retention of detrital P in the pedosphere and its conversion into biogenic forms (Syers and Walter, 1976; Crews et al., 1995), means that the P discharged in transport limited systems (such as the Amazonian and Venezuelan Llanos) may contains up to 26 times more conditionally bio-available P (DIP, DOP, ironbound and organic P) than the scarcely bio-available detrital P discharged in glacial meltwaters is (Table 6).

Glaciers and periods of glaciation may therefore have great potential to change the P dynamics and productivity of terrestrial and aquatic ecosystems in several ways (Föllmi, 1995; Chadwick et al., 1999). Firstly the great physical erosive force of advancing glaciers (Hallet et al., 1996; Hay 1998) might have lead firstly to deeply weathered soils being bulldozed off land surfaces, ironbound and organic P in such soils would become conditionally bio-available in the marine environment (a transfer of 600 Pg of C, after Sigman and Boyal, 2000). Secondly, as large areas of the continents became covered in ice physical weathering rates and export of sediment from subglacial environments may have decreased as the ice masses became predominantly

cold based and frozen to their beds (Kump et al., 2000, and references therein). Also the chemical weathering derived SRP flux from any wet based marginal areas of ice sheet would have likely been negligible, judging from the SRP fluxes from the presently glaciated Rhône and Oberaar catchments are (0.05 kmol km^{-2} yr^{-1}), this is probably due to the neutral pH of the subglacial environments (Stumm and Morgan, 1996). Thirdly, periods of deglaciation may have lead to the renewed erosion and export of freshly comminuted detrital P grains in glacial sediments and their deposition over considerable continental areas (28 % of the Northern Hemisphere's land surface may have fallen within the proglacial zone during deglaciation following the last glacial maximum, Gibbs and Kump, 1994). This detrital P may have been rapidly hydrolised to SRP in the proglacial environment. Furthermore, due to the low P binding capacity of protosoils with their thin organic horizons and low oxide contents (Egli et al., 2001; Filippelli and Souch; 1999) proglacial areas may have leaked a considerable flux of SRP into aquatic ecosystems (Pennington, 1981; Filippelli and Souch, 1999).

The evidence collected during my thesis which hints that the Rhône glacier forefield may transfer SRP into the local aquatic ecosystem is the increased rain corrected SRP flux from the Tributary catchment relative to the presently glaciated catchments (0.17 and 0.05 kmol km^{-2} yr^{-1} respectively). Further data are necessary to fully substantiate a case for the transfer SRP from an immature pedosphere to (local) aquatic ecosystems as the Tributary mass balance is based on a limited data set,

To compare the SRP fluxes generated by the dissolution of detrital P in glacial environments with SRP fluxes from the tropics, non-weathering sources of SRP need to be accounted for, namely precipitation and anthropogenic inputs: on average 0.02 kmol km^{-2} yr^{-1} of mineral P fertiliser were added to Venezuelan soils between 1985 and 1989 (Beaton

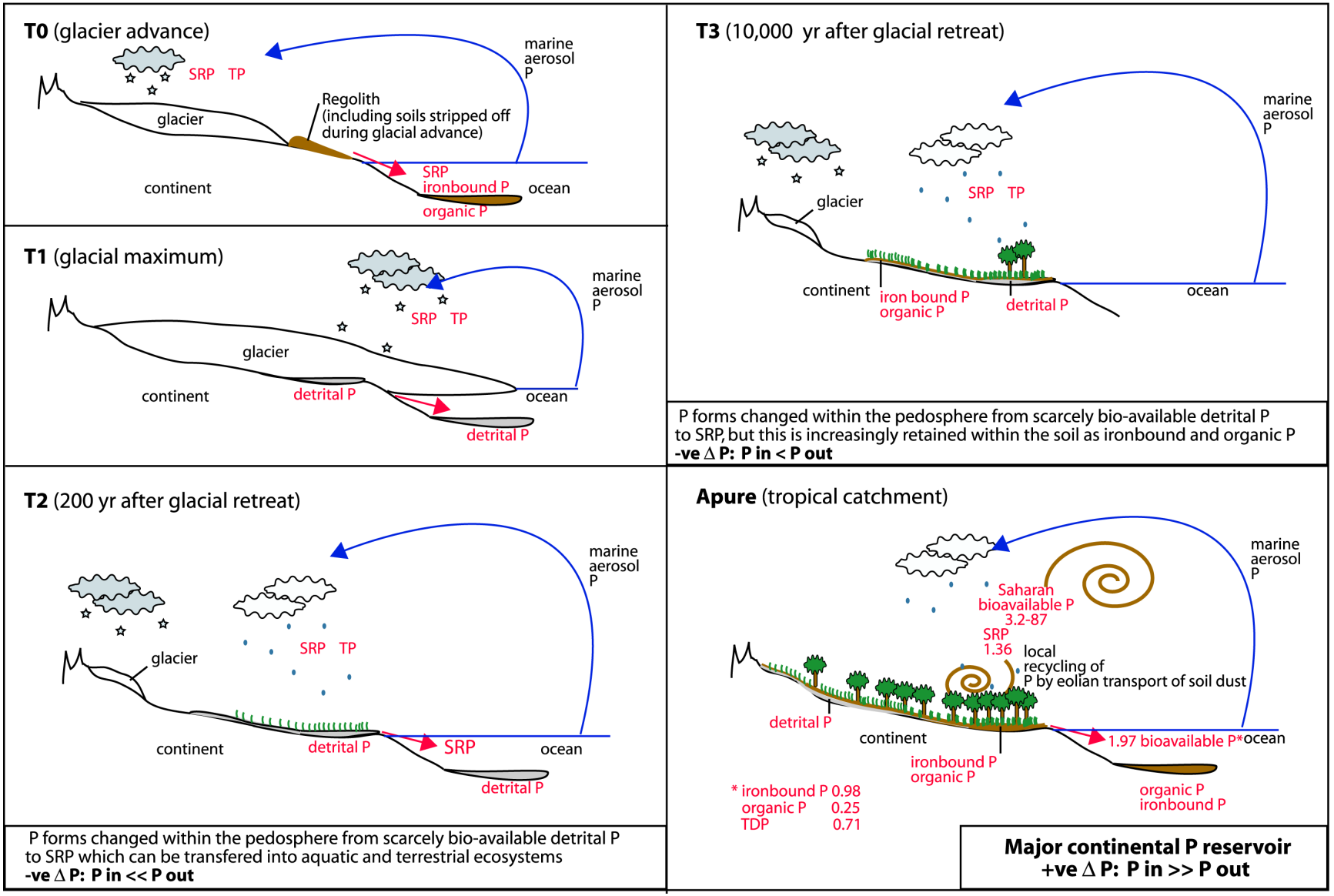


Fig 6: P cycling in tropical and glaciated continental areas, (kmol P km^{-3} yr^{-1}); Reichhof, 1986; Montes and San Jose, 1989 and Swamp et al., 1992.

et al., 1995). The regional input of soluble P by rain and occult deposition is also considerable (SRP = 1.36 kmol km^{-2} yr^{-1}; Montes and Jose, 1989). The literature hints that both locally recycled and distal inputs of SRP may be important sources: P may be recycled internally within the Apure basin by burning vegetation and through the local eolian transport of soil dust (Montes and Jose, 1989 and references therein). But, marine aerosols (Montes and Jose, 1989) and Saharan dust may also account for a portion of the locally bio-available P (3.2 - 87 kmol P km^{-2} yr^{-1}; Reichholf, 1986; Swap et al., 1992). Since the Llanos soils are oligotrophic and depleted in P (San Jose and Garcia Miragaya, 1982) such external P inputs may be important in maintaining productivity. Since the lowest estimate of distal eolian bio-available P input (3.2 kmol P km^{-2} yr^{-1}) is higher than the annual output of biologically available P from the catchment (1.97 kmol P km^{-2} yr^{-1}) the Apure basin may act as a reservoir, trapping SRP in the pedosphere in ironbound and increasingly recalcitrant organic P forms (see also Chadwick et al., 1999). Periods of glaciation (and uplift) may reactivate transport limited regimes replacing old, deeply weathered soils with immature pedospheres that transfer SRP into aquatic environments (Fig. 6).

Acknowledgements

J. Ondrus (Lab. cant. serv. environnement, Neuchâtel) performed the ICP-AES analysis. A. Moreau, M. Cornièles-Vallès and Colonel R. Mena Nava (MARNR-Venezuela) provided invaluable logistical support for the Apure sampling campaign and Swiss National Science Foundation grants 21-53997.98 and 20-61485.00 are also gratefully acknowledged.

References

Beaton J.D., Roberts T.L., Halsted E.H. and Cowell L.E. (1995) Global transfers of P in fertiliser materials and agricultural commodities: 107-137 *In:* Tiessen H. (Ed.) Phosphorus in the global environment: Transfers, cycles and management: *Scope* **54**, Wiley.

Bernath A. (1991) Zum Wasserhaushalt im Einzugsgebiet der Rhône bis Gletsch. Grebner D. (Ed.). *Züricher Geographische Schriften* **43**.

Berner R.A., and Rao J.L. (1994) Phosphorus in sediments of the Amazon River and estuary: Implications for the global flux of phosphorus to the sea. *Geochimica Cosmochimca Acta* **58**: 2333-2339.

Boström B., Persson G., and Broberg B. (1988) Bioavailability of different phosphorus forms in freshwater systems. *Hydrobiologia* **170**: 133-155.

Birkland P.W., Burke R.M., and Benedict J.B. (1989) Pedogenic gradients for iron and aluminium accumulation and phosphorus depletion in Arctic and Alpine soils as a function of time and climate. *Quaternary Research* **32**: 193-204.

Broecker W.S. (1982) Ocean chemistry during glacial times. *Geochimica Cosmochimica Acta* **46**: 1689-1705.

Cembella A.D., Antia N.J. and Harrison P.J. (1984) The utilisation of inorganic phosphorus compounds as nutrients by eukaryotic mircoalgae:

A multidisciplinary perspective. *Critical reviews in microbiology* **10**: 317-391.

Chadwick O.A., Derry L.A., Vitousek P.M., Huebert B.J. and Hedin L.O. (1999) Changing sources of nutrients during four million years of ecosystem development. *Nature* **397**: 491-497.

COHMAP (1988) Climatic changes of the last 18,000 years: Observations and model simulations. *Science* **241**: 1043-1052.

Cotner J.B., Ammerman J.W., Peele E.R., and Bentzen E. (1997) Nutrient-limited bacterioplankton growth in the Sargasso Sea. *Aquatic Microbial Ecology* **13**:141-149.

Crews T.E., Kitayama K., Fownes J.H., Riley R.H., Herbert D.A. and Mueller-Dombois D. (1995) Changes in soil phosphorus fractions and ecosystem dynamics across a long chronosequence in Hawaii. *Ecology* **76**: 1407-1424.

Delaney M.L. (1998) Phosphorus accumulation in marine sediments and the oceanic phosphorus cycle. *Biogeochemical Cycles* **12**: 563-572.

Dillon P.J. and Kirchner W.B. (1974) The effects of geology and land use on the export of phosphorus from watersheds. *Water Resources* **9**:135-145.

Edmond J.M., Palmer M.R., Measures C.I., Grant B. and Stallard R.F. (1995) The fluvial geochemistry and denudation rate of the Guayana Shield in Venezuela, Columbia and Brazil. *Geochimica et Cosmochimica Acta* **59**: 3301-3325.

Filippelli G.M., and Delaney M.L. (1994) The oceanic phosphorus cycle and continental weathering during the Neogene. *Paleoceanography* **60**: 643-652.

Filippelli G.M. and Souch C. (1999) Effects of climate and landscape development on the terrestrial phosphorus cycle. *Geology* **27**: 171-174.

Fox L.E., Sager S.L. and Wofsy S.C. (1986) The chemical control of soluble phosphorus in the Amazon estuary. *Geochimica et Cosmochimica Acta* **50**: 783-794.

Föllmi K.B. (1995) 160 m.y. Record of marine sedimentary phosphorus burial: Coupling of climate and continental weathering under greenhouse and icehouse conditions. *Geology* **23**: 859-862.

Froelich P.N., Bender M.L., Luedtke N.A., Heath G.R., and DeVries T. (1982) The marine phosphorus cycle. *American Journal of Science* **282**: 474-511.

Frossard E., Brossard M., Hedley M.J., and Metherell A. (1995) Reactions controlling the cycling of P in Soils: 107-137. *In:* Tiessen H. (Ed.) Phosphorus in the global environment: Transfers, cycles and management: *Scope* **54**, Wiley.

Gibbs M.T. and Kump L.R. (1994) Global chemical erosion during the last glacial maximum and the present: Sensitivity to changes in lithology and hydrology. *Palaeoceanography* **9**: 529-543.

Golterman H.L. (1984) Sediments, modifying and equilibriating factors in the chemistry of freshwater. *Verh. Internat. Verein. Liminol.* **22**: 23-59.

Graham W.F. and Duce R.F. (1979) Atmospheric pathways of the phosphorus cycle. *Geochimica et Cosmochimica Acta* **43**: 1195-1208.

Grobler D.C. and Silberbauer M.J. (1985) The combined effect of geology, phosphate sources and runoff on phosphate export from drainage basins. *Water Research* **19**: 975-981.

Guidry M.W., Mackenzie F.T., and Arvidson R.S. (2000) Role of tectonics in phosphorus distribution and cycling. *In:* Glenn, C.R., et al. (Eds) *Marine Authegenisis: From global to microbial:SEPM (Society for Sedimentary Geology) Special Publication* **66**.

Gurnell A.M., Brown G.H. and Tranter M. (1994) Sampling strategy to describe the temporal hydrochemical characteristics of an alpine proglacial stream. *Hydrological Processes* **8** : 1-25.

Hay W.W. (1998) Detrital sediment fluxes from continents to oceans. *Chemical Geology* **145**: 287-323.

Hudson J.J., Taylor W.D., Schindler D.W. (2000) Phosphate concentration in lakes. *Nature* **406**: 84-86

Johnsson M.J., Stallard R.F. and Meade R.H. (1988) First-cycle quartz sand in the Orinoco River basin, Venezuela and Columbia. *Journal of Geology* **96**: 263-277

Kpomblekou-a K. and Tabatabai M.A. (1994) Effect of organic acids on release of phosphorus from phosphare rocks. *Soil Science* **158**: 442-453.

Kump L.R. and Alley R.B. (1994) Global chemical weathering on glacial time scales: 46-60. *In*: Usselman T.M. and Hay W.W. (Eds.). *Material Fluxes on the Surface of the Earth*:. Geophysics Study Committee, National Research Council, National Academy Press, Washington D.C.

Lesack L.F.W., Hecky R.E. and Melack J.M. (1984) Transport of carbon, nitrogen phosphous and major solutes in the Gambia River, West Africa. *Limnology and Oceanography* **29**: 816-830.

Ludwig W., Amiotte-Suchet P. and Probst J.-L. (1999) Enhanced chemical weathering of rocks during the last glacial maximum: a sink for atmospheric CO_2? *Chemical Geology* **159**: 147-161.

Lewis W.M., and Saunders J.F. (1989) Concentration and transport of dissolved and suspended substances in the Orinoco river. *Biogeochemistry* **7**: 203-240.

Mackereth F.J.H., Heron J. and Talling J.F. (1978) Water Analysis: some revised methods for limnologists. *Freshwater biological publication* **36**.

Martin J.M., and Meybeck M. (1979)Elemental mass balance of material carried by major world rivers. *Marine Chemistry* **7**: 173-206.

McKee LJ, and Eyre BD (2000) Nitrogen and phosphorus budgets for the sub-tropical Richmond River Catchment, Austraila. *Biogeochemistry* **50**: 207-239.

Meybeck M. (1993) Natural sources of C, N, P and S, *In*: Wollast R., Mackenzie F.T., and Chou L., (Eds.) *Interactions of C, N, P and S Biogeochemical Cycles and Global Change*:

NATO ASI Series, **I 4**, Springer-Verlarg: Berlin Heidelberg.

Meybeck M. (1982) Carbon, nitrogen and phosphorus transport by world rivers. *American Journal of Science* **282**: 401-450.

Migon C. and Sandroni C. (1999) Phosphorus in rainwater: Partioning inputs and impact on the surface coastal ocean. *Limnology and Oceanography* **44**: 1160-1165.

Milliman J.D., and Meade R.H., (1983) Worldwide delivery of river sediments to ocean. *Journal of Geology* **91**: 1-19.

Molen D.T., Breeuwsma van der A, Boers P.C.M. and Roest C.W.J. (1997) Dutch policy towards phosphorus losses in agriculture: 137-149. *In*: Tunney H, Carton OT, Brookes PC, and Johnston AE. (Eds.) *Phosphorus losses from soil to water*. CAB International Wallingford.

Montes R. and San Jose J.J. (1989) Chemical composition and nutrient loading by precipitation in the Trachypogon savannas of the Orinoco Llanos, Venezuela. *Biogeochemistry* **7**: 241-256.

Murphy J. and Riley J.P. (1962) A modified single solution method for the determination of phosphate in natural waters. *Analytica Chimica Acta* **27**: 31-36.

Newbold J.D., Elwood J.W., O'Neill R.V., and Winkle W. Van (1981) Measuring nutrient spiralling in streams. *Canadian Journal of Aquatic Science* **38**: 860-863.

Pennington W. (1981) Records of a lake's life in time: the sediments. *Hydrobiologia* **79**: 197-219

Pye K. (1984) Loess. *Progress in Physical Geography* **8**: 176-217.

Reichhof J.H. (1986) Is Saharan dust a major source of nutrients to the Amazonian rain forest ? *Neotrop. Faunu Environ.* **21**: 251-255.

Reynolds C.S. and Davis P.S. (2001) Sources and bioavailability of phosphorus fractions in freshwater: a British perspective. *Biological Reviews* **76**: 27-64.

Roure F., Carnevali J.O., Gou Y. and Subieta T. (1994) Geometry and kinematics of the North Monagas thrust belt (Venezuela). *Marine Petroleum Geology* **11**: 347-362.

Ruttenberg K.C. (1992) Development of a sequential extraction method for different forms of phosphorus in marine sediments: *Limnology and Oceanography* **37**: 1460-1482.

Ruttenberg K.C. (1993) Reassesment of the oceanic residence time of phosphorus. *Chemical Geology* **107**: 405-409.

San Jose J.J. and Garcia-Miragaya J. (1982) Factores operacionales en la produccion de meteria nica de las sabanas de Trachypogon. *Boletin de la Sociedad Venezolana de Ciencias Naturales* **139**: 347 – 374-

Saunders J.F. and Lewis W.M. (1988) Transport of phosphorus, nitrogen, and carbon by the Apure River, Venezuela. *Biogeochemistry* **5**: 323-342.

Schindler D.W. (1977) Evolution of phosphorus limitation in lakes. *Science* **195**: 260-262.

Schweizer Bundesamt für Wasser und Geologie (SNGS) (1994) Technischer Bericht: Manual für die Abflussmessung nach dem Salzverdünnungsverfahren.

Sharpley A. (2000) Phosphorus Availability: D18-D36. *In*: Sumner M.E. (Ed.) Handbook of soil science: CRC Press.

Sigman D. and Boyle E. (2000) Glacial/Interglacial variations in atmospheric carbon dioxide. *Nature* **407**: 859-869.

Skirrow G. (1975) The dissolved gases-carbon dioxide: 245-300. *In*: Riley J.P. and Skirrow G. (Eds.) *Chemical Oceanography 2* 2nd edition:. London: Academic Press.

Slatt R.M. (1972) Geochemistry of meltwater streams from nine Alaskan galciers. *Geological Society of America Bulletin* **83**: 1125-1132.

Southam J.R. and Hay W.W. (1981) Global sedimentary mass balance and sea level changes. *The Sea* **7**: 1617-1684.

Stoorvogel J.J., Janssen B.H., and Breemen-Van N. (1997) The nutrient budgets of a watershed and its forest ecosystem in the Tai National Park in Côte d'Ivoire. *Biogeochemistry* **37**: 159-172.

Stumm W. and Morgan J.J. (1996) *Aquatic Chemistry*: Wiley, New York: **pp**. 1022.

Swamp R., Garstang M., Greco S., Talbot R. and Kallberg P. (1992) Saharan dust in the Amazon basin. *Tellus* **44**: 133-149.

Swiss National Hydrological and Geological Service (SNGS) (1994) Technischer Bericht: Manual für die Abflussmessung nach dem Salzverdünnungsverfahren.

Tamburini F. (2001) *Phosphorus in marine sediments during the last 150,000 years: exploring relationships between continental weathering, productivity, and climate* [Ph.D. thesis]: Switzerland, University of Neuchâtel. **pp.** 219.

Tyrell T. (1999) The relative influence of nitrogen and phosphorus on oceanic primary production. *Nature* **400**: 525-531.

Vegas-Vilarrubia T., Maass M., Rull V., Elias V., Ramon A., Ovalle C., Lopez D., Schneider G., Depetris P.J., Douglas I., (1993) Small Catchment Studies in the Tropical Zone. *In*:Moldan B. and Cerny J. (Eds) Biogeochemistry of Small Catchments: *Scope* **51**. Wiley.

Walker T.W. and Syers J.K. (1976) The fate of soil phosphorus during pedogenesis. *Geoderma* **15**: 1-19.

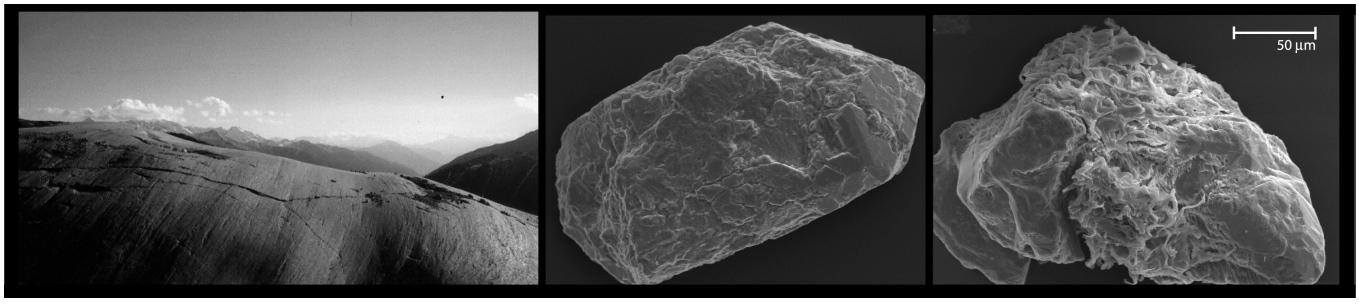
Appendix 1: Dissolved P in the Apure Watershed

Samples *	Distance from the Source	Discharge $m^3 s^{-1\dagger}$			P-SRP $\mu mol\ l^{-1}$			P-TDP $\mu mol\ l^{-1}$		P-DOP $\mu mol\ l^{-1}$	
		Feb-99	Sep-99	Nov-00	Feb-99	Sep-99	Nov-00	Sep-99	Nov-00	Sep-99	Nov-00
Head waters											
1. Tomon	20				0.1	0.3		0.5		0.1	
2. Corojo	20				0.1	0.6		0.7		0.1	
Intermediate rivers											
3. Guanare, Biscucui	137					0.5	0.3	0.5	1.0		0.6
4. Portugesa, Llanos Rd	200					0.3		0.4		0.1	
5. Bocono entry to lake	100				0.1	0.5		0.7		0.2	
6. Outflow of barage	100					0.1		0.3	0.2	0.1	0.0
7. Bocono before Guanare	213		51			0.2		0.4		0.1	
8. Guanare before Bocono (0-2m)	213		160			1.1		1.1		0.1	
9. Bocono & Guanare	216		210			0.9		1.2		0.2	
Llanos river samples											
10. Guanare before Portuguesa	400		175			1.6		1.9		0.3	
11. Portuguesa before Guanare			900			0.3		0.6		0.3	
12. Portugesa + Guanare 800 m	400					0.0	0.7	0.0	1.0		0.3
13. Portugesa + Guanare 15 km (s)	400					0.3	0.6	0.5	1.1	0.2	0.5
14. Portuguesa before Apure, San Fernando (g)	450	175	1075	625	0.1	0.6	0.4	0.7	0.8	0.1	0.4
15. Apure before Portuguesa, San Fernando (g)	950	375	3225	1875	1.8	0.6	0.6	0.7	0.8	0.1	0.2
16. Apure Boquerones	1037					0.3	0.5	0.6	0.7	0.3	0.3
17. Mouth Apure	1247	650	5000		0.4	0.7		0.4			

* The numbering corresponds to the sample points on Fig. 3

† Discharge estimates ± 10%

CHAPTER 5
appendices



Ablation period SRP (µg/l) at minimum and maximum discharge in the Rhône meltwaters (1999-2001)

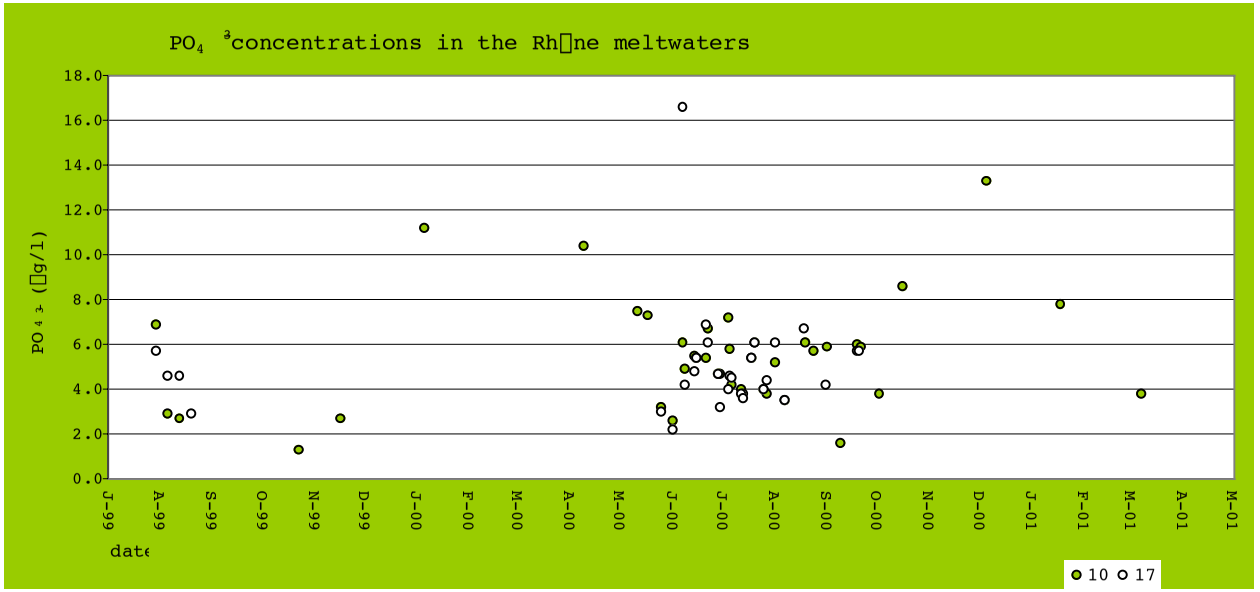
	07_99			08_99			09_99			10_99			05_00			06_00			07_00			08_00			09_00			10_00		
Date	10	17	daily	10	17	daily	10	17	daily	10	17	daily	10	17	daily	10	17	daily	10	17	daily	10	17	daily	10	17	daily	10	17	daily
1																2.6	2.2					5.2	6.1		5.9		5.9			
2																												3.8		3.8
3																														
4																			7.2	4.0	5.6									
5				2.9	4.6	3.8													5.8	4.6	5.2									
6																			4.2	4.5	4.4									
7																6.1	16.6	11.4				3.5	3.5	3.5						
8																4.9	4.2	4.6												
9																									1.6		1.6			
10																														
11													7.5		7.5															
12				2.7	4.6	3.7													4.0	3.8	3.9									
13																			3.8	3.6	3.7									
14																5.5	4.8	5.2												
15																5.4	5.4	5.4												
16																												8.6		8.6
17													7.3		7.3															
18																			5.4	5.4	5.4		6.7	6.4						
19					2.9	2.9																6.1			6.0	5.7	5.9				
20																			6.1	6.1	6.1					5.7	5.7			
21																5.4	6.9	6.2							5.9		5.9			
22										1.3		1.3				6.7	6.1	6.4												
23																														
24																						5.7		5.4						
25													3.2	3.0	3.1				4.0	4.0	4.0									
26																														
27																			3.8	4.4	4.1									
28																4.7	4.7	4.7												
29	6.9	5.7	6.3													4.7	3.2	4.0												
30																														
31																							4.2	4.2						
m			6.3			3.4						1.3			6.0			6.0			4.7			4.9			5.0			6.2

Accumulation period daily SRP concentrations in the Rhône meltwaters (1999-2001)

Date	µg/l
16/11/99	2.7
5/12/00	13
5/1/00	11
18/1/01	8
7/3/01	4
9/4/00	10
29/4/01	
m	8.20

	Ablat.	Accum.
n	63	6
mean	5.00	8.20

Month	mean flux	(kg/km²day)
January	0.003	
February		
March	0.001	
April	0.003	
May	0.023	
June	0.042	
July	0.032	
August	0.034	
September	0.015	
October	0.030	
November	0.001	
December	0.004	
Annual	**5.841**	(kg/km²/yr)



Ablation period SRP (µg/l) at minimum and maximum discharge in the Oberaar meltwaters (1999-2001)

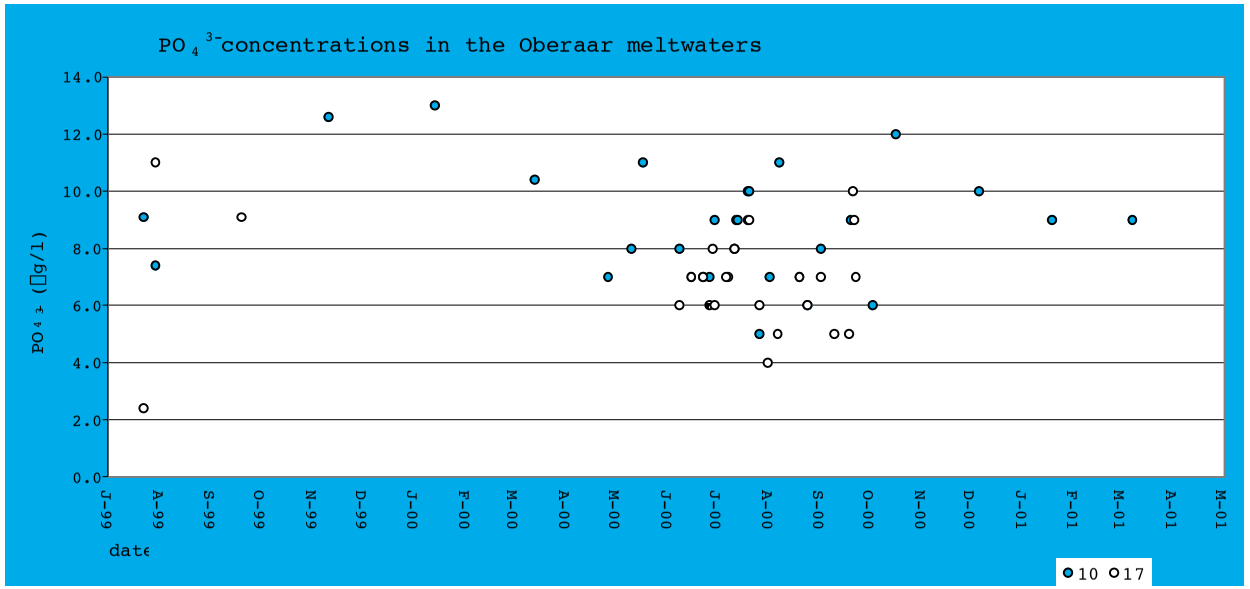
	07_99			08_99			09_99			10_99			05_00			06_00			07_00			08_00			09_00			10_00		
Date	10	17	daily	10	17	daily	10	17	daily	10	17	daily	10	17	daily	10	17	daily	10	17	daily	10	17	daily	10	17	daily	10	17	daily
1																						7.0		7.0	8.0	7.0				
2																												6.0		6.0
3																														
4																														
5																														
6																				7.0			5.0							
7																			7.0		7.0	11.0		8.0						
8																8.0	6.0	7.0												
9																										5.0	4.0			
10													8.0		**8.0**															
11																			8.0	8.0	8.0									
12																			9.0		9.0									
13																			9.0		9.0									
14																														
15																7.0	7.0	7.0												
16																												12.0		12.0
17													11.0		11.0															
18																										5.0				
19								9.1											10.0	9.0	9.5	7.0	7.0	7.0	9.0					
20																			10.0	9.0	7					10.0				
21																										9.0				
22	9.1	2.4	**5.8**													7.0	7.0	7.0								7.0				
23																														
24																						6.0	6.0	6.0						
25																														
26																7.0	6.0	6.5	5.0	6.0	7									
27																														
28																	8.0	8.0												
29	7.4	11	**9.2**													9.0	6.0	7.5												
30																														
31																				4.0	7									
m			7.5												9.5			7.2			7.9			7.0			4.0			9.0

Accumulation period daily SRP concentrations in the Oberaar meltwaters (1999-2001)

Date	µg/l
10/11/99	12.6
13/1/00	13
13/3/00	10
26/4/00	7
5/12/00	10
18/1/01	9
7/3/01	9.00
m	10.14

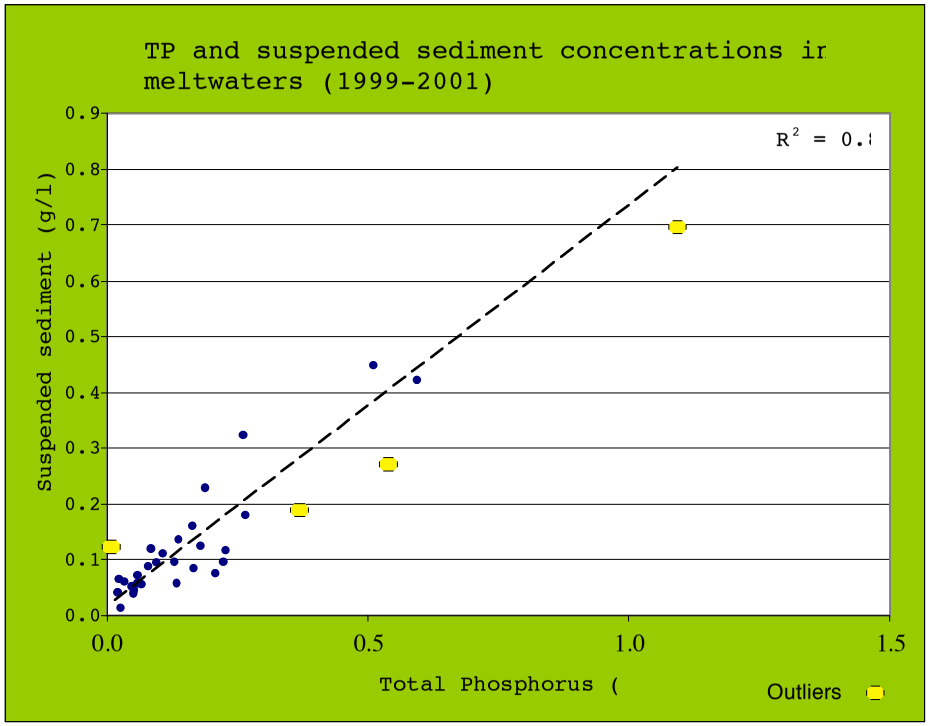
	Ablat.	Accum.
n	49	7
mean	7.58	10.14

Month	(kg/km²day)
January	0.003
February	
March	0.002
April	0.004
May	0.016
June	0.029
July	0.035
August	0.029
September	0.040
October	0.022
November	0.006
December	0.005
Annual	5.958 (kg/km²/yr)



The Relationship between Total Phosphorus (TP) and Suspended Sediment Concentrations in the Rhône Meltwaters (2000-2001)

	TP (mg/l)	Susp. Sed (g/l)	Susp. Sed outliers
10:00 h samples			
14/6/00	1.09		0.54
15/6/00	0.38		0.19
21/6/00	0.22	0.10	
22/6/00	0.08	0.09	
1/6/01	0.02	0.07	
7/7/01	0.51	0.45	
17/7/01	0.19	0.23	
7/8/00	0.13	0.06	
19/8/00	0.18	0.13	
24/8/00	0.13	0.10	
3/8/01	0.27	0.18	
1/9/00	0.05	0.04	
9/9/00	0.05	0.05	
19/9/00	0.07	0.06	
21/9/00	0.14	0.14	
16/10/00	0.55		0.23
5/12/00	0.02	0.04	
18/1/01	0.03	0.01	
7/3/01	0.02	0.04	
17:00 h samples			
8/6/00	0.08	0.12	
14/6/00	0.59	0.42	
15/6/00	0.26	0.32	
21/6/00	0.23	0.12	
22/6/00	0.21	0.08	
7/8/00	0.17	0.09	
18/8/00	0.01		0.13
31/8/00	0.06	0.07	
19/9/00	0.03	0.06	
20/9/00	0.09	0.10	
2/10/00	0.05	0.05	
29/8/01	0.11	0.11	
5/9/01	0.06	0.06	
15/8/01	0.16	0.16	

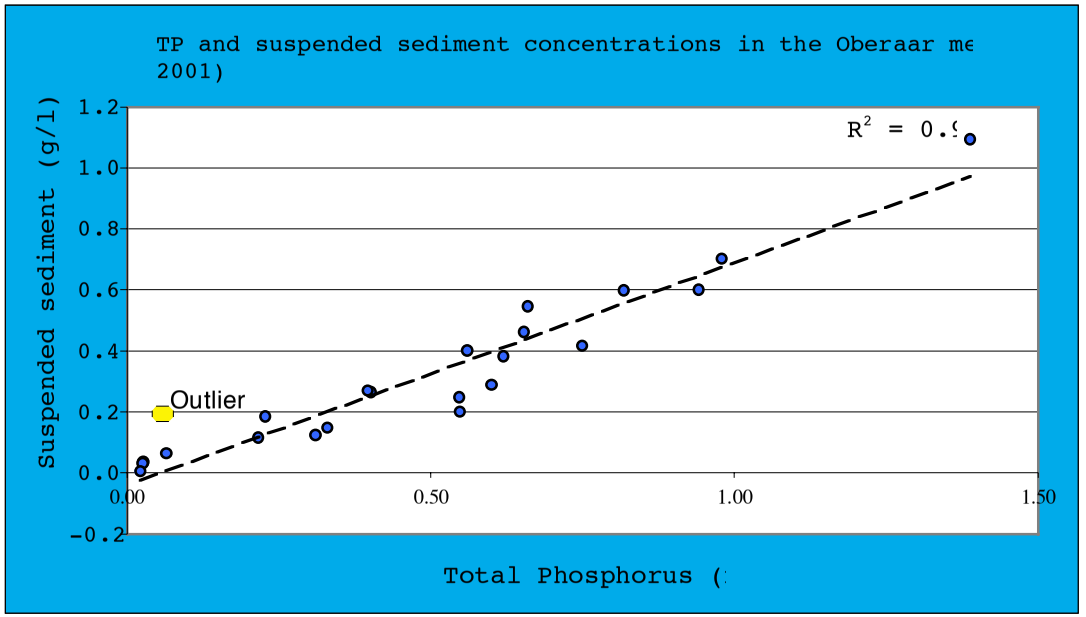


TP = (suspended sediment (g/l)/0.0.7185) - 0.017

Outliers were not included in the regression to prevent negative TP concentrations being calculated. When outliers are included $R^2 = 0.80$ & TP = (suspended sediment (g/l)/0.51) - 0.04

The Relationship between Total Phosphorus (TP) and Suspended Sediment Concentrations in the Oberaar Meltwaters (2000-2001)

	TP (mg/l)	Susp. Sed (g/l)	Susp. Sed outliers
10:00 h samples			
15/6/00	0.55	0.25	
14/6/01	0.98	0.70	
4/7/01	1.39	1.09	
3/8/01	0.82	0.60	
6/8/00	0.33	0.15	
24/8/00	0.40	0.27	
1/9/00	0.56	0.40	
9/9/00	0.23	0.19	
19/9/00	0.22	0.12	
21/9/00	0.40	0.27	
2/10/00	0.06	0.07	
16/10/00	0.55	0.20	
5/12/00	0.03	0.04	
18/1/00	0.03	0.03	
7/3/01	0.02	0.01	
17:00 h samples			
15/6/00	0.75	0.42	
6/8/00	0.31	0.12	
24/8/00	0.62	0.38	
1/9/00	0.66	0.55	
9/9/00	0.65	0.46	
18/9/00	0.60	0.29	
20/9/00	0.94	0.60	
21/9/00	0.08		0.27



TP = (suspended sediment (g/l)/0.7284) + 0.0402

Outliers were not included in the regression to prevent negative TP concentrations being calculated.
When outliers are included R^2 = 0.89 & TP = (suspended sediment (g/l)/0.69) + 0.01

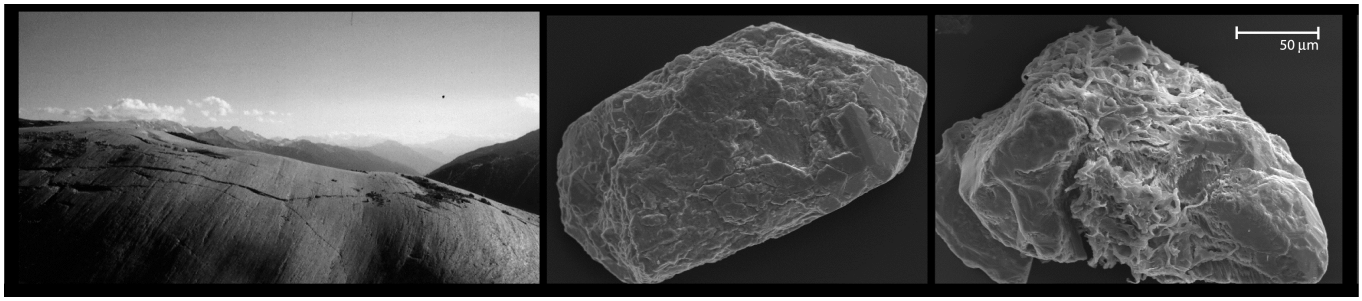
CHAPTER 6

Conversation with a Stone (III)

I knock at the stone's front door.
"It's only me, let me come in.
I hear you have great empty halls inside you,
unseen, their beauty in vein,
soundless, not echoing anyone's steps.
Admit you don't know them well yourself."

"Great and empty, true enough" says the stone,
"but there isn't any room
Beautiful perhaps, but not to the taste
of your poor senses.
You may get to know me, but you'll never know
me
my whole surface it turned toward you, though
all my insides turned away."

Wistawa Szymborska , in Nothing Twice



CHEMICAL WEATHERING IN A GLACIAL CHRONOSEQUENCE IN THE FOREFIELDS OF RHÔNE AND OBERAAR GLACIERS (SWISS ALPS): RATE AND MECHANISM OF BIOTITE WEATHERING

K. Arn, R. Hosein, T. Adatte, P. Steinmann, K.B. Föllmi*
Institut de Géologie, Université de Neuchâtel, Rue Emile-Argand 11, CH-2007 Neuchâtel, Switzerland.

Abstract

We analysed the clay mineralogy of glacial sediments in the two catchment areas of the Rhône and Oberaar glaciers (Swiss Alps) using XRD techniques, in order to identify processes and rates of alteration of moraine material in the glacier forefield. The well-dated sediments provide a chronosequence consisting of (A) recent suspended sediment in meltwater; B. terminal moraines dating from the Little Ice Age (LIA 1300-1850); and (C) tills dating from the retreat of Younger Dryas (YD 11'500 y BP). The suspended sediment is derived from mechanically abraded freshly eroded bedrock without being stored and altered subglacially and secondary weathering products have not been observed. Chemical weathering becomes increasingly important once glacial sediment is deposited in the proglacial area. With increasing age a vegetation cover develops on the morainic deposits and the initial umbrepts undergo podzolisation. XRD data in this chronosequence show an increase in pedogenically formed vermiculite and a continuous decrease in biotite with increasing sediment age. Biotite contents in the top 30 cm of the soils decrease by 25 – 50 % within 140 – 270 years. Feldspar weathering becomes apparent in proglacial sediments older than 270 years.

Biotite weathering rates were calculated using the difference in biotite content between the C-horizon and the top 30 cm of a soil profile. Reactive mineral surface areas were estimated geometrically, for their total as well as for their edge surface. The weathering rates obtained using the total mineral surface area (WR_T) are in the order of $10^{-10} – 10^{-12}$ $mol_{biotite}$ $m^{-2}{}_{biotite}$ sec^{-1}. The weathering rates using the edge surface area (WR_E) are in the order of $10^{-10} – 10^{-11}$ $mol_{biotite}$ $m^{-2}{}_{biotite}$ sec^{-1}. The calculated rates are several orders of magnitude faster than known field weathering rates. This is related to: (1) The predominance of fine-grained particles (<63 μm) in glacial sediment which are mechanically disaggregated and preferentially leached; and (2) The studied glacial sediments are well drained and highly permeable and no heterogeneities in flow paths through soils were observed. We suggest that glacially derived material is subjected to enhanced chemical weathering, starting immediately after deposition in the pro-glacial zone and subsequently continuing for thousands of years after glacier retreat.

This chapter has been submitted to Chemical Geology

Introduction

Glaciers are important agents of physical erosion and glacial abrasion produces a considerable fraction of fine-grained sediment (<63 μm). The high surface/mass ratio and the presence of strained minerals in this fraction condition the material for subsequent chemical weathering. This process begins immediately after erosion and mobilisation in the subglacial domain of temperate glaciers (e.g. Tranter et al., 1993; Gurnell et al., 1994; Sharp et al., 1995; Anderson et al., 1997, Fairchild et al., 1999 and Hosein et al., submitted). It may also continue once the sediment is beyond the glacier margins, within proglacial deposits such as moraines and alluvial plains where chemical weathering may be intensified after glacier retreat (Anderson et al., 2000).

The interest in chemical weathering processes in glacial domains is related to its impact on the global carbon cycle: directly, by the consumption of atmospheric CO_2 during silicate weathering, as well as indirectly, by the mobilisation of nutrients such as phosphorus, iron, potassium, and calcium, which regulate productivity rates and photosynthetic uptake of atmospheric CO_2 (Sharp et al., 1995; Föllmi, 1995 and Hallet et al., 1996). A better understanding of changes in the global carbon cycle related to glacial periods depends, therefore, on a better understanding of chemical weathering processes in glaciated areas and glacial sediments of different ages. Extensive literature exists on soil development in glacially derived sediments in chronosequences (e.g.,

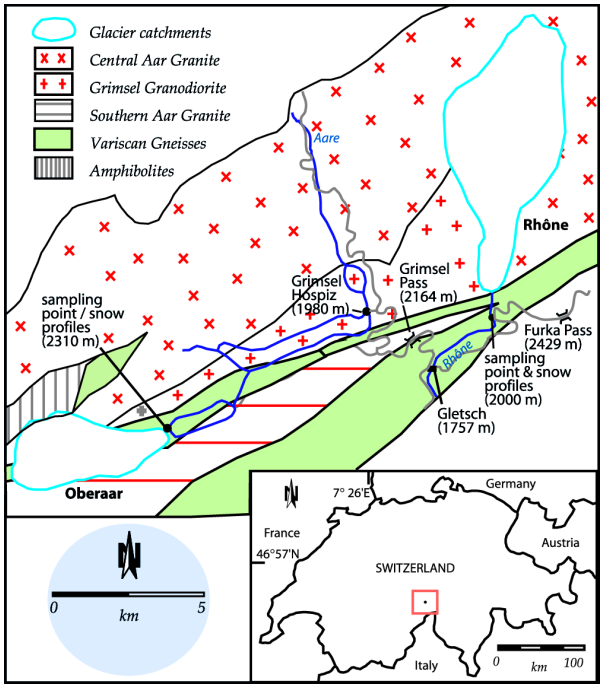


Fig. 1: *Map of the field areas with geology of the Aar Massif modified after Oberhänsli et al. (1988) and todays glacier catchments.*

Claridge and Campbell, 1984; Birkeland et al., 1987; Lidmar-Bergström et al., 1999; Righi et al., 1999 and Egli et al., 2001).

In glacial environments the vermiculitisation of biotite leads to the preferential release of K^+ ions in glacial meltwaters (Drever and Douglas, 1986, Anderson et al., 1997). Biotite as the source of K^+ could hold as a proxy of chemical weathering in glacial regimes. Biotite field weathering rates in different climatic regimes are commonly calculated by a mass balance method (e.g., Swoboda-Colberg and Drever, 1993; Nagy, 1995; Murphy et al., 1998). Reported laboratory based biotite weathering rates are calculated for different conditions (Table 6b); they are normally two to three orders of magnitude higher than field rates (e.g., Velbel, 1993a; Turpault

Table 1: Different parameters of the two catchments.

	Oberaar			Rhone		
Geographical position	46° 32' N 8° 14' E			46° 35' N 8° 23' E		
Surface of catchment	11.2 km2			23 km2		
Altitude	2310 - 3631 m (a.s.l.)			1750 - 3630 m a.s.l.		
Glacier cover today (%)	57%			73%		
Annual mean temperature *	- 1° C§			+ 1.2° C§		
Annual mean precipitation *	2100 mm			2200 mm		
Geology of catchments:	Today	LIA	YD	Today	LIA	YD
Central Aar Granite	38%	38%	25%	90%	82-86%	40%
Grimsel Granodiorite	7%	7%	12%	10%	8-9%	20%
Variscan Gneisses	42%	42%	38%		10-5%	20%
Ultramafic Inclusions	1%	1%	1%			
Southern Aar Granite	12%	12%	24%			
Mesozoic metasediments						20%

* Schwab et al. (2001)
§ within proglacial area, 2300 m at Oberaar, 1757 m at Rhone

LIA, Little Ice Age
YD, Younger Dryas

and Trotignon, 1994; Nagy, 1995; Kalinowski and Schweda, 1996).

In this contribution we studied the forefields of the Rhône and Oberaar glaciers, located in the Swiss Alps (Fig. 1). The areas experience similar climatic conditions and underwent comparable deglaciation phases in the Holocene. Both glaciers are presently subjected to considerable retreat and loss in volume. Both areas are contained within the crystalline rocks of the Aar Massif (Stalder, 1964, and Abrecht, 1994; Fig. 1). The lithologies are quite homogeneous and comparable (Table 1), except for the presence of a zone of highly deformed Variscan basement gneisses and schists in the Oberaar catchment area (Oberhänsli et al., 1988).

The goals of this study are threefold: 1) To reconstruct processes and timing of weathering of primary minerals in the proglacial zone; 2) to calculate biotite weathering rates based on the decreasing biotite content of soil profiles over 100s to 1000s of years; and 3) to consider the impact which glaciers may exert on global weathering rates.

Sampling Sites

Two profiles (O_{140A} and O_{140B}; Fig. 2) were dug in a moraine ridge that was deposited during the maximum extent of the Little Ice Age (LIA) within the Oberaar catchment (1860, Ammann, 1977). Another profile (O_{YD}) was dug within a patchy till cover beyond the extent of the LIA-moraines: This till is interpreted to date back to the retreat of the glacier after the Younger Dryas (YD; 11'500 BP; C. Schlüchter, Bern, pers.comm.). Hormes et al. (2001) show evidence for eight Holocene phases of reduced glacier extent in the area of the Unteraargletscher, a

glacier catchment adjacent to the Oberaar. Their first post YD phase of glacier contraction, with glaciers smaller than at present, occured 9910-9550 cal yr BP (14-C dated woods). "YD" is used in this work as age for glacial sediments dating back to this first post YD phase. Vegetation cover in the proximal forefield of the Oberaar glacier (ca. 2300 m above sea level, a.s.l.) consists of pioneer plants typical for proglacial areas that recently freed from ice. Some alpine meadows and peat lands appear in the more distal parts (Ammann, 1977).

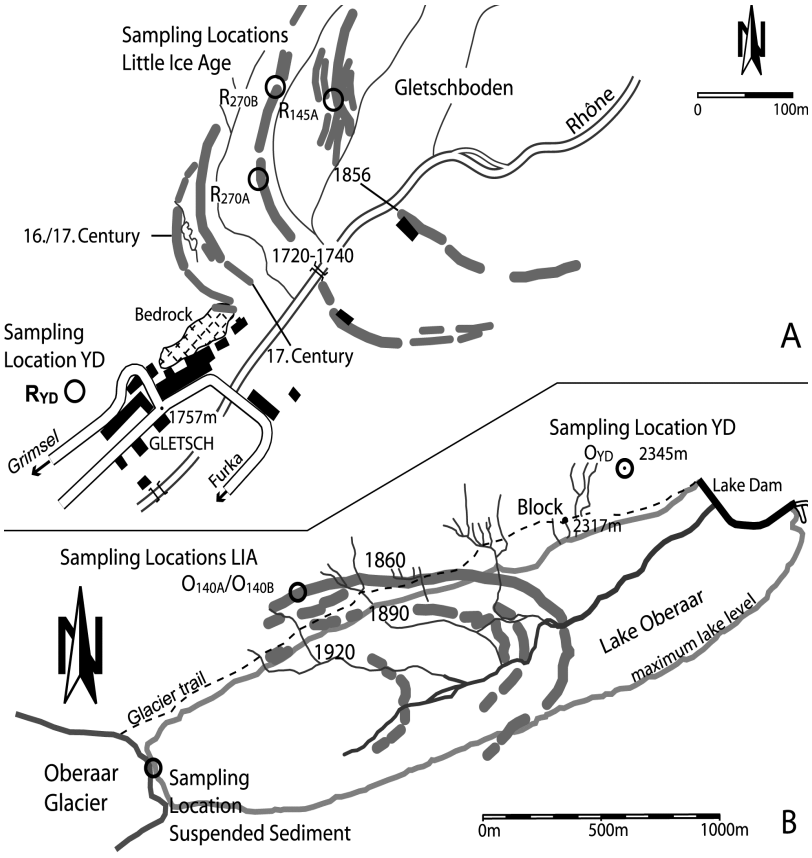


Fig. 2: Situation maps: (A) Rhone glacier forefield after Zumbühl (1988), and (B) Oberaar glacier forefield after Ammann (1977). For profile description see text and Table 2.

The maximum extent of the Rhône glacier during the Little Ice Age (LIA) was around 1600 (Zumbühl, 1988). Two profiles (R_{270A}, and R_{270B}; Fig. 2) were dug in moraine ridges dating from the beginning of the 18th century, and one profile (R_{145A}) was made in the terminal moraine dating from 1856. A further profile (R_{YD}; Fig. 2) was dug in a patchy till cover in a scoured morphology beyond the limits of LIA, which also dates back to the retreat of YD, as described in the Oberaar catchment. The vegetation in the glacier forefield (at 1750 m a.s.l.) mainly consists of alpine meadows and peat lands with alder bushes.

Soil profiles

The LIA profiles are located on the crest of moraine ridges. All moraine profiles show a sandy to silty texture and contain some clay, and the YD profiles are not significantly enriched in clays. The general grainsize distribution implies a good porosity , allowing precipitation to percolate through the tills. Soil description are given in Table 2 (the names of soil types and horizons are given according to USDA, 1998, USDA, 1999; soil types are also given according to the recommendations of A.F.E.S., 1998).

The young soils dating back to 1856 – 1860 are best described as orthent (entisols) or "regosols" after USDA and AFES, respectively: In these profiles (O_{140A}, O_{140B}, R_{145A}) an organo-mineral Ah horizon of 5 cm was observed which overlies a transition zone (AC) of 30 – 40 cm and the unweathered C-horizon. A Bw horizon could not be distinguished with certainty. The 270 year old soils (R_{270A}, R_{270B}) were found to be umbrebts (inseptosols) or "brunisol oligosaturé" after USDA and AFES, respectively: An organo-mineral Ah horizon (5 cm) covers a 10 to 15 cm thick Bw horizon. The underlying transition zone reaches down to at least 50 cm. Within the top 30 cm of all the LIA profiles the root density is high and the moraines are of a browny (top) to rusty color. Below 30 – 40 cm the moraines look fresh and grey in color, and roots rarely reach below 30 – 40 The oldest soils dating back to the retreat of the YD are humods (spodosols) or "podzosols ocriques" after USDA and AFES, respectively. The YD profiles from both areas are strongly weathered throughout. In profile O_{YD} (Oberaar) a discontinuous E horizon of 10 cm thickness is present under a 5 cm thick Oh and a 5 – 10 cm thick Ah horizon. Below that a Bhs (at 20 – 30 cm depth) overlies a Bw horizon (at 30 – 60 cm depth). At 60 cm depth the profile reaches unweathered consolidated bedrock (R). In profile R_{YD} (Rhône) a typical E horizon of 10 cm thickness is present under a 10 cm thick Ah horizon. Below that a Bhs (at 20 – 40 cm depth) overlies a Bw horizon (at 40 – 70 cm depth). Between 30 and 40 cm depth a rusty layer is visible, pointing to the periodic existence of a water layer. At the bottom of the YD profiles is a Bw horizon, and a C horizon could not be distinguished. The top 30 cm of these profiles are organic rich and of a dark brownish color (matrix) including lighter zones. Below that the soil is of a rusty color and some roots reach down to the bottom of the profiles. The clasts are strongly weathered and decay easily.

Laboratory methods

Integrated samples (2 – 3 kg) were taken in soil profiles every 10 cm down to a depth of 60 – 100 cm. The measured parameters of each 10 cm slice were averaged for the top 30 cm and for the bottom 20 – 30 cm, which corresponds to the C-horizon for the LIA profiles. This division was used because of the significant transitions observed at 30 cm depth in all profiles: The rhizosphere is restricted to the top 30 cm layer, and changes in clay mineralogy, pH, and colour of the samples are observed at this limit as well. Suspended sediment was collected from both glaciers during the two ablation seasons (1999 and 2000) by filtering meltwaters through 0.45 μm cellulose-acetate filters in the field. Bedrock was randomly sampled within the areas.

All samples were analysed at the GEA laboratory of the Geological Institute of the University of Neuchâtel. Prior to analysis samples were oven-driedat 40 °C and divided into subsamples. Granulometric analyses of the glacial sediments were performed using sieving sizes of 4 cm to 63 μm and the fraction < 63 μm was analysed on a Granulometry Laser Oriel CIS, together with the suspended sediment samples. Bulk rock and clay

mineralogy of the samples were analysed following the procedure of Adatte et al. (1996). Approximately 20 g of each bedrock sample was ground with a "jaw" crusher to obtain small chips (1 to 5 mm). Approx. 5 g of dried glacial sediment and bedrock chips were ground to a homogenous powder with particle sizes <40μm. 800 mg of this powder were pressed (20 bars) in a powder holder covered with blotting paper and analysed by XRD. Bulk rock composition was determined by XRD (SCINTAG XRD 2000 Diffractometer) based on methods described by Klug and Alexander (1974), Kübler (1983), and Adatte et al. (1996). This method for the semi-quantitative analysis of the bulk rock mineralogy uses external standards.

Separation of different grain-size fractions (< 2μm and 2-16 μm) for clay mineralogy analysis of glacial sediments and dust was obtained by centrifugation using the time-settling method based on Stokes law. Each fraction was pipetted onto a glass plate and air-dried at room temperature. The analyses were performed with a SCINTAG XRD 2000 Diffractometer. The intensities of selected XRD peaks characterising each clay mineral present in the size fraction (chlorite, phengite, biotite, biotite-

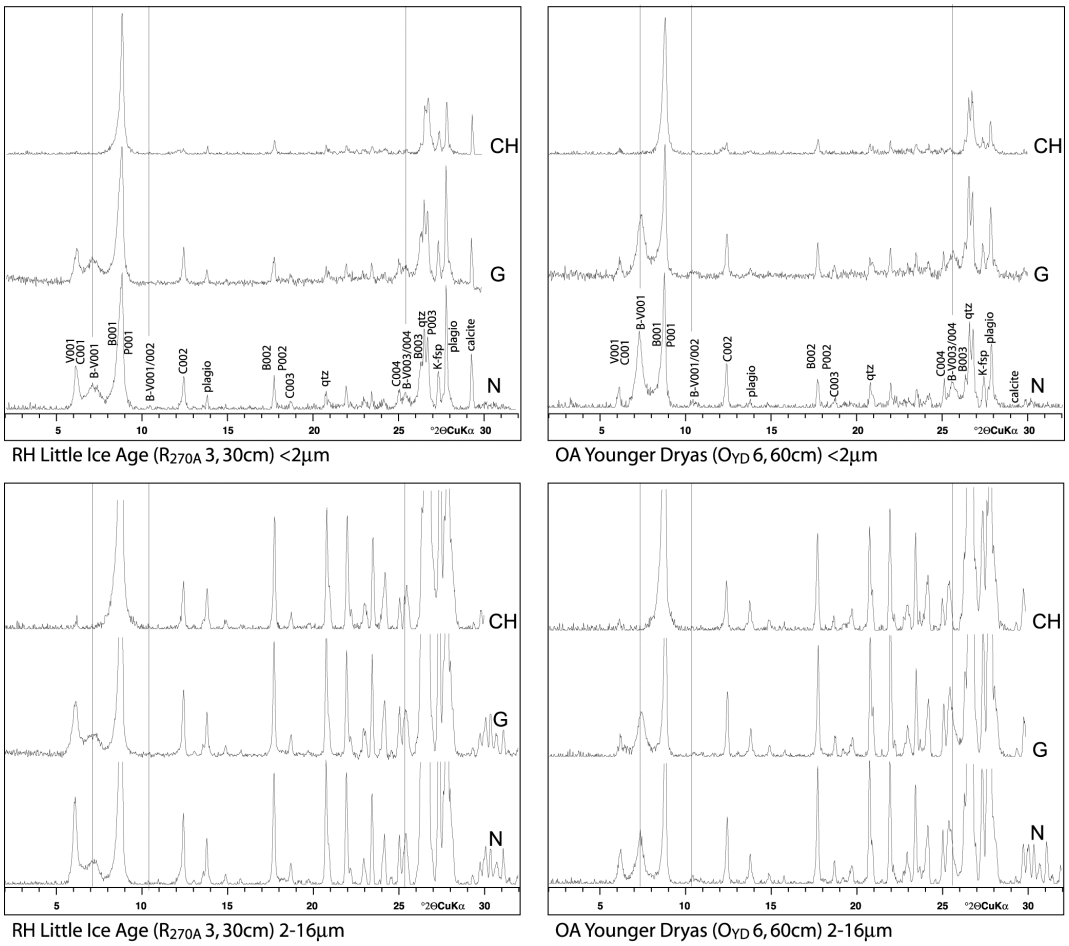


Fig. 3: *XRD-plots after different pretreatments (<2 µm and 2-16 µm fraction of samples $R_{270A}3$ and $O_{YD}6$): (N) normal, air dried; (G) ethylen-glycol solvation; (CH) heated for two hours at 450 °C; see text for discussion.*

vermiculite mixed-layers, and vermiculite) were measured. Detection limit is ≥ 0.3 %. In the 2-16μm fraction also quartz, K-feldspar, plagioclase, and calcite were measured. Mineral ratios were calculated

using raw intensity data (peak heights). Determination of biotite-vermiculite mixed-layers is achieved by the method of Moore and Reynolds (1997). Peaks of biotite (B001), phengite (P001), vermiculite (V001), and biotite-vermiculite mixed layers (B-V001) have been obtained by deconvolution of the 5-10 ° 2θ – interval, by using a Pearson seven function. The samples were pretreated with ethylene-glycol solvation and heated to 450° C. Positions of peaks of vermiculite and biotite-vermiculite mixed layers did not move in the glycol sample and collapsed to 10 Å in the heated one (Fig. 3). Soil pH was measured with a glass electrode on 1:1 deionized water: soil suspension.

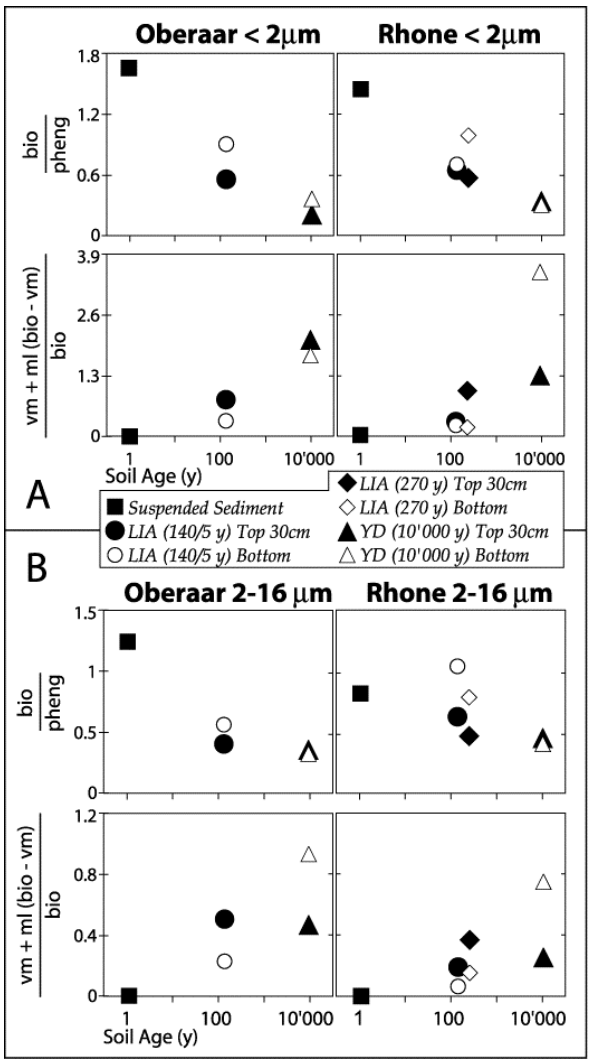


Fig. 4: *Raw intensity ratios (biotite/phengite & (vermiculite + biotite-vermiculite mixed-layers)/biotite) of Oberaar and Rhone sediments of different ages (moraines and suspended sediment; vm = vermiculite, ml(bio-vm) = biotite-vermiculite mixed-layers).*

Results

The whole rock mineralogical analyses show that all moraine and suspended sediment samples reflect the bedrock mineralogy of the two areas; which consists of quartz, potassic feldspar (microcline), plagioclase (albite), phyllosilicates, calcite, and chlorite, with some additional amphibole (actinolite) in the Oberaar catchment.

The XRD analysis of clay minerals shows the presence of chlorite, phengite, biotite, biotite-vermiculite mixed layers (= hydrobiotite, Moore and Reynolds, 1997), and vermiculite (Tables 3 & 4). The existence of some traces of smectite, mica-smectite mixed-layers or gibbsite can not be excluded; their maximum concentration, however, is less than 0.5 % in samples from the most developped horizons of the profiles, thus they are not considered to be significant in our work. In the <2μm and 2-16μm fractions of the moraine samples several trends in mineral distribution are visible in the evolution from the LIA to the YD profiles. The mineral ratios are plotted in a chronological order in Figures 4, 5, and 6.

Table 2: Chronosequence parameters.

	Oberaar glacier forefield							**Rhone glacier forefield**									
Soiltype [†]	**Orthent (Entisols)**				**Humod (Spodosols)**			**Orthent (Entisols)**			**Umbrebt (Inseptisols)**				**Humod (Spodosols)**		
"Référence" [§]	**Regosol (140 y)**				**Podzosol ocrique (10 ky)**			**Regosol (145 y)**			**Brunisol oligosaturé (270 y)**				**Podzosol ocrique (10 ky)**		
sample depth	soil depth	soil	O_{140A}	O_{140B}	soil depth	soil	O_{YD}	soil depth	soil	R_{145A}	soil depth	soil	R_{270A}	R_{270B}	soil depth	soil	R_{YD}
(cm)	(cm)	horizon[†]	pH	pH	(cm)	horizon[†]	pH	(cm)	horizon[†]	pH	(cm)	horizon[†]	pH	pH	(cm)	horizon[†]	pH
		Oh			0-5	Oh			Oh			Oh				Oh	
0-10	0-5	Ah	5.4	7.6	5-10	Ah	6.7	0-5	Ah	5.0	0-5	Ah	4.6	4.6	0-10	Ah	n.a.
10-20	5-30	AC	6.3	6.7	10-20	E	6.5	5-30	AC	5.2	5-20	Bw	4.8	4.7	10-20	E	5.4
20-30			6.7	6.6	20-30	Bhs	6.1			6.0	20-30	BwC	4.9	5.3	20-30	Bhs	5.4
30-40	30-	C	7.1	6.6	30-40	Bw	5.5	30-	C	6.4	30-40	(Bw)C	5.9	6.0	30-40	Bhs *	5.5
40-50			7.2	6.6	40-50	Bw	5.7			6.6	40-	C	6.0	6.1	40-50	Bw	5.5
50-60			7.2	7.1	50-60	Bw	5.8			6.5			6.1	6.5	50-60	Bw	5.9
60-70			7.7	7.5		R				6.4			6.2	n.a.	60-70	Bw	5.8
70-80			7.9	7.2						6.5			6.3	6.5			
80-90			8.2	7.1						6.7			6.5				
90-100			8.1	6.9						6.9			6.2				

[†] USDA (1998, 1999)

[§] A.F.E.S. (1998)

* former water layer visible (rusty rocks)

n.a. not analysed

Table 3: Clay mineralogy of the fraction <2 µm and 2 - 16 µm of glacial sediments from the Oberaar catchment.

Age	Sample	Depth	fraction < 2µm		fraction 2-16µm				
			v + bv / biotite	biotite/ phengite	v + bv / biotite	biotite/ phengite	qtz/ K-fsp	qtz/ plagio	cc/ qtz*
Oberaar moraine samples									
LIA	$O_{140A}1$	0-10	0.592	0.755	0.487	0.309	0.160	0.027	n.d.
140y	$O_{140A}2$	10-20	0.396	0.745	0.540	0.449	0.444	0.071	n.d.
	$O_{140A}3$	20-30	0.577	0.733	0.311	0.435	0.264	0.042	0.149
	$O_{140A}4$	30-40	0.521	0.794	0.373	0.474	1.243	0.128	0.202
	$O_{140A}5$	40-50	0.372	0.652	0.267	0.522	0.316	0.037	0.068
	$O_{140A}6$	50-60	0.527	0.670	0.370	0.353	0.074	0.014	0.076
	$O_{140A}7$	60-70	0.307	0.924	0.187	0.689	0.479	0.078	0.254
	$O_{140A}8$	70-80	0.472	0.929	0.182	0.622	0.210	0.035	0.168
	$O_{140A}9$	80-90	0.321	0.953	0.189	0.538	0.362	0.045	0.095
	$O_{140A}10$	90-100	0.556	0.907	0.264	0.544	0.159	0.040	0.264
Av.	Top <30	0-30	0.522	0.744	0.446	0.398	0.290	0.047	0.149
	stdev		*0.109*	*0.011*	*0.120*	*0.077*	*0.144*	*0.022*	
Av.	Bottom C	>70	0.449	0.929	0.211	0.568	0.244	0.040	0.175
	stdev		*0.119*	*0.023*	*0.045*	*0.047*	*0.106*	*0.005*	*0.085*
LIA	$O_{140B}1$	0-10	1.483	0.311	0.339	0.608	0.519	0.091	0.042
140y	$O_{140B}2$	10-20	0.612	0.412	0.663	0.359	0.445	0.047	0.034
	$O_{140B}3$	20-30	1.051	0.540	0.726	0.321	0.837	0.107	0.047
	$O_{140B}4$	30-40	0.186	1.179	0.410	0.303	0.249	0.043	0.052
	$O_{140B}5$	40-50	0.184	1.945	0.236	0.509	0.215	0.031	0.148
	$O_{140B}6$	50-60	0.164	1.697	0.275	0.497	0.272	0.033	0.065
	$O_{140B}7$	60-70	0.147	1.930	0.118	0.548	0.147	0.022	0.033
	$O_{140B}8$	70-80	0.083	0.856	0.288	0.544	0.516	0.090	0.056
	$O_{140B}9$	80-90	0.339	0.555	0.193	0.653	0.235	0.038	0.087
	$O_{140B}10$	90-100	0.220	1.422	0.232	0.556	0.317	0.059	0.057
Av.	Top <30	0-30	1.049	0.421	0.576	0.430	0.600	0.082	0.041
	stdev		*0.435*	*0.115*	*0.208*	*0.156*	*0.208*	*0.031*	
Av.	Bottom C	>70	0.214	0.944	0.238	0.584	0.356	0.062	0.067
	stdev		*0.128*	*0.440*	*0.047*	*0.060*	*0.145*	*0.026*	*0.018*
YD	$O_{YD}1$	0-10	1.343	0.332	0.593	0.399	1.176	0.948	n.d.
10ky	$O_{YD}2$	10-20	1.274	0.142	0.316	0.311	0.086	0.046	n.d.
	$O_{YD}3$	20-30	3.592	0.247	0.498	0.359	3.302	0.461	0.027
	$O_{YD}4$	30-40	2.737	0.371	2.191	0.193	1.031	0.317	0.070
	$O_{YD}5$	40-50	1.816	0.291	0.974	0.303	0.459	0.152	0.116
	$O_{YD}6$	50-60	1.631	0.492	0.895	0.445	0.961	0.264	0.098
Av.	Top <30	0-30	2.069	0.240	0.469	0.356	1.521	0.485	
	stdev		*1.319*	*0.095*	*0.140*	*0.044*	*1.636*	*0.452*	
Av.	Bottom C	>40	1.724	0.391	0.935	0.374	0.710	0.208	0.107
	stdev		*0.131*	*0.142*	*0.055*	*0.101*	*0.355*	*0.079*	*0.013*
Oberaar suspended sediment samples									
recent	O36 F290		0	1.618	0	1.513	0.472	0.124	
	K46 F223		0	1.431	0	1.024	0.287	0.045	
	K39 F217		0	1.631	0	1.140	0.308	0.051	
	K8 F41		0	2.001	0	1.282	0.828	0.128	
	Av. (n=24)			1.670		1.240	0.474	0.087	0.35 **
	stdev			*0.239*		*0.210*	*0.250*	*0.045*	*0.280*

v = vermiculite, bv = biotite-vermiculite mixed-layers

*) cc/qtz ratios from whole rock analysis

**) average cc/qtz ratios from suspended sediment

n.d. not detected

Table 4: Clay mineralogy of the fraction <2 µm and 2 - 16 µm of glacial sediments from the Rhone catchment.

Age	Sample	Depth	fraction < 2µm		fraction 2-16µm				
			v + bv / biotite	biotite/ phengite	v + bv / biotite	biotite/ phengite	qtz/ K-fsp	qtz/ plagio	cc/ qtz*
Rhone moraine samples									
LIA	$R_{145A}1$	0-10	0.292	0.732	0.045	0.947	0.131	0.048	0.0607
145y	$R_{145A}2$	10-20	0.259	0.664	0.077	0.526	0.374	0.137	0.0949
	$R_{145A}3$	20-30	0.266	0.556	0.442	0.423	0.198	0.065	0.101
	$R_{145A}4$	30-40	0.414	0.696	0.050	0.862	0.201	0.070	0.0552
	$R_{145A}5$	40-50	0.379	0.497	0.093	0.383	0.149	0.062	0.148
	$R_{145A}6$	50-60	0.141	0.902	0.065	1.319	0.099	0.043	n.d.
	$R_{145A}7$	60-70	0.363	0.791	0.120	0.908	0.147	0.056	0.0897
	$R_{145A}8$	70-80	0.168	0.723	0.074	0.921	0.160	0.068	0.139
	$R_{145A}9$	80-90	0.215	0.664	0.052	1.021	0.191	0.075	0.0349
	$R_{145A}10$	90-100	0.182	0.712	0.049	1.207	0.215	0.090	0.2155
Av.	Top <30	0-30	0.272	0.651	0.188	0.632	0.235	0.083	0.086
	stdev		*0.017*	*0.089*	*0.221*	*0.278*	*0.125*	*0.047*	*0.022*
Av.	Bottom C	>70	0.189	0.700	0.058	1.050	0.189	0.078	0.130
	stdev		*0.024*	*0.032*	*0.014*	*0.145*	*0.027*	*0.011*	*0.091*
LIA	$R_{270A}1$	0-10	1.105	0.290	0.478	0.189	0.181	0.051	0.148
270y	$R_{270A}2$	10-20	1.421	0.316	0.403	0.457	0.232	0.076	0.114
	$R_{270A}3$	20-30	0.711	0.875	0.295	0.902	0.487	0.192	0.057
	$R_{270A}4$	30-40	0.236	0.868	0.146	0.712	0.091	0.037	0.023
	$R_{270A}5$	40-50	0.861	0.483	0.142	0.812	0.325	0.098	0.051
	$R_{270A}6$	50-60	0.035	0.734	0.323	0.800	0.066	0.027	0.102
	$R_{270A}7$	60-70	0.105	0.716	0.225	0.917	0.458	0.148	0.221
	$R_{270A}8$	70-80	0.222	1.049	0.115	0.825	0.089	0.031	0.064
	$R_{270A}9$	80-90	0.278	1.105	0.090	0.746	0.078	0.033	0.037
	$R_{270A}10$	90-100	0.087	1.006	0.220	0.776	0.000	0.000	0.141
Av.	Top <30	0-30	1.079	0.494	0.392	0.516	0.300	0.106	0.107
	stdev		*0.356*	*0.331*	*0.092*	*0.360*	*0.164*	*0.075*	*0.046*
Av.	Bottom C	>70	0.196	1.053	0.142	0.782	0.056	0.021	0.081
	stdev		*0.098*	*0.049*	*0.069*	*0.040*	*0.048*	*0.019*	
LIA	$R_{270B}1$	0-10	0.823	0.349	0.262	0.236	0.186	0.056	0.180
270y	$R_{270B}2$	10-20	0.949	0.676	0.420	0.431	0.183	0.051	0.122
	$R_{270B}3$	20-30	0.669	0.891	0.339	0.606	0.232	0.070	0.080
	$R_{270B}4$	30-40	0.586	0.667	0.723	0.636	0.155	0.065	n.d.
	$R_{270B}5$	40-50	0.806	0.443	0.266	0.910	0.062	0.030	n.d.
	$R_{270B}6$	50-60	0.356	0.927	0.138	0.685	0.126	0.059	0.044
	$R_{270B}8$	70-80	0.143	0.764	0.167	0.829	0.075	0.038	0.089
Av.	Top <30	0-30	0.814	0.638	0.341	0.425	0.200	0.059	0.127
	stdev		*0.140*	*0.273*	*0.079*	*0.185*	*0.027*	*0.010*	*0.050*
YD	$R_{YD}1$	0-10	1.203	0.366	0.128	0.565	1.328	0.189	n.d.
10 ky	$R_{YD}2$	10-20	1.032	0.247	0.277	0.365	1.237	0.178	0.089
	$R_{YD}3$	20-30	1.589	0.437	0.342	0.463	0.606	0.147	0.044
	$R_{YD}4$	30-40	n.a.	n.a.	0.925	0.375	0.424	0.087	n.d.
	$R_{YD}5$	40-50	4.301	0.413	1.083	0.492	0.987	0.204	n.d.
	$R_{YD}6$	50-60	4.605	0.226	0.859	0.485	0.547	0.134	0.024
	$R_{YD}7$	60-70	2.335	0.399	0.623	0.322	1.352	0.166	n.d.
Av.	Top <30	0-30	1.274	0.342	0.515	0.401	0.756	0.137	0.067
	stdev		*0.286*	*0.134*	*0.357*	*0.054*	*0.427*	*0.046*	
Av.	Bottom C	>50	3.470	0.312	0.741	0.403	0.949	0.150	0.024
	stdev		*1.605*	*0.122*	*0.167*	*0.115*	*0.569*	*0.023*	
Rhone suspended sediment samples									
recent	F272		0	1.633	0	1.528	0.264	0.104	
	F91		0	3.705	0	0.488	0.314	0.122	
	F235		0	0.225	0	0	0.306	0.127	
	F74		0	0.172	0	0.444	0.222	0.092	
	Av. (n=23)			1.434		0.615	0.277	0.111	0.09 **
	stdev			*1.659*		*0.647*	*0.043*	*0.016*	*0.072*

The relative content of secondary minerals in the LIA profiles is generally higher in the top 30 cm of the profiles. In the YD profiles this trend is reversed, with a higher relative content of secondary minerals in the bottom parts of the profiles (except for the <2μm fraction of Oberaar). The relative vermiculite content (2-16μm fraction) of the top 30 cm of the YD profiles is even lower than in the LIA profiles. The YD profiles are more deeply weathered than the LIA profiles. Fig. 7 shows how the vermiculite content increases with depth within the Rhône R_{YD} profile.

In the 140 year old moraines at Oberaar the ratios of (vermiculite + biotite-vermiculite mixed layers) / biotite are twice as high in the top 30 cm of the profiles as in the bottom parts (Fig. 4). The ratio in the Oberaar YD profile is again two times higher with higher values for the bottom parts of the profiles (except OA < 2μm fraction). The biotite content decreases correspondingly: The biotite/phengite ratios are half as high in the LIA profiles compared to the suspended sediments, and again half as high in the YD profile compared to the LIA profiles, always having higher values for the bottom parts of the profiles. The moraine profiles of Rhône glacier catchment show the same trends. The biotite content of Rhône suspended sediment is comparable to the LIA profiles (R_{270A} & R_{270B}).

Oberaar quartz/K-feldspar ratios are almost twice as high as the Rhône ones (Fig. 5). Compared to the suspended sediment the values from the LIA profiles are 6 to 36 % and 15 to 75 % lower for top 30 cm and bottom parts and for Oberaar and Rhône profiles, respectively. In the YD profiles the ratios are approximately doubled, with significantly higher values for the top 30 cm of the profiles. The quartz/plagioclase ratios in the LIA profiles are comparable between the two areas. They are 26 to 41 % and 25 to 75 % lower than in the suspended sediments for top 30 cm and bottom parts and for Oberaar and Rhône profiles, respectively. In the YD profiles the ratios are approximately doubled, with significantly higher values for the top 30 cm of the profiles especially at Oberaar.

The calcite/quartz ratio of the suspended sediment (calculated on bulk profiles from whole rock mineralogy; Fig. 6 and Table 3 & 4) is higher for Oberaar than for Rhône (0.35 vs. 0.09). In the Oberaar LIA profiles this ratio is diminished by 69 % (to 0.11) relative to the suspended sediment (0.35). The ratio is again decreased in the YD profile (0.08). The Rhône calcite/quartz ratio in the LIA profiles is

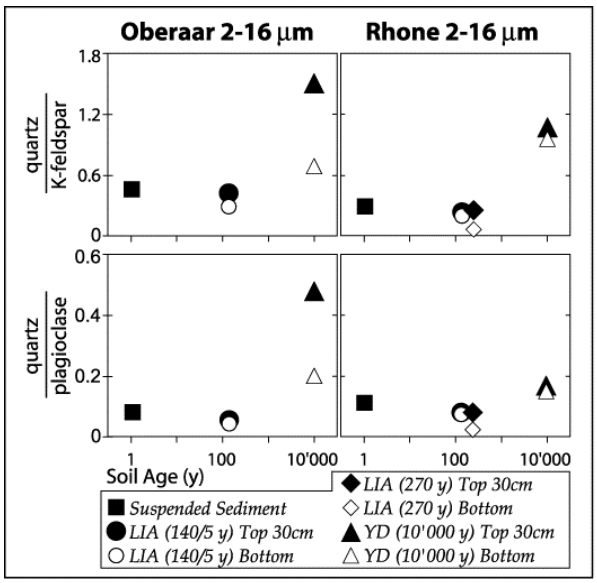


Fig. 5: *Raw intensity ratios (quartz/K-feldspar & quartz/plagioclase) of Oberaar and Rhone sediments of different ages (moraines and suspended sediment, 2-16 µm fraction).*

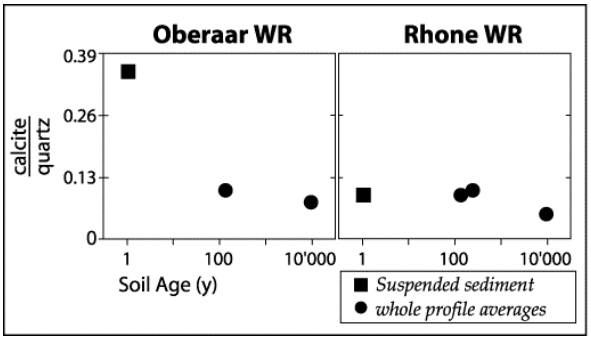


Fig. 6: *Raw intensity calcite/quartz ratios of suspended sediment and entire profiles calculated from whole rock analysis (XRD). Suspended sediment (OA n = 19; RH n = 15).*

comparable to the suspended sediment (0.09 to 0.10), only the YD profile shows significantly lower values (0.05).

Biotite field weathering rate

We calculated the decrease in biotite by comparing the biotite/phengite ratio between the C-horizon (bottom 30 cm) and the top 30 cm of the profiles in % for the 0 – 2 and 2 – 16 μm fractions that were analysed for clay minerals (Tables 3 & 4). Consequently we calculated the amount of biotite (kg) contained within the C-horizon using the corresponding biotite content (%) of the two analysed grain-size fractions (0 – 2 and 2 – 16 μm) combined with the average moraine density of 1500 kg m^{-3} (Egli et al., 2001). We also took into consideration the overestimation in clay minerals of these grain-size fractions which is due to preparation as well as orientation effects: By comparing the phyllosilicate/quartz ratio obtained by whole rock XRD analysis (bulk samples) to the corresponding grain-size fraction data (clay mineral analysis), the overestimation in clay minerals was calculated to be ≥ 20 times for the 0 – 2 μm and 2 – 8 times for the 2 – 16 μm fraction, which corresponds to 95 – 100 % and 50 – 85 % of clay minerals in these grain-size fractions, respectively. This gives us an upper and lower boundary limit for the weathering rates. With a biotite formula by Marquer (1987 & pers. comm.), who worked in the same area and performed several chemical analyses of the micas contained within Grimsel Granodiorite (biotite = $(K_{0.952}, Na_{0.012})$ $(Mg_{1.164}, Fe_{1.276}, Al^{VI}_{0.294}, Ti_{0.099}, Mn_{0.023}, Cr_{0.003})$ $(Si_{2.826}, Al^{IV}_{1.175})$ $O_{10}(OH)_2$) we calculated the amount of biotite which is lost per year relative to the amount of biotite in the C-horizon (t = 0). However, the detailed composition of biotite does not significantly influence the final weathering rates.

Using the grain-size distribution for particles < 16 μm we interpolated the distributions of the particles < 1 μm using an exponential function (Table 5). We obtained $R^2 \geq 0.95$. In order to calculate the relative surface area of biotite using a geometric approach we assume that biotite breaks down into regular shaped

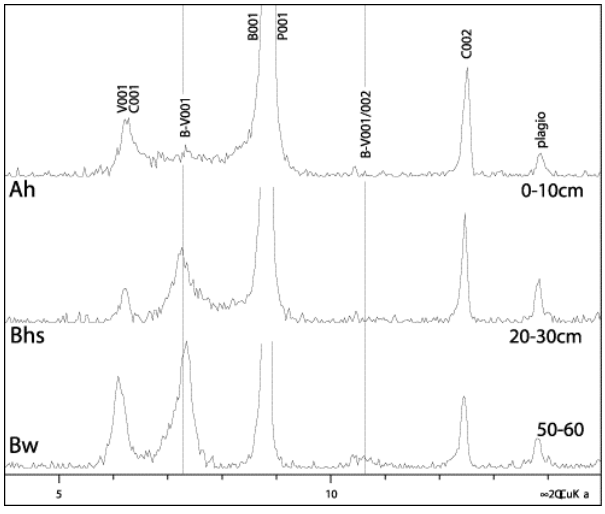


Fig. 7*: Accumulation of vermiculite as a function of depth in the 2-16 µm fraction of the RYD profile.*

flakes or platelets with a constant diameter/thickness ratio. We use radius/height (r/h) ratios of 5, 10, and 15 (cf. Swoboda-Colberg and Drever, 1993) which gives us average surface areas for each grain-size division (surface of cylinder: $S_c = 2\pi r^2 + 2\pi rh$). With a biotite density of 3.09 g cm^{-3} we calculated the total relative surfaces S_T (m^2 g^{-1}; S_c / V; $S_c = 2\pi r^2 + 2\pi rh$ and $V = \pi r^2 h$) as well as the relative edge surfaces S_E (m^2 g^{-1}; S_e / V; $S_e = 2\pi rh$ and $V = \pi r^2 h$), where dissolution processes most likely happen (Nagy, 1995).

The results for the biotite weathering rate are summarised in Table 6a and are further explained in the discussion section. Table 6a shows biotite loss in % of the two grain-size fractions and in mol yr^{-1}. Total surface areas S_T (m^2 g^{-1}) are given for the different radius/height ratios (5, 10, and 15) together with the corresponding edge surface areas S_E (m^2 g^{-1}). The latter remain constant for different radius/height ratios. Finally the calculated weathering rates are shown for total surface area (WR_T, pmol m^{-2} sec^{-1}) as well as for edge surface area (WR_E, pmol m^{-2} sec^{-1}). Table 6b consists of a compilation of different weathering rates calculated by different approaches, and are discussed below.

Table 5: Grainsize distribution in different soil profiles, fractions < 1 µm from interpolation of fractions < 16 µm.

Grain size fraction	OA_{140A}	RH_{145A}	RH_{270A}
16µm	34.62	35.18	42.39
8µm	37.44	37.83	37.36
4µm	20.95	19.78	15.62
2µm	5.33	5.47	3.65
1µm	1.142	1.180	0.719
0.5µm	0.391	0.411	0.209
0.2µm	0.095	0.102	0.041
0.1µm	0.032	0.036	0.012

Discussion

Validity of data: a) Reworked material

We suggest that the amount of pre-weathered material in our soil profiles is rather small and well homogenised with the freshly eroded sediments for several reasons: 1) Our profiles show characteristic soil zonation processes which already occur in the young LIA moraine profiles (Table 2) and a gradient is visible in the distribution of secondary minerals: the contents of secondary minerals of the top 20 – 30 cm of the LIA profiles are significantly higher than the ones of the C horizons (below 30 – 40 cm depth) in these profiles (Fig. 4). This suggests that a significant amount of secondary minerals is newly formed. 2) The YD profiles lie in the same altitude as the LIA ones and correspond to the altitudes of the YD accumulation zone. The YD material is therefore deposited during the YD retreat of the glaciers. The glaciers "cleaned out" their systems during the maxima, meaning that the material of our soil profiles was deposited as fresh material during the retreat, when the equilibrium line was already back up in the catchment. 3) Furthermore, apatite mineral grains

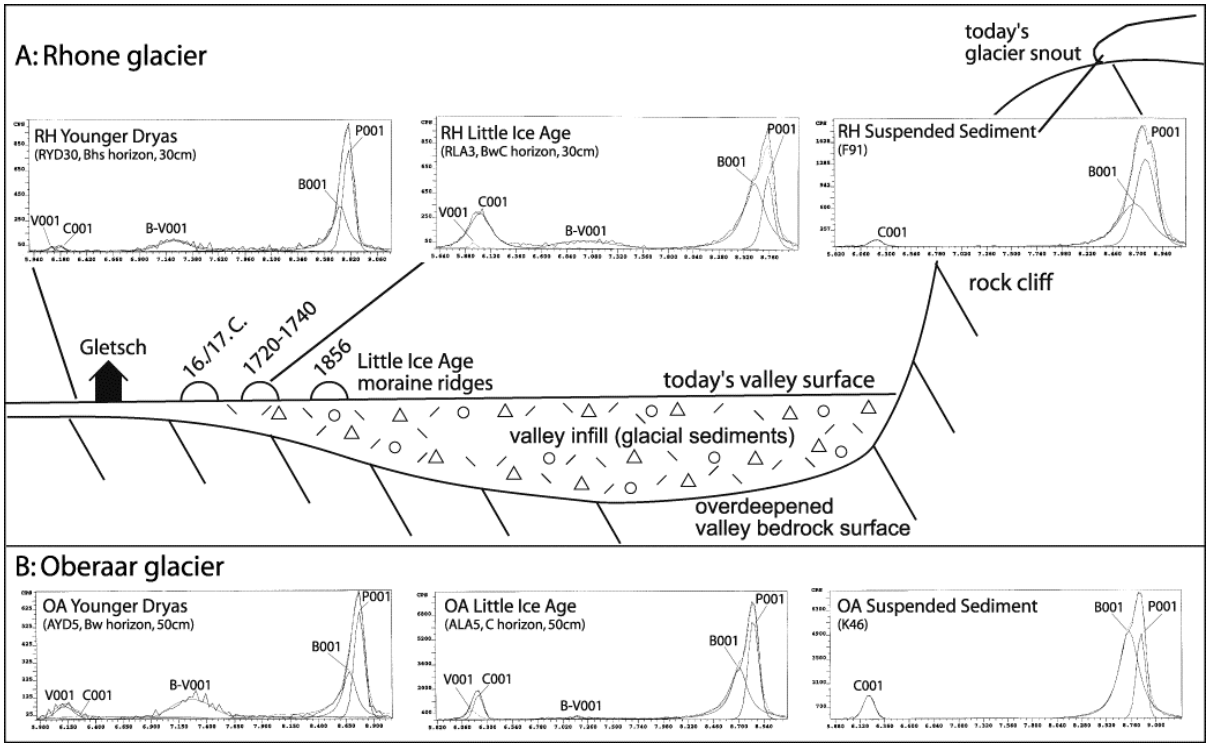


Fig. 8A: *Schematic profile along valley floor of the Rhone proglacial area. Bedrock surface is overdeepened during LGM and YD because two glaciers joined here; overdeepening exaggerated. Valley infill isolated and prevented bedrock surface from active erosion processes during LIA glacier advance. Time mineralogical evolution of different sediments (2-16 µm fraction): suspended sediment => LIA moraines => YD moraines.*
Fig. 8B: *The mineralogic evolution of different sediments from Oberaar glacier (2-16 µm fraction): suspended sediment => LIA moraines => YD moraines.*

from suspended sediment and bottom LIA profiles (C horizons) do not show significant differences with regard to their surface morphologies, suggesting that the material of the C horizons is not chemically weathered to a larger extent (Hosein et al., submitted).

b) Geology of catchments during different times

During LIA and YD the surface areas of our two glaciers were larger and consequently included different lithologies than they do recently. Approximate bedrock distributions for different times are given in Table 1. Lithological distribution of the Oberaar LIA catchment corresponds to the present-day distribution (Fig. 1 & 2). During YD the Oberaar glacier filled its catchment more completely, and larger portions of the Grimsel Granodiorite and the Southern Aar Granite were ice covered than today. However, we expect only small differences in the composition of the initial parent materials between LIA and YD soil profiles.

During the maximum extent of YD, two glaciers existed in the Rhône catchment, which joined each other in the plane of Gletsch: The Rhône glacier from the north and the Mutt glacier from the south-east (Furkapass, see Fig. 1). The confluence of these two glaciers led to an over deepening of the valley and finally, with their retreat, to a glacial sediment infill consisting of a mixture of the lithologies which were

contained in the glacier catchment at that time (Fig. 1 & 8A). A first order estimation of the lithologies of the YD glacier catchment gives a distribution of 40 % Central Aar Granite, 20 % Grimsel Granodiorite, 20 % Variscan Gneisses, and 20 % Mesozoic metasediments. The initial parent material of our YD soil profile contained therefore also Variscan Gneisses and Mesozoic metasediments, and is for this reason not directly comparable to the parent material of LIA soil profiles. During LIA, the Mutt glacier did not join the Rhône glacier (Zumbühl, 1988). The Rhône glacier spread out widely over the plane of Gletsch, not eroding the YD valley infill but depositing the LIA terminal moraines on top of it (Fig. 2 & 8A). The 5 – 10 % of Variscan Gneisses were isolated and protected from reworking processes. Therefore the lithological distribution is comparable between Rhône LIA and todays catchment.

Biotite weathering: a) General

The clay mineralogy of the suspended sediment of both glaciers is comparable as is also the mica compositions of various sediment samples from both glacier catchments (Fig. 9). We may therefore compare their decay processes between our two catchment areas.

The zone of increased weathering of biotite coincides with the zone of high root density, which suggests that weathering is biochemically accelerated by the network of roots and associated microorganisms. Mechanically disaggregated biotite (by abrasion) is preferentially leached to release different cations (specially K, Mg, Fe, and Si; Barker et al., 1997 and Barker et al., 1998). The marginal zones of the frayed-out biotite are gradually opened up and transformed into biotite-vermiculite mixed-layers and subsequently into vermiculite. Therefore glacially derived sediments should show increased biotite weathering rates (see below). Fresh inner parts of the biotites (that were not glacially disaggregated to the same extent) are leached much more slowly.

The chronosequential evolution of the glacial sediments we analysed is clearly visible in Fig. 8: Secondary minerals are missing in the suspended sediment, but they build up within LIA moraines and are widespread in YD moraines. In more developed and consequently more mature soils (at lower altitude

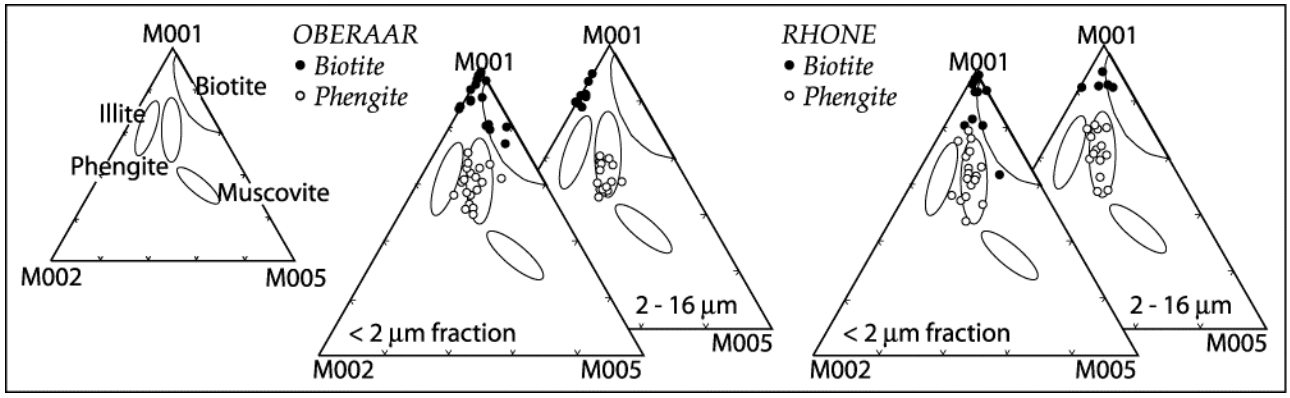


Fig. 9: *Mica compositions of glacial sediments (<2 µm and 2-16 µm fraction) in a triangular diagram 001 (10Å), 002 (5Å), and 005 (2Å) after Rey and Kübler, 1983.*

and on forested site) compared to this work, Righi et al. (1999) found partially weathered dioctahedral phengite within the eluvial horizon, which was transformed into a mica-smectite mixed-layer mineral. In our area we do not see a decrease in the phengite content within this layer over time and we do not find significant traces of any gibbsite, smectite, or mica-smectite mixed-layers within any of our soil samples.

b) Biotite weathering rate

One important aspect of calculating biotite weathering rates and comparing them to literature values is that due to its perfect basal cleavage, the basal surfaces of biotite flakes are not very reactive during weathering, and most of the dissolution occurs at the edges of the grains (Turpault and Trotignon, 1994). Smaller grains will have much more edge relative to basal surface than larger grains. Therefore the total weathering rates (WR_T) which are calculated using total surface area S_T (including the basal surfaces) may be lower than the edge weathering rates (WR_E) using edge surface areas S_E.

Our edge weathering rates WR_E are one order of magnitude higher than our total weathering rates WR_T (Table 6a) which is due to the different relative surface areas used. The edge weathering rates WR_E are the same for the different r/h ratios as the radius stays constant per size fraction and changes in r/h therefore correspond to changes in h which do not affect the relative surface areas S_E ($m^2\ g^{-1}$) as they are normalised to volume. Our field-based, total weathering rates WR_T calculated using total surface area S_T are in the same order of magnitude as fast

Table 6a: Biotite weathering rates compilation for different soil profiles and assumed parameters.

Catchment	Time-span	Loss % 0-2µm	Loss % 2-16µm	Loss (mol yr^{-1})	Loss (mol yr^{-1})	r/h[#]	S_T ($m^2\ g^{-1}$)	S_E ($m^2\ g^{-1}$)	WR_T (pmol $m^{-2}\ sec^{-1}$)		WR_E (pmol $m^{-2}\ sec^{-1}$)	
	yr			low	high				high	low	high	low
Oberaar	140	19.93	30.00	24.88	40.60	5	1.357	0.226	104.24	106.15	625.46	636.87
						10	2.487		56.86	57.90		
						15	3.618		39.09	39.80		
Rhone	145	6.94	39.80	79.32	133.85	5	1.358	0.226	128.73	132.93	772.41	797.59
						10	2.489		70.22	72.51		
						15	3.620		48.28	49.85		
Rhone	270	53.11	34.04	14.53	23.31	5	1.127	0.188	82.14	80.59	492.82	483.52
						10	2.065		44.80	43.96		
						15	3.004		30.80	30.22		
Oberaar*	10,000	74.14	51.26	0.67	1.05	5	1.357	0.226	2.80	2.74	16.81	16.45
						10	2.487		1.53	1.50		
						15	3.618		1.05	1.03		
Rhone a[§]	10,000	66.77	40.61	0.47	0.75	5	1.127	0.188	2.67	2.61	16.00	15.65
						10	2.065		1.45	1.42		
						15	3.004		1.00	0.98		
Rhone b[†]	10,000	49.97	55.73	1.74	2.85	5	1.358	0.226	2.82	2.83	16.94	17.00
						10	2.489		1.54	1.55		
						15	3.620		1.06	1.06		

* Surface areas calculated from C-horizon of profile O_{140A}

§ Surface areas calculated from C-horizon of profile RH_{270A}

† Surface areas calculated from C-horizon of profile RH_{145A}

[#] r/h = ratio radius/height of platelet, where radius = average of particle size fraction (see Table 5).

laboratory rates (10^{-10} – 10^{-12} $mol_{biotite}$ $m^{-2}{}_{biotite}$ s^{-1}; Acker and Bricker, 1992, Nagy, 1995, Murphy et al., 1998, Table 6b). If we compare the weathering rates calculated using edge surface area S_E (WR_E, 10^{-10} – 10^{-11} $mol_{biotite}$ $m^{-2}{}_{biotite}$ s^{-1}), they are two orders of magnitude slower than the analogue laboratory rates by Turpault and Trotignon (1994). This discrepancy between field and laboratory rates is well known (e.g. Swoboda-Colberg and Drever, 1993, Velbel, 1993a).

The weathering rates calculated for LIA soil profiles are comparable between Rhône and Oberaar, their variance is due to the differences in biotite loss (%) within the profiles and initial biotite contents at time t = 0. Due to their age the weathering rates calculated for YD soil profiles are 1 – 2 orders of magnitude slower. YD total weathering rates (WR_T) correspond to laboratory rates obtained by Swoboda-Colberg and Drever (1993). LIA soil profile C-horizon values are used to calculate YD weathering rates. For Oberaar this assumption might be valid, as the eroded lithologies did not change much between YD and LIA (Table 1). For Rhône, however, this assumption is less solid, as outlined above. Therefore, this approach to calculate longer-term weathering rates might not be very sensitive.

c) Possible explanations for the higher weathering rates

We base our calculation on material which is enriched in small particle fractions through glacial mechanical abrasion processes. Mechanically disaggregated and frayed-out biotites are preferentially leached. Due to the alpine environment total precipitation and therefore throughflow is probably increased compared to other field sites. Therefore our glacially derived material may show faster biotite weathering rates.

Due to effects of sample preparation, we are looking at size fractions < 16 μm. Larger size fractions have less relative reactive surface area (Hodson, 2002), especially with regard to edge surface area S_E. As we use a geometric approach to calculate the relative surface area, the r/h ratio remains a major uncertainty. In other weathering rate studies BET surfaces were used, calculated according to Brunauer et al. (1938). The surface areas calculated nongeometrically are always higher than the geometric areas, due to surface roughness and surface steps (Swoboda-Colberg and Drever, 1993) as well as to interlayer surface area (Kalinowski and Schweda, 1996). Our final weathering rates may be increased by this effect and should be seen as maximum rates.

Our study is performed in highly permeable and well-drained glacial sediments where waters percolate easily through the soil matrix and are furthermore rather dilute (low-ionic strength rain waters). The effect of heterogeneities in flow path through soils is of minor importance compared to most field studies, in which weathering rates for silicate minerals are calculated with mass balance equations using surface and groundwater ion concentrations related to estimated mineral surface area (Swoboda-Colberg and Drever, 1993, Velbel, 1993b, White, 1995, Murphy et al., 1998). This effect is quite dominant in such studies, where dissolution may be minimized because soil porewaters only percolate along macropores. In these studies, such effects explained

the large discrepancy between field weathering rates and laboratory rates. In laboratory studies, the solutions flow through the matrix (micropores); this increases the overall solute concentration and may have a negative effect on the weathering rate. However, electrolyte effects on dissolution kinetics of biotite at low temperature are small (Kalinowski and Schweda, 1996).

As biotite dissolves and secondary phases (vermiculite) increase there is a loss of reactive surface area in field conditions. Less and less biotite might be in direct contact to soil porewaters. This effect should be taken into consideration for the longer time step of 10,000 years that we are looking at.

Other observed weathering reactions

Calcite is highly reactive in dilute waters (glacial meltwaters or dilute soil waters) because of its dissolution rate at near neutral pH (10^{-5} mol m^{-2} s^{-1}; Plummer et al., 1978), which is approximately seven orders of magnitude higher than the dissolution rate of plagioclase feldspar ($\approx 10^{-12}$ mol m^{-2} s^{-1}; Blum and Stillings, 1995). Oberaar suspended sediment contains three times as much calcite as Rhône (Hosein et al., submitted), which is due to the presence of calcite bearing Variscan Gneisses (with up to 5 wt% calcite, Stalder, 1964). Calcite in the Oberaar LIA moraine profiles is decreased to one third compared to the suspended sediment (Fig. 6). In Rhône LIA profiles this dissolution effect is less visible. In both areas the calcite content is again decreased in the time step to the YD profiles. The short-term weathering of calcite starts as soon as the bedrock-flour becomes in contact with dilute meltwater in the subglacial environment. At Oberaar it is well advanced after 140 years. However, in both areas it continues after 140 – 270 years and its effects are still visible in the longer term (time-step to YD).

The quartz/K-feldspar and quartz/plagioclase ratios show the differences in bedrock between the two catchments (Tables 3 & 4). Suspended sediment is taken here as the average composition of the bedrock that is recently eroded. Oberaar suspended sediment is richer in plagioclase (lower quartz/plagioclase ratios) in comparison to the Rhône catchment. Rhône glacier suspended sediment, on the other hand, contains more K-feldspar (Fig. 5). This difference may be explained by the smaller content of K-feldspar within the Variscan Gneisses of the Oberaar catchment compared to the other lithologies (Stalder, 1964). The feldspar content of the different LIA profiles corresponds more or less to the suspended sediment values (Fig 5). The differences are due to different transport mechanisms (e.g. ice, water). The increased quartz/K-feldspar and quartz/plagioclase ratios in the top parts of the profiles show the more intense weathering of K-feldspar and plagioclase in the top soil layers compared to the bottom parts. The ratios increase with time: In the YD profiles they are more than doubled (Fig 5). Therefore the weathering of K-feldspar and plagioclase is rather slow and only becomes significant on time scales longer than 270 years.

Table 6b: Compilation of weathering rates of biotite measured in laboratory and field experiments.

Study	Analysis	Surface approach	Approx. weathering rates
Laboratory			
Acker and Bricker, 1992	acidic solutions; H_2SO_4; pH 3 - 5.5; 22 ± 1.5 °C oxidizing / reducing solutions saturated vs. unsaturated flow conditions	BET	10^{-11} - $10^{-12.5}$
Swoboda-Colberg and Drever, 1993	75 - 150 µm size fraction of soil from field site room temperature pH 4 - 4.5 (analogue pH of bulk soil solution field site) deionised water, HCl to adjust pH	geometric r/h = 10	$10^{-11.4}$
Turpault and Trotignon, 1994	0.1N HNO_3; pH 1.08 ± 0.02; 24 °C Single cut crystals of biotite with decr. thickness => S_T ≈ const.; S_E decr. const. thickness cut along external (001) interface => ST incr.; SE ≈ const. const. thickness cut perpendicular to external (001) interface => ST ≈ const.; SE incr.	"geometric" S_E vs. S_T norm. to S_E	≈10^{-8}
Kalinowski and Schweda, 1996	aqueous solutions; pH 1 - 4; room temperature	BET	$10^{-11.9}$ †
Field			
Swoboda-Colberg and Drever, 1993	plot irrigation with HCl; pH 2 - 3 soil solution combined with grain-size distribution and mineralogy of soil	geometric r/h = 10	10^{-14}
Murphy et al., 1998	massbalance equation inclusive density and volume of phyllosilicate grains, porewater chemistry and flux & soil porosity	BET	10^{-15}

† as cited in Murphy et al. 1998

Conclusions

There are two domaines of weathering in glacial environments, the subglacial and proglacial zones: "Long-term" weathering processes take place in the proglacial area where conditions associated with pedogenesis, such as increased acidity, increase the overall chemical weathering rates. The calcite concentration of proglacial sediments decreases drastically in the first hundred years after deposition and the chemical weathering of biotite and feldspar grains is also increased after their deposition in the proglacial area. Biotite weathers to form biotite-vermiculite mixed-layer clays and subsequently vermiculite after 140 years (LIA moraine profiles, especially within the top 30 cm of the soils), and continues more slowly in YD profiles.

We present a new approach to calculate weathering rates using the decrease of biotite between the C-horizon and the top 30 cm of the soils and a geometrical calculation of the mineral surface area. We calculate weathering rates using total mineral surface area in the order of 10^{-10} – 10^{-11} $mol_{biotite}$ $m^{-2}_{biotite}$ sec^{-1} for a time-scale of hundreds of years. Weathering rates using the edge surface area are in the order of 10^{-10} $mol_{biotite}$ $m^{-2}_{biotite}$ sec^{-1}. These elevated

weathering rates are due to a combination of the enrichment in small particles which are glacially abraded and the high throughflow due to the high precipitation volumes at these alpine fieldsites. However, the particle sizes as well as the geometrical approach considered here could have a further effect on our calculation. Therefore our weathering rates should be seen as maximum rates. A slow-down of the weathering processes is visible comparing weathering rates calculated over hundreds and thousands of years.

The subglacial domain is dominated by "short-term" weathering reactions driven by the dissolution of freshly ground fine particles in dilute glacial meltwaters. The most reactive mineral in this context is calcite.

Acknowledgements

We thank David Nisbet and Marlen Schaller for field support. The manuscript benefited from the discussions with J.-M. Gobat (soil science), S. Bleuler and C. Schlüchter. This study was supported by Swiss National Science Foundation Grants 21-53997.98 and 20-61485.00.

References

A.F.E.S. (1998) A sound reference base for soils. The "référentiel pédologique". INRA, Paris, **pp.** 322

Abrecht J. (1994) Geologic units of the Aar massif and their pre-Alpine rock associations: a critical review. *Schweizerische Mineralogisch-Petrographische Mitteilungen* **74**: 5-27.

Acker J.G. and Bricker O.P. (1992) The influence of pH on biotite dissolution and alteration kinetics at low temperature. *Geochimica et Cosmochimica Acta* **56**: 3073-3092.

Adatte T., Stinnesbeck W. and Keller G. (1996) Lithostratigraphic and mineralogic correlations of near K/T boundary clastic sediments in NE Mexico: Implications for origin and nature of deposition. *In:* G. Ryder, D. Fastovsky and S. Gartner (Eds.) *The Cretaceous-Tertiary events and other catastrophes in Earth history*. Special Paper Geological Society of America: 211-226.

Ammann K. (1977) Der Oberaargletscher im 18., 19., und 20. Jahrhundert. *Zeitschrift für Gletscherkunde und Glazialgeologie*, **XII**: 253-291.

Anderson S.P., Drever J.I., Frost C.D. and Holden P. (2000) Chemical weathering in the foreland of a retreating glacier. *Geochimica et Cosmochimica Acta* **64**: 1173-1189.

Anderson S.P., Drever J.I. and Humphrey N.F., (1997) Chemical weathering in glacial environments. *Geology* **25**: 399-402.

Barker W.W., Welch S.A. and Banfield J.F., (1997) Biogeochemical weathering of silicate minerals. *Reviews in Mineralogy; Mineralogical Society of America* **35**: 391-428.

Barker W.W., Welch S.A., Chu S. and Banfield J.F. (1998) Experimental observations of the effects of bacteria on aluminosilicate weathering. *American Mineralogist* **83**: 1551-1563.

Birkeland P.W., Burke R.M. and Shroba R.R. (1987) Holocene alpine soils in gneissic cirque deposits,

Colorado Front Range. *U.S. Geological Survey Bulletin* **1590**: **pp.** 21.

Blum A.E. and Stillings L.L. (1995) Feldspar dissolution kinetics. *Reviews In Mineralogy* **31**: 291-351.

Brunauer S., Emmett P.H., Teller E. (1938) Adsorption of gases in multimolecular layers. *Journal of the American Chemical Society* **60**: 309-319.

Claridge G.G.C. and Campbell I.B., (1984) Mineral transformation during the weathering of dolerite under cold arid conditions in Antarctica. *New Zealand Journal of Geology and Geophysics* **27**: 537-545.

Drever J.I. and Hurcomb D.R. (1986). Neutralization of atmospheric acidity by chemical weathering in an alpine drainage basin in the North Cascade Mountains. *Geology* **14**: 221-224.

Egli M., Mirabella A. and Fitze P. (2001) Clay mineral formation in soils of two different chronosequences in the Swiss Alps. *Geoderma* **104**: 145-175.

Fairchild I.J. et al. (1999) Solute generation and transfer from a chemically reactive alpine glacial-proglacial system. *Earth Surface Processes and Landforms* **24**: 1189-1211.

Föllmi K.B. (1995) 160 m. y. record of marine sedimentary phosphorus burial: Coupling of climate and continental weathering under greenhouse and icehouse conditins. *Geology* **23**: 859-862.

Gurnell A.M., Brown G.H. and Tranter M. (1994) Sampling strategy to describe the temporal hydrochemical characteristics of an alpine proglacial stream. *Hydrological Processes* **8**: 1-25.

Hallet B., Hunter L. and Bogen J. (1996) Rates of erosion and sediment evacuation by glaciers: A review of field data and their implications. *Global and Planetary Change* **12**: 213-235.

Hodson M. E. (2002) Variation in element release rate from different mineral size fractions from the B horizon of a granitic podzol. *Chemical Geology*: in press.

Hormes A., Müller B. U., Schlüchter C. (2001) The Alps with little ice: evidence for eight Holocene phases of reduced glacier extent in the Central Swiss Alps. *The Holocene* **11**: 255-256.

Hosein R., Arn K., Steinmann P., Adatte T. and Föllmi, K. (*Submitted)* Calcite, the principal control on cation fluxes from the Rhône and Oberaar glaciers, Switzerland. *Geochimica et Cosmochimica Acta.*

Hosein R., Arn K., Lee M., Steinmann P., Föllmi K. (*Submitted)* Apatite weathering in glacial chronosequences (Rhône and Oberaar Glaciers, Switzerland). *Geology.*

Kalinowski B.E. and Schweda P. (1996) Kinetics of muscovite, phlogopite, and biotite dissolution and alteration at pH 1-4, room temperature. *Geochimica et Cosmochimica Acta* **60**: 367-385.

Klug H.P. and Alexander L. (1974) X-ray diffraction procedures for polycrystalline and amorphous materials. John Wiley and Sons Inc., New York.

Kübler B. (1983) Dosage quantitatif des minéraux majeurs des roches sédimentaires par diffraction

X. *Cahiers de l'Institut de Géologie de Neuchâtel* **ADX**: 1-12.

Lidmar-Bergström K., Olsson S. and Roaldset E. (1999) Relief features and paleoweathering remnants in formerly glaciated Scandinavian basement areas. *Special Publications of the international Association of Sedimentology* **27**: 275-301.

Marquer D. (1987). Transfert de matière et déformation progressive des granitoïdes. Exemple des massifs de l'Aar et du Gothard (Alpes centrales suisses). [PhD thesis] Rennes: **pp.** 250.

Moore D. and Reynolds R. (1997) X-ray diffraction and the identification and analysis of clay-minerals. Oxford University Press, Oxford: pp. **332**

Murphy S.F., Brantley S.L., Blum A.E., White A.F. and Dong H. (1998) Chemical weathering in a tropical watershed, Luquillo Mountains, Puerto Rico: II. Rate and mechanism of biotite weathering. *Geochimica et Cosmochimica Acta* **62**: 227-243.

Nagy K.L. (1995) Dissolution and precipitation kinetics of sheet silicates. *Reviews In Mineralogy* **31**: 173-233.

Oberhänsli R., Schenker F. and Mercolli I. (1988) Indications of Variscan nappe tectonics in the Aar Massif. *Schweizerische Mineralogisch Petrographische Mitteilungen* **68**: 509-520.

Plummer L.N., Wigley T.M.L. and Parkhurst D.L. (1978) The kinetics of calcite dissolution in CO_2-water systems at 5 - 60 °C and 0 - 1.0 atm CO_2. *American Journal of Science* **278**: 179-216.

Rey M. and Kübler B. (1983) Identification des micas des séries sédimentaires par diffraction X, à partir de la série harmonique (001) des préparations orentées. *Schweizerische Mineralogisch Petrographische Mitteilungen* **63**: 13-36.

Righi D., Huber K. and Keller C. (1999) Clay formation and podzol development from postglacial moraines in Switzerland. *Clay Minerals* **34**: 319-332.

Schwab M., Frei C., Schär C. and Daly C. (2001) Mean annual precipitation throughout the European Alps 1971-1990. *In:* Federal Office for Water and Geology (Ed) *The Hydrological Atlas of Switzerland*. Bundesamt für Landestopographie, Bern.

Sharp M.J., Tranter M., Brown G.H. and Skidmore M. (1995) Rates of chemical denudation and CO_2 draw down in a glacier-covered alpine catchment. *Geology* **23**: 61-64.

Stalder H.A. (1964) Petrographische und mineralogische Untersuchungen im Grimselgebiet (Mittleres Aarmassiv). *Schweizerische Mineralogische und Petrographische Mitteilungen* **44**: 187-389.

Swoboda-Colberg N.G. and Drever J.I. (1993) Mineral dissolution rates in plot-scale field and laboratory experiments. *Chemical Geology* **105**: 51-69.

Tranter M., Brown G., Raiswell R., Sharp M. and Gurnel A. (1993) A conceptual model of solute acquisition by Alpine glacial meltwaters. *Journal of Glaciology* **39**: 573-581.

Turpault M.-P. and Trotignon L. (1994) The dissolution of biotite single crystals in dilute HNO_3 at 24 °C: Evidence of an anisotropic corrosion process of micas in acidic solutions. *Geochimica et Cosmochimica Acta* **58**: 2761-2775.

USDA (1998) *Keys to soil taxonomy*. United States Department of Agriculture: **pp**. 328

USDA (1999) *Soil taxonomy: A basic system of soil classification for making and interpreting soil surveys*. United States Department of Agriculture, pp. **870**

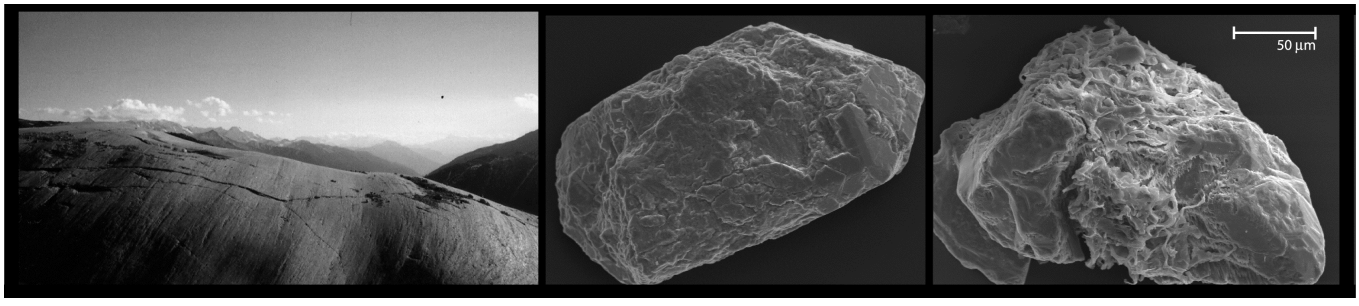
Velbel M.A. (1993a) Constancy of silicate-mineral weathering-rate ratios between natural and experimental weathering: Implicatioins for hydrologic control of differences in absolute rates. *Chemical Geology* **105**: 89-99.

Velbel M.A. (1993b) Temperature dependence of silicate weathering in nature: How strong a negative feedback on longterm accumulation of atmospheric CO_2 and global greenhouse warming? *Geology* **21**: 1059-1062.

White A.F. (1995) Chemical weathering rates of silicate minerals in soils. *Reviews in Mineralogy* **31**: 407-461.

Zumbühl H.J. (1988) Der Rhônegletscher in den historischen Quellen. *In:* H.J. Zumbühl and H. Holzhauser (Eds), *Die Alpen: Alpengletscher in der Kleinen Eiszeit*. Schweizer Alpen-Club SAC, Bern: **pp.** 166-233.

CHAPTER 6
appendices



RHONE PROFILES	Depth cm	Phyllosilicates %	Quartz %	K-Feldspar %	Plagioclase %	Calcite %	Unquantified %
R_{145yr}							
	0_10	3.6	20.4	8.6	45.2	0.9	21.2
	10_20	1.8	45.1	5.3	41.8	0.5	5.6
	20_30	3.2	26.8	24.0	37.9	0.8	7.2
	30_40	1.4	17.0	11.7	5.3	0.5	64.1
	40_50	3.6	15.0	9.1	7.6	0.0	64.8
	50_60	2.1	15.0	7.8	24.2	0.0	50.9
	60_70	1.5	20.5	15.0	30.0	0.6	32.3
	70_80						
	80_90	2.4	32.7	28.6	36.7	0.5	0.0
	90_100	2.9	21.5	6.1	18.4	1.1	50.1
R_{270yr}							
	0_10	1.6	25.1	13.6	29.6	0.9	29.1
	10_20	2.2	28.8	17.2	34.9	0.0	16.9
	20_30	3.1	17.6	8.7	24.7	0.8	45.0
	30_40	2.7	12.5	14.9	24.0	0.0	46.0
	40_50	1.6	35.1	9.8	16.2	0.5	36.8
	50_60	2.5	41.0	22.3	27.1	1.1	6.0
	60_70	1.4	27.0	10.8	24.2	0.0	36.6
	70_80	3.3	52.9	9.0	28.5	0.0	6.3
	80_90	2.5	24.1	19.3	29.6	0.5	23.9
	90_100	1.1	26.4	14.7	35.1	1.3	21.3
R_{270yr} '							
	0_10	4.1	24.9	20.1	33.3	1.6	16.0
	10_20	2.3	32.5	19.7	25.8	1.3	18.3
	20_30	1.4	29.4	15.7	26.3	0.7	26.5
	30_40	2.5	30.0	8.6	24.2	1.0	33.7
	40_50	1.7	17.0	13.3	50.1	0.8	17.2
	50_60	1.7	17.0	13.3	50.1	0.8	17.2
	60_70	3.6	36.8	60.1	28.9	0.7	0.0
	70_80						
$R_{11.6kyr}$							
	0_10	4.2	34.4	9.7	36.9	0.0	14.9
	10_20	4.2	26.2	4.3	26.2	0.5	38.6
	20_30	4.2	33.7	11.1	25.4	0.0	25.6
	30_40	3.1	13.5	8.6	45.9	0.0	29.0
	40_50	3.6	47.6	43.4	27.4	0.0	0.0
	50_60	11.7	21.1	11.0	32.4	0.4	23.4
	60_70	3.6	1.6	18.5	35.3	0.0	41.0

OBERAAR PROFILES	Depth cm	Phyllosilicates %	Quartz %	K-Feldspar %	Plagioclase %	Calcite %	Unquantified %
O_{140yr}							
	0_10	9.0	16.1	4.7	29.9	0.0	40.4
	10_20	5.7	18.6	2.4	18.5	0.0	54.9
	20_30	6.2	23.1	1.9	28.6	1.6	38.7
	30_40	5.1	13.2	2.2	36.6	2.8	40.0
	40_50	3.5	19.5	1.9	40.0	0.4	34.6
	50_60	5.8	33.0	7.8	36.2	0.6	16.6
	60_70	5.2	22.3	7.5	19.6	1.0	44.4
	70_80	7.8	19.1	15.9	38.2	1.5	17.5
	80_90	4.9	25.9	7.2	22.0	0.6	39.4
	90_100	8.4	32.5	5.4	32.8	1.7	19.3
O_{140yr} '							
	0_10	6.1	34.9	4.6	30.4	0.0	24.1
	10_20	7.6	34.6	7.6	34.2	0.4	15.6
	20_30	9.9	18.4	10.1	48.2	0.0	13.4
	30_40	9.0	23.2	6.3	45.2	0.0	16.3
	40_50	7.9	40.7	6.3	54.8	0.6	0.0
	50_60	12.5	28.5	5.1	44.7	0.5	8.7
	60_70	11.3	24.1	6.8	54.1	1.2	2.6
	70_80	10.5	30.6	8.4	51.0	0.9	0.0
	80_90	8.7	41.1	6.5	30.9	0.9	11.9
	90_100	9.1	27.1	6.8	38.0	0.6	18.3
$O_{11.6kyr}$							
	0_10	13.3	11.2	9.0	12.8	0.0	53.7
	10_20	4.3	29.9	32.6	28.7	0.0	4.5
	20_30	8.1	34.6	50.6	28.4	0.0	0.0
	30_40	3.4	33.1	20.5	27.2	0.6	15.1
	40_50	5.8	26.4	42.5	27.6	0.7	0.0
	50_60	5.5	30.9	21.5	32.9	0.9	8.3

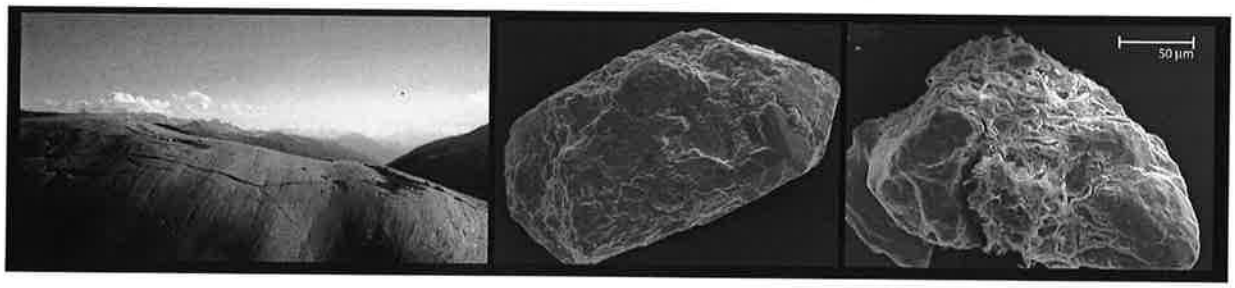
CHAPTER 7

Conversation with a Stone (IV)

I knock at the stone's front door.
"It's only me, let me come in.
I don't seek refuge for eternity.
I'm not unhappy.
I'm not homeless
My world it worth returning to.
I'll enter and exit empty handed
And my proof I was there
will be only words,
which no-one will beleive."

"You shall not enter", says the stone
"you lack the sense of taking part.
No other sense can make up for your
missing sense of taking part
Even sight heightened to become all seeing
will do you no good without a sense of
taking part.
You shall not enter, you have only a sense
of what that sense should be,
only its seed, imagination."

Wistawa Szymborska , in Nothing Twice



SR ISOTOPE SYSTEMATICS IN TWO GLACIATED CRYSTALLINE CATCHMENTS: RHÔNE AND OBERAAR GLACIERS (SWISS ALPS)

K. Arn[1], R. Hosein[1], D. Aubert[2], P Steinmann[1], J. Kramers[3] and K.B. Föllmi[1]

[1]Institut de Géologie, Université de Neuchâtel, 2007 Neuchâtel, CH

[2]EOST, ULP/CNRS, Centre de Géochimie de la Surface, UMR 7517, 67084 Strasbourg Cedex, France

[3]Gruppe Isotopengeologie, Geologisches Institut, Universität Bern, Erlachstrasse 9a, 3012 Bern CH

Abstract

We studied subglacial chemical weathering processes and the Sr isotope composition of runoff and particulate material in the two glaciated catchments of Oberaar (OA) and Rhône (RH) glacier (Swiss Alps). Both areas are contained within the crystalline rocks of the Aar Massif, and the lithologies are quite homogeneous and comparable, except for the presence of a zone of highly deformed Variscan basement gneisses and schists in the Oberaar cachment, that may contain up to 9 % calcite.

We analysed meltwaters and precipitation as well as bulk suspended sediment and local bedrock. Furthermore we analysed the easy leachable fraction from the rocks and suspended sediment, using a 4.2 M acetic acid attack.

Ca/Na ratios are 5.0 – 13.3 and 1.8 – 2.4 in OA and RH meltwaters, respectively, which indicates that meltwaters in both catchments are enriched in Ca compared to suspended sediments. This suggests that the main source of Sr in meltwaters is derived by preferential weathering of calcite. Sr ratios of RH meltwaters ($^{87}Sr/^{86}Sr$ = 0.7251 – 0.7258) are lower than those of RH bulk suspended sediment (0.7279 – 0.7334). The Rhône suspended sediment composition is interpreted as a mixture of Grimsel Granodiorite (0.7101) and Central Aar Granite (0.7449). We explain the lower meltwater Sr ratio by the preferential weathering of disseminated calcite which has a relatively low calcite $^{87}Sr/^{86}Sr$ ratio (estimated 0.720 – 0.730). Furthermore early and nonstoichiometric cation release exert another impact on the meltwater signal. OA meltwaters (0.7137 – 0.7174) show a higher isotopic ratio compared to OA suspended sediment (0.7130 – 0.7148) which reflects the preferential weathering of the calcite contained within the Variscan gneisses (estimated 0.7160 ± 0.001).

The $^{87}Sr/^{86}Sr$ ratio measured in rain is 0.7104 (n = 5). An influence of rain on Rhône meltwater $^{87}Sr/^{86}Sr$ ratio is not neglectable. The high Sr isotopic singature of Oberaar meltwaters compared to that of the corresponding suspended sediment and also to the low Sr isotopic ratio of rainwater (0.7104) suggests that the atmospheric contribution is not visible in the Oberaar meltwaters.

Disseminated calcite exerts a major impact not only on the meltwater major ion composition but also on its Sr systematics.

Introduction

Flux rates and isotopic ratios of Sr have been analysed in stream water settings in order to trace mineral weathering reactions and weathering rates of individual silicate phases and compare them with the isotopic characteristics of the catchments source rocks (e.g., Blum et al., 1993, Blum and Erel, 1995, Taylor and Blum, 1995, Clow et al., 1997). The chemical weathering of Sr from minerals is not necessarily stoichiometric and is dominated by the rapid dissolution of Sr-rich and highly reactive minerals or mineral inclusions; e.g., disseminated calcite (Clow et al., 1997, Blum et al., 1998, Jacobson and Blum, 2000, Jacobson et al., 2002) or apatite (Aubert et al., 2001). Biotite releases considerable amounts of highly radiogenic Sr during the initial stages of weathering, where the initial weathering rates may exceed those for feldspar (Blum and Erel, 1995, Blum and Erel, 1997, Arn et al., submitted). In laboratory dissolution experiments Brantley et al. (1998) show that early Sr release from feldspars is nonstoichiometric and not isotopically identical to the starting material. The nonstoichiometric release is attributed to secondary phases present in minute proportions, and/or to leaching of cations from damaged sites. They further propose that abraded feldspar particles formed during glaciation will show this initial transient nonstoichiometric release.

Recently detailed studies of the meltwater chemistry (major ions as well as Sr systematics) were performed in glaciated catchments draining different types of rock substrata (e.g., Anderson et al., 2000, Sharp et al., 2002, Tranter et al., 2002). In these studies it was shown that carbonate weathering has a dominant influence on bulk meltwater chemistry, even in catchments of predominantly silicate lithologies with only trace amounts of carbonates (Clow et al., 1997, Blum et al., 1998, Anderson et al., 2000, Jacobson and Blum, 2000, Jacobson et al., 2002, Tranter et al., 2002).

Sr flux rates and isotopic ratios in stream waters also reflect the intensity of weathering. Sr isotopic budgets for Himalayan rivers are used to infer increased erosion rates in this mountain range (Galy et al., 1999, Galy and France-Lanord, 2001). They are relevant as indicators of silicate weathering rates and of the relative importance of carbonate and silicate weathering sources within different Himalayan settings (Harris, 1995, English et al., 2000).

The Sr isotopic ratios in continental riverine runoff are used as a proxy for the rate of chemical weathering on continents. They control the Sr isotopic signature of deposited marine carbonates together with other Sr sources, such as submarine hydrothermal sources and deep-sea sediment pore waters (Blum and Erel, 1995, Palmer and Edmond, 1989, Hodell et al., 1990, Hodell and Woodruff, 1994). Steep gradients in the Sr isotopic ratio towards more radiogenic values in marine carbonates in the late Eocene – Holocene are explained by the intensified weathering of continental source rocks associated with the uplift of the Tibetian plateau and Himalayan mountain range (e.g. Raymo et al., 1988, Raymo and Ruddiman, 1992, Edmond, 1992).

Subglacial and proglacial weathering processes increase the chemical weathering of primary minerals

(Sharp et al., 1995, Hallet et al., 1996, Anderson et al., 1997; Tranter et al., 2002, Hosein et al., submitted) and enhance the release of Sr by several mechanisms: (1) glacial grinding and abrasion of rock generating ultrafine particles (< 63 µm) with increased total reactive surface area, (2) selective weathering of bedrock components with relatively high Sr isotopic ratios, (3) the continuous supply of these minerals and the larger discharge and increased flushing of glacial sediments and soils, (4) the presence of mechanically damaged surfaces, enhancing the nonstoichiometric dissolution due to their transiently reactive surface area.

We studied subglacial chemical weathering processes and the Sr isotope composition of bedrock, runoff and particulate material in the two glaciated catchments of Oberaar (OA) and Rhône (RH) Glaciers (Swiss Alps), which are both situated in the crystalline rocks of the Aar massif. Our goal was to estimate the influence of preferential dissolution of major and trace minerals on the bulk meltwater signal. We suggest that the lithological differences between the two areas in this framework of granitic rocks exert major influences on the bulk meltwater isotope chemistry and the mineralogy of the particulate flux (suspended sediment). We show that dissolution of disseminated calcite and nonstoichiometric Sr release from silicates are important sources of Sr and determine Sr isotopic ratios in runoff. A novel element in this work is that glaciated purely crystalline terrains have not been studied in the same detail as mixed crystalline sedimentary or sedimentary terrains.

Field areas

The Rhône and Oberaar Glaciers are located to the east and west of the Grimselpass (2100m above sea level) in the central Swiss Alps, respectively (Fig. 4.1 and Table 4.1). The glaciers experience similar climatic conditions (Schwab et al., 2001) and are presently subjected to considerable retreat and loss in volume. Both areas are contained within the crystalline rocks of the Aar Massif (Stalder, 1964, and Abrecht, 1994; Fig 4.1), and the lithologies are quite homogeneous and comparable, except for the presence of a zone of highly deformed Variscan basement gneisses and schists in the Oberaar area (Oberhänsli et al., 1988).

The Central Aar Granite and the Southern Aar Granite contain quartz, potassic feldspar (microcline), plagioclase (oligoclase), and micas (mainly biotite). The Grimsel Granodiorite is richer in mica (biotite)

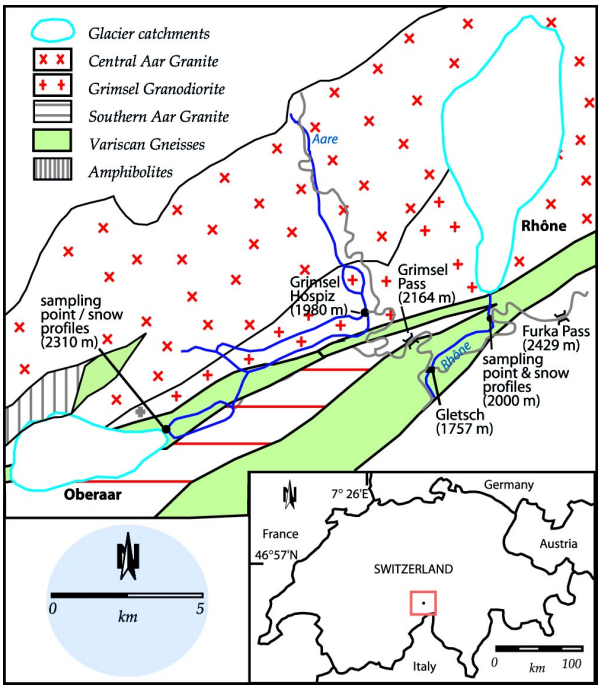


Fig. 1: *Location of the catchments, together with the main geology of the area*

and contains several meter to decameter sized basic lenses higher up in the Oberaar catchment.

The Variscan Gneisses show recrystallized quartz, plagioclase (20 – 50 vol%; oligoclase), and 8 – 20 % biotite and may contain some potassic feldspar (microcline). These gneisses are heterogeneous on a small scale and contain up to 9 wt% calcite (compare also Stalder (1964), who found up to 5 vol% calcite). Sulfide mineralization is evident in these rocks, as visible in many rusty stains on weathered surfaces and the higher SO_4 flux in the meltwater (Hosein et al., submitted).

Table 1: Comparison of the field areas.

	Oberaar		Rhone	
Geogr. Position	46° 32' N 8° 14' E		46° 35' N 8° 23' E	
Surface of catchment	11.2 km^2		23 km^2	
Altitude	2310 - 3631 m a.s.l.		1750 - 3630 m a.s.l.	
Glacier cover today (%)	57%		73%	
Annual mean temperature †	- 1° C §		+ 1.2° C §	
Annual mean precipitation †	2100 mm		2200 mm	
Geology of catchments:	total*	ice covered#	total*	ice covered¥
Central Aar Granite	38%	26%	90%	76±1%
Grimsel Granodiorite	7%	3%	10%	24±1%
Variscan gneisses	42%	60%		
Ultramafic Inclusions	1%			
Southern Aar Granite	12%	11%		

† Schwab (2001)
§ within proglacial area; 2300 m at Oberaar, 1757 m at Rhone
* from geological maps of areas, see text for references.
# Ultramafic inclusions neglected, see text for explanations.
¥ calculated in this work, see text for explanations.

Sampling and Analytical Methods

Weekly (summer) to monthly (winter) bulk meltwater samples (1000 ml) were taken at both glaciers throughout the years 1999 to 2001 and a representative collection was used for Sr-analyses. The samples were immediately filtered in the field using 0.45 µm cellulose nitrate filters, acidified using suprapure HNO_3, and stored in prewashed (10% HNO_3) polypropylene bottles at 4° C. Suspended sediment was collected from both glaciers during the ablation seasons (1999 to 2001) by filtering meltwaters in the field. The sediment samples were oven-dried at 40° C. Rain samples were taken during the 2000 and 2001 ablation seasons: A polypropylene bottle was connected to a plastic funnel via a polypropylene tube (all equipment was prewashed with 10% HNO_3). The bottle was left for a maximum of 24 hours before the rainwater was filtered and stored like the meltwaters. 17 samples of bedrock were randomly taken within the proglacial areas and on the valley walls beside the glaciers. The bedrock samples include the major lithologies of the two catchment areas. Subglacially precipitated carbonate deposits were sampled in both catchments, they appear quite widespread in front of the retreating glaciers. Whole-rock samples plus carbonate deposits were crushed and milled to a fine powder in an agate mill.

A first series of samples was analysed at the Geological Institut of the University of Berne according to the following procedure:

Approximately 100 ml of water was evaporated and the residue dissolved in 1 ml of 3M HNO_3. From a first serie of suspended sediment and rock powders, 1 – 2 g were leached with 4.2M acetic acid for 30 min (weak acid samples, WA). The supernatant was centrifuged twice, evaporated, dissolved with 14M HNO_3 and again evaporated, before being dissolved in 1 ml of 3M HNO_3. The leaching residue was dried, approximately 0.15 mg was digested for 72 hours at 120°C in closed Savilex vessels containing a mixture of 35M HF and 14M HNO_3 (residue total digestion samples, RT). The evaporated samples were taken into solution with 6M HCl and H_2O (pure), evaporated again and subsequently dissolved in 1 ml

of 3M HNO_3. In a second serie approximately 0.06 mg of suspended sediment (4 samples) and of carbonate deposit (1 sample) was digested for 72 hours at 120°C in closed Savilex vessels with 14M HNO_3 (strong acid samples, SA). The supernatant was centrifuged, evaporated and subsequently dissolved in 1 ml of 3M HNO_3.

All samples were spiked with approximately 0.05 – 0.06 mg of an ^{84}Sr spike, all acids used were purified by double distillation. All samples were centrifuged prior to the separation of Sr from other ions using columns with Sr spec-pure resin. Strontium samples were stored in 0.01M HNO_3 and some of them were diluted with 0.35M HNO_3 prior to analyses. The samples were analysed on a Nu Instruments® Multiple Collector Inductively Coupled Plasma-Mass Spectrometer (MC-ICP-MS) in static mode. During the analyses 19 standards (NBS 987) were measured with an average $^{87}Sr/^{86}Sr$ of 0.710286 (2 s.d. = 0.000019).

A second serie of samples was analysed in the Centre de Géochimie de la Surface in Strasbourg. Bedrock samples representative for the catchment lithologies and two suspended sediment and meltwater samples were analysed for their Sr isotopic composition and their chemistry. The chemistry, including Sr, was measured on an ICP-MS. For the analyses of the Sr isotopic composition powders of the samples were digested for 7 days in closed Savilex vessels containing a HF, HNO_3, and $HClO_4$ mixture (bulk samples, TD). Strontium was separated from other ions using a cation exchange resin with 1.5 and 4M HCl as eluents. The total procedural blank was < 0.5 ng. $^{87}Sr/^{86}Sr$ ratios were determined on a VG Sector® multicollector thermal ionisation mass spectrometer (TIMS). Strontium was deposited on a W filament with Ta_2O_5 as activator. Mass fractionation corrections were applied by normalising the average $^{87}Sr/^{86}Sr$ ratios to the $^{86}Sr/^{88}Sr$ ratio of 0.1194. The accuracy of the $^{87}Sr/^{86}Sr$ analyses was evaluated by determining the NBS 987 standard. A mean value of $^{87}Sr/^{86}Sr$ = 0.710258 (2 s.d. = 0.000026, n = 9) was obtained during analyses.

A third serie of samples was analysed at the Geochemical and Environmental Analyses (GEA) Laboratory of the University of Neuchatel. 1 – 2 g from the bedrock and subglacial carbonate powders were leached with 4.2 M acetic acid for 30 min (WA samples). The supernatant was pipetted of and filtered using 0.45 µm cellulose nitrate filters and a syringe. The leachates were measured on a quadrupole ICP-MS together with 10 further meltwater samples. Detection limit of this quantitative method is < 100 ppt for Ca and < 1 ppt for Sr.

Total inorganic carbon was determined on about 100 mg of ground rock powder, using Rock Eval 6 standard bulk rock pyrolysis (Espitalié et al., 1986 and Lafargue et al., 1996). The inorganic or mineral carbon contents (MINC) were calibrated with marble standards and expressed as wt% calcite. For low concentrations the error is 20 % (RSD); for higher concentrations (≥ 0.5 wt%) the error is 5 % (RSD) or less.

Major cations of the meltwater samples were measured by ion chromatography (Dionex DX 500, Hosein et al., submitted). The error is ± 5 % for concentrations of < 100 ppb and ± 2 % for concentrations of 100 ppb – 1 ppm.

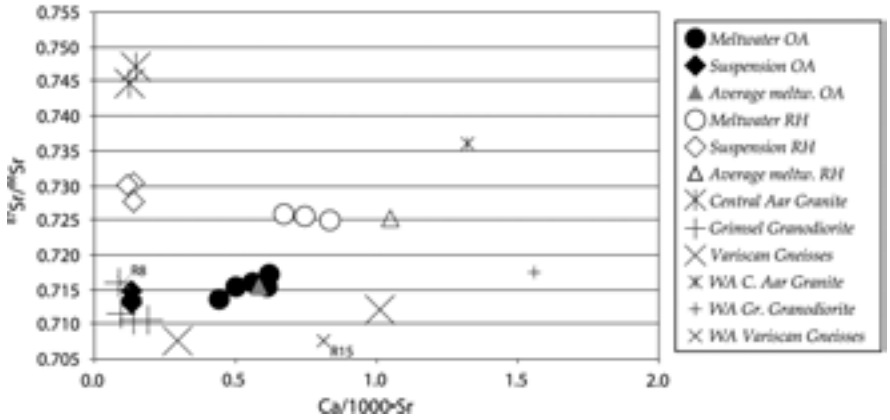


Fig. 2: *$^{87}Sr / ^{86}Sr$ vs. Ca / (1000•Sr) for water, bedrock and suspended sediment samples from both catchments.*

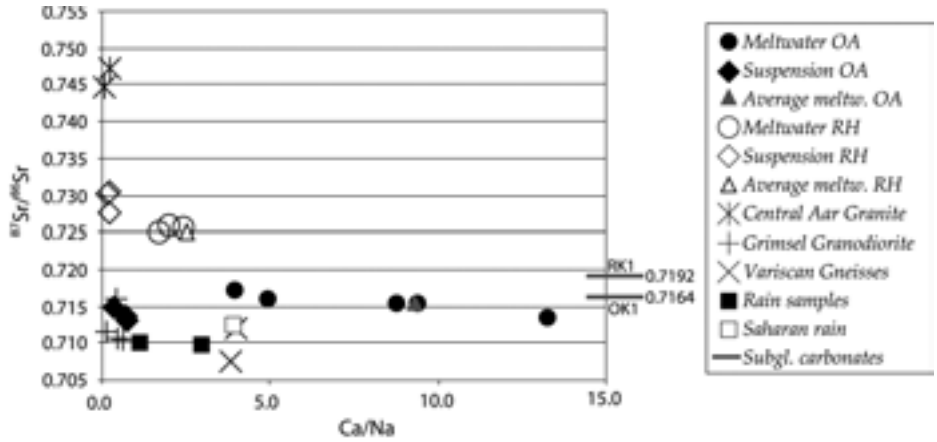


Fig. 3 : *$^{87}Sr / ^{86}Sr$ vs. Ca / Na for water, bedrock and suspended sediment samples from both catchments.*

Results

The results of the chemical and Sr isotopic analyses are given in Table 4.2 & 4.3 and Fig. 4.2 & 4.3. Our obtained $^{87}Sr/^{86}Sr$ ratios for bedrock correspond well with previously published data of the same rocks. The $^{87}Sr/^{86}Sr$ ratio for Central Aar Granite (0.7449) concurs with the data from Challandes (2001). Also the Grimsel Granodiorite $^{87}Sr/^{86}Sr$ ratios (0.7106 & 0.7115) correspond to published data (0.7088 – 0.7114, Challandes, 2001) with exception of sample R1 (0.7161). For Southern Aar Granite a $^{87}Sr/^{86}Sr$ ratio of 0.7356 from Schaltegger and Krähenbühl, 1990) was adopted. For the Variscan Gneisses two $^{87}Sr/^{86}Sr$ ratios (0.7121 and 0.7078) were measured. Published values for this lithology lack. For Rhône suspended sediments we obtained $^{87}Sr/^{86}Sr$ ratios between 0.7279 and 0.7306, for Oberaar suspended sediments the values lie between 0.7130 and 0.7148.

The meltwaters of both glaciers have comparable Sr concentrations: 0.006 – 0.027 and 0.079 – 0.479 µmol l^{-1} for Rhône and Oberaar meltwater samples, respectively. The $^{87}Sr/^{86}Sr$ ratios of the meltwaters

Table 2: Results of the different bedrock and suspended sediment analyses.

Sample			Sr	87/86Sr		2s	Calcite†	Ca	Ca/(1000*Sr)	Na	Ca/Na
			µmol g^{-1}			error	wt%	µmol g^{-1}		µmol g^{-1}	
Bedrock											
Central Aar Granite											
R17	TD	*	0.422	0.744946	±	0.000026	0.11	52	0.122	526	0.098
R17	RT		0.413	0.745898	±	0.000012					
R17	WA		0.019	0.736238	±	0.000072					
R17	WA	NE	0.007					9.4	1.328		
CAGr		¥	1.050	0.747077	±	0.000109		159	0.151	660	0.240
Aar10		#	0.902	0.731928	±	0.000028					
	Bio		1.142	0.741252	±	0.000167					
	K-Feldspar		0.711	0.733796	±	0.000058					
Aar12		#	0.799	0.737147	±	0.000032					
	Bio		6.518	0.739120	±	0.000043					
	Plagio		0.833	0.744114	±	0.000269					
Aar17		#	0.811	0.744057	±	0.000056					
	Bio		0.148	0.748567	±	0.000098					
	Plagio		0.822	0.743363	±	0.000079					
Grimsel Granodiorite											
R6	TD	*	1.941	0.711526	±	0.000024	0.27	185	0.096	874	0.212
R6	RT		1.488	0.711554	±	0.000025					
R6	WA		0.004	0.717531	±	0.000020					
R6	WA	NE	0.003					4.2	1.565		
R1		*	3.139	0.716050	±	0.000024		285	0.091	597	0.478
R9		*	3.630	0.710569	±	0.000026		503	0.138	911	0.552
Aar31		#	4.212	0.708837	±	0.001640					
	Bio		0.594	0.716423	±	0.000046					
	Kfs		3.311	0.710056	±	0.000085					
AD20		#	2.686	0.710093	±	0.000029					
	Bio		1.435	0.713651	±	0.000394					
	Plagio		1.498	0.710527	±	0.000075					
ACIIh		#	2.573	0.711382	±	0.000053					
	Bio		0.726	0.715351	±	0.000074					
	Plagio		3.409	0.711191	±	0.051440					
Southern Aar Granite											
SAGr		¥	0.869	0.735627	±	0.005317					
Variscan gneisses											
R8	TD	*	1.792	0.712059	±	0.000024	0.15	1818	1.014	450	4.040
R8	RT		2.282	0.711808	±	0.000014					
R8	WA		0.003	0.716165	±	0.000020					
R8	WA	NE	0.011					1.2	0.104		
R15	TD	*	4.121	0.707763	±	0.000022	9.01	1230	0.298	321	3.832
R15	RT		2.990	0.707828	±	0.000014					
R15	WA		0.865	0.707644	±	0.000050					
R15	WA	NE	0.494					403	0.816		
Suspended sediment											
Oberaarglacier											
OAP6	TD	*	1.838	0.714783	±	0.000013		241	0.131	569	0.423
OA3	RT		2.193	0.713794	±	0.000032					
OA3	WA		0.134	0.713426	±	0.000024					
OA1	SA		2.717	0.712984	±	0.000014		355	0.131	453	0.783
OA2	SA		2.705	0.713787	±	0.000008		351	0.130	500	0.702
Rhône glacier											
RH3.8.	TD	*	1.164	0.730245	±	0.000015		141	0.121	639	0.220
RH3	RT		1.117	0.730570	±	0.000013					
RH3	WA		0.055	0.733371	±	0.000016					
RH1	SA		1.142	0.730583	±	0.000021		162	0.142	621	0.261
RH2	SA		1.176	0.727853	±	0.000029		168	0.143	597	0.281
Carbonate deposit											
OK1			1.725	0.7164363	±	0.000013					
OK1	WA	NE	0.100					385	3.858		
RH1			0.160	0.719159	±	0.000024					

* measured at Centre de Géochimie de la Surface in Strasbourg

NE measured at GEA Lab, University of Neuchatel

¥ Schalteggerand Krähenbühl, 1990

Challandes et al. 2001

† From RockEval analyses, GEA Lab, University of Neuchatel

Table 3: Results of the different water samples analyses.

Sample		Sr	87/86 Sr		2 sigma	Ca	Ca/ (1000*Sr)	Na	Ca/Na
		µmol l^{-1}			error	µmol l^{-1}		µmol l^{-1}	
Meltwater									
Oberaarglacier									
O51		0.403	0.715619	±	0.000024	203.74	0.51	23.04	8.84
O65		0.197	0.713730	±	0.000023	86.78	0.44	6.52	13.31
O75		0.146	0.715419	±	0.000020	90.27	0.62	9.57	9.44
O80		0.109	0.717371	±	0.000046	140.90	1.30	16.96	8.31
P6	*	0.125	0.715950	±	0.000013	69.98	0.56	14.00	5.00
P4	NE	0.218				136.90	0.63		
P7	NE	0.079				83.40	1.05		
K8	NE	0.301				136.77	0.45		
P8	NE	0.240				108.87	0.45		
P9	NE	0.479				231.07	0.48		
K25	NE	0.238				99.52	0.42		
Rhoneglacier									
A111		0.149	0.725554	±	0.000159	9.48	0.06	3.91	2.42
A142		0.234	0.725840	±	0.000192	12.22	0.05	6.09	2.01
RH3.8.	*	0.107	0.725067	±	0.000014	9.00	0.08	5.00	1.80
P046	NE	0.008				23.65	2.82		
A067	NE	0.007				20.18	2.77		
P093	NE	0.006				9.10	1.51		
P071	NE	0.009				19.31	2.09		
P142	NE	0.010				27.77	2.87		
A169	NE	0.027				45.06	1.69		
Rain									
O45R		0.004	0.712375	±	0.000010	67.08	16.51	16.96	3.96
RR1		0.004	0.709957	±	0.000108	2.49	0.69	2.17	1.15
RR2		0.016	0.709745	±	0.000024	11.72	0.72	3.91	3.00
RR3		0.042	0.709788	±	0.000013				
RR4		0.011	0.709972	±	0.000033				
Carbonate deposit									
OK1			0.7164363	±	0.000013				

* measured at Centre de Géochimie de la Surface in Strasbourg

NE measured at GEA Lab, University of Neuchatel

sampled throughout the ablation season show little variation (0.7251 – 0.7258 for Rhône and 0.7137 and 0.7174 for Oberaar samples).

The $^{87}Sr/^{86}Sr$ ratios of the rain samples measured are quite similar (0.7097 – 0.7100), except for one sample (0.7124) that was taken during a one day rain event associated with the precipitation of brownish to redish colored dust suggesting its provenance is from outwith the catchment and may have a Saharan source (Lenaz et al., 1986, Kübler et al., 1990). The chemistry of this water shows a high Ca concentration, and the $^{87}Sr/^{86}Sr$ ratio is slightly higher than the average of the other analysed rain samples (Fig. 4.3).

The weak acid attack (WA) of Central Aar Granite gave a $^{87}Sr/^{86}Sr$ ratio of 0.7362 which is lower than that of the corresponding total digested sample (R17, TD = 0.7449). The WA $^{87}Sr/^{86}Sr$ ratio of Grimsel Granodiorite is higher than the corresponding TD (R6, WA = 0.7175 and TD = 0.7115). One WA $^{87}Sr/^{86}Sr$ ratio of the two samples of Variscan Gneisses is higher than the corresponding TD (R8, WA = 0.7162 and TD = 0.7121) whereas the other WA $^{87}Sr/^{86}Sr$ ratio is approximately the same (R15, WA = 0.7076 and TD = 0.7078).

All bedrock lithologies of the two catchments contain measurable amounts of calcite (Table 4.2). The calcite content in Grimsel Granodiorite (0.11 wt%) is lower than in Central Aar Granite (0.27 wt%). The Variscan Gneisses contain 9 and 0.15 wt% of calcite, respectively. The large differences in calcite contents in the Variscan Gneisses point towards the heterogeneity of these rocks (Arn et al., submitted).

The strong acid attack of Oberaar suspended sediment (SA samples: 0.7130 & 0.7138; 14M HNO_3) gave ratios close to the residue sample (RT, 0.7138) but smaller than the bulk sample (TD, 0.7148). The WA $^{87}Sr/^{86}Sr$ ratio of the suspended sediment (0.7134) is similar, and lies between the two WA $^{87}Sr/^{86}Sr$ ratios of the Variscan Gneisses (0.7076 & 0.7162). The heterogeneity of the Variscan Gneisses is also reflected in the scattering of the suspended sediment samples. The Rhône suspended sediment WA $^{87}Sr/^{86}Sr$ ratio (0.7334) is higher than the residue (RT, 0.7306) and the bulk sample (TD, 0.7302), and may be comparable to the WA $^{87}Sr/^{86}Sr$ ratio of Central Aar Granite (0.7362). The strong acid attack (SA: 0.7279 & 0.7306; 14M HNO_3) gives values comparable to the residue and the bulk sample, which is probably related to the leaching of a significant part of silicate minerals. Due to the more homogeneous bedrock of the Rhône catchment its suspended sediment shows less scatter. In the suspended sediment leaving a glacier a significant amount of minerals may already be leached subglacially and the further leaching of suspended sediment might not correspond to the initial leach. Therefore we do not use the suspended sediment WA $^{87}Sr/^{86}Sr$ ratios for the following discussion of Sr sources in the meltwaters.

Discussion

General

The Sr isotopic signal of the meltwaters is usually dominated by contributions from disseminated calcite due to its high dissolution rate and its preferential weathering in subglacial environments (as is reported from other glaciated areas, e.g., Tranter et al., 1993,

Tranter et al., 2002, Anderson et al., 1997, White et al., 1999, Hosein et al., submitted). Compared to the suspended sediment, the meltwaters from both glaciers show a Ca enrichment relative to Na (increased Ca/Na ratio) which points towards the preferential weathering of a mineral with a high Ca concentration (calcite, apatite; Fig. 4.3). For Oberaar glacier the Ca enrichment is higher. As the concentrations of PO_4 measured in meltwaters from both glaciers are comparable (Hosein et al., submitted), the main source of Sr in the meltwaters can not be apatite but rather disseminated calcite contained within the different bedrock lithologies. Furthermore, easily hydrated ions derived from freshly cleaved silicate surfaces may exert another impact on the meltwater signal. Their early release is nonstoichiometric and may not correspond to the bulk mineral signature (Brantley et al., 1998).

All granitic rocks in our areas contain measurable amounts of disseminated calcite, with up to 9 wt% calcite in the Variscan Gneisses (Table 4.2). For all the rock and suspended sediment samples, the $^{87}Sr/^{86}Sr$ ratios of WA samples (which are dominated by disseminated calcite) are quite similar to the ratios measured in the bulk samples (TD samples). Disseminated calcite seems to have more or less equilibrated with the surrounding rock during Alpine metamorphism of the Aar Massif (O. Müntener, pers. comm.). However, the small differences in the $^{87}Sr/^{86}Sr$ ratios of the WA samples compared to the bulk rock values allow us to discuss the different sources of Sr present in the meltwaters.

Suspended sediment represents bedrock that was recently mechanically abraded at the glacier base (Benn and Evans, 1998, Drewry, 1986) and its mineralogy shows an average of the different bedrock compositions of todays glacier catchments (Arn et al., submitted). The composition of suspended sediment is affected by the composition of glacier covered bedrock type, by mechanical effects of abrasion and transport, as well as by the overall resistance (or hardness) of a lithology and its minerals against mechanical erosion.

Rhône systematics:

a) Suspended sediment vs. catchment lithologies.

Using a mass balance approach we calculate the portions of the two bedrock lithologies within the catchment. Knowing the $^{87}Sr/^{86}Sr$ ratios and Sr concentrations of the two main lithologies in the Rhône catchment (Table 4.2) and considering suspended sediment to be a mixture of the two recently mechanically eroded bedrock lithologies (see above; bulk suspended sediment (TD) $^{87}Sr/^{86}Sr$ ratio and Sr concentration) we calculated the portions of these lithologies within the suspended sediment. This calculation gives approximately 76 ± 1 % of Central Aar Granite and 24 ± 1 % of Grimsel Granodiorite (Table 4.1). Assuming equal erodability (no difference in the overall hardness) indicates that also the areal distribution of the two lithologies is approximately 76 and 24 %. The values are quite different from an estimated distribution using different maps, which give approximately 90 and 10 % for Central Aar Granite and Grimsel Granodiorite, respectively (Table 4.1). However, the available maps are not precise for the glacier covered parts of

the catchment, hence our calculated distribution of the two lithologies is probably more reliable.

b) Rhône meltwater signal. At Rhône glacier the $^{87}Sr/^{86}Sr$ ratio of the meltwater is smaller than of the suspended sediment. Meltwater $^{87}Sr/^{86}Sr$ ratios lie between the two bedrock WA samples (Central Aar Granite 0.7362; Grimsel Granodiorite 0.7175, Fig. 4.2 & 4.3, Table 4.2 & 4.3) but according to the lithological distribution they are not corresponding to the WA values. Furthermore, the average Ca/1000•Sr ratio of meltwater samples is higher than the two WA bedrock samples (Fig. 4.2). We propose four reasons for this fact: (1) During the weak acid attack more than calcite was dissolved, the WA signal is influenced by other minerals. As the Central Aar Granite WA value (0.7362) lies below the TD value (0.7449) and other single mineral values are higher (0.7371 – 0.7486, except 0.7338 for one K-feldspar sample; see Table 4.2) the pure granite calcite $^{87}Sr/^{86}Sr$ ratio has to be lower than the WA value. Accordingly, as the WA $^{87}Sr/^{86}Sr$ ratio of Grimsel Granodiorite is the highest of all Granodiorite values (Table 4.2), the pure granodiorite calcite $^{87}Sr/^{86}Sr$ ratio has to be equal or more likely higher admitting that also for Grimsel Granodiorite more than calcite was leached by the weak acid attack (WA). As a broad estimation we propose the disseminated calcite of Rhône catchment lithologies to be between 0.7200 (granodiorite) and 0.7300 (granite) with a higher Ca/1000•Sr ratio than the average meltwater. Because the Ca enrichment relative to Na in Rhône meltwaters compared to Rhône suspended sediment is significant, we assume that calcite dissolution exerts the dominant impact on the meltwater chemistry. (2) The nonstoichiometric Sr release during initial subglacial weathering could have a lowering effect on the $^{87}Sr/^{86}Sr$ ratios which is visible in our meltwaters. The feldspars from Grimsel Granodiorite have a higher Sr concentration (1.498 – 3.409 µmol g^{-1}) compared to Central Aar Granite feldspars (0.711 – 0.822 µmol g^{-1}). They could therefore dominate the nonstoichiometric Sr release, and,according to their lower $^{87}Sr/^{86}Sr$ ratios (0.7101 – 0.7112 compared to 0.7338 – 0.7441 for Central Aar Granite feldspars), they could have a decreasing effect on the meltwater $^{87}Sr/^{86}Sr$ ratios. (3) The dissolution of subglacially precipitated carbonate could exert another lowering influence on the meltwater values (0.7192, Fig. 4.3). The significant occurrence of such carbonates in front of Rhône glacier assumes them to exist also beneath the actual glacier, where they can get involved in the subglacial weathering processes. (4) At Rhône the lower $^{87}Sr/^{86}Sr$ ratios in meltwaters compared to bulk suspended sediment may imply that atmospheric input (with its low $^{87}Sr/^{86}Sr$ ratio and high Ca/Na values) also exerts a visible impact on the meltwater signal (Fig. 4.3).

a) Oberaar systematics:

Comparing Oberaar lithologies and suspension: At Oberaar the lithological architecture is visible from the broad geomorphological framework: The main valley incision was performed on the easier erodable zone of Variscan Gneisses which make up approximately 60 % of the total glacier covered area (Table 4.1). The remaining 40 % at the glaciers sides are composed of granitic rocks which are harder and less erodable. The lithologies are elongated parallel

to the main valley geometry from the glacier snout to the top of the catchment (the Oberaar Joch). Taking into account the ratio of glacier cover, the average suspended sediment flux (kg km^{-2} yr^{-1}) of Oberaar glacier is 2 times higher than Rhône glacier (Hosein et al., submitted). Knowing the areal distribution of 60 % : 40 % and taking the erodability of granitic rocks to equal 1 we calculate the erodability of the Variscan Gneisses to be 2.7 to get an overall flux that is 2 times higher. This corresponds to an influence of the gneiss on the bulk suspended sediment of 73 %. Beside the areal distribution this higher influence is due to effects of anisotropy and glacier dynamics (e.g., higher ice overweight along central parts of glacier).

b) Oberaar meltwater signal

In accordance to the values of the two samples of Variscan Gneisses the $^{87}Sr/^{86}Sr$ ratios of Oberaar suspended sediment (TD) and the meltwater are lower than the ones of Rhône (Fig. 4.2 & 4.3, Table 4.2 & 4.3). The Oberaar meltwaters show a stronger Ca-enrichment relative to Na compared to the suspended sediment than Rhône meltwaters (Fig. 4.3). This is due to the clear dominance of the Variscan Gneisses (with their higher erodability and their higher calcite content compared to the granitic lithologies) in this catchment. Watching the WA $^{87}Sr/^{86}Sr$ ratios of the two samples of Variscan Gneisses, the meltwater $^{87}Sr/^{86}Sr$ ratios would be expected to plot lower, which implies that our two samples do not seem to be representative for the Variscan Gneisses (=> outliers!). This shows clearly the *high* heterogeneity of these gneisses, they are not adequately represented by the two samples we measured (cf. also the different calcite content of the two samples, R8 = 0.15 wt%, R15 = 9 wt%). According to the Sr ratio of the meltwaters, we would expect an average gneiss calcite $^{87}Sr/^{86}Sr$ ratio to be 0.7160 ± 0.001. Furthermore, the $^{87}Sr/^{86}Sr$ ratio of a sample of subglacially precipitated carbonate deposits is about the same (0.7164, Fig. 4.3), whereas its Ca/Na ratio is higher than all the meltwater samples measured. As the carbonate deposits are quite widespread in this catchment (own observations at the glacier snout), their subglacial dissolution could also exert a major impact on our meltwater signals.

Because Oberaar meltwater $^{87}Sr/^{86}Sr$ ratios are higher than the suspended sediment (and than all the rain values), the atmospheric impact is minor relative to the other discussed Sr sources (Fig. 4.3).

Comparison to other works

Sharp et al. (2002) discuss the relationship between subglacial weathering processes and the Sr isotope systematics of meltwater runoff from Robertson Glacier, (Alberta, Canada) a glacier that rests on predominantly carbonate bedrock. During times of quick flow conditions with high discharge, when meltwaters are dilute and their residence times within the glacier are short, the contribution of carbonates to the Sr flux in runoff dominates. Opposite, during distributed flow conditions, when meltwater-rock contact times are long, significant amounts of K-silicate minerals present in the catchment exert a visible impact on the meltwaters.

On the other hand, Anderson et al. (2000) show in their research for streams draining the catchment of the retreating Bench Glacier (south-central Alaska,

glacier within metagraywacke-metapelite bedrock), that the dominant contribution to solute flux in the glacier outlet stream is by generally biotite alteration. The carbonate source only became dominant in proglacial streams draining sediments of increasing age of exposure.

The measured $^{87}Sr/^{86}Sr$ ratios of our meltwaters lie too close to each other (& their Sr concentrations are scattering too much) to significantly attach their values to such trends (and they are too few).

Conclusions

This is the first work which analyses Sr isotopes in purely crystalline glaciated terrains. Generally, meltwaters draining crystalline glaciated catchments reflect the high $^{87}Sr/^{86}Sr$ ratios of the underlying bedrocks. Meltwater composition is defined by different short-term subglacial processes: At Oberaar we showed that the dissolution of disseminated calcite exerts a major impact not only on meltwater major ion composition but also on its Sr systematics. Also Rhône glacier meltwaters draining a solely granitic catchment show a clear impact of disseminated calcite dissolution. Here the influence of nonstoichiometric Sr release from silicates and from precipitation seems to be visible as well.

The dominance of calcite dissolution was confirmed in the Oberaar catchment (where the Variscan Gneisses contain more calcite and are easier erodable than the other granitic rocks) by comparing the $^{87}Sr/^{86}Sr$ ratio of the meltwaters to the $^{87}Sr/^{86}Sr$ ratios of disseminated (& subglacially precipitated) calcite.

Outlook

In this work we analysed the Sr systematics of crystalline glaciated terrains. We showed clearly that disseminated calcite exerts a dominant impact on meltwater Sr characteristics, even in a pure crystalline catchment, e.g., the Rhône catchment. Hosein et al. (submitted) show that as soon as there is a higher amount of calcite (2.3 % in Oberaar compared to 0.5 % in Rhône catchment) it dominates the meltwater dissolved load. Sr isotope systematics help to clarify our knowledge about subglacial weathering processes. On the other hand our work also shows the limits of the Sr systematics, where heterogeneities in Sr content of lithologies complicate the interpretations (Oberaar catchment with Variscan Gneisses).

To resolve the remaining uncertainties with our findings we would therefore propose several points to consider during a continued survey of the two catchment areas:

(1) In order to get insight in the exact Sr systematics of disseminated calcite we propose step wise leaching experiments starting with ultrapure water and weaker acids (pH 4), in analogue to the work of Sharp et al. (2002). Leaching with 4.2M acetic acid was shown to be too strong.

(2) During a further field mission we would try to get more samples of the Variscan Gneisses ($n > 10$) as well as of the granitic rocks, in order to compare the scatter between them and to be able to conclude what could be an average value for the gneisses of the area.

(3) Same time we would get more meltwater and suspended sediment samples (n = 15 – 20), in order to get insight in their variance and trends (quick-flow / dilute-flow) during the ablation season. Accumulation season samples could give information about weathering processes during longer sediment-water contact times.

(4) The calcite content should be measured on all bedrock samples and on suspended sediments.

(5) During a further field mission several rainwater samples could be collected to countercheck the data obtained within this work.

Acknowledgements

This work benefited from the collaboration with Dominique Aubert (Strasbourg) and Jan Kramers (Berne) who are gratefully acknowledged. We thank Virginie Matera (Neuchatel) and Ingeborg Hebeisen (Berne) for laboratory assistance. This study was supported by Swiss National Science Foundation Grants 21-53997.98 and 20-61485.00.

References

Abrecht J. (1994) Geologic units of the Aar massif and their pre-Alpine rock associations: a critical review. *Schweizerische Mineralogisch-Petrographische Mitteilungen* **74**: 5-27.

Anderson S.P., Drever J.I., Frost C.D. and Holden P., (2000) Chemical weathering in the foreland of a retreating glacier. *Geochimica et Cosmochimica Acta* **64**: 1173-1189.

Anderson S.P., Drever J.I. and Humphrey N.F. (1997) Chemical weathering in glacial environments. *Geology* **25**: 399-402.

Arn K., Hosein R., Adatte T., Steinmann P. and Föllmi K.B. (*submitted*) Chemical weathering in a glacial chronosequence in the forefields of Rhône and Oberaar Glaciers (Swiss Alps): Rate and mechanism of biotite weathering. *Chemical Geology.*

Aubert D., Stille P. and Probst A. (2001) REE fractionation during granite weathering and removal by waters and suspended loads: Sr and Nd isotopic evidence. *Geochimica et Cosmochimica Acta* **65**: 387-406.

Benn D.I. and Evans D.J.A. (1998) *Glaciers and glaciation.* Arnold Publishers, London: **pp** 734.

Blum J.D. and Erel Y. (1995) A silicate weathering mechanism linking increases in marine 87Sr/86Sr with global glaciation. *Nature* **373**: 415-418.

Blum J.D. and Erel Y. (1997) Rb-Sr isotope systematics of a granitic soil chronosequence: The importance of biotite weathering. *Geochimica et Cosmochimica Acta* **61**: 3193-3204.

Blum J.D., Erel Y. and Brown K. (1993) 87Sr/86Sr ratios of Sierra Nevada stream waters: implications for relative mineral weathering rates. *Geochimica et Cosmochimica Acta* **58**: 5019-5025.

Blum J.D., Gazis C.A., Jacobson A.D. and Chamberlain C.P. (1998) Carbonate versus silicate weathering in the Raikhot Watershed within the High Himalayan Crystalline Series. *Geology* **26**: 411-414.

Brantley S.L., Chesley J.T. and Stillings L.L., (1998) Isotopic ratios and release rates of strontium

measured from weathering feldspars. *Geochimica et Cosmochimica Acta* **62**: 1493-1500.

Challandes N. (2001) *Comportement des systèmes isotopiques 39Ar-40Ar et Rb-Sr dans les zones de cisaillement: Exemples du massif de l'Aar (Massifs cristallins externes) et de la nappe de Suretta (Alpes centrales suisses).* [PhD Thesis] Université de Neuchâtel, Neuchâtel.

Clow D.W., Mast M.A., Bullen T.D. and Turk J.T. (1997) Strontium 87/ strontium 86 as a tracer of mineral weathering reactions and calcium sources in an alpine/subalpine watershed, Loch Vale, Colorado. *Water Resources Research* **33**: 1335-1351.

Drewry D. (1986) *Glacial Geological Processes.* Edward Arnold Ldt., London, **pp.** 276

Edmond J.M. (1992) Himalayan tectonics, weathering processes, and the strontium isotope record in marine limestones. *Science* **258**: 1594-1597.

English N.B., Quade J., DeCelles P.G. and Garizone C.N. (2000) Geologic control of Sr and major element chemistry in Himalayan Rivers, Nepal. *Geochimica et Cosmochimica Acta* **64**: 2549-2566.

Espitalié J., Deroo G. and Marquis F. (1986) La pyrolyse Rock-Eval et ses applications - III partie. *Rev. Inst. Fr. Pet.* **41**: 73-89.

Galy A. and France-Lanord C. (2001) Higher erosion rates in the Himalaya: Geochemical constraints on riverine fluxes. *Geology* **29**: 23-26.

Galy A., France-Lanord C. and Derry L.A. (1999) The strontium isotopic budget of Himalayan Rivers in Nepal and Bangladesh. *Geochimica et Cosmochimica Acta* **63**: 1905-1925.

Hallet B., Hunter L. and Bogen J. (1996) Rates of erosion and sediment evacuation by glaciers: A review of field data and their implications. *Global and Planetary Change* **12**: 213-235.

Harris N. (1995) Significance of weathering Himalayan metasedimentary rocks and leucogranites for the Sr isotope evolution of seawater during the early Miocene. *Geology* **23**: 795-798.

Hodell D.A., Mead G.A., and Mueller P.A. (1990) Variation in the strontium isotopic composition of seawater (8 Ma to present): Implications for chemical weathering rates and dissolved fluxes to the oceans. *Chemical Geology* **80**: 291-307.

Hodell D.A. and Woodruff F. (1994) Variations in the strontium isotopic ratio of seawater during the Miocene; stratigraphic and geochemical implications. *Paleoceanography* **9**: 405-426.

Hosein R., Arn K., Steinmann P., Adatte T., Huon S., and Föllmi K.B. (*in prep*) Phosphorus weathering: 4 case studies from the Swiss Alps and Venezuela.

Hosein R., Arn K., Steinmann P., Adatte T., and Föllmi K.B. (*submitted*) Carbonate and silicate weathering in two presently glaciated, crystalline catchments in the Swiss Alps. *Geochimica et Cosmochimica Acta*.

Jacobson A.D. and Blum J.D. (2000) Ca/Sr and 87Sr/86Sr geochemistry of disseminated calcite in Himalayan silicate rocks from Nanga Parbat: Influence on river-water chemistry. *Geology* **28**: 463-466.

Jacobson A.D., Blum J.D., Chamberlain C.P., Poage M. and Sloan V.F. (2002) Ca/Sr and Sr isotope systematics of a Himalayan glacial chronosequence: Carbonate versus silicate weathering rates as a function of landscape surface age. *Geochimica et Cosmochimica Acta* **66**: 13-27.

Kübler B., Jantschik R. and Huon S. (1990) Minéralogie et granulométrie des poussières éoliennes, dites "Sahariennes", du 24 avril 1989 à Neuchâtel. Leur importance pour l'environnment, les sols et les sédiments. *Bulletin de la Société Neuchâteloise des Sciences naturelles* **113**: 75-98.

Lafargue E., Espitalié J., Marquis F. and Pillot D. (1996) Rock Eval 6 applications in hydrocarbon exploration, production and in soil contamination studies, Latin American *Congress on Organic Geochemistry, Cancun.*

Lenaz R., Landuzzi V. and Tomadin L. (1986) Apports et concentration des masses de poussières éoliennes sur le bassin oriental et occidental de la Méditerrannée. *Memoires de la Société Geologique Italienne* **36**: 189-200.

Oberhänsli R., Schenker F. and Mercolli I. (1988) Indications of Variscan nappe tectonics in the Aar Massif. Schweizerische *Mineralogisch Petrographische Mitteilungen* **68**: 509-520.

Palmer M.R. and Edmond J.M. (1989) The strontium isotope budget of the modern ocean. *Earth and Planetary Science Letters* **92**: 11-26.

Raymo M.E. and Ruddiman W.F. (1992) Tectonic forcing of late Cenozoic climate. *Nature* **359**: 117-122.

Raymo M.E., Ruddiman W.F. and Froelich P.N. (1988) Influence of late Cenozoic mountain building on ocean geochemical cycles. *Geology* **16**: 649-653.

Schaltegger U. and Krähenbühl U. (1990) Heavy rare-earth element enrichment in granites of the Aar Massif (Central Alps, Switzerland). *Chemical Geology* **89**: 49-63.

Schwab M., Frei C., Schär C. and Daly C. (2001) Mean annual precipitation throughout the European Alps 1971-1990. *In:* Federal Office for Water and Geology (Ed.) *The Hydrological Atlas of Switzerland.* Federal Office for Topography, Bern, Switzerland.

Sharp M.J., Creaser R.A. and Skidmore M. (2002) Strontium isotope composition of runoff from a glaciated carbonate terrain. *Geochimica et Cosmochimica Acta* **66**: 595-614.

Sharp M.J., Tranter M., Brown G.H. and Skidmore M. (1995) Rates of chemical denudation and CO2 drawdown in a glacier-covered alpine catchment. *Geology* **23**: 61-64.

Stalder H.A. (1964) Petrographische und mineralogische Untersuchungen im Grimselgebiet (Mittleres Aarmassiv). *Schweizerische Mineralogische und Petrographische Mitteilungen* **44**: 187-389.

Taylor A. and Blum J. (1995) Relation between soil age and silicate weathering rates determined from the chemical evolutin of a glacial chronosequence. *Geology* **23**: 979-982.

Tranter M., Brown G., Raiswell R. Sharp, M. and Gurnel A. (1993) A conceptual model of solute acquisition by Alpine glacial meltwaters. *Journal of Glaciology* **39**: 573-581.

Tranter M. Sharp M.J., Lamb H.R., Brown G.H., Hubbard B.P. and Willis I.C. (2002) Geochemical weathering at the bed of Haut Glacier d'Arolla, Switzerland - A new model. *Hydrological Processes* **16**: 959-993.

White A.F., Bullen T.D., Vivit D.V., Schulz .S. and Clow D.W., (1999) The role of disseminated calcite in the chemical weathering of granitoid rocks. *Geochimica et Cosmochimica Acta* **63**: 1939-1953.

CHAPTER 8

Conversation with a Stone (V)

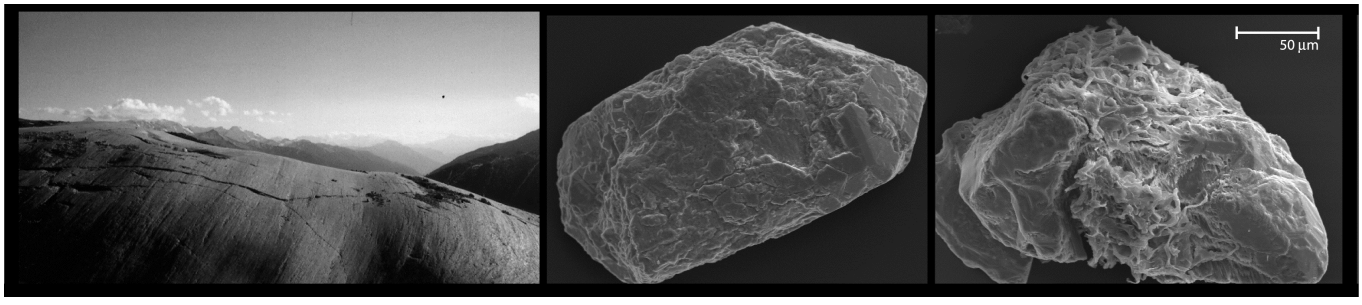
I knock at the stone's front door
"It's only me, let me come in.
I haven't got two thousand centuries,
so let me come in under your roof."

"If you don't believe me", says the stone,
just ask the leaf, it will tell you the same
Ask a drop of water, it will say what the
leaf has said.
And finally, ask a hair from your own head.
I am bursting with laughter, yes laughter,
vast laughter,
although I don't know how to laugh."

I knock at the stone's front door.
"It's only me, let me come in."

"I don't have a door", says the stone.

Wistawa Szymborska , in Nothing Twice



DISCUSSION
THE DENUDATION RATES OF ACCESSORY MINERALS; CALCITE, PYRITE AND APATITE, IN 2 CRYSTALLINE GLACIERISED CATCHMENTS IN THE SWISS ALPS: POTENTIAL CONSEQUENCES FOR BIOGEOCHEMICAL WEATHERING RATES ON GLACIAL-INTERGLACIAL TIMESCALES

During our theses Kaspar Arn and I have studied the mechanical and physical weathering of crystalline rocks in subglacial and proglacial environments, by assessing the weathering products derived from such systems. A catchment approach was employed, using two small basins presently containing the Oberaar and Rhône glaciers, and a third recently glaciated watershed, the Rhône Tributary. All three catchments are located within the crystalline Aar Massif in central Switzerland in close proximity to each other, they span a similar altitude range and therefore experience comparable mean annual temperatures and precipitation volumes and runoff (*Chapter 2; Chapter 3, Table 1*; this chapter, Table 1). This allows for a meaningful comparison of the dissolved and suspended composition of the meltwaters draining their subglacial environments, where active abrasion and plucking generate reactive rock flour with a median grain size in the 4-8 μm range. Calculating the product of runoff composition and volume allows us to estimate the present-day solute and solid fluxes leaving the watersheds. These fluxes are corrected for atmospheric inputs in order to quantify both the mechanical and chemical subglacial annual erosion rates within the two catchments and the atmospheric CO_2 (transiently) drawn down by such chemical weathering reactions. Integrated weathering process over centenial to millenial time slices were also studied as a part of our theses, by assessing the changing mineralogical composition of proglacial sediments over time (*chapters 4 and 6)*.

The first lesson we learnt in comparing our two small, presently glaciated catchments is that despite the fact they were chosen for their physical similarities, the strongly foliated, gneissic texture of the central section of the Oberaar catchment (42 %) leads to elevated suspended sediment and solute concentrations in the meltwaters draining this watershed. An increase of less than 2 % in the calcite content of the suspended (and subglacial) sediments, coupled with the greater amount of freshly comminuted sediment in contact with the Oberaar meltwaters (due to the higher erodability of the foliated gneissic zone), appears to elevate Ca^{2+} fluxes by an order of magnitude, from 10's of keq km^{-2} yr^{-1} to 100's of keq km^{-2} yr^{-1}. In addition the higher sulphide content of the Oberaar catchment's bedrock and the oxidation of such sulphide minerals contributes a higher flux of protons to the Oberaar meltwaters leading to a quadrupling of the cation denudation flux from the Oberaar catchment relative to the Rhône (Table 1). Many authors have underlined the dominant influence of calcite

Table 1: Chemical Denudation Fluxes from a range of glacial environments and the parameters that may affect denudation rates

Catchment	Specific runoff ($m\ yr^{-1}$)	Bedrock	Catchment area (Km^2)	Ice cover (%)	Thermal regime	Cationic denudation rate ($\sum meq+\ m\text{-}2\ yr\text{-}1$)	Transient CO_2 drawdown ($kg\ C\ km^{-2}\ yr^{-1}$)
Ice Sheet							
Lewis River draining Barnes Ice Cap	0.71	migmatic granite-gneiss	205	89	Polythermal ?	94	
Maritime glaciers (Svalbard)							
Scott Turnerbreen	0.52	Sedimentary/mixed	13	32	Cold-based	160	110
Austre Broggernbreen	1.3	Sandstone, shale, phyllite, schists, quartzite & carbonate	9.9	71	Cold-based	240	1100
Broggernbreen (lower site)	0.99	Sandstone, shale, phyllite, schists, quartzite & extensive carbonate	32	53	Polythermal	500	2600
Finsterwalderbreen	0.60	Phyllites, quartzites, sandstones, shales, limestones & siltstones	69	65	Polythermal	325	915
Hannabreen	0.8	Carbonate, schist & sandstone	13.3	69	Polythermal	320	2300
Erdmanbreen	0.81	Sandstone, dolerite, phyllite, schist, quartzite	16	70	Polythermal	190	490
Midre Lovénbreen	1.4	Schist, quartzite, phyllite, minor carbonate & sandstone	6.2	80	Polythermal	560	765
Maritime glaciers (Iceland)							
Tungufljot	2.1	Basalt	720	25		720	9800
Hvita-south, Gullfoss	2.1	Basalt	2000	19		1100	13000
Hvita-west kljafoss	1.8	Basalt	1700	21		650	8300
Temperate valley glaciers							
Europe							
Rhône†	3.1	granite	26.6	73	Warm-based	147-178	774
Oberaar†	2.4	granite & strongly foliated gneiss	11.03	57	Warm-based	681	2317
Haut Glacier d'Arolla	2	schists and gneisses	12	54	Warm-based	640	2000
Gornergletscher	1.4	gneisse, micaschist, gabbro,serpentine, 5% - calcareous micaschist and dolomite	82	83	Warm-based	450	
Tsidjiore Nouve		Metamorphosed Limestones	4.8	97	Warm-based	510	
N. America							
South Cascade Glacier	3.9	phlogopite-actinolite schists, greenstones, quartz diorite, basaltic and lamprophyric dykes	6.1	34	Warm-based	676	3300
Worthington Glacier	7.7	metagraywake, metapelite	13	83	Warm-based	1600	
Berendon Glacier	3.7	siltstones, conglomerates and volcanoclastic	53	62	Warm-based	947	
Asia							
Batura Glacier	2	Carbonate-rich	608	60	Warm-based	1500	
Chhota-Shigri Glacier	3.5	Plutonic/metamorphic	40	25	Warm-based	750	
Dokriani Glacier	1.1	Plutonic/metamorphic	23	45	Warm-based	462	
Continental/global averages			390*				3000§

† This study:

* Livingstone (1963)

§ Gaillardet et al. (1999)

Other data are from a compilation by Hodson et al. (2000)

weathering on the chemical signature of glacial meltwaters draining crystalline catchments (e.g. Eyles et al., 1982; Drever and Hurcomb, 1986; Anderson et al., 1997, 2000; West et al., 2002). The mechanical style of subglacial erosion leads to the exposure of large surface areas of freshly crushed, chemically reactive minerals such as calcite and pyrite in crystalline rocks and associated late stage hydrothermal calcite veining. This accentuates the chemical weathering of these minerals in the subglacial environment, because at near neutral pHs the dissolution rate of calcite (10^{-5} mol m^{-2} s^{-1}; Plummer et al., 1978) is approximately 11 orders of magnitude faster than the dissolution rate of albite ($\approx 10^{-16}$ mol m^{-2} s^{-1}; Chou and Wollast, 1985). Therefore although runoff volume is generally held to be the primary control on solute denudation rates (Table 1; Bluth and Kump, 1994; Anderson et al., 1997) variations of the in the pyrite and calcite content of the bulk rock have a much bigger impact on the solute fluxes from the glaciated areas we have studied than do differences in runoff (Rhône runoff = 3.1 m yr^{-1}; Oberaar runoff = 2.4 m yr^{-1}). Moreover table 1 shows that lithology is an important control of cationic denudation rates in a wider range of glacial settings (see also Hodson et al. 2000).

After quantifying the cation denudation fluxes from Rhône and Oberaar catchments we assessed the relative importance of long- and short-term CO_2 draw down within the watersheds. The cation denudation fluxes were separated into their carbonate and silicate weathering derived components and we assumed that protons from carbonic acid were shared equally between carbonate and silicate minerals (see Sharp et al., 1995 for an alternative approach). Our calculation showed that an order of magnitude more CO_2 was drawn down by weathering reactions in the Oberaar catchment compared to the Rhône over the 1999-2001 study period, with 150 % more long term CO_2 draw down in the Oberaar catchment (*see chapter 3*). When

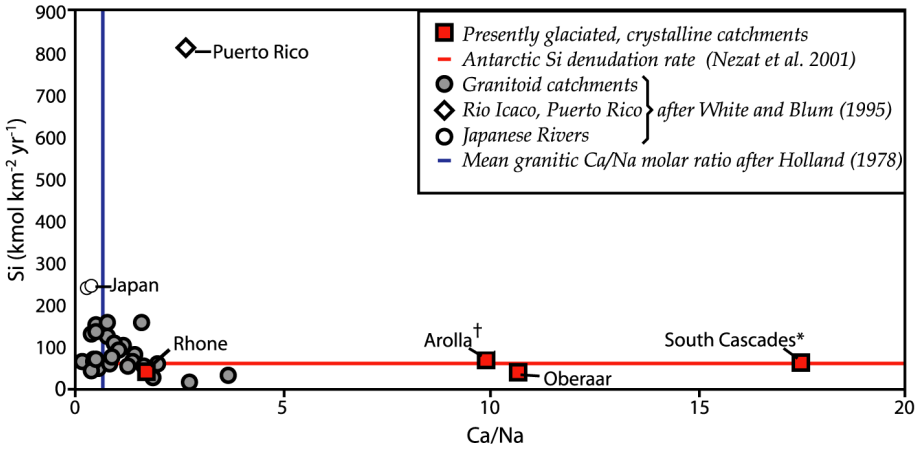


Fig. 1: Silicate and carbonate weathering in presently glaciated and non-glaciated granitoid catchments (All fluxes are corrected for precipitation inputs)

† *Sharp et al. (1995) & * Axtmann and Stallard (1995), cyclical salt corrections; White and Blum (1995), volumetric correction.*

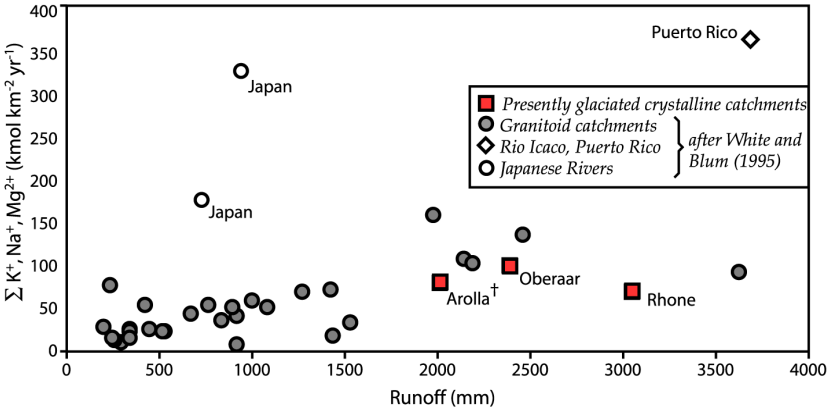


Fig. 2: Molar fluxes of cations derived from silicate weathering against runoff in presently glaciated and non-glaciated granitoid catchments (All fluxes are corrected for precipitation inputs).
† Sharp et al. (1995), cyclical salt corrections; White and Blum (1995), volumetric correction.

compared to a broader data set we see that increasing the calcium content (and friability) of bedrock concomitantly increases the localised transient CO_2 draw down (silicate + carbonate weathering) with more calcic lithologies sequestering higher volumes of atmospheric CO_2 (Table 1 after Hodson, 2000). Yet, although cation denudation rates three times higher than Summerfield's (1991) estimated global average denudation rate (14.8 t km^{-2} yr^{-1}) have been reported from wet-based temperate glacial catchments (Sharp et al., 1995), transient CO_2 draw down is not elevated in glacial environments relative to the continental average (3000 kg km^{-2} yr^{-1}; Gaillardet et al., 1999; see table 1). This suggests that while chemical weathering and transient CO_2 draw down are not necessarily retarded in modern subglacial environments these processes are not sped up here either. Long-term CO_2 draw down, driven by silicate weathering, does not appear to be affected, either favorably or adversely by increased ice cover either: silica fluxes from glaciated and non-glaciated temperate catchments underlain by granitoid lithologies are comparable, irrespective of their glacier cover. Only silica fluxes issuing from Japananese and Puerto Rican catchments with granitoid geology, which experience higher temperatures and/or precipitation inputs, plot as positive outliers in our comparison (Fig: 1). But, silica fluxes may not be the best indicator of silicate weathering in weathering limited glacial environments (Stallard, 1992) where silicate weathering is incongruent (Kump et al., 2000 and references therein). Therefore we have also compared the silicate-derived-cation-fluxes from presently glaciated and non-glaciated systems (Fig. 2; see chapter 3 for discussion). But, again here there is no obvious distinction between presently glaciated and non-glaciated catchments with similar runoff.

A second potential mechanism for the sequestration of atmospheric CO_2 is the biological carbon pump, which is thought to be limited by phosphorus on geological timescales (Broecker and Peng, 1982; Tyrell, 1999). The main detrital P-bearing mineral group is apatite. This mineral is present as an accessory phase in crystalline rocks, but

while the accessory phases calcite and pyrite dominate the subglacial meltwater composition, the near neutral pH of glacial melts inhibit subglacial dissolution of apatite (Fig. 3, after Stumm and Morgan, 1996). Our P mass balance indicates that only 0.04-0.05 kmol km^{-2} yr^{-1} of detrital P may be dissolved in the subglacial environments of the Rhône and Oberaar glaciers, but that the subglacial comminutation of bedrock may mechanically precondition apatite grains for chemical weathering in the proglacial environment. The fluxes of total phosphorus we have calculated for the Rhône and Oberaar catchments rank among the highest in the world (*Chapter 5, table 6*) and 97 % of this phosphorus is in the particulate form of detrital phosphorus, which in our catchments will be principally apatite (*see chapters 4 & 5*). Moreover the relative softness of apatite grains leads to extensive mechanical pitting of their surfaces during transport through the subglacial system. Consequently, the apatite grains delivered to proglacial areas have elaborate microtopographies and therefore large, reactive surface areas. While heavily pitted whole apatite grains were found in the 125-250 μm fraction of moraines and meltout sediments, no apatite fragments were found in the 63-125 μm fraction. Thereby suggesting that apatites are crushed into sub 63 μm particles through abrasion, for example by quartz grains which are mechanistically twice as hard as apatite grains. Such mechanical preconditioning renders grains more reactive leading to accelerated chemical dissolution in the proglacial area, where

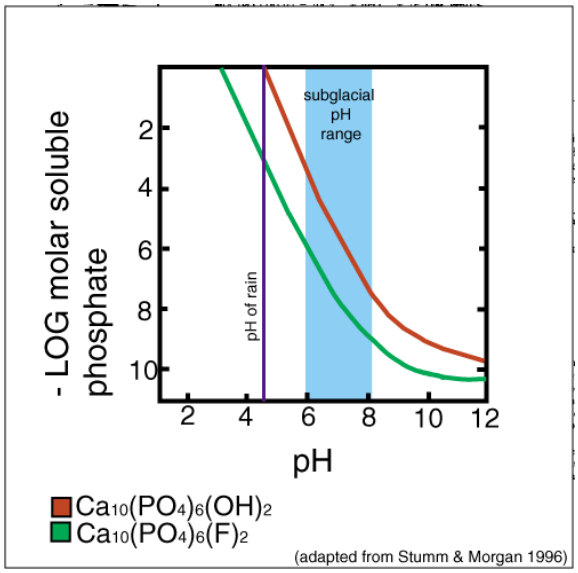


Fig. 3: *The relationship between pH and apatite solubility*

acid aerosols, sulphide oxidation and biological processes in the developing, acidic pedosphere all serve to lower the pH of interstitial pore waters (*chapter 7*). Three tests made during this thesis point towards elevated P weathering rates in the proglacial environments of the Rhône and Oberaar glaciers:

Firstly, the ESEM study of apatite grain surface morphologies showed extensive etching on the surfaces of proglacial grains, which was most pervasive at the tops of soil profiles where organic matter has accumulated (*see chapter 5 for a soil description*). The pit textures on the proglacial grains are indicative of corrosive dissolution etching, unlike

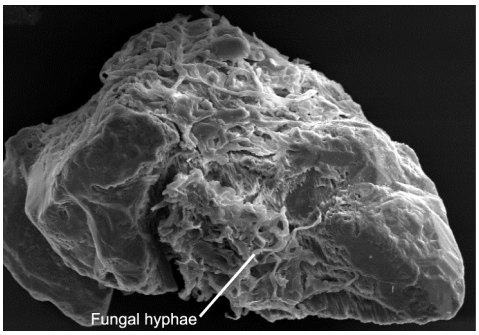


Fig. 4: *Apatite grain showing denticular weathering structures covered in fungal hyphae* (***O*** $_{140\ yr,}$ *0-10 cm).*

the mechanically pitted and dissolution rounded morphologies observed on the surfaces of apatite grains weathered solely in the subglacial environment. This indicates that weathering solutions are more acidic in the proglacial environment. Varied etching textures on the proglacial apatite grain surfaces imply that both diffuse and localised acid hydrolysis reactions dissolve detrital phosphorus in the glacier forefield (*see appendix 3, chapter 4*). Fungal hyphae had colonised apatite grains from the tops of profiles and they appear to biogeochemically mediate dissolution of the grains, as the grain surfaces were locally etched into denticular pits where they were covered by the hyphae (Fig. 4). This localised corrosion may be due to the secretion of organic acids, (such as oxalic acid; Kpomblekou and Tabatabai, 1994).

The second test involved measuring the P content of runoff from the presently glaciated catchments, where meltwaters are in contact with freshly abraded sediment, and the P content of the Rhône Tributary. The latter stream drains a catchment filled mainly with 11.6 kyr granitic and granodiorite drift which is colonised by alpine meadow vegetation. We observed that dissolved P concentrations were elevated in the tributary and it's dissolved, soluble reactive P (SRP) flux is elevated with respect to the SRP fluxes from the presently glaciated catchments. We calculate that 0.17 kmol km^{-2} yr^{-1} of SRP is eroded from the Rhône Tributary catchment. This weathering rate it is comparable with Meybeck's (1993) world average SRP flux, which importantly, is not corrected for atmospheric inputs (0.13 kmol km^{-2} yr^{-1}). The glacial catchments are less favorable environments for the chemical weathering and erosion of SRP (0.05 kmol km^{-2} yr^{-1}).

For the third test integrated detrital P weathering rates were calculated for the 145 yr, 270 yr and 11.6 kyr profiles dug in the Rhône forefield. Detrital P concentrations in the profiles and in "parent material" were measured using a sequential extraction method (Ruttenberg, 1992) and Ti concentrations, measured by X-ray fluorescene, were used to correct for volume changes in the profiles over time. The detrital P weathering rates we calculate for the 3 integrated time slices are all elevated compared the world average P concentration in natural runoff (0.13 kmol km^{-2} yr^{-1}; Meybeck, 1993). The detrital P chemical weathering rates integrated over 145 yr; 270 yr and 11.6 kyr are calculated as 10, 9 and 0.32 kmol km^{-2} yr^{-1}, respectively.

The chemical erosion rate of SRP from the Rhône Tributary catchment, which drains predominantly 11.6 kyr aged sediments and the detrital P chemical weathering rate calculated for the 11.6 kyr profile in the Rhône forefield are of the same order of magnitude. This cross check implies that our calculations are rather robust. Moreover it seems logical that the SRP erosion rate should be on average lower than the present-day detrital P chemical weathering rate, since there is considerable evidence that dissolved P is rapidly sorbed on iron hydroxides and clays, as well as being incorporated into living organic matter in the pedosphere (Walker

and Syers, 1976; Birkland et al., 1989; Crews et al., 1995; this study, chapter 4). Our observation of increased chemical erosion of weathering derived SRP in the recently glaciated Rhône Tributary catchment implies that the proglacial zone may transfer bio-available SRP to the aquatic biosphere for up to tens of thousands of years after glacial retreat (see also Filippelli and Souch, 1999). The immature pedosphere is a poor SRP sink, as clay minerals, iron oxides and organic matter are only beginning to form in the recently deposited overburden. The accelerated oxidation of freshly comminuted sulphide minerals in the proglacial environment may provide an important proton source for the acid hydrolysis of apatite grains before biological agents of corrosion obtain a foothold (see Retallack, 1990; Anderson et al., 2000; Wadham et al., 2001). The impact that detrital P weathering (in proglacial areas) can have on riverine SRP fluxes depends on the amount of weathering derived SRP retained within the evolving pedosphere (Fig. 5).

Studies of modern wet based glaciers may give meaningful insights into weathering underneath polythermal ice sheets. The southern margins of the LGM ice sheets, where most weathering is thought to have taken place were also wet based (e.g. Sugden, 1978): and it is likely that channelised drainage systems evolved under the southern margins of the Laurentide ice sheet in the summer months, as they do under temperate valley glaciers (Nienow et al., 1996; Nienow, personal communication). This would have allowed for localised subglacial interactions between fine-grained sediment and CO_2 rich meltwater (Kump and Alley, 1994; Kump et al., 2000 and references therein). But, despite these potentially favorable conditions the general glacial weathering literature as a whole suggests that it is unlikely that CO_2 draw down increased under underneath ice sheets, particularly since contemporary subglacial environments do not show evidence of elevated CO_2 sequestration (Table 1; Gibbs and Kump, 1994; Tranter et al., 2002).

It has been suggested that chemical weathering may be more significant in the proglacial areas in front of the ice sheets, where reactions between fine grained material, and CO_2 enriched runoff are more unfettered. There have been several studies measuring chemical weathering rates in proglacial catchments, by studying the composition of runoff (Anderson et al., 2000; Wadham et al., 2001) and the changing mineralogical composition of proglacial sediments over time (Darmody et al., 1987; *chapter 4; chapter 7*). These studies report increased weathering rates of reactive mineral phases such as calcite, pyrite and biotite in proglacial sediments deposited during the Little Ice Age relative to equivalent subglacial weathering rates. Anderson et al. (2000) also observed an increasingly congruent style of silicate weathering in proglacial sediments that were deposited at the LGM. Anderson et al. (2000) suggest this rise may be a result of increased biogeochemical weathering in the evolving pedosphere.

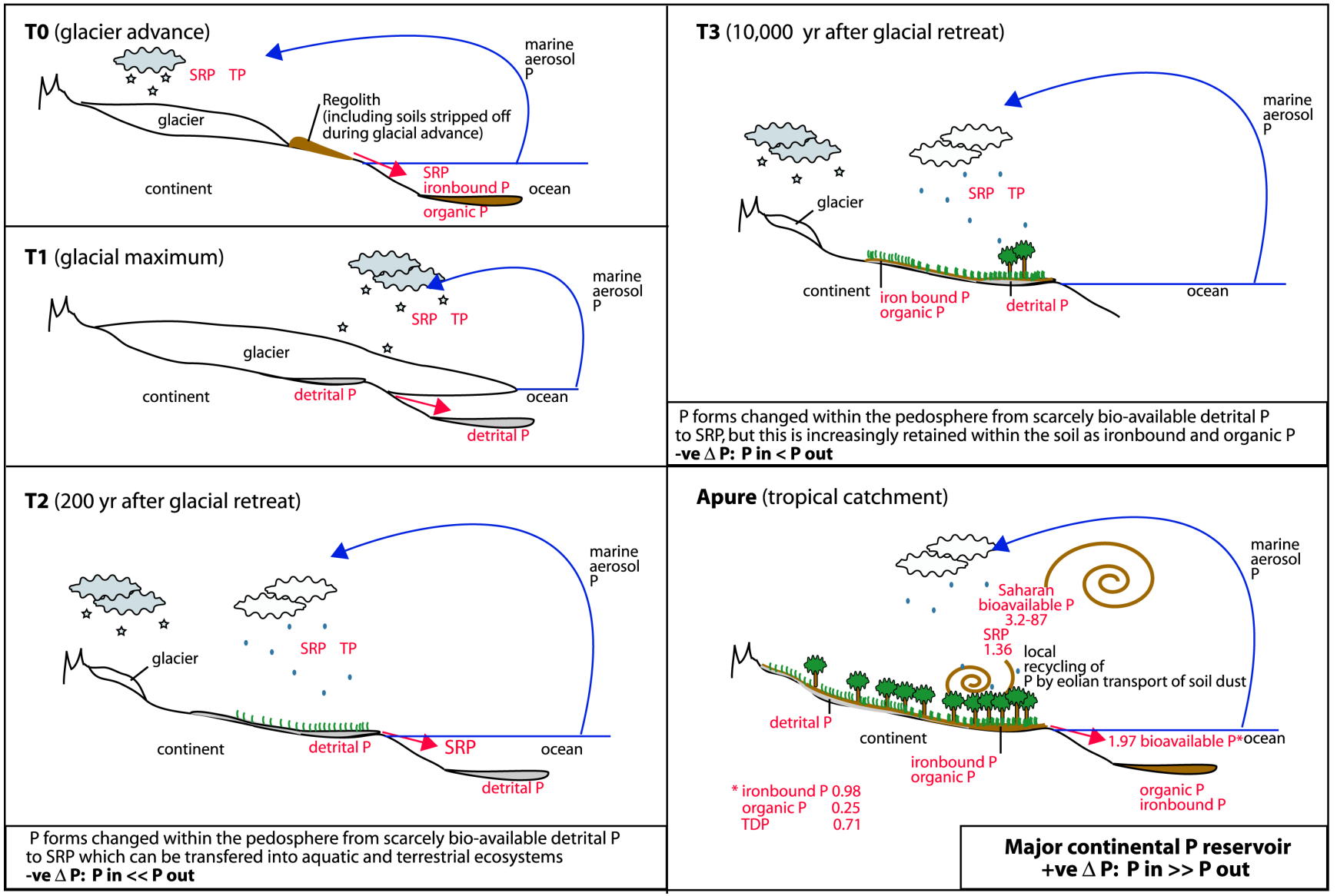


Fig 5: *P cycling in tropical and glaciated continental areas, values are taken from chapters 5 (kmol P km^{-3} yr^{-1}); Reichhof, 1986; Montes and San Jose, 1989 and Swamp et al., 1992.*

There are several commonalities between the glacial forefields we have studied and those exposed by deglaciation after the LGM, which may allow us to scale up our findings and draw some wider inferences about chemical weathering post LGM: Firstly our catchments are underlain by crystalline bedrock, and this was the dominant lithology underneath the Northern Hemisphere ice sheets at the LGM (Gibbs and Kump, 1994; i.e. the North American, Fennoscandian and Scottish shields), although smaller scale carbonate (and salt) outcrops could have a significant impact on local chemical and physical erosion fluxes (Meybeck, 1987). Moreover granites have median P concentrations compared to other continental rock types; therefore applying our calculated weathering rates to wider continental areas will generate conservative detrital P erosion fluxes (sandstone, 170; ultramafic rocks, 195; carbonates, 400; low Ca granites, 600; high Ca granites, 920; basalts, 1130; deep sea clays, 1300 P, ppm). Secondly temperature and precipitation may be important (co)factors. There is a growing body of evidence suggesting a positive correlation between temperature and silicate weathering rates. Meybeck (1987) observed that 38% of the global silica flux comes from the tropics, and positive correlations between temperature and/or precipitation have been observed by Vebel (1993) and White and Blum (1995). Also Birkland et al., (1989) observed that climatic conditions also play an important role in controlling detrital P weathering rates, whereby cold, dry, arctic climes hamper detrital P dissolution rates, whereas warm, wet conditions accelerated them. After the LGM 28 % of the Northern Hemisphere's landmass between 40° and 80° latitude underwent deglaciation. The decreased dustiness reported during this period is interpreted as evidence of increase soil moisture and precipitation (e.g. Broecker, 2000 and references therein). Therefore the climatic conditions and the parent material in our temperate glacier catchments may not be dissimilar to those which prevailed in post LGM proglacial areas (CLIMAP, 1981). Furthermore, the trend we have observed in our chronosequences, of a rapid decrease in detrital P concentrations at the tops of profiles on kyr time scales and a concomitant increase in ironbound and organic P forms, has been observed by other authors in a wide range of proglacial environments throughout the world (e.g. Walker and Syers, 1976; Birkland et al., 1989). This would imply that the trend we observe the Rhône chronosequence applies to detrital P weathering in proglacial sediment deposits in general.

Table 2: Riverine HCO_3^- fluxes[%]

Catchments	Area 10^6 km^2	HCO_3^- kmol km^{-2} yr^{-1}
Global Data Set		
Amazon	5.90	462
Zaire	3.70	823
Mississippi	3.25	309
Ob	3.11	236
Parana	2.87	119
Yenisei	2.57	279
Lena	2.47	237
Amur	1.93	124
Nil	1.87	122
Changjiang	1.82	921
Ganges/Brahmaputra	1.66	1,116
Mackenzie	1.62	291
Niger	1.54	72
Zambesi	1.41	29
Murray	1.13	16
St Lawrence	1.11	600
Orinoco	1.03	219
Indus	0.91	654
Mekong	0.85	526
Yukon	0.84	467
Huanghe	0.82	235
Danube	0.77	801
Orange	0.72	27
Colorado	0.71	67
Columbia	0.66	374
Si Kiang	0.46	1,411
Limpopo	0.34	37
North Dvina	0.33	798
Godavari	0.31	474
Magdelena	0.29	703
Fraser	0.25	390
Yanna	0.24	71
Mahandi	0.19	483
Rio Negro	0.18	189
Hungho	0.16	975
Average		*419*
Small Glacier Covered Catchments		
South Cascade Glacier[*]		922
Haut Glacier d'Arolla[$]		332
Oberaar °		467
Rhône °		101
Average		*455*

[%] Data on non-glaciated catchments were taken from Ludwig et al., 1998 and references therein

[*] Axtmann and Stallard, 1995

[$] Sharp et al., 1995

° This study

At the LGM 18.4 * 10^6 km^2 more land was ice covered than at present (Gibbs and Kump, 1994). The melting of this ice, post 18 kyr, gave way to a period of elevated annual glacial runoff which reached its peak 14.3 kyr ago in the Northern Hemisphere, with glacial melt from the Cordilleran, Fennoscandian, Kara, Barents and Greenland ice sheets contributing 30 % of the global riverine discharge, compared to the 0.6- 1 % that glacial melt contributes to the global riverine discharge today (Tranter et al., 2002). The following discussion considers how the global continental weathering rate of SRP and HCO_3^- may be affected by periods of glacial retreat such as the Bölling-Allerod, when climate warming, increased atmospheric concentrations of CO_2 and glacial runoff are documented:

The average HCO_3^- flux generated by subglacial weathering in presently glaciated catchments with crystalline bedrock (455 kmol km^{-2} yr^{-1}) is comparable with the average HCO_3^- flux from non-glaciated catchments (table 2). If we assume that this subglacial HCO_3^- erosion flux holds for the forefields of the Laurentide and Fennoscandanavian ice sheets, where carbonate weathering rates may even be accelerated compared to those observed in temperate subglacial environments with the same bedrock (Anderson et al., 2000; Wadham et al., 2001), then when the ice sheets had receded to 1/2 their LGM extent, exposing 9200000 km^2 of land, the combined HCO_3^- from these recently deglaciated areas could have been up to 4.2 * 10^9 kmol yr^{-1}. This value is comparable with the present-day global riverine HCO_3^- flux: Ludwig et al. (1999) estimate that the present-day global riverine HCO_3^- flux to the oceans is 5.93 * 10^9 kmol yr^{-1}.

The impact of deglaciation on the global DIP flux to the oceans can be assessed in the same way: If we again base our calculation on a time when the LGM ice mass was halved exposing 9200000 km^2 of land and assume a conservative chemical SRP erosion flux of 0.17 kmol km^{-2} yr^{-1} (i.e. what we measure in the Rhône Tributary catchment) this gives a flux of 1.564 * 10^6 kmol SRP yr^{-1} from this recently deglaciated area. The maximum present-day global riverine reactive P flux (dissolved inorganic + dissolved organic + particulate organic + iron bound particulate P) is 1.485 * 10^8 kmol yr^{-1} (Compton et al., 2000 and references therein). Therefore this hypothetical SRP flux following deglaciation post LGM represents $1/10^{th}$ of the present-day global flux of potentially bioreactive P forms.

These calculations give a feel for the of impact of SRP and HCO_3^- fluxes during glacial periods in Earth History. The numbers hint that periods of deglaciation may significantly increase global HCO_3^- and to a lesser extent SRP fluxes to the oceans. This may have important implications for marine alkalinity (Archer and Maier-Reimer, 1994); (marine) productivity and long-term CO_2 drawdown, as SRP (Redfield, 1958; Broecker and Peng 1982; Tyrell, 1999) and HCO_3^- are potentially bio-enhancing (Milligan and Morel, 2002). CO_2 partial pressures are often below the saturation limit for photosynthesis in marine ecosystems and this can limit productivity unless phytoplankton can utilise other forms of carbon (Riebesell et al., 1993; Badger et al., 1998). Milligan and Morel (2002) have demonstrated that the siliceous tests of (marine) diatoms can act as a pH buffer, enabling the enzymatic conversion of HCO_3^- into CO_2, which can then be used in photosynthesis by these organisms. Therefore changes in the HCO_3^- concentration of ocean surface waters may effect diatom productivity rates and subsequently atmospheric CO_2 content.

Paradoxically CO_2 draw down increases during periods of glaciation, and not during interglacial stadials! There are of course many other factor which should be considered in modeling changes in the HCO_3^- and SRP concentrations of ocean surface waters on glacial-interglacial timescales and their subsequent effect on productivity and atmospheric CO_2: Regarding SRP the following factors may be important: the partitioning of the P flux on ocean shelves, relative to the abyss, which has repercussions for the rate at which P is recycled from the sediment back into the water column (faster for shelf sediments) or whether it is in fact incorporated in sediments at all (as maybe the case for deep depot-centers; Delaney, 1988). The rate of overturn of the oceans is also important and its effect on the production rate of authigenic minerals P minerals in sediments, (so-called sink switching; Ruttenberg, 1993). The more efficient this process is, the lower the P residence time in the ocean, although the fact that authigenic minerals are operationally defined by the SEDEX method leads to a tendency to over estimate authigenic P and underestimate residence times (Ruttenberg, 1992).

HCO_3^- concentrations are also controlled by a complicated set of intereacting processes including: rates of continental input of organic and inorganic

carbon, marine productivity rates; the depth of the lysocline which controls the locus of carbonate deposition; organic carbon deposition and degradation rates, which in turn affect carbonate dissolution and oceanic circulation patterns (Broecker 1982; Archer and Maier-Reimer, 1994 and references therein; Sigman and Boyle, 2000).

Given that the continental ice sheets in this present ice age were initiated at 3.0-3.1 Ma (Einarsson and Albertson, 1988; Raymo et al., 1989) and that organic and total P accumulation rates in marine sediments are observed to increase sharply from this time to the present (Föllmi, 1995; 1996) oceanic P concentrations must have been controlled by increased continental weathering rates, since the deep water marine reservoir would be drained of dissolved P over this period, by the precipitation of P in solid authigenic and ironbound phases, according to the P residence times estimated by Ruttenberg (1993;16-38 kyr) and Colman and Holland (2000; 10 kyr; see also Delaney, 1998). The Laurentide ice sheet may have advanced and retreated up to 6 times during this 3.0 Ma period, and mountain glaciers in Europe and America may have waxed and waned up to 9 and 21 times respectively (Bowen et al., 1986). Therefore proglacial areas were highly dynamic systems over this time: detrital P may have been deposited and chemically weathered on large continental areas by retreating ice masses, supplying biological reactive DIP (and HCO_3^-) in to the marine realm for 10's of kyr before the pedosphere evolved sufficiently to become an effective reservoir trapping P in ironbound and organic P forms. P inputs to the oceans would then be reduced until the next ice advance, when soils may have been cleared off the continents delivering ironbound P and organic P to the oceans, providing another source of conditionally bio-available P to the marine biosphere (Fig 5). Glacial weathering and erosion may therefore be a very important process in maintaining the elevated organic and total P accumulation rates observed in marine sediments of Oligocene age and younger (Föllmi, 1995), since mechanical erosion rejuvenates the pedosphere, clearing out conditionally bio-available ironbound and organic P forms into aqueous ecosystems and restocking it with detrital P (*chapter 5; Fig.6*; Walker and Syers, 1976; Chadwick et al., 1999).

My conclusion is that continental weathering, associated with periods of glacial retreat, in concert with increased runoff and exposure of large volumes of fine, reactive sediment may briefly release bio-enhancing nutrients such as phosphorus (and potentially HCO_3^-), increasing the upper limit for marine productivity and the sequestration of atmospheric CO_2 (Falkowski, 1997). But the increased eolian iron flux to the (Southern) oceans, due to enhanced aridity during glacial periods may be a more finely tuned pacer of marine productivity and CO_2 draw down during glacial periods (Martin, 1990; Falkowski, 1997; Watson et al., 2000). Ultimately the cause(s) of enhanced CO_2 draw down during glacial stadials still remain a holy grail (Sigman and Boyle 2000).

References

Anderson, S.P., Drever J.I. and Humphery N.F. (1997) Chemical weathering in glacial environments. *Geology* **25**: 399-402.

Anderson S.P., Drever J.I., Frost C.D. and Holden P. (2000) Chemical weathering in the foreland of a retreating glacier. *Geochimica et Cosmochimica Acta* **64**: 1173-1189.

Archer D. and Maier-Reimer E. (1994) Effect of deep-sea sedimentary calcite preservation on atmospheric CO_2 concentration. *Nature* **367**: 260-263.

Axtmann E.V. and Stallard R.F. (1995) Chemical weathering in the South Cascade Glacier basin, comparison of subglacial and extra-glacial weathering. *In*: *Geochemistry of Seasonally Snow-Covered Catchments (Proceedings of a Boulder Symposium, July 1995)* IAHS **228**: 431-439.

Badger M.R., Andrews T.J., Whitnes S.M., Ludwig M., Yellowlees D.C., Leggat W. and Price D.G. (1998) The diversity and coevolution of Rubisco, plastids, pyrenoids, and chloroplast-based CO_2-concentrating mechanisms in algae. *Canadian Journal of Botany* **76**: 1052-1071.

Berger W.H. (1990) The Younger Dryas cold spell-a quest for causes. *Palaeogeography, Palaeoclimatology, Palaeoecology* **89**: 219-237.

Birkland P.W., Burke R.M. and Benedict J.B. (1989) Pedogenic gradients for iron and aluminium accumulation and phosphorus depletion in Arctic and Alpine soils as a function of time and climate. *Quaternary Research* **32**: 193-204.

Bluth G.S. and Kump L.R. (1994) Lithological and climatological controls of river chemistry. *Geochimica et Cosmochimica Acta* **58**: 2341-2359.

Bowen D.Q., Richmond G.M., Fullerton D.S., Sibrava V., Fulton R.J. and Velichko A.A. (1986) Correlation of Quaternary Glaciations in the northern hemisphere. In Sibrava V., Bowen D.Q. and Richmond (Eds.) Quaternary Glaciations in the Northern Hemisphere. *Quaternary Science Reviews* **5**: 509-501 and Chart 1.

Broecker W.S. (1982) Ocean geochemistry during glacial time. *Geochimica et Cosmochimica Acta* **46**: 1689-1705.

Broecker W.S. (2000) Abrupt climate change:causal constraints provided by the paleoclimate record. *Earth-Science Reviews* **51**: 137-154.

Broecker W. and Peng T.-H. (1982) *Tracers in the sea*. Lamont-Doherty Geological Observatory, Palisades, N.Y: **pp** 690.

Chadwick O.A., Derry L.A., Vitousek P.M., Huebert B.J. and Hedin L.O. (1999) Changing sources of nutrients during four million years of ecosystem development. *Nature* **397**: 491-497.

CLIMAP Project Members (1981) Seasonal reconstruction of the earth's surface at the last glacial maximum. *Geological Society of America.* Map and Chart Series **36**.

Colman A.S. and Holland H.D (2000) The global diagenetic flux of phosphorus from marine sediments to the oceans: Redox sensitivity and the control of atmospheric oxygen levels. *In*: Marine

Authigenesis. From Global to Microbial, *SEPM Special Publication* **66**: 21-33.

Compton J., Mallinson D., Glenn C.R., Filippelli G., Föllmi K., Shields G. and Zanin Y. (2000) Variations in the Global Phosphorus Cycle: *In:* Marine Authigenesis. From Global to Microbial, *SEPM Special Publication* **66**: 21-33.

Crews T.E., Kitayama K., Fownes J.H., Riley R.H., Herbert D.A. and Mueller-Dombois D. (1995) Changes in soil phosphorus fractions and ecosystem dynamics across a long chronosequence in Hawaii. *Ecology* **76**: 1407-1424.

Broecker W.S. (1982) Ocean geochemistry during glacial time. *Geochimica et Cosmochimica Acta* **46**: 1689-1705.

Darmody R.G, Thorn C.E. and Rissing J.M. (1987) Chemical Weathering of Fine Debris from a series of Holocenee Moraines: Storbreen, Jotunheimen, Southern Norway. *Geografiska Annaler* **69**: 405-413.

Delaney M.L. (1988) Phosphorus accumulation in marine sediments and the oceanic phosphorus cycle. *Global Biogeochemical Cycles* **12**: 563-573.

Drever J.I. and Hurcomb D.R. (1986) Neutralization of atmospheric acidity by chemical weathering in an alpine drainage basin in the North Cascade Mountains. *Geology* **14**: 221-224.

Einarsson T. and Albertson K.J. (1988) The glacial history of Iceland during the past three million years: 227-235. *In*: Shackleton N.J., West R.G. and Bowen D.Q. (Eds) *The Past Three Million Years: Evolution of Climatic Variability in the North Atlantic Region.* Cambridge University Press.

Eyles N., Sassevilee D.R., Slatt R.M. and Rogerson R.J. (1982) Geochemical denudation rates and solute transport mechanisms in a maritime temperate glacier basin. *Canadian Journal of Earth Sci*ence **19**: 1570-1581.

Falkovski P.G. (1997) Evolution of the nitrogen cycle and its influence on the biological sequestration of CO_2 in the ocean. *Nature* **387**: 272-275.

Föllmi K.B. (1995) 160 m.y. Record of marine sedimentary phosphorus burial: Coupling of climate and continental weathering under greenhouse and icehouse conditions. *Geology* **23**: 859-862.

Föllmi K.B. (1996) The phosphorus cycle, phosphogenesis and marine phosphate-rich deposits. *Earth-Science Reviews* **40**:55-124.

Filippelli G.M. and Souch C. (1999) Effects of climate and landscape development on the terrestrial phosphorus cycle. *Geology* **27**: 171-174.

Gaillardet J., Dupré B., Louvat P. and Allégre C.J. (1999) Global silicate weatheirng and CO_2 consumption rates deduced from the chemistry of large rivers. *Chemical Geology* **159**: 3-30.

Gibbs M.T. and Kump L.M. (1994) Global chemical erosion during the last glacial maximum and the present: Sensitivity to changes in lithology and hydrology. *Paleoceanography* **9**: 529-543.

Hodson A., Tranter M., and Vatne G. (2000) Contemporary rates of chemical denudation and

atmospheric CO_2 sequestration in glacier basins: an Arctic perspective. *Earth Surface Processes and Landforms* **25**: 1447-1471.

Holland D.H (1978) The chemistry of the Atmosphere and the Oceans. Wiley-Interscience, New York. **pp** 351.

Kpomblekou-a K. and Tabatabai M.A. (1994) Effect of organic acids on release of phosphorus from phosphare rocks. *Soil Science* **158**: 442-453.

Kump L.R. and Alley R.B. (1994) Global chemical weathering on glacial time scales. *In*: Usselman TM and Hay WW (Eds). *Material Fluxes on the Surface of the Earth*: 46-60. Geophysics Study Committee, National Research Council, National Academy Press, Washington D.C.

Kump L.R.., Brantley S.L. and Arthur M.A. (2000) Chemical weathering, atmospheric CO_2, and climate. *Annual Reviews of Earth Planet Science* **28**: 611-667.

Livingstone D.A. (1963) Chemical compositions of rivers and lakes. *U.S. Geological Survey Proffesional Paper* **440-G**: 64 pp.

Ludwig W., Amiotte-Suchet P. Munhoven G. and Probst J-L. (1998) Atmospheric CO2 consumption by continental erosion: present-day controls and implications for the last glacial maximum. *Global and Planetary Change* **16-17**: 107-120.

Martin J.H. (1990) Glacial-interglacial CO_2 change: The iron hypothesis. *Paleoceanography* **5**: 1-13.

Meybeck M. (1987) Global chemical weathering of surficial rocks estimated from river dissolved loads. *American Journal of Sci*ence **287**: 401-428.

Meybeck M. (1993) Natural sources of C, N, P and S: 163-193. *In*: Wollast R. Mackenzie F.T. and Chou L. (Eds.) Interactions of C, N, P and S Biogeochemical Cycles and Global Change. *NATO ASI Series:* **I 4**. Springer-Verlarg, Berlin Heidelberg.

Milligan A.J. and Morel F.M.M. (2002) A proton buffering role for Silica in Diatoms. *Science* **297**:1948-1850.

Nezat C.A, Lyons B.W. and Welch K.A. (2001) Chemical weathering in streams of a polar desert (Taylor Valley, Antarctica) *GSA Bulletin* **113**: 1401-1408.

Plummer L. N., Wigley T. M. L., and Parkhurst D.L. (1978) The kinetics of calcite dissolution in CO_2-water systems at 5-60°C and 0.0-1.0 atm CO_2. *American Journal of Science* **278**: 179-216.

Raymo M.E., Ruddiman W.F., Backman J., Clement B.M. and Martinson D.G. (1989) Late Pliocene variation in Northern Hemisphere ice sheets and North Atlantic deep water circulation. *Paleoceanography* **4**:413-446.

Redfield A.C. (1958) The biological control of chemical factors in the environment. *American Scientist* **46**: 3 205-221.

Retallack G.J. (1990) Soils of the Past: *A n Introduction to Paleopedology*. Unwin Hyman, Winchester. **pp** 520.

Riebesell U., Wolf-Gladrow D.A. and Smetacek V.S. (1993) Carbon dioxide limitation of marine phytoplankton growth rates. *Nature* **361**: 449-251.

Ruttenberg K.C. (1992) Development of a sequential extraction method for different forms of phosphorus in marine sediments. *Limnology and Oceanography* **37**: 1460-1482.

Ruttenberg K.C. (1993) Reassessment of the oceanic residence time of phosphorus. *Chemical Geology* **107**: 405-409.

Sharp M., Tranter M., Brown G.H. and Skidmore M. (1995) Rates of chemical denudation and CO_2 draw down in a glacier-covered alpine catchment. *Geology* **23**: 61-64.

Sigman D.M. and Boyle E.A. (2000) Glacial/interglacial variations in atmospheric carbon dioxide. *Nature* **407**: 859-869.

Stallard R.F. (1992) Tectonic Processes, Continental Freeboard, and the Rate-controlling Step for Continental Denudation. *In*: Butcher S.S. et al., (Eds) Global Biogeochemical Cycles. Academic Press, New York. **pp.** 93-121.

Stumm W. and Morgan J.J. (1996) *Aquatic Chemistry*. Wiley, New York: **pp** 1022.

Sugden D.E. (1978) Glacial erosion by the Laurentide ice sheet. *Journal of Glaciology* **20**: 367-394.

Summerfield M. (1991) *Global geomorphology:* Harlow, United Kingdom, Longman **pp** 537.

Tranter M., Sharp M.J., Lamb H.R., Brown G.H., Hubbard B.P. and Willis I.C. (2002) Geochemical weathering at the bed of Haut Glacier d'Arolla, Switzerland – a new model. *Hydrological Processes* **16**: 959-993.

Tyrell T. (1999) The relative influences of nitrogen and phosphorus on oceanic primary production. *Nature* **400**: 525-531.

Vebel M.A. (1993) Temperature dependence of silicate weathering in nature: How strong a negative feedback on longterm accumulation of atmospheric CO_2 and global greenhouse warming? *Geology* **21**: 1059-1062.

Wadham J.L., Cooper R.J., Tranter M. and Hodgkins R (2001) Enhancement of solute fluxes in the proglacial zone of a polythermal glacier. *Journal of Glaciology* **47**: 378-386.

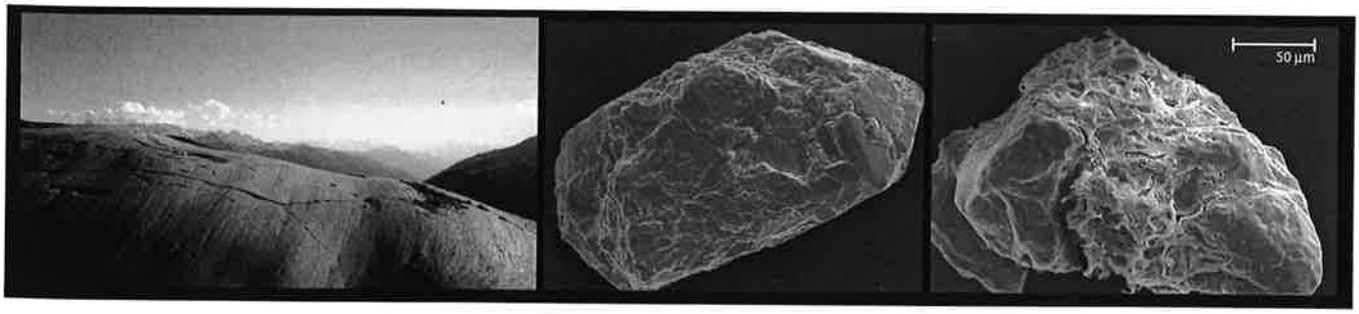
Walker T.W. and Syers J.K. (1976) The fate of phosphorus during pedogenesis. *Geoderma* **15**: 1-19.

Watson A. J., Bakker D. C. E., Ridgwell A. J., Boyd P. W., and Law C. S. (2000) Effect of iron supply on Southern Ocean CO_2 uptake and implications for glacial atmospheric CO_2. *Nature* **407**: 730-733.

West J.A., Bickle M.J., Collins R. and Brasington J. (2002) Small-catchment perspective on Himalayan weathering fluxes. *Geology* **30**: 355-358.

White A.F. and Blum A.E. (1995) Effects of climate on chemical weathering in watersheds. *Geochimica Cosmochimica Acta* **59**: 1729-1747.

APPENDICES



TESTS ON THE EFFECT OF GRANULOMETRY ON THE SEQUENTIAL EXTRACTION OF DIFFERENT PHOSPHORUS FORMS.

Introduction

The phosphorus (P) phases in the suspended and bedload of the Apure River System, Venezuela and in the suspended sediments and proglacial chronosequences of the Rhône and Oberaar glaciers, central Switzerland were identified using the SEDEX method. This extraction sequence was originally designed by Ruttenberg (1992) for use on marine sediments. Although it draws on previous soil science extraction schemes to distinguish iron bound (step I) , detritally bound (step III) and organic bound phases (step VI) a new step (II) is introduced, to remove authegenic carbonate fluorapatite by a weak acid extraction. We use all four extraction steps defined by Ruttenberg, despite the fact our sediments are not of marine origin and interpret step II as fine, reactive detrital P based on the experiment described below.

Ruttenberg (1992) points out that a sediment's granulometry and surface texture can affect its reactivity and consequently the extraction step in which it is solublised. She states therefore that samples should be ground as little as possible to achieve a grain size of < 125 μm for the method to be optimal. In our glacial suspended sediments the modal grain size is between 4-8 μm and the apatite mineral group is relatively soft compared to other minerals which it is in contact with in the subglacial environment (Vicker's hardness; 535 kg^{-1} mm^{-2}) suggesting that apatite would be partitioned into the finer sediment fraction. Also, as particles are freshly ground with many surface indentations they will be more reactive according to Ruttenberg (1992) than apatite grains rounded by riverine transport. The apatite grains analysed in the proglacial areas of the Rhône and Oberaar glaciers are similarly fresh, with fracture surfaces and extensive surface etchings upon increasing sediment age, suggesting that they too will be rather reactive and extracted to some extent in step II.

Methods

To test the effect of granulometry on extraction by the sedex method blue rock apatite was crushed in an agate mill for 5 minutes (Sample A) and 10 seconds to acheive different granulometries. The sample crushed for 10 seconds was separated into two sub-samples B (< 63 μm), and C (64-125 μm) using sieves. The granulometry of samples A and B was measured using a Laser Oriel Granulometer (table 1). The three crushed apatite samples, A, B and C were then diluted with pure quartz sand (10 mg of apatite and 90 mg of quartz sand).

Table 1: The granulometry of apatite samples A, B and C.

Size Fraction (μm)	Granulometry of sample A (%)	Granulometry of sample B (%)	Granulometry of sample C (%)
0_2	13	6	
2_4	21	16	
4_8	31	26	
8_16	16	20	
16_36	14	28	
36_64	5	4	
64-125	0	0	100

A: whole sample crushed for 5 minutes
B: < 63 μm fraction of the sample crushed for 10 seconds
C: 64-125 μm fraction of sample crushed for 10 seconds

Sample A has the finest grainsize, with a modal grainsize in the 4-8 μm fraction, whereas sample B has a modal grainsize within the 16-32 μm fraction (sample C's grains are all between 64 and 125 μm, as predefined by the method).

All samples were treated by the SEDEX method in duplicate (see *chapter 2, appendix 5* for a detailed description of the method). A blank containing 100 % quartz sand was also passed.

Results

No P was extracted from the quartz blank in any step of the extraction method nor was any P extracted from any of the samples in step I. Step II extracted 90 % of the P from sample A, 70% of the P from sample B and only 30 % of the P from sample C. Whereas step III extracted approximately 10, 27 and 66 % of the detrital P from phases A, B and C respectively. In all three samples approximately 1-5 % of the apatite P is extracted by step VI (see fig. 1).

These results are reproducible with the duplicate samples giving low 1 σ standard deviations, see Table 2.

Table 2: standard deviation (1 sigma) on the P concentrations (mg/g) n =2.

Sample	Step II	Step III	Step VI
A	0.21	0.00	0.00
B	0.12	0.04	0.02
C	0.09	0.19	0.04

Conclusions

The granulometry of the apatite has a direct effect on the step in which it is extracted by the sedex method. The finer the apatite grains, the more P is removed by step II. We therefore interpret step II as an indicator of chemically reactive apatite. Our test may also favour dissolution associated with this step due to the freshly ground nature of our grain surfaces. Authigenic P can form in terrestrial environments,

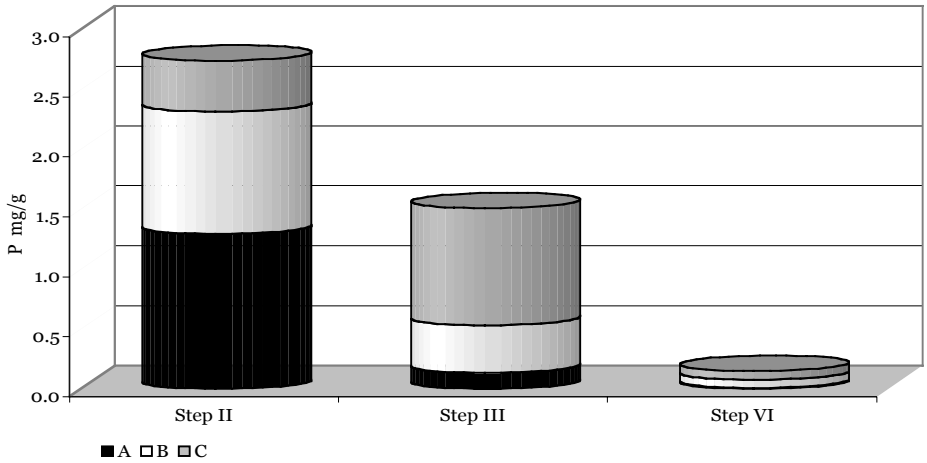


Fig. 1: *P phases extracted from apatite samples of different granulometries*

but it does not normally form in acidic soils

(Addiscot and Thomas, 1999; Sharpley, 2000) such as those found in the glacial catchments, and authigenic precipitates were not observed on any detrital grains in the moraines during the ESEM study.

In addition authigenic P is considerably more abundant in calcareous soils which are not prevelant in the Apure catchment and therefore we interpret the P extracted in step II of the tropical and glacial samples as reactive detrital P.

A component of P remains after the detrital P extraction irrespective of the original grain size of the apatite, with 5 % detrital apatite being identified as organic P in the coarser B and C samples. Therefore the interpretation of organic P at low concentrations, such as those found within the glacial suspended sediment samples should be qualified by other measurements e.g. total organic carbon.

CONFERENCE ABSTRACTS

First author papers

(oral unless otherwise indicated)

A comparison of soluble reactive and total dissolved phosphate concentrations and dynamics, in temperate-glacial and humid-tropical fluvial systems.

R. Hosein, K. Arn, K.B. Föllmi, P. Steinmann (2000) Swiss Sed., Fribourg

Soluble reactive phosphate (SRP) and total dissolved phosphate (TDP) concentrations have been studied in two contrasting weathering environments:

a) two small, temperate, mountain glacier catchments; the Rhone and Oberaar glaciers, in Switzerland over a one-year ablation period

b) A large, humid-tropical watershed, the Apure river system, Venezuela, which runs from the Venezuelan Andes to the Orinoco river. The Venezuelan watershed was sampled once during the dry season (February) and once at the end of the rainy season (September).

Comparing present-day biogeochemical weathering in glacial and tropical environments may initially seem counter-intuitive. Classically chemical weathering studies looked to the tropics, following the rational that a 10 °C increase in temperature doubles chemical reaction rates. But another physical control of reaction rates is the reactive surface area of the "chemicals". Glacier milks contain particles of high surface area to volume ratio. In temperate glaciers such particles may remain in isolated contact with subglacial waters for periods of months.

Our initial results suggest that SRP and TDP concentrations in the two environments are comparable. Oberaar glacier values lie between 35 and 65 μg/l, those of the Rhone glacier are between 10 and 40 μg/l . February tropical values are consistently lower than or equal to temperate values, whereas the September tropical data falls into the same range as the temperate results.

In this light we suggest that the importance of biogeochemical weathering in glaciated environments might be greater than is presently recognised.

Can icehouse-greenhouse transitions be modeled by extrapolating data sets from temporate-glacial and humid tropical environments ?

R. Hosein, K. Arn, K.B. Föllmi, P. Steinmann, C.J. Burton†, M.J. Russell†. (2000) *EGS, Nice:*

† Division of Earth Sciences, Gregory Building, Lilybank Gardens, University of Glasgow, Glasgow G12 8QQ, UK

How, in a greenhouse climate, could late Ordovician temperature drop by 10 °C (Brenchley et al., 1995), creating an icehouse period of less than 1my? $\partial^{13}C$ curves demonstrate increased productivity at the glacial maximum. Contemporaneous excursions in our chemostratigraphy (P_2O5, Fe_2O_3) support the argument for increased nutrient supply driving productivity and thus CO_2 drawdown. If nutrient supply had an important role in climate change (albedo can only explain 47% of temperature change) then identifying the nutrient source may improve our understanding of climate forcing.

Here we have explored a glaciated continent's potential to be a significant nutrient source by analysing phosphate in waters from a humid-tropical and two temporate glacial catchments. Initial results suggest that concentrations of soluble reactive (SRP) phosphate in temporate glacial waters are comparable with concentrations in tropical waters (10 – 65 μg/l & 5 – 30 μg/l SRP respectively). We suggest glacial, bio-geochemical weathering rates may be greater than presently recognised and encourage the inclusion of the continental weathering data in models of climate change.

Comparing phosphate weathering rates in glacial and tropical environments: Implications for feedbacks to global climate through coupled phosphate-carbon cycles

R. Hosein, K. Arn, K.B. Föllmi, P. Steinmann (2000) IGS British Branch, Annual Meeting, Southampton:

Raymo (1991) has highlighted the importance of feedbacks between silicate weathering and CO_2 draw down in climate change models. It is suggested that silicate weathering rates are strongly temperature dependent (Brady, 1991). Therefore although glacial environments do sequester CO_2 (Sharp et al., 1995) the global rate of CO_2 removal from the atmosphere could be anticipated to decrease during a glaciation, reducing the potential for a negative feedback. A second mechanism of CO_2 draw down could be a biogeochemical one: Given phosphate would be the limiting factor and applying Redfield molar ratios 106 moles of CO_2 could be taken up by aquatic biomass for every mole of phosphate available to them.

We compare phosphate fluxes (as soluble reactive phosphate-SRP) from glacial and tropical environments to see whether temperature is clearly the limiting factor in weathering phosphate-bearing minerals. The values from both environments fall into a similar range. We suggest that the crushing, grinding action of glaciers plays an important role in increasing the surface area of minerals and that surface area may, in part, control the rate of phosphate weathering.

On paper the effieciency of phosphate limited CO_2 draw down depends on the C:P molar ratio chosen for calculations. In the Oberaar and Rhone catchments, multiplying the P flux values, 17 and 29 kg/km^2/year respectively, by the Redfield molar ratio (draw down by living algae) implies that 1416 and 696 kg-C/Km^2/yr respectively of carbon could be sequestered from the atmosphere. If a higher C:P molar ratio ,e.g 1: 500, as found in the decayed organic matter of land plants, is chosen the CO_2 draw down increases considerably. This would suggest glacial P fluxes could have an impact on pCO_2 ,if the organic matter was not reoxidised, at a similar order of magnitude to silicate weathering 2137 kg-C/km^2/yr (Sharp et al., 1995) in the glacial environment.

Adsorbed cation fluxes from the Rhone and Oberaar Glaciers

R. Hosein, K. Arn, K.B. Föllmi, P. Steinmann (2001) EUG 11, Strasbourg, poster:

Suspended sediment samples were taken during the 1999 ablation season from the Rhône and Oberaar glacier meltwater streams. 40 of these samples were leached with 3 x 10 ml aliquots of 1N ammonium acetate. This leachate was measured for Ca^{2+},Mg^{2+}, Na^+ and K^+ ions using a flame AAS.

We found, firstly that the adsorbed cation concentration was not constant during the ablation season for any ion. On an annual scale sediment exported during "flushing events", namely days with high rain fall, contained elevated concentrations of adsorbed ions (mg/g). The change in the adsorbed ions can also be seen on an hourly scale, during a 24 h study of a rain event. On the 27/7/99 - 28/7/99 heavy rain fell on the Rhône catchment between 19.00 and 04.00. An increase in the Ca^{2+} and Na^+ adsorbed load was observed at 23.00 and 01.00. Post rainstorm adsorbed cation concentrations returned to their lower values.

Secondly the ratio of dissolved to adsorbed ion concentrations does not appear constant during the ablation season and is also perturbed by flushing events.

We suggest the concentration of adsorbed ion cations can be up to 100 % of the dissolved load. This observation has important implications for chemical mass balance studies in glaciated areas. Potential CO_2 draw down by chemical weathering in glaciated areas may be higher if the total concentration of the adsorbed weathering products has previously been underestimated.

A SEM study of the chemical weathering rates of apatites in two glaciated catchments in the Swiss Alps

R. Hosein, M. Lee[†], K. Arn, K.B. Föllmi, P. Steinmann (2001) Earth System Processes Edinburgh:

[†] Division of Earth Sciences, Gregory Building, Lilybank Gardens, University of Glasgow, Glasgow G12 8QQ, UK

Apatite is a common phosphorus-bearing mineral. Quantifying its weathering rate is important as phosphorus (as PO_4) is a biolimiting nutrient whose only source is rock weathering (it has no geseous phase). Its rate of supply to the environment may affect the rate which carbon is taken up biologically. Using a mass balance method (inputs of phosphate in the form of rain and snow subtracted from its output in river water) we calculate an annual weathering flux of 10 - 12 kg/km^2/year for the catchments of the Rhône and Oberaar glaciers, Switzerland. Both areas have a granitic bedrock.

An alternative way to estimate weathering rates is to look at mineral etching, using scanning electron microscope imaging. If sediment age and pit depth is known, then a weathering rate can be calculated for the individual minerals in the sediment. This method is used here as a first-order test to constrain the weathering rates estimated by the mass balance method. It may also demonstrate varying weathering rates in different environments (periglacial, subglacial) in the same catchment.

We hope to compare the degree of etching in glacial sediments of different ages, taken from within our catchments. Apatites have been isolated from recent glacial-fluvial, lacustrine and melt-out sediment, from 1850-moraines and moraine dating from before 1300. Apatites from the oldest moraine, which is all we have analysed to date, show evidence of etching, possibly following previous weakenings in the crystal lattice caused by fission tracks. Results will be presented as weathering rates of phosphorus for the apatite grains and compared to our mass balance rate results.

Detrital phosphorus weathering rates and mechanisms: comparing tropical and glacial catchments.

R. Hosein, K. Arn, S. Huon[†], K.B. Föllmi (2002) 12th Goldschmidt Conference, Davos:

[†] Univ. P.M. Curie, Lab. Biogéochimie isotopique (LBI), UMR 7618, Paris

Continental biogeochemical weathering of apatite is the primary source of phosphorus (P). Variations in weathering intensity may influence the global P flux and therefore primary production rates, which are important with regard to the carbon cycle and climate change. To assess the relative importance of the phosphorus flux in tropical and glacial environments we compared the distribution of phosphorus phases in suspended sediments from the Apure river system, Venezuela with those from meltwater streams of the Oberaar and Rhône glaciers, central Switzerland. Additionally two chronosequences were sampled in the forefields of the Oberaar and Rhône glaciers, comprising Little Ice Age moraines and tills of the Younger Dryas. Iron-bound P, organic P, and detrital P phases are quantified by a sequential extraction (SEDEX) method. In the glacial suspended sediment detrital P is the main phase. The Apure system suspended sediment becomes impoverished in detrital P and enriched in iron and organic bound P in rivers further from the source. In the glacial Younger Dryas samples the detrital P phase is replaced by organic and iron-bound P. Initial calculations give approximate apatite weathering rates of 0.3 g m^{-2} yr^{-1} for the Little Ice Age moraines and 0.01 g P m^{-2} yr^{-1} for the Younger Dryas tills. These weathering rates are one order of magnitude higher than the continental average value. Our results show that alpine glaciers have potential to accelerate detrital P weathering, especially in the first 100's of years after deposition of glacial sediment. Finally we present a global data set demonstrating that the flux of Total P in meltwaters from presently glaciated catchments is elevated when compared to riverine fluxes from presently non-glaciated catchments.

Phosphorus phases in 2 alpine glacial meltwater streams and a proglacial tributary draining crystalline catchments in the Swiss Alps

R. Hosein, K. Arn, P. Steinmann, K.B. Föllmi (2002) IGS British Branch Annual Meeting Glasgow:

The bio-availability of phosphorus (P) and its potential impact on bio-productivity and atmospheric CO_2 sequestration varies, depending on the form and the environment it is in. Detrital P is the primary source of P to the biosphere and physical erosion rates control detrital P supply. Total P concentrations in the Rhone and Oberaar glacier meltwaters are directly proportional to their suspended sediment concentrations. We calculate present-day detrital P fluxes from the Rhone and Oberaar glaciers of 7 and 11 kmol km^{-2} yr^{-1} respectively, representing 93 – 95 % of the total P flux. These fluxes are among the highest recorded particulate P fluxes in the world. But retention of detrital P minerals in terrestrial deposits may be vital to convert them into bio-available forms, as detrital P is not bio-available in aquatic environments. Protosols develop on alpine glacial deposits within a timespan of hundreds of years and the low pH and biological processes associated with the pedosphere enhances dissolution of the main detrital P bearing mineral, apatite. Soluble reactive P (SRP) concentrations in the Rhone and Oberaar glacier meltwaters are lower than SRP concentrations in the Rhone tributary that drains 11.6 kyr (Younger Dryas aged) sediments on which alpine meadow has developed. We calculate an SRP weathering flux from the Rhone tributary of 0.36 kmol km^{-2} yr^{-1}, whereas the Rhone and Oberaar glacier SRP flux is 0.16 kmol km^{-2} yr^{-1}. This implies that apatite dissolution is faster in the proglacial environment. The released SRP is biologically available. The ironbound and organically bound P phases, which have accumulated in the 11.6 kyr sediment, are also more bio-available than detrital P in freshwater and marine environments.

Second author papers

(oral unless otherwise indicated)

Weathering and climate change

K.B. Föllmi, R. Hosein, K. Arn, F. Tamburini, T. van Westrenen, B. van de Schootbrugge, P. Steinmann, T. Adatte (2000) EGS 25 Nice:

Weathering is important in regulating the long-term carbon cycle. Temporal changes in biogeochemical weathering rates modulate the uptake of atmospheric CO_2, and changes in biogeochemical weathering rates lead to changes in the release rates of biophile elements (such as P, Si, Ca, Fe), which modulate transformation rates of in-organic carbon into organic carbon through photosynthesis. Variations in weathering may, therefore, exert an important control on a row of globally interlinked processes such as productivity, transformation of inorganic carbon into organic carbon, oxygen contents, as well as climate.

Presently, in the field of research on weathering, several main topics have been identified as partially unresolved: 1) Quantification of weathering rates in the geological past; 2) The degree of dependency of biogeochemical weathering rates on total weathering rates; and 3) The influence of glaciation on total and biogeochemical weathering rates. These topics are relevant to several open questions, such as 1) to what extend continental weathering did contribute to phases of enhanced marine productivity during the Neogene and Quaternary, dependent on climate change; and 2) which types of feedback mechanisms may have developed between weathering and climate change in the case glaciation events did contribute to enhanced biogeo-chemical weathering.

Present-day (bio)geochemical weathering in glaciated areas

K. Arn, R. Hosein, K.B. Föllmi, P. Steinmann (2000) Swiss Sed, Fribourg:

The influence of glacial activity on (bio-) geochemical weathering and its rates was studied in the two catchment areas of the Rhône and Oberaar glaciers. In a first-year field campaign (1999) water was measured and sampled five days a week at Rhône and twice a week at Oberaar glacier, always at 10 am and 5 pm, that is during those parts of the day in which water discharge reaches its minimum and maximum, respectively.

Results of the first field season show that concentrations of major cations and anions (Ca, Mg, Na, K, Al, Si, P, Cl, NO_3, SO_4, HCO_3) are generally higher (up to 10-40 %) at minimum flow (10 am) than at maximum flow (5 pm). Concentrations are also lower from the middle of July until the beginning of September this year, probably relating to the seasonal evolution of daily mean temperature. Chloride and pH don't follow this trend. Increases in chloride are more likely to correspond to rain events. The big rain event at the beginning of July corresponds to the highest estimated discharge values. This in turn lead to a dilution of solutes; bedload transport was obvious.

Suspension load was estimated from filtering water samples. Grainsize and x-ray analyses will be performed and presented. An initial comparison of phosphate values from this two glaciated catchment areas and from a tropical weathering regime (Orinoco basin, Venezuela) is presented in a related talk by Rachel Hosein.

Present-day glacial activity and geochemical weathering

K. Arn, R. Hosein, K.B. Föllmi, and P. Steinmann (2000) EGS 25, Nice:

The influence of glacial activity on (bio-) geochemical weathering and its rates was studied in the two catchment areas of the Rhône and Oberaar glaciers, both in the Swiss Alps. In a first-year field campaign (1999) water was measured and sampled five days a week at Rhône and twice a week at Oberaar glacier, always at 10 am and 5 pm, that is during those parts of the day in which water discharge reaches its minimum and maximum, respectively.

Results of the first field season show that concentrations of major cations and anions (Ca, Mg, Na, K, Al, Si, P, Cl, NO_3, SO_4, HCO_3) are generally higher (up to 10 – 40 %) at minimum flow (10 am) than at maximum flow (5 pm). Concentrations are also lower from the middle of July until the beginning of September this year, probably relating to the seasonal evolution of daily mean temperature. Chloride and pH don't follow this trend. Increases in chloride are more likely to correspond to rain events. A big rain (and snowmelt) event at the beginning of July corresponds to the highest estimated discharge values what lead to a dilution of solutes.

Suspension load was estimated from filtering water samples. Suspension concentration seems to follow the discharge hydrograph and therefore also corresponds to rain events. Grainsize and X-ray analyses will be performed and presented to show the mineralogical evolution of the weathering environment over an ablation season.

The importance of lithology in mass balance calculations of glaciated areas

K. Arn, R. Hosein, K.B. Föllmi, and P. Steinmann (2000) *IGS British Branch Annual Meeting, Southampton:*

The influence of glacial activity on (bio-) geochemical weathering and its rates is studied in the two catchment areas of the Rhône and Oberaar glaciers (Swiss Alps). The two areas were chosen because of their homogeneous lithology, both are lying in the crystalline rocks of the Aar massif. That should simplify the comparison of the dissolved chemistries between the two areas. Glacial meltwater was measured and sampled regularly over more than one ablation season, always at 10 am and 5 pm, that is during those parts of the day in which water discharge reaches its minimum and maximum, respectively.

In both areas the dissolved chemistry is showing the well known trends of higher concentrations during minimum discharge (10 am) than during maximum discharge (5 pm). Furtheron concentrations are also lower from middle of July until beginning of September, relating to the seasonal evolution of daily mean temperature. Chloride and pH don't follow this trend. Increases in chloride are more likely to correspond to rain events. The big rain event at the beginning of July 1999 corresponds to the

highest estimated discharge values. This in turn leads to a dilution of solutes; bedload transport was obvious.

A preliminary comparison of the results from the two catchments shows that concentrations of major cations and anions (Ca, Mg, Na, K, PO_4, Cl, NO_3, SO_4, HCO_3) are generally higher at Oberaar glacier than at Rhôneglacier and therefore, the fluxes seem to be independent on the ratio of glacier cover (glacier cover Oberaar < Rhoneglacier). The Si fluxes of the two areas on the other hand are in the same order of magnitude. This observations imply that the lithology of the Oberaar catchment has to be less homogeneous. Specially Na-normalized Mg–Ca as well as HCO_3–Ca plots are showing a generally more pure granitic solute source in Rhône catchment, whereas a small portion of a gneissic-schisty zone in Oberaar catchment seems to be of a major importance for the dissolved chemistry.

Suspension load was estimated from weighing sample filters and from measuring turbidity during ablation season 2000. Particulate output and therefore physical erosion is also higher at Oberaar glacier. Local to regional weather patterns and their flushing influences are observed in both neighbouring catchments.

Subglacial vs secondary weathering in two glaciated areas in the Swiss Alps

K. Arn, R. Hosein, T. Adatte, K.B. Föllmi, and P. Steinmann (2001) EUG 11, Strasbourg: (poster).

The influence of glacial activity on (bio-) geochemical weathering and its rates is studied in the two catchment areas of the Rhône and Oberaar glaciers (Swiss Alps). In sampling glacial meltwaters and measuring their dissolved chemistry two main questions arose: (1) Are they a result of primary weathering, that means of dissolution of freshly ground fines or are there also reworking processes going on (weathering of soils and moraines up in the catchments)? (2) Can secondary weathering, after the deposition of moraines, be visible in the mineralogy of such deposits?

Suspended sediment from two ablation seasons was collected when filtering meltwaters: Whole rock mineralogy (filters) as well as the <2 μm grainsize fraction represent mainly the lithology of the catchment. There is no sign of secondary products like vermiculite. Therefore the suspended sediment has to origin from subglacial mechanical erosion of fresh bedrock.
Several profiles within moraine walls of different age (mainly walls from little ice age 1600-1850 as well as walls more than 500 years old) showed secondary weathering: The ratios of mica/clorite and K-Feldspar/Plagioclase respectively, increase with increasing age from 1.5 (value from recent sediment) to 2-3 and from 0.2 to 0.5-0.85 respectively. The older moraines showed an especially high vermiculite content of 5-30 % compared to mica and chlorite. The appearance of these secondary clay minerals seems to be dependent also on siltosity of the moraines (if compared with the granulometry).

This shows that alteration occurs in moraine deposits in a temperate alpine environment, even though the moraines are at altitudes of more than 2000 m a.s.l. and at low yearly average temperatures. Therefore in calculating regional to global weathering fluxes from glaciated areas, secondary weathering should not be neglected.

The importance of gradual chemical weathering on nutrient release in two glaciated areas in the Swiss Alps

K. Arn, R. Hosein, T. Adatte, K.B. Föllmi, and P. Steinmann (2001) Abstract for oral presentation at Earth System Processes, Edinburgh:

In order to identify processes and rates of alteration of moraine material in the glacier forefield, we studied chemical weathering processes of glacial sediments and rates in the two catchment areas of the Rhône and Oberaar glaciers (Swiss Alps).

We use mineralogy and bulk chemistry (XRD and XRF data) of glacial sediments of different ages from both glaciers; i.e. suspended sediment in meltwater, recent englacial melt-out sediment, terminal moraines dating from little ice age LIA (1300-1850), and older tills. Two of the main questions are: (1) How much does subsequent weathering of sediment after deposition contribute to the overall chemical denudation rate of a catchment? (2) How long is its influence significant? The answers could be used to assess weathering rates during glacial periods.

XRD data show an increase of pedogenic formed vermiculite and a continuous decrease of biotite with increasing age of the sediment. Chlorite seems to be more or less stable in tills up

to LIA, in the oldest deposited tills there is a significant decrease. Suspended sediment is fresh, secondary weathering products are missing. Melt-out sediment contains vermiculite suggesting it may be derived from reworked lateral moraines that were previously weathered.

XRF element distributions have been compared to mineralogy in our profiles, which should give an insight in nutrient leaching processes. The distribution of some elements can directly be related to mineral weathering reactions, eg. biotite => vermiculite: The concentration of Fe_2O_3, K_2O, and MgO decreases as biotite content becomes less. In the pre-LIA tills Fe_2O_3 is completely leached in the top 30 cm of the profile.

This gradual convergence of biotite to vermiculite over a time scale of 100's of years emphasises the importance of secondary weathering in glaciated cachments. This pedogenic processes allow the slow release of Fe, probably biolimiting nutrient in proglacial alpine areas.

Sr isotope systematics in two glaciated crystalline catchments in the Swiss Alps

K. Arn, R. Hosein, K.B. Föllmi, and P. Steinmann, J. Kramers,[†] D. Aubert[§] (2002) 12th Goldschmidt Conference, Davos:

[†] Gruppe Isotopengeologie, Geol. Inst., Uni Bern, Erlachstrasse 9a, CH-3012 Bern

[§] EOST, ULP/CNRS, Centre de Géochimie de la Surface, UMR 7517, 1 rue Blessig, F-67084 Strasbourg

The Sr isotope systematics are useful in the identification of the relative importance of different sources contributing to chemical weathering fluxes. We studied subglacial chemical weathering processes and the Sr isotope composition of runoff and particulate material in the two glaciated catchments of Oberaar (OA) and Rhone (RH) glacier (Swiss Alps). Both areas are contained within the crystalline rocks of the Aar Massif, and the lithologies are quite homogeneous and comparable, except for the presence of a zone of highly deformed variscide basement gneisses and schists in the Oberaar cachment.

We analysed meltwaters (RH $^{87}Sr/^{86}Sr$ = 0.7257 / OA 0.7155), suspended sediment (RH 0.7292 / OA 0.7134), precipitation (0.7104) and dust (0.7109), local bedrock (0.7101 – 0.7377), and subglacially precipitated calcite that is now exposed in front of the glaciers (RH 0.7182 / OA 0.7164).

RH meltwater ratio is smaller than RH suspended sediment (total digestions) which can be interpreted as a mixture of granodiorite (0.7101) and granite (0.7377). We explain this by the preferential weathering of calcite (disseminated or in veins), which has a relatively low $^{87}Sr/^{86}Sr$ ratio. An enrichment in Ca relative to Na in the meltwaters compared to suspended sediments is visible in both areas (OA > RH). In addition meltwaters could also be influenced by atmospheric input. The role of this will be assesed by mass balance calculations. The fact that OA meltwaters show an increased ratio compared to OA suspended sediment points to a minor atmospheric influence on our meltwaters: Increased OA meltwater ratios are better explained by the weathering of freshly ground biotite. The concentration of suspended sediment is higher for OA than for RH. OA suspended sediment contains more biotite due to the gneissic rocks within this catchment, what is also visible in the more elevated K flux.

The first order reaction in our catchments is weathering of calcite, but in addition, in the OA catchment biotite weathering exerts an other major influence on the meltwater $^{87}Sr/^{86}Sr$ ratio.

*Quantifying the impact of accessory calcite on meltwater chemistries draining two crystalline catchments, the Rhone and Oberaar glaciers, Switzerland**

K. Arn, R. Hosein, P. Steinmann, T. Adatte, K.B. Föllmi (2002) IGS British Branch Annual Meeting Glasgow:

Annual suspended sediment and dissolved fluxes have been calculated for the presently glaciated Rhone and Oberaar catchments. The catchments lie on the crystalline rocks of the Aar massif in central Switzerland. There are minor lithological differences between the two catchments; The central section of Oberaar catchment is underlain by a schistose zone containing < 5 % calcite, whereas the Rhone catchment only contains granitic and granodioritic bedrock with < 1 % calcite.

Meltwaters from the two catchments were sampled over two years (1999-2001). Monthly samples were taken during the accumulation period (winter) whereas during the ablation period (summer) samples were taken twice daily. There

is a considerable difference in the total dissolved fluxes from the two catchments, which is principally the calcium flux from the Oberaar catchment being 5 – 6 times higher than that from the Rhone. We attribute this to the elevated calcite flux from the Oberaar glacier: Calcite concentrations are 3 times higher in the Oberaar suspended sediment and 1.6 – 2 times as much suspended sediment is exported from the Oberaar catchment than from the Rhone. This leads to a calcite flux of approximately 16 t km^{-2} yr^{-1} from the Oberaar catchment, whereas the calcite flux from the Rhone catchment is only 3 t km^{-2} yr^{-1}. The calcium fluxes from these alpine glaciers is directly proportional to the calcite content of their suspended sediment, and the higher calcite content of the Oberaar sediment causes 3 times more atmospheric CO_2 to be sequestered in the Oberaar catchment compared to the Rhone.

Nisbet, Rachel Hafiza Hosein

Address Ch. du Reposoir 23,
Lausanne 1007

Tel. (home) 021 601 4330

D.o.B. 02/11/76

Nationality British

Education

'99 - '02: Institut de Géologie, University of Neuchâtel, Switzerland.

Ph. D. thesis: Biogeochemical weathering processes in the glacierised Rhône and Oberaar catchments, Switzerland and the Apure catchment, Venezuela. My supervisor is Karl Föllmi.

The project was undertaken by myself and another Ph. D. student, thereby giving me experience in teamwork and collaborative project development. My thesis included six months of fieldwork, sampling meltwaters, snow, rain, dust and proglacial sediments in the Rhône and Oberaar glacier catchments in the Valais in order to calculate chemical and physical denudation fluxes from these presently glaciated areas.

During my thesis I also had the opportunity to further my research experience via two further collaborations: I was invited to participate in a project studying the hydrochemistry of the Apure watershed, Venezuela, organised by Sylvain Huon, of the Biogéochimie Isotopique Group of the Université Pierre & Marie Curie, Paris. Additionally, I initiated my own collaboration with Martin Lee of the Division of Earth Sciences at the University of Glasgow examining the surface morphologies of apatite grains from glacial sediments of different ages.

I have presented my results at several international conferences, including the European Union of Geosciences meeting (EUG; Strasbourg, 2000), the Earth Surface Processes meeting (Edinburgh; 2001) and the world's biggest international geochemical conference, the Goldschmidt (Davos; 2002).

I held a teaching assistant post, giving lectures and practicals on general geology, sedimentology and geophysiology, these classes were mainly taught in French. I also participated in departmental geological fieldtrips in the Swiss Alps and Germany.

'94 - '98: Department of Geology, University of Glasgow, Scotland.

In 1998 I graduated with a B.Sc. (Hons) 2.1 in Geology and Applied Geology. I also received prizes for motivating class morale, and for palaentology upon graduation. During my degree I took courses in hydro-, petroleum- and engineering geology, sedimentology and environmental chemistry. I enjoyed fieldwork and found a field trip to southern Spain, where we studied recently created mountain environments, particuarly interesting.

'87 - '94 Queen Katherine School, Kendal, Cumbria, England.

A Levels: English Literature (B) Biology (B) Chemistry (B) General Studies (B) German (C).
G.C.S.E.'s: 9 A's and 1 B.

Experience and Employment

'03 Invited speaker at the "Evolution of the Earth's Surface" meeting, Glasgow, organised by the Mineralogical Society, Clay Minerals Group.

'98: Volunteer in a wood recycling initiative (Brighton, UK)

'97 & '98: Fossil excavation projects.

During two, one month trips I learnt methods of fossil excavation and preservation on UNESCO protected sites in Germany (Messel, Eocene and the Westerwald, Oligocene). I also benifitted from the opportunity to hone my spoken German.

'96: Spitsbergen Expedition: As member of a twenty strong expedition to the high Arctic I was tested as a field scientist, report editor, public speaker and more!

Appendix III

Interests
Skiing, mountain biking and singing.

Languages
I am a native English speaker, fluent in French and German (spoken) and possessing very basic Spanish.

Computer Skills
Comfortable with Mac's and PC's. Familiar with MS office, Adobe Illustrator and Photoshop.

References

Prof. Dr Karl Föllmi (Karl.Föllmi@unine.ch)

Dr Chris Burton (C.Burton@earthsci.gla.ac.uk)